Self-Assembly and Self-Organisation of Discotic Micelles formed in Aqueous Solutions of the Salts of Fluorinated Carboxylic Acids

Ashok Neil Parbhu

Department of Chemistry and Biochemistry

Massey University

New Zealand

Submitted in accordance with the requirements

degree Doctor of Philosophy

March 1994

Abstract

The phase behaviour of a series of discotic micellar liquid crystal systems found in aqueous solutions of perfluorinated carboxylic acids has been determined mainly by the use of ^{2}H and ^{133}Cs NMR. All the systems exhibited an isotropic micellar solution phase which underwent transitions to first a micellar nematic N_D^+ and then a micellar lamellar L_D phase on decreasing temperature or increasing the surfactant concentration. It was found that the self-organisation could be understood within the framework of a hard particle interaction and the changes in the phase transition temperatures on the addition of salt, change of counter-ion, and substitution of different chain length fluorocarbons were the result of changes in the micellar self-assembly.

The effect of amphiphile chain length was investigated by studying the caesium salts of perfluorinated carboxylic acids with chain lengths of 7, 9 and 10 carbons, in $^{2}H_2O$. A comparison with the caesium pentadecafluorooctanoate (CsPFO)/$^{2}H_2O$ system shows the four systems exhibit universal phase behaviour with the phase transition temperatures at any given volume fraction of surfactant being simply displaced in temperature. In addition, the variation in the axial ratio of the discotic micelles along the transition lines has been established from the magnitudes of the ^{2}H quadrupole splittings of $^{2}H_2O$. It has been shown that for any given thermodynamic state of the system axial ratios of the discotic micelles decrease with increasing chain length, *i.e.* the micelle aggregation number increases. At the phase transition temperatures, however, the micelles have the same axial ratio irrespective of the length of the fluorocarbon chain.

The influence of inorganic electrolyte on the mesophase behaviour has been studied in the CsPFO/CsCl/$^{2}H_2O$ and ammonium pentadecafluorooctanoate (APFO)/NH_4Cl/ $^{2}H_2O$ systems. The addition of electrolyte has the effect of increasing the phase transition temperatures in both systems. ^{2}H NMR has been used in conjunction with low angle x-ray scattering to probe changes in the micelle structure as a function of electrolyte. It has been shown that electrolyte promotes growth of the micelle, *i.e.* a decrease in the axial ratio. But, as in the case of changing the chain length, the axial ratio of the discotic micelle is the same at the phase transition temperatures for any given volume fraction of amphiphile.

The role of the counter-ion and co-ion have also been established by ^{133}Cs and ^{35}Cl NMR. The effect of counter-ion has been investigated by progressively substituting APFO for CsPFO on a mole for mole basis. The Cs^+ ions are shown to be preferentially "bound" over NH_4^+ ions, but the micelle size is the same at the phase transition temperatures. Co-ion effects on the phase behaviour of the added salt systems has been probed by substitution of Cl^- ions with F^-, Br^-, and I^- ions. It has been shown that the co-ion has no significant effect on the phase behaviour.

Table of Contents

List of Symbols

a	(1) head group area
	(2) length of the minor axis
a/b	micelle axial ratio
α'	contribution of a monomer in the toroidal, semicylindrical rim to the excess free energy
$\boldsymbol{B}$	magnetic field
b	length of the major axis
β	$1/k_BT$
β^b	free energy difference corresponding to the work needed per monomer to form part of an infinite bilayer out of surfactant ions present in solution
β_{Cl}	bound fraction of chloride ions
β_{Cs}	bound fraction of caesium ions
c	electrostatic energy
χ_{Cl}	nuclear quadrupole coupling constant of the ^{35}Cl nucleus.
χ_{Cs}	nuclear quadrupole coupling constant of the ^{133}Cs nucleus
χ_D	nuclear quadrupole coupling constant for ^2H in heavy water
Cep	critical end point
$\Delta\tilde{\nu}$	quadrupole splitting,
$\Delta\chi$	anisotropy in the magnetic susceptibility
$\Delta\chi_a$	anisotropy in the magnetic susceptibility of an amphiphile
e	elementary charge
ε_0	permittivity in a vacuum
ε	relative permittivity

ϕ	volume fraction of amphiphile
ϕ_p	total particle volume fraction
γ	magnetogyric ratio
γ_I	interfacial tension
$g_i(a)$	bulk energy and entropy effects associated with the packing of the hydrophobic tails
g_N	nuclear g factor
η	asymmetry parameter
$h_i(a)$	interfacial tension and electrostatic energy contributions to chemical potential
I	isotropic micellar solution phase
I	nuclear spin quantum number
i	surfactant environment
LC	liquid crystal region
L_D	lamellar phase
μ	magnetic moment
$\tilde{\mu}^0$	chemical potential
μ_N	nuclear magneton
$\boldsymbol{n}$	mesophase director
n_a	number of moles of amphiphile
n_b	number of bound water molecules per amphiphile
n_e	number of moles of electrolyte
N_D^+	nematic phase
$\langle P_2(\cos\alpha)\rangle_s$	shape factor

P	spin angular momentum
Q	nuclear quadrupole moment
q_{zz}	component of the nuclear quadrupole-electric field gradient coupling parallel to the direction of the magnetic field,
S	order parameter
s	aggregation number
σ	chemical shift shielding tensor.
$S_{O\text{-}D}$	order parameter relating the average orientation of the O-^{2}H bond of a water molecule with respect to the micelle surface
s_{rim}	number of surfactants in the rim
T^*	temperature of the theoretical second order transition
Tcp	tricritical point
T_{IL}	temperature of the upper boundary to the isotropic-to-lamellar transition
T_{IN}	temperature of the upper boundary to the isotropic-to-nematic transition
T_{LI}	temperature of the lower boundary to the isotropic-to-lamellar transition
T_{LN}	temperature of the lower boundary to the nematic-to-lamellar transition
T_{NI}	temperature of the lower boundary to the isotropic-to-nematic transition
T_{NL}	temperature of the upper boundary to the nematic-to-lamellar transition
Tp(I,N,L)	triple point
v	space filling volume associated with each molecule
W	monomer solution phase
w_a	mass fraction of amphiphile
w_c	mass fraction of electrolyte
x_a	mole fraction of amphiphile

X_{APFO}	mole fraction of APFO of the total mole fraction of amphiphile
x_e	mole fraction of electrolyte
x_w	mole fraction of amphiphile heavy water
y	relative stability parameter
ψ_0	electrostatic potential at the surface
z	the charge

List of Abbreviations

APFO	Ammonium pentadecafluorooctanoate
C10	CsNFD/^2H_2O system
C7	CsTFH/^2H_2O system
C8	CsPFO/^2H_2O system
C9	CsHFN/^2H_2O system
cmc	critical micelle concentration
CsNFD	caesium nonadecafluorodecanoate
CsHFN	caesium heptadecafluorononanoate
CsPFO	caesium pentadecafluorooctanoate
CsTFH	caesium tridecafluoroheptanoate
EL	Eriksson and Ljunggren model
MBG	McMullen, Ben-Shaul, and Gelbart model
o.d.	outer diameter
RbPFO	rubidium pentadecafluorooctanoate
TH	Taylor and Herzfeld model

Acknowledgments

I am grateful to Associate Professor Ken Jolley for his support throughout my postgraduate studies. I am indebted to him for many things; his encouragement, confidence in my work, and his friendship, but primarily it is his patience for which I am most appreciative.

I would like to express appreciation to Associate Professor Gavin Hedwig for his guidance and encouragement.

I am grateful to my colleagues at Massey University, Dr David Parker, Dr Mark Smith, Dr Pat Edwards, and Mr Scott Thomsen, and for their assistance and encouragement. I also would like to thank my colleagues at Leeds University Dr Johnathan Clements and Dr Gerson Orquies for providing me with x-ray and conductivity data. Thankyou to Professor Neville Boden for helpful discussions.

Thankyou to the technical staff of the science faculty for their assistance.

I am grateful for the financial assistance granted for travel to Leeds by both the New Zealand Royal Society and the British Council. The research experience that I gained has proved to be invaluable. Thankyou to the Massey University Vice Chancellors Committee for my Ph.D. scholarship

I am truly indebted to Karen Morgan for her support to the very end.

Finally I would like to acknowledge (again) my appreciation to my family; Mum, Dad, Bharat, and Ramila, for their continued encouragement.

Chapter 1

Introduction

Lyotropic liquid crystals are formed by aggregates of amphiphillic molecules dispersed in a solvent. Amphiphilic molecules characteristically consist of a hydrophobic and hydrophilic moiety. There are two levels of ordering. On increasing the amphiphile concentration of the molecular solution, the amphiphilic molecules initially undergo self-assembly to form aggregates, the concentration at which this occurs is called the critical micelle concentration (cmc). The aggregates at higher concentrations can undergo self-organization to form liquid crystalline mesophases. A variety of different phases can be formed dependent on the size and shape of the amphiphile aggregate.

Conventional hydrocarbon surfactants exhibit an essentially universal phase behaviour in water (figure 1.1), irrespective of the structure of the polar groups. Mesophases with one- (lamellar), two- (hexagonal and rectangular), and three-dimensional (cubic) translational order occur, but nematic (orientable) states are conspicuously absent. The dominant feature is that the transition from one mesophase to the next is associated with a dramatic change in the topology of the aggregate. The interpretation of this universal phase behaviour is therefore reduced to obtaining an understanding of the factors that govern the variation of the stability of the various aggregates with concentration and temperature.

In 1967 Lawson and Flautt [1] demonstrated that a solution of sodium decylsulphate in water containing small amounts of decanol and sodium sulphate was homogeneously aligned by the magnetic field in NMR experiments. Rosevear[2] then observed that the same solutions exhibited a Schlieren opto-micrographical texture, a characteristic signature of a nematic phase. Using X-ray and neutron diffraction, Charvolin and co-workers[3, 4] have shown that these solutions consist of rod- or disc-shaped micelles with long range orientational ordering of their symmetry axes (figure 1.2). The early reported nematic phases were located over narrow concentration ranges in complex mixtures of amphiphile, solvent, and salts or alcohols. For a long time it was thought that a third component, either salt or alcohol, was essential for the production of stable nematic phases. However, several binary systems which exhibit nematic phases have now been observed[5]. The decylammonium chloride (DACl)/water system for example, which was long thought to require salts to form a stable nematic phase, exhibits such a phase over the amphiphile mass fraction w_a range of 0.42 to 0.49[6]. The disodium cromoglycate/water system also exhibits a nematic phase from $w_a = 0.10$ to 0.15[7]. These are examples of hydrocarbon amphiphiles where the nematic range is typically limited to very small concentration ranges.

Figure 1.1 Schematic phase diagram for a conventional amphiphile in water, reproduced from reference[8]. ϕ_A is the volume fraction of amphiphile, T the temperature, and K is crystalline surfactant.

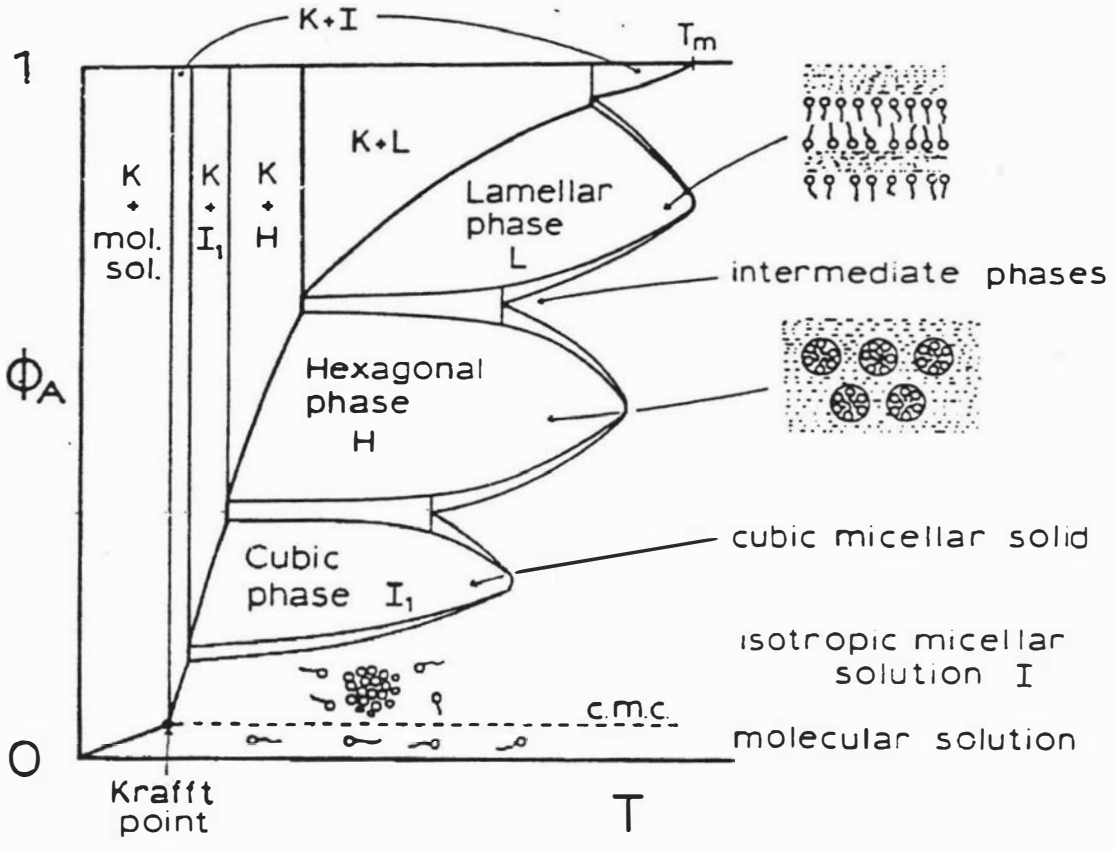

Figure 1.2 Schematic representation of possible structures of aggregates and their associated mesophases formed by conventional amphiphiles in water. Reproduced from reference[8].

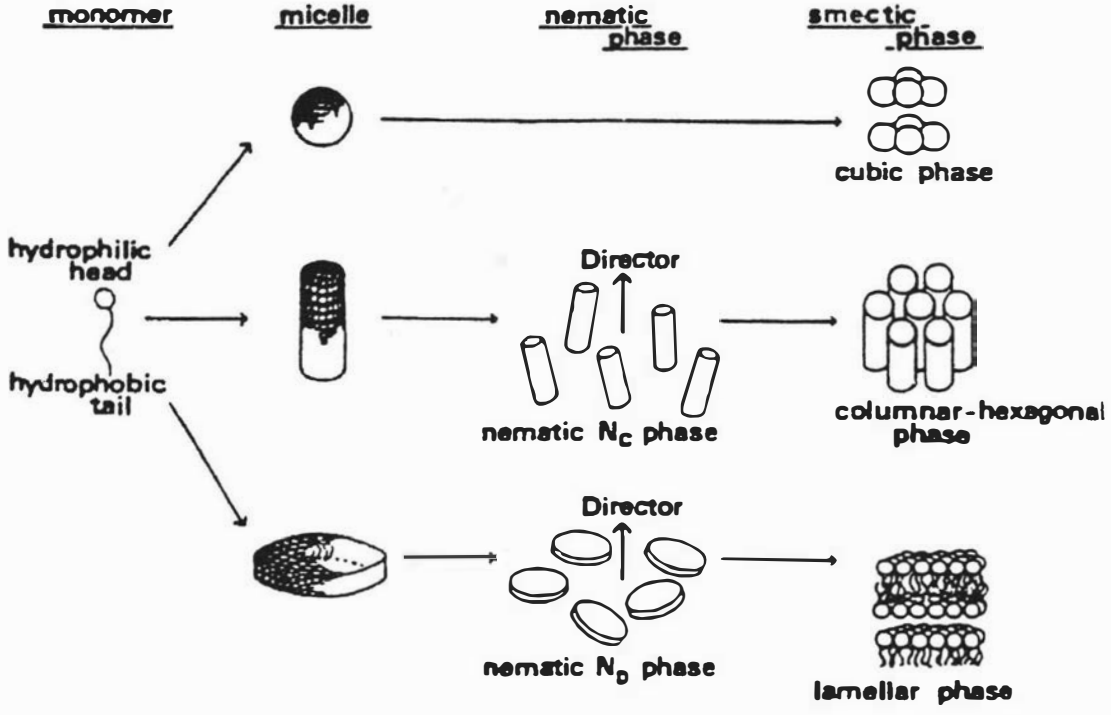

On the other hand, salts of short chain perfluorocarbon carboxylic acids form solutions of discotic micelles which are stable over wide concentration and temperature intervals. Unlike the conventional hydrocarbon systems the phase changes in the perfluorinated systems do not undergo dramatic changes in the aggregate topology on traversing phase transition boundaries. Typically, the discotic micelles, with increasing concentration undergo a sequence of disorder/order transitions to form first a nematic phase and, subsequently, a smectic lamellar phase. The nematic phase N_D is characterised by long-range orientational correlations in the micelles, whilst in the dilute lamellar phase L_D the micelles are arranged on equidistant planes. The discotic micelles have a positive diamagnetic susceptibility (N_D^+) which gives rise to monodomain samples in applied magnetic fields and short magnetic relaxation times[9], both of which make them amenable to experimental interrogation.

The caesium[10], ammonium[11], rubidium[12], and tetramethyl ammonium[13] salts of short chain perfluorocarbon carboxylic acids form a N_D^+ phase while the sodium and potassium salts are not sufficiently soluble to form liquid crystal phases. The lithium salt behaves somewhat like a classical soap-like surfactant, exhibiting hexagonal and bilayer-type lamellar phases, but no nematic phase, and the parent acid exhibits phospholipid type vesicle and lamellar phases. The corresponding salt of heptadecafluorononanoic acid yield similar phase diagrams, with corresponding transition temperatures about 25 K higher[14]. Each of the systems that undergo the I-to-N_D^+ and N_D^+-to-L_D disorder/order series of transitions exhibit a generic phase behaviour.

Of the salts that form discotic micelles the caesium pentadecafluorooctanoate (CsPFO)/^2H_2O system is the archetypal system. A high resolution phase diagram of this system has been established and is shown in figure 1.3[15]. The phase diagram exhibits the extensive nematic phase intermediate to the isotropic micellar solution phase I, and the discotic lamellar phase. The range of the discotic nematic phase extends from a amphiphile mass fraction of w_a = 0.225 to 0.632 and temperatures from T = 285.3 to 351.2 K. The N_D^+-to-L_D transition is second order to low concentrations but crosses over to first order at a tricritical point Tcp at w_a = 0.43; T = 304.80 K. Investigation of the CsPFO/^2H_2O system have shown that the micelle size decreases along the phase transitions with increasing concentration of amphiphile, from an aspect ratio *a/b* of 0.21 (aggregation number s of 351) at w_a = 0.2 to *a/b* = 0.38 (s = 80)at w_a = 0.6[15]. It has also been shown that the micelle size decreases as a function of increasing temperature[15].

The CsPFO/water system phase behaviour has also been established[16] to high precision. A comparison of the two systems in volume fraction, temperature space shows an isotope effect on changing the solvent. Substituting H_2O for ^2H_2O lowers both T_{NI} and T_{NL} at corresponding concentrations: at ϕ = 0.15, $T_{NI}(^2H_2O)$ - $T_{NI}(H_2O)$ is 3.9 K and $T_{NL}(^2H_2O)$ - $T_{NL}(H_2O)$ is 4.3 K; these differences decrease with increasing ϕ (temperature) and eventually vanish at $\phi \approx 0.41$ (80 °C). The micelle sizes were shown to

1.3 Phase diagram for the CsPFO/^2H_2O system[15], temperature versus the mass fraction of amphiphile, w. Nomenclature: K, crystal; L_D , lamellar phase; N_D^+, nematic phase with positive diamagnetic anisotropy and discotic micelles; I, isotropic micellar solution phase; Tcp, the lamellar-nematic tricritical point; Tp(I,N,L), the isotropic micellar solution-nematic-lamellar triple point.

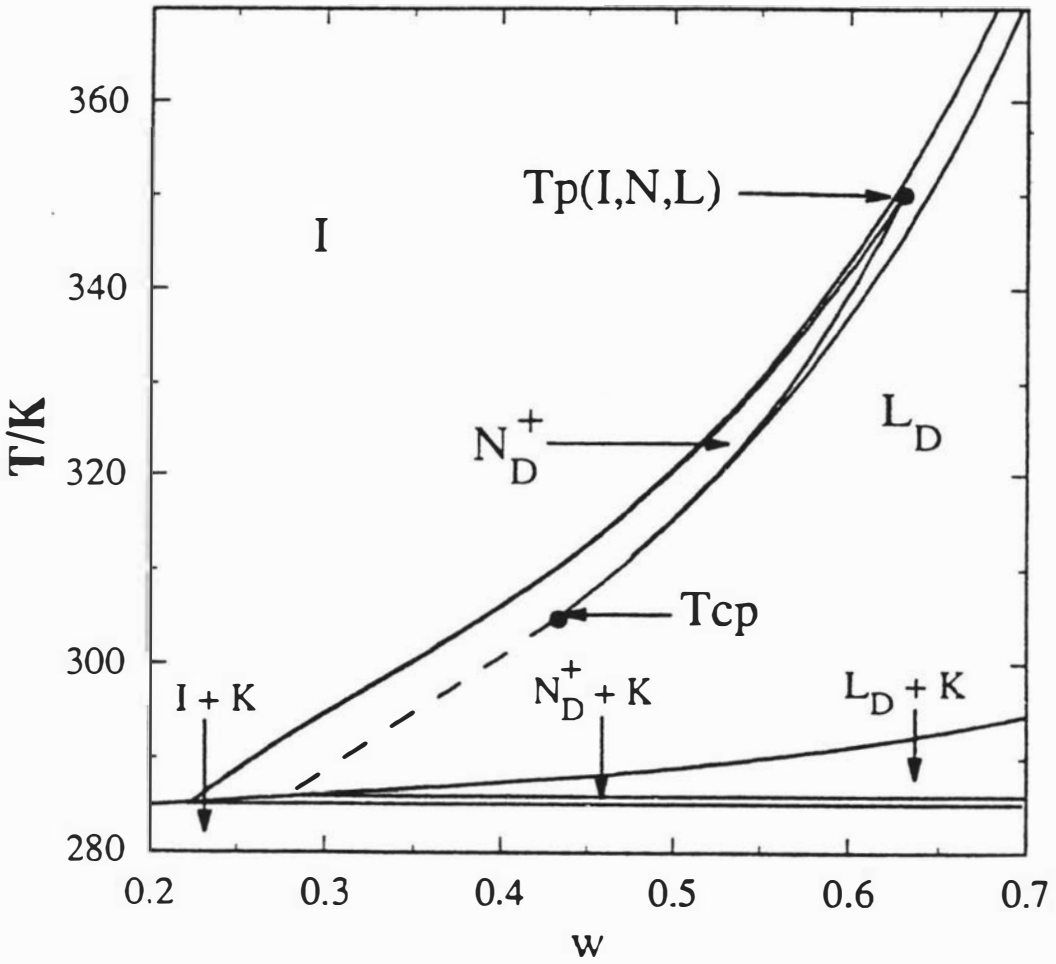

be essentially the same at T_{NI} (T_{LN}) at corresponding concentrations. They also decrease as the temperature is raised. It follows that the micelles must be larger in ^2H_2O than in H_2O at corresponding concentrations and temperatures below 80 °C. This "isotope effect" on the micelle size is attributed to tighter binding of Cs^+ to surface carboxylate groups *via* bridging water molecules in the case of ^2H_2O.

Changing the counter-ion has a much greater effect on the phase behaviour. The ammonium pentadecafluorooctanoate(APFO)/^2H_2O system high resolution phase diagram has been established[11] and exhibits similar phase behaviour as the CsPFO/^2H_2O system but with phase transition temperatures at corresponding volume fractions about 23 K lower[14], although ϕ versus *a/b* is the same in both systems[17].

Simple statistical mechanical models suggest that discotic micelles are intrinsically unstable and should undergo spontaneous growth to form infinite bilayers as is the case for phospholipids for example[18]. However, theoretical models have been proposed to account for their intrinsic stability. McMullen and co-workers[19, 20] used a micelle model consisting of an oblate right-circular cylinder (body) closed by a half-toroidal rim. The chemical potential of a surfactant molecule is different in the "body" than in the "rim" because of changes in both the surface interactions and the elasticity free energy difference in those two environments. They showed that only small discotic micelles can be stable, and that the chemical potential of the surfactant in the rim can be only slightly greater than in the body so that the entropy of mixing off-sets their explosive growth into infinite bilayers.

For thermotropic liquid crystals it is the entropic free energy,[21] which drives order-disorder transitions. Onsager obtained a relationship between the particle number density and their eccentricity (l/σ, where l is the lenght of the rod and σ its diameter) for very long rods ($l/\sigma > 100$). Recent treatments have established corresponding relationships between the diameter and thickness of discs which enable comparisons with theory to be undertaken. For the CsPFO/^2H_2O and APFO/^2H_2O system it has been shown that the volume fraction versus *a/b* ratic (*a* is the minor axis and *b* is the major axis of the ellipsoidal micelle) is close to that predicted from an Onsager hard particle model modified to include particles with low eccentricity[21-27]. The measured *a/b* ratios are higher than those predicted at low ϕ values. In the case of thermotropics, the particles can be considered to have a constant geometry (apart from possibly conformational changes) irrespective of the thermodynamic state of the system. In micellar liquid crystals, however, the micelle sizes are expected to vary with concentration and temperature and to depend upon the nature of the forces between the micelles and also upon any coupling to the symmetry and order of the mesophase. This will have a marked effect on the phase behaviour. Taylor and Herzfeld[28] have recently considered liquid crystal phases formed in reversibly self-assembling systems (micellar liquid crystals) within the framework of a hard-particle model. Their model allows for polydispersity which is expected to

significantly affect the structure of any translationally ordered phases which occur[29]. The effect of including polydispersity is to favour a translationally ordered lamellar phase consisting of layers of discotic micelles rather than the characteristic columnar phases exhibited in thermotropic discotic systems[30]. They also calculated *a/b* ratios as a function of ϕ at both the I-to-N_D^+ and N_D^+-to-L_D transitions.

The object of this study is to investigate factors that govern the size and shape of the aggregates, and the mechanism of the disorder/order phase transitions of the short chain fluorinated surfactants in aqueous solution. In order to achieve this aim a study of the effect of systematic perturbations on the phase behaviour of the fluorinated surfactant/^2H_2O system has been undertaken.

The effect of changing the chain length of the perfluorocarbon chain has been revealed by determining the phase behaviour for the homologous systems caesium tridecafluoroheptanoate (CsTFH)/^2H_2O, caesium heptadecafluorononanoate (CsHFN)/^2H_2O, and caesium nonadecafluorodecanoate (CsNFD)/^2H_2O over accessible temperature and concentration ranges using ^2H NMR spectroscopy[15] to define the phase transition temperatures. These results, together with previously determined phase diagram for the caesium pentadecafluorooctanoate (CsPFO)/^2H_2O system, were used to investigate how the chain length affects the size of the micelles and in turn the phase transition temperatures. It is shown that the behaviour of all these binary systems can be represented by a universal phase diagram plotted in reduced temperature versus volume fraction space where the temperature is scaled by the temperature at the tricritical point Tcp. The I-to-N_D^+ phase transition appears to be governed by hard particle forces at high surfactant concentrations whilst at lower concentrations longer range softer forces seem to be important too. Thus the actual shape of the phase diagram in reduced temperature/volume fraction space is primarily governed by the effects of temperature and composition on the self-assembly behaviour of the discotic micelles.

The effect of added electrolyte was determined by studying the phase behaviour of the CsPFO/CsCl/^2H_2O and APFO/NH_4Cl/^2H_2O systems. Added electrolyte can effect both the inter-micellar and intra-micellar forces as a result of electrostatic screening and specific surface interactions.

It is shown that at a fixed temperature, electrolyte induces growth in the micelles (*i.e.* it affects the self-assembly of the micelles) but at the phase transition temperatures the micelle size is unchanged from that in the binary system at the corresponding surfactant concentration (*i.e.* it has little effect on the self-organization of the micelles). Thus, the primary effect of the electrolyte is to change the intra-micellar interactions. The counter-ion and co-ion binding at the micelle surface has been investigated using ^{133}Cs and ^{35}Cl NMR as well as co-ion substitution experiments. It will be shown that the co-ion has no significant part to play in the micelle self-assembly.

The role of the counter-ion has been further investigated by a counter-ion substitution experiment in which NH_4^+ ions are proportionally exchanged for Cs^+ ions at a fixed amphiphile to ^2H_2O mole ratio. Specific counter-ion surface interactions are revealed with the Cs^+ ion being preferentially bound.

References

1. K. D. Lawson, T. J. Flautt, *J. Am. Chem. Soc.* **8921**, (1967).

2. F. Rosevear, *J. Soc. Cosmet. Chem.* **19**, 581 (1968).

3. J. Charvolin, A. M. Levelut, E. T. Samulski, *J. Physique Lett.* **40**, L587-L592 (1979).

4. Y. Hendrikx, J. Charvolin, M. Rawiso, L. Liebert, M. C. Holmes, *J. Phys. Chem.* **87**, 3991-3999 (1983).

5. M. Boidart, A. Hochapfel, M. Laurent, *Mol. Cryst. Liq. Cryst.* **154**, 61-67 (1988).

6. M. R. Rizzatti, J. D. Gault, *J. Colloid Interface Sci.* **110**, 285-262 (1986).

7. H. Lee, M. M. Labes, *Mol. Cryst. Liq. Cryst.* **84**, 137-157 (1982).

8. N. Boden, R. J. Bushby, K. W. Jolley, M. C. Holmes, F. Sixl, *Mol. Cryst. Liq. Cryst.* **152**, 37 (1987).

9. N. Boden, K. W. Jolley, *Phys. Rev. A* **45**, 8751-8758 (1992).

10. N. Boden, et al., *J. Physique* **47**, 2135-2144 (1986).

11. N. Boden, J. Clements, K. W. Jolley, D. Parker, M. H. Smith, *J. Chem. Phys.* **93**, 9096-9105 (1990).

12. C. Rosenblatt, *J. Colloid. Interface. Sci.* **131**, 236-241 (1989).

13. K. Reizlein, H. Hoffmann, *Progr. Colloid & Polymer Sci.* **69**, 83-93 (1984).

14. K. Fontell, B. Lindman, *J. Phys. Chem.* **87**, 3289-3297 (1983).

15. N. Boden, S. A. Corne, K. W. Jolley, *J. Phys. Chem.* **91**, 4092-4105 (1987).

16. N. Boden, K. W. Jolley, M. Smith, *J. Phys. Chem.* **97**, 7678-7690 (1993).

17. N. Boden, P. J. B. Edwards, K. W. Jolley, in *Structure and Dynamics of Strongly Interacting Colloids and Supramolecular Aggregates in Solution* S.-

H. Chen, J. S. Huang, P. Tartaglia, Eds. (Kluwer academic Publishers, Dordrecht, 1992), vol. 369, pp. 433-461.

18. S. Kirchner, G. Cevc, *Europhysics Letters* **23**, 229-235 (1993).

19. W. E. McMullen, A. Ben-Shaul, W. M. Gelbart, *J. Colloid Interface Sci.* **98**, 523-536 (1984).

20. W. E. McMullen, W. M. Gelbart, A. Ben-Shaul, *J. Phys. Chem.* **88**, 6649-6654 (1984).

21. L. Onsager, *Ann. N. Y. Acad. Sci.* **51**, 627-659 (1949).

22. D. Frenkel, R. Eppenga, *Phys. Rev. Lett.* **49**, 1089-1092 (1982).

23. D. Frenkel, B. M. Mulder, J. P. McTague, *Phys. Rev. Lett.* **52**, 287-290 (1984).

24. M. P. Allen, D. Frenkel, J. Talbot, *Comput. Phys. Rep.* **9**, 301 (1989).

25. M. P. Allen, R. W. Wilson, *Jounal of Computer-Aided Molecular Design* **3**, 335 (1989).

26. D. Frenkel, B. M. Mulder, *Mol. Phys.* **55**, 1171 (1985).

27. B. Tjipto-Margo, G. T. Evans, *J. Chem. Phys.* **93**, 4254 (1990).

28. M. P. Taylor, J. Herzfeld, *Phys Rev A* **43**, 1892-1905 (1991).

29. T. J. Sluckin, *Liq. Cryst.* **6**, 111 (1989).

30. S. Chandrasekhar, *Liq. Cryst.* **14**, 3-14 (1993).

Chapter 2
Materials and Methods

2.1 Chemicals

Deuterium oxide, 99.9 atom % deuterium, was obtained from both Aldrich and Sigma Chemical Company. Tridecafluoroheptanoic acid, pentadecafluorooctanoic acid heptadecafluorononanoic acid, and nonadecafluorodecanoic acid were obtained from both Aldrich and Riedel-de Haen (98% purity). All H_2O used in the preparation of samples was deionised and doubly distilled. Caesium fluoride, chloride, bromide and iodide were obtained from Aldrich, as was the ammonium chloride. All of the inorganic salts had a purity of at least 99.9%

The caesium salts of tridecafluoroheptanoic (CsTFH), pentadecafluorooctanoic (CsPFO), heptadecafluorononanoic (CsHFN), and nonadecafluorodecanoic (CsNFD) acids were prepared by neutralising an aqueous solution of the appropriate perfluorinated carboxylic acid with an aqueous solution of caesium carbonate, where a simple acid-carbonate reaction occurred with the evolution of carbon dioxide. Although the perfluorinated carboxylic acid is only sparingly soluble in water, all the acids are solubilized as the reaction proceeds and the water soluble salt is formed.

The Rubidium salt of pentadecafluorooctanoic acid (RbPFO) was prepared using rubidium carbonate as the base and ammonium pentadecafluorooctanoate (APFO) was prepared by neutralising a pentadecafluorooctanoic acid solution with a solution of ammonium hydroxide (30 %).

Each neutralization reaction was followed using indicator paper (BDH). Once the acid solution was neutralized the resulting amphiphile solution was freeze dried to remove the water. The amphiphile was generally recrystallized, twice, using a 50/50 v/v n-hexane/n-butanol mixture, although for more soluble amphiphiles such as the ammonium salt the fraction of non-polar solvent was increased.

The recrystallized amphiphile was dried under vacuum (0.5 mm Hg) at 318 K for periods of 12 to 36 hours to ensure the removal of any traces of the organic solvent used in the recrystallization. This was essential as tiny amounts of solvent can markedly affect the phase transition temperatures. Residual butanol in the sample causes the transition temperature to be lowered. The purified dried amphiphile was stored in a desiccator to keep it moisture free until required. Prior to the preparation of a sample the amphiphile was again placed under vacuum to ensue complete dryness. This is important because any additional water would make a difference in the calculation of the composition of the sample. Any inorganic salts used to prepare samples were also dried under vacuum before use.

2.2 Preparation Of Samples

All samples used in this study were prepared gravimetrically using a Mettler AT 261 Delta Range balance. Masses were measured to a precision of ±0.00002. As sample preparation methods are critical in obtaining consistent results in studies involving lyotropic liquid crystal systems each sample preparation method is outlined in detail below.

2.2.1 NMR Sample Preparation

Samples for use in the NMR spectrometer were produced by weighing ^2H_2O and solute directly into a 5 mm o.d. NMR tube that had been shortened to a length of 100 mm. The NMR tube had previously been soaked in concentrated nitric acid and then rinsed repeatedly with distilled water after which it was dried in an oven. The concentrated acid solubilized any organic or inorganic contaminants in the NMR tube, which could then be flushed out by the distilled water.

The solute was added though a long funnel whilst the ^2H_2O was introduced by means of a long hypodermic syringe needle so as to avoid contact with the upper section of the tube. This is essential to prevent any alterations in concentration due to evaporation of ^2H_2O or the decomposition of amphiphile when the tubes are flame sealed. This method allowed samples to consistently be prepared with an accuracy in composition of ± 0.001 mass fraction.

When a series of samples required a constant ratio of ^2H_2O to amphiphile a bulk standard solution of the required mass fraction of amphiphile was prepared. This was done by weighing directly into a glass ampoule, which was then immediately flame sealed to avoid concentration changes due to either evaporation or the absorption of water by the hygroscopic ^2H_2O. The sample was then heated in an oven to about fifteen degrees above the isotropic-to-nematic transition temperature and inverted repeatedly until a homogeneous isotropic phase was formed. The NMR samples were then prepared by weighing both the inorganic salt and the standard amphiphile solution directly into 5 mm o.d. NMR tubes. Immediately prior to use the amphiphile solution was heated into the isotropic phase and thoroughly mixed to ensure concentration homogeneity. The amphiphile solution was added using a constant volume micropipettor with a long hypodermic syringe needle, so that the sample could be placed in the base of the NMR tube. The inorganic salt was added through a long glass funnel that fitted inside the NMR tube.

Once the components were added the NMR tube was sealed with "parafilm" and then centrifuged, to ensure that there was no sample material adhering to the upper portion of the tube. The tube was then flamed sealed, and a section of 5 mm glass tubing fused on to bring the total length, sample tube plus extension tube, to 655 mm. The sample could then be loaded into the sample temperature control cell shown in figure 2.1.

Figure 2.1 Double-pass water flow sample cell used to control the sample temperature during NMR experiments. The water is pumped to the cell by a Colora WK3 cryostat.

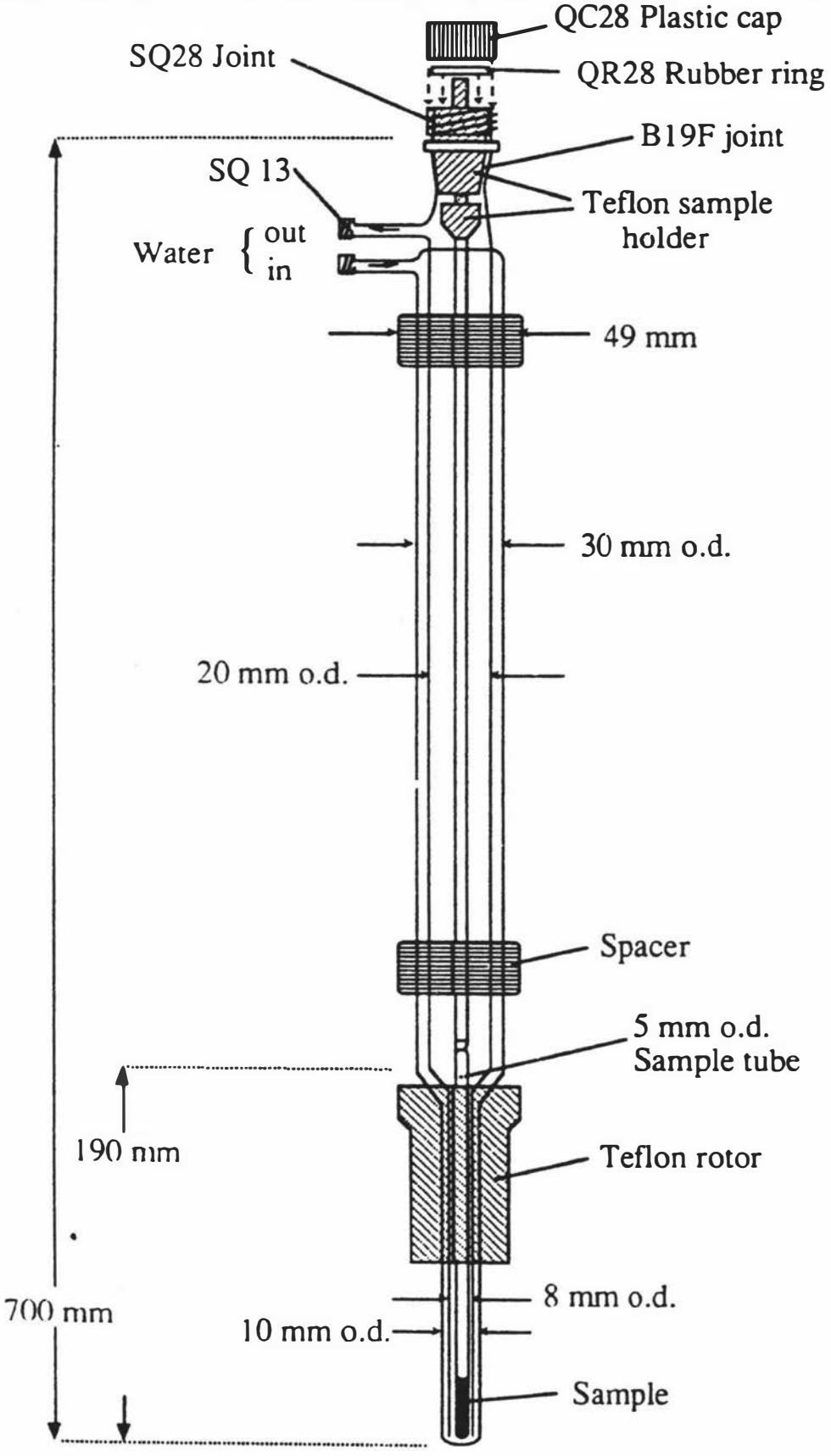

Samples stored at room temperature gave reproducible results (*i.e.* the phase transition temperatures were invariant) over a period of several months. Samples kept at elevated temperatures (>353 K), however underwent decomposition within a few days.

2.2.2 Polarizing Optical Microscopy Sample Preparation

Prior to obtaining precise transition temperatures using NMR spectroscopy, the phase behaviour was often coarsely determined using optical microscopy to detect changes in texture on passing through phase transitions. Samples for use in polarizing optical microscopy were made up by weighing into glass vials which were then flame sealed. Prior to loading of the samples into the microslide the solution was heated into the isotropic phase and thoroughly mixed. The microslides used had the dimensions 2 mm x 50 mm x 0.5 mm with an optical path length of 0.2 mm and were supplied by Camlab, Cambridge. The microslide was first passed through a moderate blue flame to remove any water that might be absorbed onto the surface of the glass, before being allowed to cool to room temperature in a desiccator. The microslide was then inserted into a slit in a rubber septum that was fitted to a syringe. The slit was only wide enough to accommodate the microslide thus allowing the solution to be drawn up into the microslide by raising the plunger of the syringe until the microslide was about two thirds full. The end of the microslide that was in the septum was then flame sealed by drawing out the end of the microslide in a flame with a pair of tweezers. This had to be performed relatively quickly so as to avoid heating of the sample, and possible consequent changes in sample composition, or even decomposition of the amphiphile. Once the end was flame sealed the solution was centrifuged in a microcentrifuge until all the sample solution resided at the sealed end. The open end was then flame sealed as before. The success of the sealing process was tested by placing the sealed microslide in warm water. In poorly sealed samples air bubbles were seen to escape as the air inside the microslides expanded. Two slides were prepared for each sample and in cases where the phase transition temperatures for these samples differed by more than 0.2 K the results were rejected. Once loaded into the microslides the samples could not be mixed effectively and so measurements were made immediately following sample preparation.

2.2.3 Densitometer Sample Preparation.

Dilute isotropic solutions for density measurements were prepared in 10 mL volumetric flasks equipped with close fitting lids. The amphiphile was added through a long funnel whilst the water was added via a long hypodermic syringe needle. Solutions were made up to the required molality by first weighing in the amphiphile and then calculating the mass of water that was required to be added in order to obtain the required concentration. Once a solution had been prepared, the lid was placed on the flask and then sealed with parafilm. Solutions sealed in this manner showed no measurable change

of mass over a two day period. Once sealed the solutions were mixed by repeated inversion of the flask. The solutions were allowed to stand for 12 hours to allow the foam produced during the mixing process to dissipate. Prior to use the flasks were carefully inverted twice to insure that the solution composition was homogeneous.

2.2.4 Qualitative Phase Detection Sample Preparation.

Samples used to establish the phase transitions for the construction of the triangular phase diagram were prepared in screw top vials (10 mL) that were fitted with teflon sealed tops. The solute and the ^2H_2O were each weighed directly into the vials. The solutions were then mixed by heating the sample into the isotropic phase and inverting the vial repeatedly. Tests performed on the seals of the tops showed that, even at 353 K, there was no measurable change in the mass of the samples over a period of days. The phase transitions were determined simply by observation between crossed polarisers.

2.3 Instrumentation

2.3.1 Nuclear Magnetic Resonance

NMR was used to detect phase transition temperatures and also to monitor changes in the size of the mesophase aggregates. The NMR spectra were obtained using a JEOL JNM-GX270 spectrometer with an Oxford Instruments 6.34 Tesla wide bore superconducting magnet. ^{133}Cs and ^2H spectra were collected using the NM-G27T10 10 mm tuneable probe, while ^{35}Cl spectra were collected using the NM-G27T10L 10 mm low frequency tuneable probe.

The instrument parameters given in table 2.1 are typical values and were altered as necessary to meet the requirements of specific experiments. There are two pulse widths quoted for ^2H, the short pulse width corresponds to the situation where the probe was tuned to ^2H and the long pulse for when it was tuned to ^{133}Cs (detuned from ^2H). When the probe is detuned a longer pulse width is required to rotate the magnetisation through 90° but the quality of the ^2H spectra is not affected. Detuning allows the collection of both ^2H and ^{133}Cs spectra in a very short space of time. This is achieved by using both of the terminals of the GX-270 machine, one terminal with the parameters set for ^2H observation and the other set for ^{133}Cs observation. As soon as the ^{133}Cs accumulation is completed the ^2H accumulation can be started. This procedure enabled ^2H and ^{133}Cs spectra to be obtained at exactly the same temperatures.

Phase transition detection was achieved primarily by monitoring ^2H and ^{133}Cs spectra as a function of temperature. ^{35}Cl measurements were not very useful in the determination of phase transitions. It is a less sensitive nucleus than ^{133}Cs, and although it is more sensitive than ^2H, there are many more ^2H nuclei in the samples. Also the very

short quadrupole relaxation time for ^{35}Cl in liquid crystalline mesophases results in quadrupole peaks that are very broad with a consequent poor signal to noise ratio.

Table 2.1. Typical Values Used For NMR Experimental Parameters

Nucleus	^{2}H	^{133}Cs	^{35}Cl
Experimental Mode	SGNON*	SGNON	SGNON
Observation Freq.	41.47 MHz	35.44 MHz	26.34 MHz
Sweep width	2 kHz	10-60 kHz	10-30 kHz
Data Points	8 192	32 768	8 192
Broadening Factor	0.1 Hz	1 Hz	5-10 Hz
Accumulations	4	16	1 000
$\pi/2$ Pulse Width	20 or 200 µs	19µs	30 µs
Pulse Delay	2 s	0.5 s	0.5 s

* SGNON:- single pulse, no decoupling

2.3.1.1 NMR Temperature Control and Measurement

In determining phase transition temperatures it is important to have both stable and accurate temperature control of the sample. Temperature control was maintained by mounting the extended sample tube into a double pass water flow sample cell[1] (see figure 2.1). The cell was constructed by the glass blower of the Department of Chemistry and Biochemistry to fit the dimensions of the Oxford Instruments 6.34 T wide-bore magnet. The cell can be easily customized to suit the dimensions of other magnets, either superconducting or iron. The sample cell was connected to a Colora WK3 cryothermostat through thermally insulated silicone-tubing. The control water had a relatively high flow rate so that there was no measurable temperature gradient over the sample length.

The temperature was measured by a copper/constantan thermocouple using an ice slurry reference point. The thermocouple was placed as close to the sample as was consistent with good resolution. The thermocouple potential was measured with a Philips PM2535 systems multimeter, to an accuracy of 0.1 µV. The thermocouple was calibrated at 2 K intervals to an accuracy of ±10 mK, against a Hewlett-Packard 2804A digital quartz thermometer with a 2805A temperature probe, the calibration curve is given in figure 2.2. The measured thermocouple potential was transformed into temperature (K) by linear interpolation between the calibration points using a simple computer program.

Figure 2.2 Calibration curve for the copper/constantan thermocouple used to measure the temperature during NMR experiments. $T / °C = -0.49796\ V^2 + 25.35537\ V + 0.130907$.

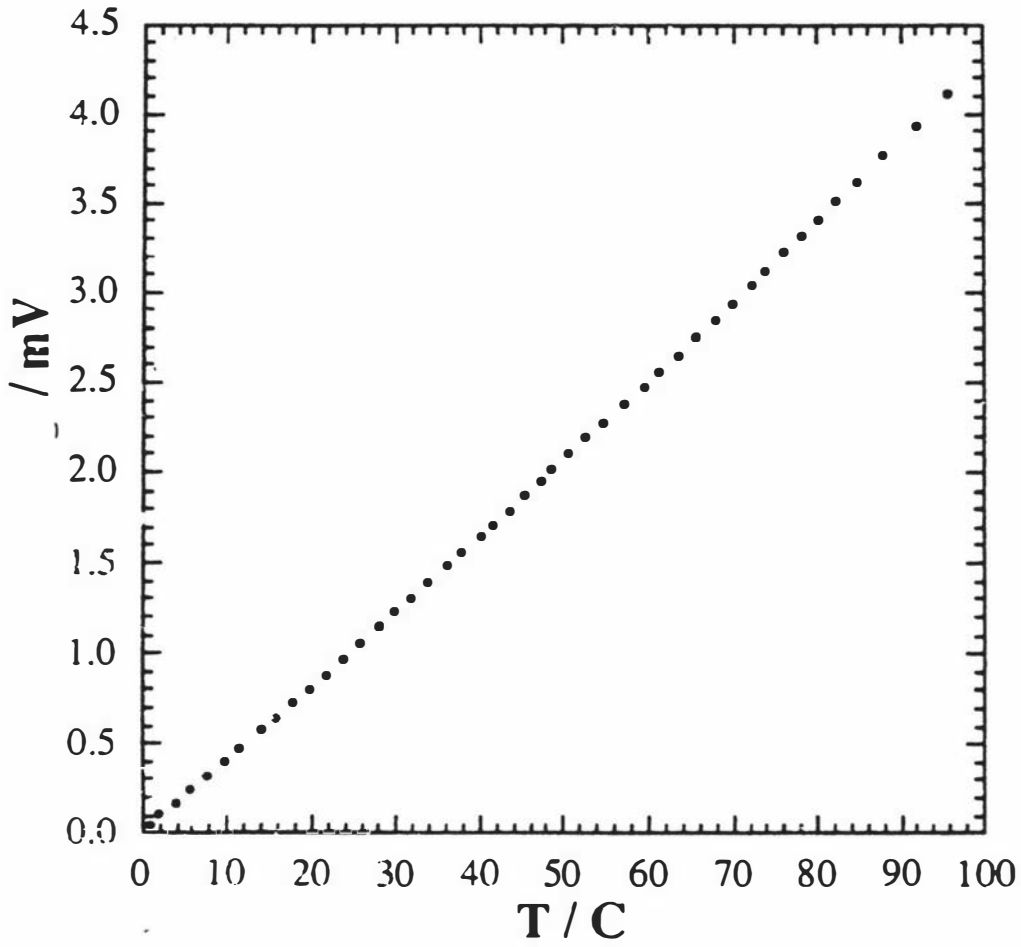

2.3.2 Polarising Microscopy

Polarising Microscopy, using a Nikon 104 polarising microscope, was routinely used to determine the phase transition temperatures for the lyotropic liquid crystal systems studied and to identify the nature of the phases formed[2]. The sample temperature was controlled using a 'home built system' as described below.

2.3.2.1 Polarising Microscopy Temperature Control and Measurement

The heating stage (Figure 2.3) was constructed by the mechanical and electronics workshops of the Department of Chemistry and Biochemistry. This stage consists of a brass block mounted upon a cast iron ring, which in turn was mounted directly on to the stage mount of the microscope. Glass microslides containing the sample were placed in a brass slide-holder which fitted tightly into a channel milled in the brass block. The holder can be moved within the channel, so that different parts of the sample can be viewed. Over the top of the brass block a copper shield was placed to minimise possible thermal gradients as a result of the sample being in contact with air. To further minimise temperature gradients when in use the whole unit was covered with a coat of insulating glasswool. The iron ring has a copper pipe soldered to it which is connected to a Colora WK3 cryo-thermostat via rubber tubing. This provides a heat sink for the brass block through the thermal contact with the mounting screws. The brass block is heated by two cartridge heaters that reside within the block either side of the sample to minimise the temperature gradient across the sample (see figure 2.3). The power to the cartridge heaters is controlled by a Omron E5AX temperature controller which monitored the block temperature via a thermistor placed in the block close to the sample. The digital readout (resolution 0.1 K) from the Omron temperature controller was calibrated against the temperature at the sample as monitored by a copper/constantan thermocouple, over the operating range of 278 K to 393 K.

2.3.3 Density Measurements

Density measurements were used to determine the apparent molar volume of the amphiphiles and also for cmc determinations. All density measurements were obtained using a Anton Paar DMA 602 vibrating tube density measuring cell with an Anton Paar DMA 60 density meter. The solution densities were measured relative to that of pure water. The calibration constant of the density meter was determined from the known densities of water[3] and air[4]. The reproducibility of an individual density measurement was better than 3×10^{-6} g cm^{-3}. The experimental conditions were set to measure the period of 10,000 oscillations of the tube with every fourth measurement recorded. Typically three recordings were collected to indicate the period of oscillation was constant.

Figure 2.3 Schematic diagram of the heating stage constructed to control and measure the temperature during polarising microscopy experiments.

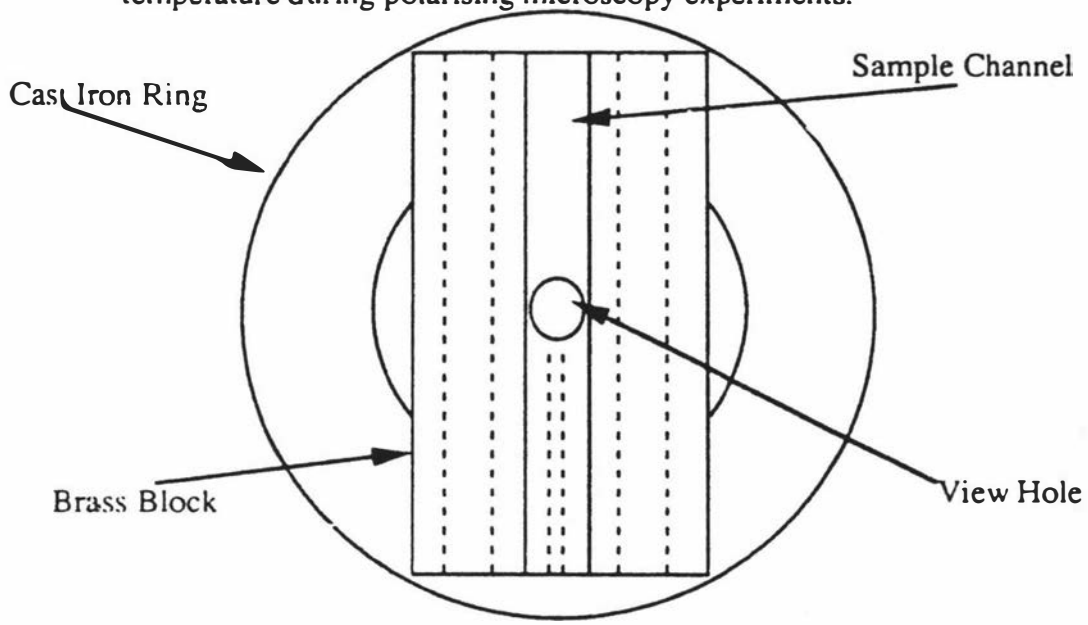

Top View

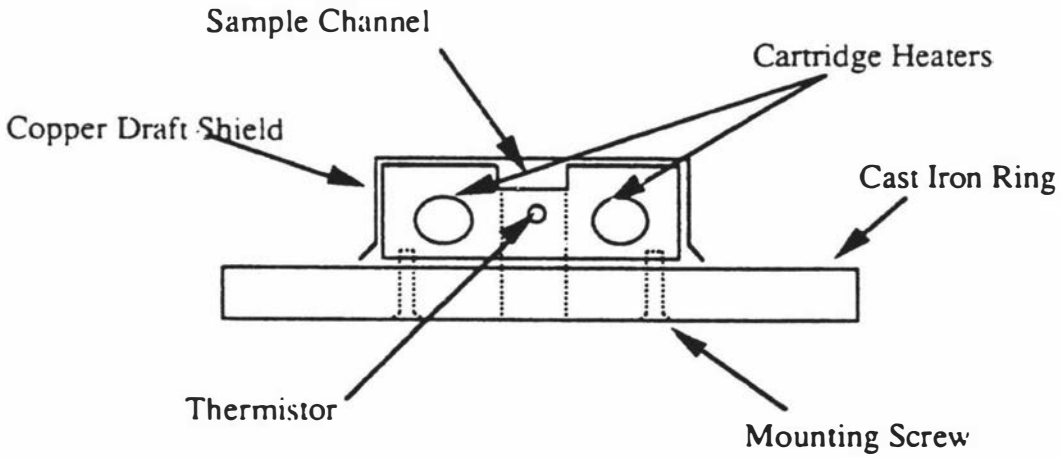

Side Veiw

Brass Sample Slide-holder

2.3.3.1 Density Temperature Control and Measurement

To maintain a constant temperature over the sample during the experiment the density cell is contained within a water jacket. The temperature of the water circulating around the density cell water jacket was controlled by a Tronac Inc. PTC-41 precision temperature controller, to an accuracy of ± 1 mK.

The temperature of the water was monitored by a Hewlett Packard 2804A Quartz thermometer in the waterbath, whilst the temperature in the density cell was determined from the resistance of a thermistor as measured by a Fluka 8050A digital multimeter The thermistor was first calibrated against the quartz thermometer. Since there was a fast flow of water from the waterbath to the cell there was no significant difference in temperature between the cell and the waterbath.

2.3.4 Qualitative Phase Detection

Since anisotropic mesophases of liquid crystals exhibit optical birefringence, this property was used to coarsely establish isotopic, anisotropic and biphasic regions. This was achieved by observing samples of various compositions as a function of temperature through crossed polaroid sheets.

2.3.4.1 Qualitative Phase Detection Temperature Control and Measurement

The samples were maintained at the required temperature in a heating block that was thermostatically controlled to within ±1 K. The temperature of the heating block was measured with a glass thermometer.

References

1. N. Boden, S. A. Corne, P. Halford-Maw, D. Fogarty, K. W. Jolley, *J. Mag. Resonance* **98**, 92-108 (1992).
2. K. Radley, A. Saupe, *Mol. Cryst. Liq. Cryst.* **44**, 227-236 (1978).
3. G. S. Kell, *J. Chem. Eng Data* **12**, 66-69 (1967).
4. R. C. Weast, *Handbook of Chemistry and Physics* (The Chemical Rubber Co., Ohio, 1971) 51st ed.

Chapter 3

NMR

Nuclear magnetic resonance of quadrupole nuclei is an excellent experimental technique for mapping phase boundaries and studying the nature and mechanism of phase transitions in lyotropic amphiphilic liquid crystals. This is because the quadrupole splitting is a characteristic signature of each kind of phase and is also a function of composition and temperature. It can, therefore, provide detailed information about the uniformity of composition and temperature in bulk samples. It is a particularly useful method when traversing phase coexistence regions in that the signal from each component is observable and the relative amounts of the phases can be monitored.

Primarily ^{2}H, ^{35}Cl and ^{133}Cs NMR have been used in this study. In the following sections the basic theory of the NMR of quadrupole nuclei will be developed and the dependence of the quadrupole splittings on the size and shape of the aggregate, and the fraction of bound counter-ion will be discussed. In ordered phases ^{133}Cs spectra reveal a large anisotropy in the chemical shift shielding tensor which provides a useful method for detecting some phase transitions. The relationship of the chemical shift anisotropy to the structure and order of the liquid crystal mesophase is described and illustrative spectra are presented. The methods used to determine the phase transition temperatures for each sample will also be described.

3.1 The Zeeman Interaction

For a spinning nucleus the magnitude of the spin angular momentum vector, $\boldsymbol{P}$, is defined by the nuclear spin quantum number, I, such that

$$P = \hbar\sqrt{I(I+1)} \qquad [3.1]$$

The direction of $\boldsymbol{P}$ is defined by the quantum number, m_I, which represents the component of the spin angular momentum along the reference z-direction.

$$P_z = \hbar m_I \qquad (m_I = I, I-1, I-2 \ldots -I) \quad [3.2]$$

A charged nucleus with spin angular momentum will generate a magnetic moment, μ, related to $\boldsymbol{P}$ by

$$\mu = \frac{g_N \mu_N \mathbf{P}}{\hbar} \qquad [3.3]$$

where g_N is the nuclear g factor and μ_N is the nuclear magneton $\left(= \frac{e\hbar}{2m_p} = 5.05095 \times 10^{-27}\ \mathrm{J\ T^{-1}}\right)$. This is commonly written in the form,

$$\mu = \gamma \mathbf{P} \qquad [3.4]$$

where γ is the magnetogyric ratio ($\gamma \equiv g_N \mu_N / \hbar$). The magnitude of μ is thus given by

$$\mu = \gamma\hbar\sqrt{I(I+1)} \qquad [3.5]$$

with components along the reference direction, μ_z of

$$\mu_z = \gamma\hbar m_I \qquad [3.6]$$

In the absence of a magnetic field the energy of an isolated nucleus is independent of direction and therefore independent of m_I. In the presence of a magnetic field, $\boldsymbol{B}$, a magnetic moment has energy,

$$E = -\mu.\boldsymbol{B} \qquad [3.7]$$

with components in the field direction (along the z-axis)

$$= -\mu_z B_0 \qquad [3.8]$$

$$= -\gamma\hbar m_I B_0 \qquad [3.9]$$

i.e. there are $2I+1$ energy levels each separated by $|\gamma\hbar B_0|$

Transitions can be made to occur between energy levels by using electromagnetic radiation of the appropriate frequency.

$$\Delta E = h\nu = \gamma\hbar B_0 \Delta m_I \qquad [3.10]$$

i.e.

$$\nu = \frac{\gamma}{2\pi} B_0 \qquad (\Delta m_I = \pm 1) \qquad [3.11]$$

So in the absence of any extra perturbing interactions all nuclei of a given species will have the same resonance frequency, ν, and a spectrum consisting of a single absorption line comprised of $2I$ superposed components. The effects of Heisenberg Uncertainty, relaxation, and inhomogeneities in the magnetic field (causing a distribution of resonance conditions through the bulk of the sample) cause the absorption line to have a finite width. There are a number of effects which can cause a change in the permitted energy levels which lead to shifts in the resonance frequencies. Two such effects, which are relevant to the present study, give rise to quadrupole splittings and ^{133}Cs chemical shifts.

3.2 Quadrupole Splitting

At the field used in this study and in the perfluorinated systems, the Zeeman interaction is much larger than the quadrupole interaction and the latter may be regarded as a small perturbation of the former. The origin of the quadrupole interaction is the non-spherically symmetric nuclear charge distribution for a nucleus with $I > 1/2$. This gives rise to a nuclear electrical quadrupole moment which interacts with an external electrical field gradient to create additional nuclear energy states. The energy levels of a nucleus with $I > 1/2$ in the presence of an electric field gradient are given by[1],

$$E_m = -\gamma\hbar B_0 m_I + \frac{3m_I^2 - I(I+1)}{4I(2I-1)} hq_{zz}. \qquad [3.12]$$

Figure 3.1 shows the effect of the quadrupole perturbation (2nd term in equation[3.12]) on the Zeeman levels energy level diagram for a ^{133}Cs nucleus.

The nematic phases of perfluorinated carboxylate salts in ^2H_2O are diamagnetically positive and the mesophase director, ***n***, undergoes spontaneous alignment along the direction of the field, ***B***, to give a uniaxial macroscopically aligned sample. Such a sample will give a first order spectrum for any spin $I>1/2$ consisting of $2I$ equally spaced lines with separation, referred to as the quadrupole splitting, $\Delta\tilde{\nu}$ given by[2-4]

$$\Delta\tilde{\nu}(\phi) = \frac{3}{2I(2I-1)}\tilde{q}_{zz}P_2(\cos\phi) \qquad [3.13]$$

The upper tilde denotes partially averaged quantities. The averaging arises as the result of reorientations that take place at a faster rate than the time-scale of the experiment (10^5 s^{-1}), including local reorientation of the bound species and diffusion over the micelle surface. $\tilde{q}_{zz}$ is the partially averaged component of the nuclear quadrupole-electric field gradient interaction tensor measured parallel to ***n*** in a perfectly ordered mesophase and is given by

$$\tilde{q}_{zz} = \sum_n p_n\chi_n\left[S^n_{cc} + \frac{1}{3}\eta_n\left(S^n_{aa} - S^n_{bb}\right)\right] \qquad [3.14]$$

where S_{ij} are elements of the Saupe ordering matrix at the n^{th} site that has a statistical weight p_n, $\chi_n = \left(\frac{e^2qQ}{h}\right)$ is the corresponding quadrupole coupling constant and η_n is the asymmetry parameter. The actual values for χ_n and η_n may vary from site to site and will thus be determined by the detailed structure of the micelle.

In micellar liquid crystal systems it is useful to be able to separate the contributions to the quadrupole splitting that arise from micellar and order parameter fluctuations. This is done[5, 6] by redefining $\tilde{q}_{zz}$ such that

$$\tilde{q}_{zz} = |\tilde{q}_{zz}|_s S \qquad [3.15]$$

where $|\tilde{q}_{zz}|_s$ now contains terms which depend only on the detailed structure of the aggregate and on the solution concentration (*i.e.* it is the value of $\tilde{q}_{zz}$ in a perfectly ordered crystal) and S is an order parameter which represents an average of the orientations of the micellar axes with respect to ***n***.

The contributions to S can be further reduced to

$$S = \overline{\langle P_2(\cos\beta)\rangle}\langle P_2(\cos\theta)\rangle \qquad [3.16]$$

$$= \overline{P}_{2,m}P_{2,n} \qquad [3.17]$$

where θ is the angle between the local director and the mesophase director ***n*** and β is the angle between the micelle and the local director , *i.e* $P_{2,n}$ describes local director fluctuations, and $\overline{P}_{2,m}$ describes the average orientation of the micelle with respect to a local director (figure 3.2).

Figure 3.1 Energy level diagram for a ^{133}Cs nucleus in the presence of an electric field gradient[7].

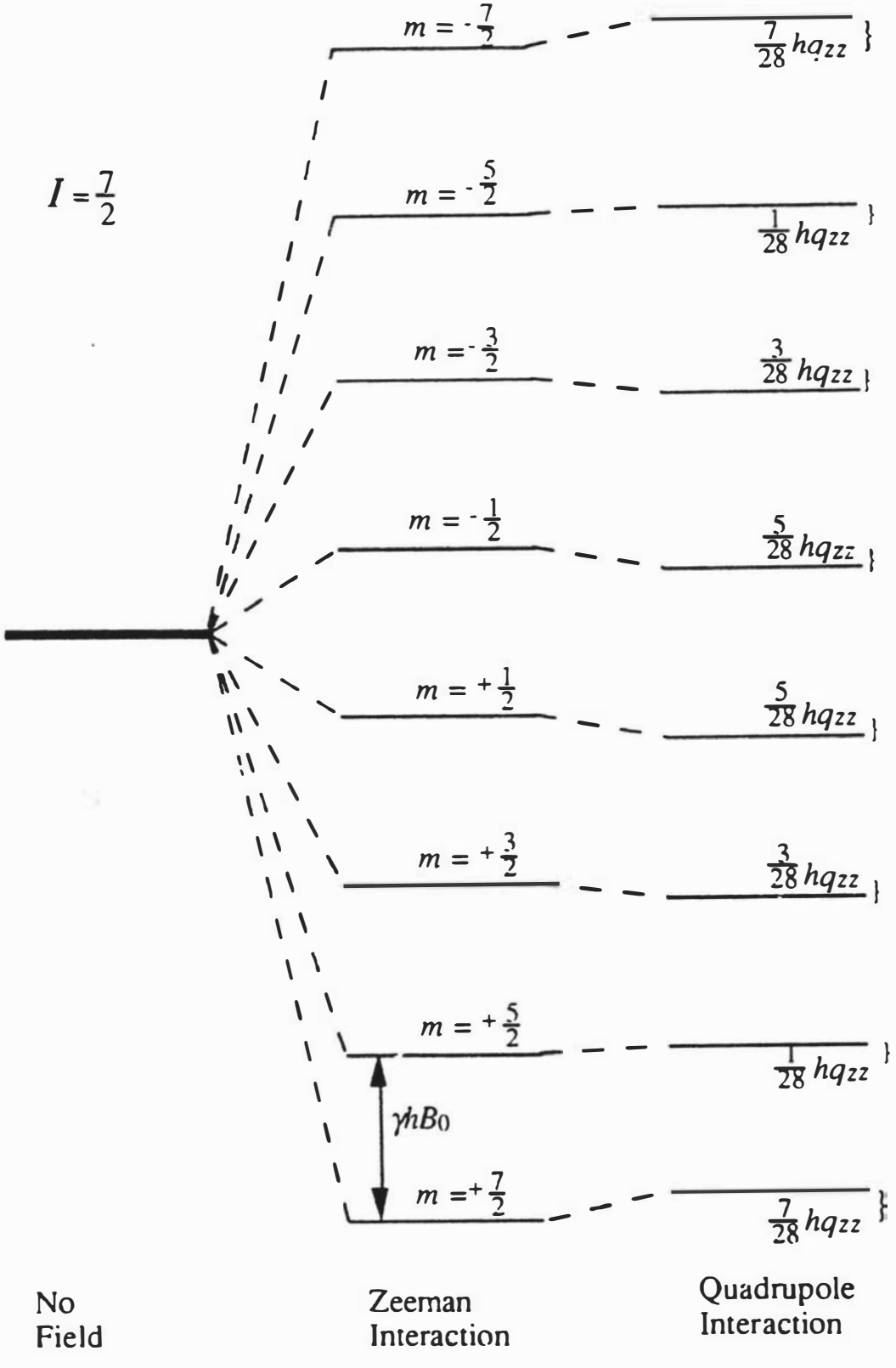

From equation [3.13] and [3.15 we can write[8]

$$\boxed{\Delta\tilde{\nu}(\phi) = \frac{3}{2I(2I-1)}|\tilde{q}_{zz}|_s SP_2(\cos\phi)} \qquad [3.18]$$

Figure 3.2 Representation of fluctuations contributing to the order parameter S.

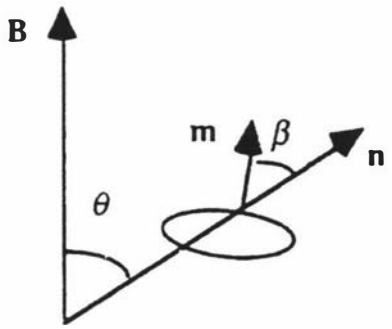

3.2.1 Deuterium Quadrupole Splitting

The observed ^2H quadrupole splitting of heavy water represents an average over a statistically representative set of sites. For a molecule of heavy water in the solvent there are two distinct sites; water molecules in the solvent bulk where the quadrupole interactions average to zero ($\tilde{q}_{zz}=0$) and water molecules associated with the micellar surface. Exchange between bound and unbound water molecules occurs rapidly with respect to the time scale of the NMR experiment to give a single sharp doublet the splitting of which corresponds to a weighted average of heavy water molecules in all possible sites ($\tilde{q}_{zz}\neq 0$). From equation[3.18], the quadrupole splitting for a ^2H nucleus ($I=1$) in heavy water becomes

$$\Delta\tilde{\nu}(\phi) = \frac{3}{2}|\tilde{q}_{zz}|_s SP_2(\cos\phi) \qquad [3.19]$$

with $|\tilde{q}_{zz}|_s$ being given by[5]

$$|\tilde{q}_{zz}|_s = \langle P_2(\cos\alpha)\rangle_s \chi_D\left(\frac{x_a}{x_w}\right) n_b S_{O-D} \qquad [3.20]$$

χ_D is the quadrupole coupling constant for ^2H in heavy water, x_a and x_w are the mole fractions of amphiphile and heavy water respectively, n_b is the number of bound water molecules per amphiphile and S_{O-D} is an order parameter representing the averaging due to the local orientational motion of the O-^2H bonds of these bound water molecules. $\langle P_2(\cos\alpha)\rangle_s \left\{= \frac{1}{2}\langle 3\cos^2\alpha - 1\rangle_s\right\}$, where α is the angle between the normal to the micelle surface and the micelle symmetry axis and the angular brackets denote an average over the micelle surface, accounts for the diffusive motion of the molecules over the surface of the micelle.

3.2.2 Caesium Quadrupole Splitting

For ^{133}Cs (I =7/2) the spectrum is made up of seven evenly spaced lines with relative intensities of 7:12:15:16:15:12:7 with a separation of[9]

$$\Delta\tilde{\nu}(\phi) = \frac{1}{14}|\tilde{q}_{zz}|_s SP_2(\cos\phi) \qquad [3.21]$$

where

$$|\tilde{q}_{zz}|_s = \langle P_2(\cos\alpha)\rangle_s \chi_{Cs}\beta_{Cs}. \qquad [3.22]$$

β_{Cs} is the fraction of caesium ions 'bound' to the surface of the micelle and χ_{Cs} is the quadrupole coupling constant of the ^{133}Cs nucleus. In the caesium spectra only one set of lines is observed for any given phase indicating that the exchange between bound and unbound caesium ions is fast on the time-scale of the experiment. The origin of the field gradient at the nucleus is probably a distortion of the ion hydration shell from spherical symmetry in those ions 'bound" to the surface of the micelle[4,9,10].

3.2.3 Chlorine Quadrupole Splitting

The spectrum for ^{35}Cl (I=3/2) will consist of three equally spaced lines of relative intensities 3:4:3, and with peak separation given by

$$\Delta\tilde{\nu}(\phi) = \frac{1}{2}|\tilde{q}_{zz}|_s SP_2(\cos\phi) \qquad [3.23]$$

where

$$|\tilde{q}_{zz}|_s = \langle P_2(\cos\alpha)\rangle_s \chi_{Cl}\beta_{Cl} \qquad [3.24]$$

β_{Cl} is the fraction of chloride ions 'bound' to the surface of the micelle and χ_{Cl} is the quadrupole coupling constant of the ^{35}Cl nucleus. As in the case of caesium spectra the observation of only one set of lines in any given phase indicates the exchange between bound and unbound chloride ions is fast on the time-scale of the NMR experiment. In addition the electric field gradient at the nucleus is also probably a result of a perturbation of the spherically symmetric hydration shell as a consequence of the "bound" ions being in the vicinity of the charged surface.

3.3 ^{133}Cs Chemical Shift Anisotropies

In the presence of an external magnetic field B_0, local magnetic fields are generated at the nucleus as a result of circulations of the surrounding electrons induced by the applied field. The resonance condition of equation[3.11] can be written

$$\nu = \frac{\gamma}{2\pi} B_0(1-\sigma) \qquad [3.25]$$

where σ is the chemical shift shielding tensor. The σ tensor elements reflect the symmetry of the electronic environment of the nucleus.

The chemical shift of a nucleus in an anisotropic liquid crystalline phase is composed of an isotropic and an anisotropic part. In an isotropic liquid only the isotropic part is visible. The origin of chemical shifts of $^{133}Cs^+$ ions in solution is overlap between the outer orbitals of the ion and those of the solvent[4]. The $^{133}Cs^+$ ion is easily polarizable[11], giving comparatively large changes in the chemical shift, so that in a non-macroscopically aligned liquid crystalline sample the chemical shift anisotropy can readily be observed[4, 11]. For the case of a macroscopically aligned discotic micellar mesophase, the partially averaged chemical shift is given by[9]

$$\tilde{\sigma}_{zz}(\phi) = \sigma_i + \frac{2}{3}\sum_n p_n\left[S^n_{cc}\left\{\sigma^n_{cc} - \frac{1}{2}\left(\sigma^n_{aa} + \sigma^n_{bb}\right)\right\} + \frac{1}{3}\left(S^n_{aa} - S^n_{bb}\right)\left(\sigma^n_{aa} - \sigma^n_{bb}\right)\right]P_2(\cos\phi) \qquad [3.26]$$

where σ_i is the chemical shift in the isotropic phase and σ_{ii} represent the principle axes (a,b,c) of the chemical shift shielding tensor. Averaging of the chemical shift arising from the diffusive motion of the caesium ion over the surface sites must also be allowed for. As in the case of the quadrupole splittings, for a uniform distribution of the ions over the micelle surface, this averaging is given by $\langle P_2(\cos\alpha)\rangle_s = \langle 3/2\cos^2\alpha - 1/2\rangle_s$. After averaging due to the microscopic motion of the Cs^+ ions is taken into consideration, equation[3.26] reduces to[9]

$$\tilde{\sigma}_{zz}(\phi) = \sigma_i + \frac{2}{3}\langle P_2(\cos\alpha)\rangle_s \beta_{Cs}\left(\sigma_{//} - \sigma_\perp\right)_M S P_2(\cos\phi) \qquad [3.27]$$

where $(\sigma_{//})_M$ and $(\sigma_\perp)_M$ are, respectively, the components of the axially symmetric ^{133}Cs chemical shielding tensor parallel and perpendicular to the micelle surface, and $\sigma_i = 1/3\left\{\mathrm{Tr}\sigma^b\right\}\beta + (1-\beta)\sigma^f$, with the superscripts denoting "bound" and "free" counter-ions.

In an isotropic phase ($S = 0$) the observed shift is given by σ_i. In a macroscopically aligned phase (ϕ=0°;$S\neq 0$), the second term in equation[3.27] is non zero. This will give rise to a discontinuity in the ^{133}Cs shift at an isotopic-to-nematic transition of magnitude[9]

$$\tilde{\sigma}_{zz}(0^\circ) - \sigma_i = \frac{2}{3}\Delta\tilde{\sigma} = \frac{2}{3}\langle P_2(\cos\alpha)\rangle_s \beta_{Cs}\left(\sigma_{//} - \sigma_\perp\right)_M S \qquad [3.28]$$

where

$$\Delta\tilde{\sigma} = \tilde{\sigma}_{zz}(0^\circ) - \tilde{\sigma}_{zz}(90^\circ) \qquad [3.29]$$

This discontinuity in the chemical shift enables the isotropic-to-nematic and isotropic-to-lamellar phase transitions to be determined from ^{133}Cs chemical shift measurements. For a first order nematic-to-lamellar transition the discontinuity in $\bar{\sigma}_{zz}(0°)$ in a macroscopically aligned sample arises from discontinuities in $\langle P_2 \cos\alpha \rangle_s$ and S across the transition[9]. It has been shown that the ^{133}Cs quadrupole splittings and chemical shift anisotropies scale with changes in $\langle P_2 \cos\alpha \rangle_s$, S, and β_{Cs+}[9], and both may be used to detect phase transitions. The best method to use depends on the particular phase transition to be determined. The ways in which measurements of quadrupole splittings and shift anisotropies can be used to precisely locate phase transitions are discussed in the following sections.

3.4 Appearance of NMR Spectra

Illustrations of spectra in the isotropic phase I, nematic phase N_D^+, and polycrystalline lamellar phase L_D for ^2H, ^{133}Cs and ^{35}Cl nuclei are given in figures 3.3, 3.4, and 3.5 respectively. In the isotropic micellar solution phase the order parameter S is zero. Thus only the Zeeman interaction is observed and the spectra of all three nuclei consist of a single peak (figures 3.3a, 3.4a, and 3.5a).

For macroscopically ordered nematic and lamellar mesophases $0 < S < 1$ and the quadrupole splitting for ^2H, ^{133}Cs, and ^{35}Cl spectra are given by equations[3.19], [3.21], and [3.23] respectively. Thus the ^2H spectrum of heavy water consists of a symmetrical doublet (figure 3.3b), the ^{133}Cs spectrum consists of seven equally spaced lines (figure 3.4b), and the ^{35}Cl spectrum is composed of three equally spaced lines (figure 3.5b) with the expected intensity distributions. The ordered spectrum shown is for the nematic phase in each case. The appearance of the spectrum of a macroscopically aligned lamellar phase is identical to that of the corresponding nematic phase spectra but the magnitude of the quadrupole splittings is greater in the L_D phase.

Macroscopically ordered lamellar phases are easily prepared by cooling in the spectrometer magnetic field from the isotropic micellar solution phase, through the nematic phase, where the nematic director aligns along the magnetic field, into the lamellar phase where the lamellar director becomes locked into the mesophase. If the cooling takes place outside of a magnetic field an unorientated sample is obtained in

Figure 3.3 ^{2}H NMR spectra [12] for a CsPFO/CsCl/$^{2}H_2O$ sample with a mass ratio of CsPFO to $^{2}H_2O$ of 1:1 and mass fraction of CsCl w_e of 0.0434. The phases represented are; (a) Isotropic micellar solution phase, (b) Nematic phase, (c) Lamellar phase with an isotropic distribution of local directors.

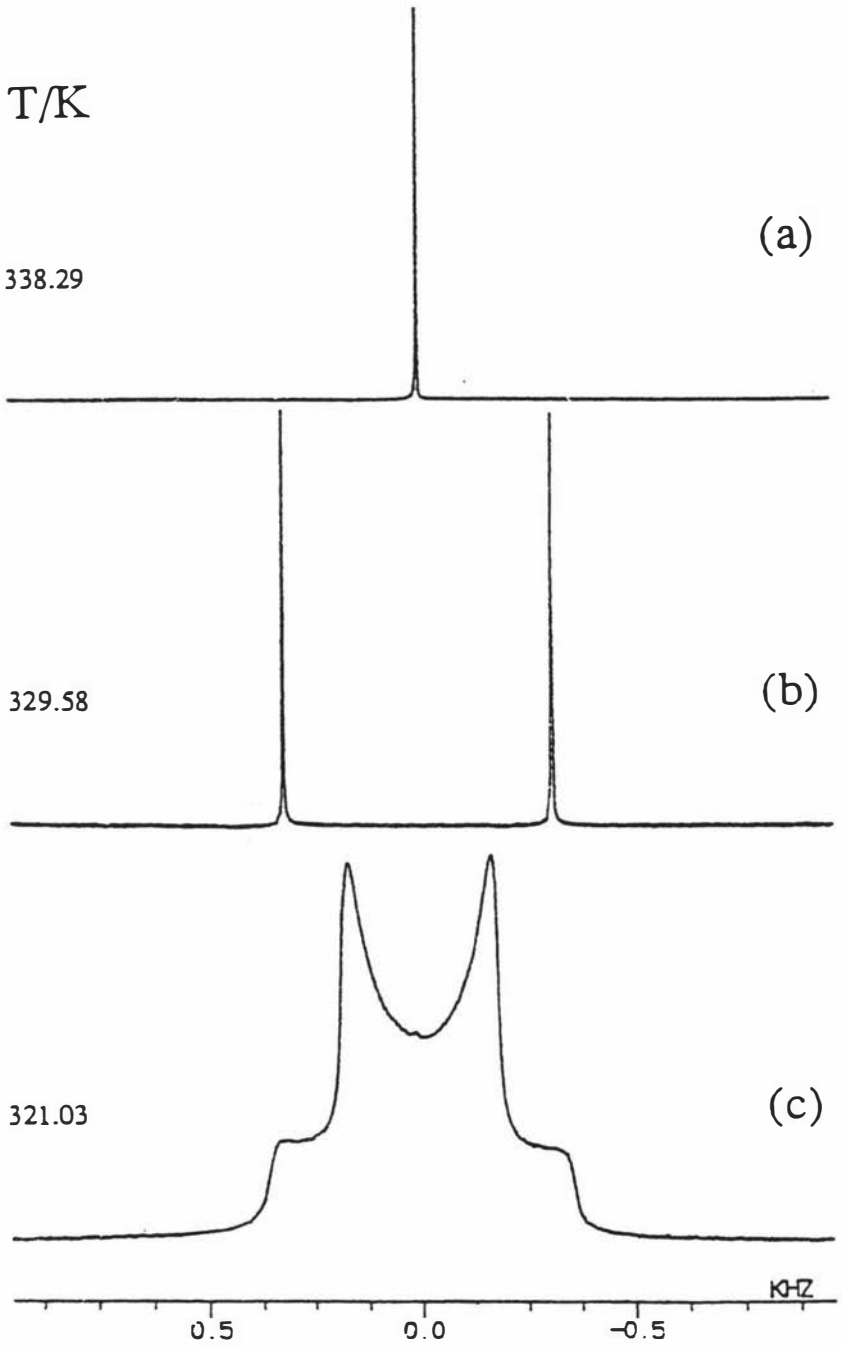

Figure 3.4 ^{133}Cs NMR spectra[12] for a CsPFO/CsCl/$^{2}H_2O$ sample with a mass ratio of CsPFO to $^{2}H_2O$ of 1:1 and mass fraction of CsCl w_c of 0.0434. The phases represented are; (a) Isotropic micellar solution phase, (b) Nematic phase, (c) Lamellar phase wit an isotropic distribution of local directors.

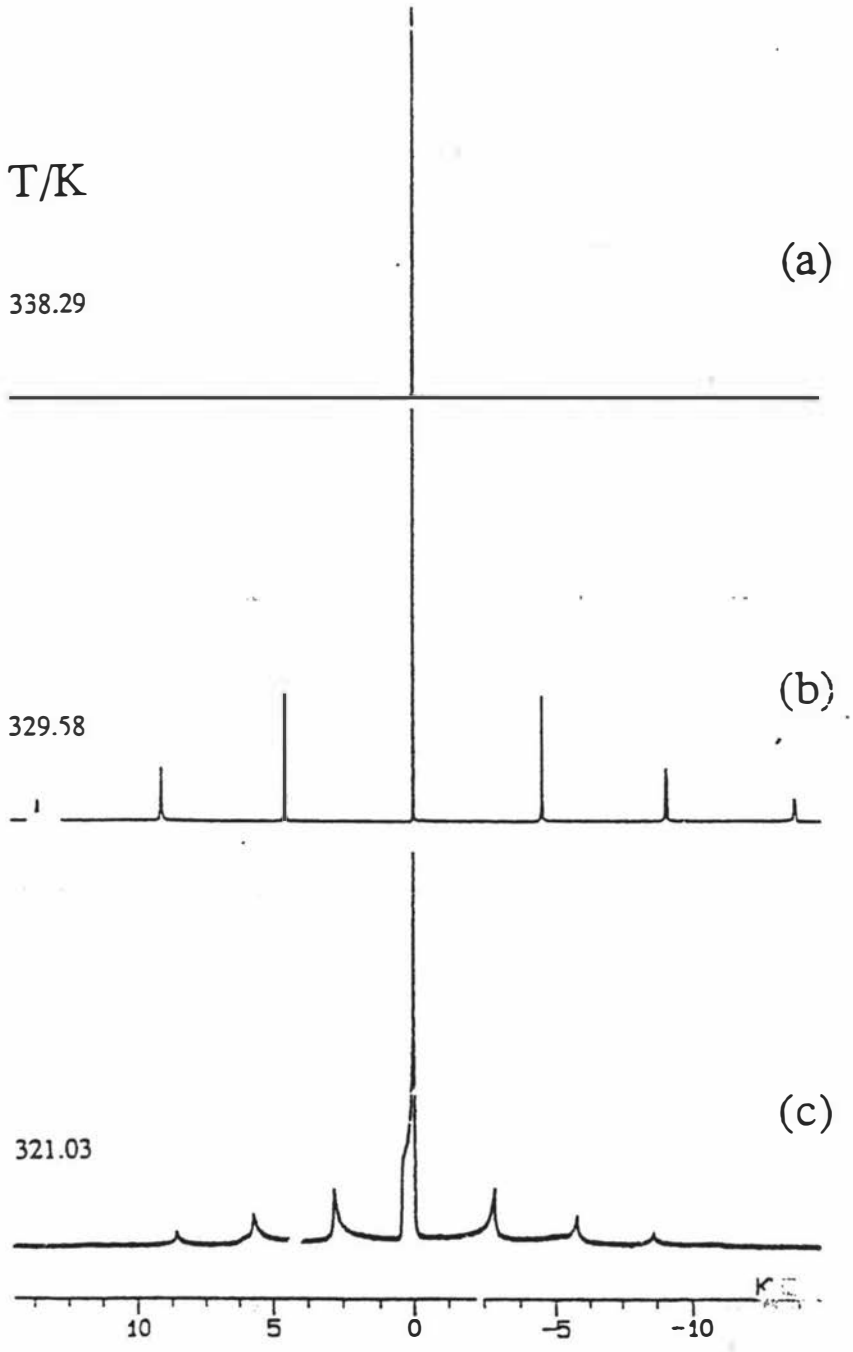

Figure 3.5 ^{35}Cl NMR spectra[12] for a CsPFO/CsCl/$^{2}H_2O$ sample with a mass ratio of CsPFO to $^{2}H_2O$ of 1:1 and mass fraction of CsCl w_e of 0.0434. The phases represented are; (a) Isotropic micellar solution phase, (b) Nematic phase, (c) Lamellar phase with an isotropic distribution of local directors.

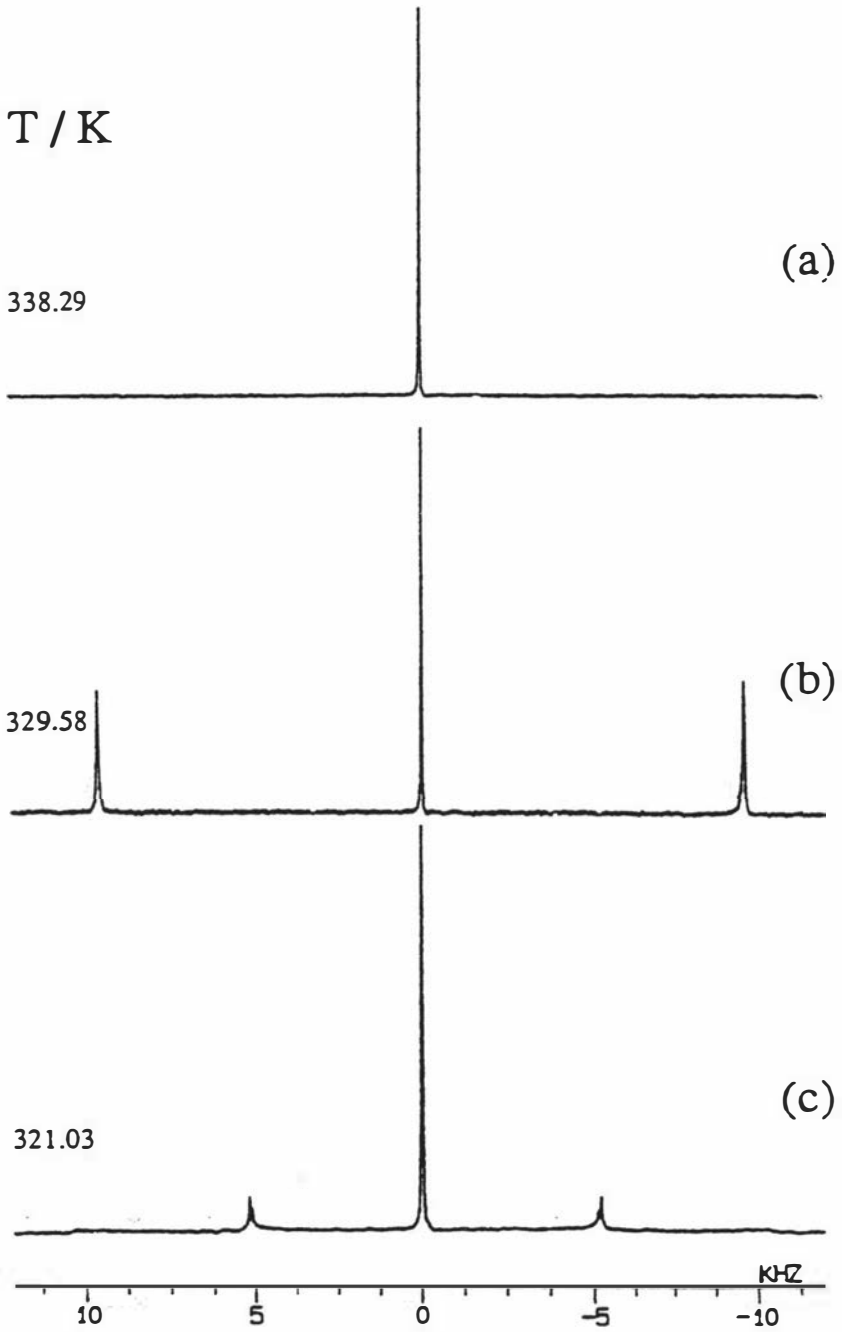

which there is a random orientation of local lamellar directors. Since the lamellar phase will not reorientate in a magnetic field (*i.e.* it has an infinite valued rotational viscosity coefficient[5]), the observed spectra reflect an isotropic distribution of director orientation. For the ^2H nucleus (figure 3.3c) the unorientated spectrum consists of a "Pake" doublet, where singularities are evident at $\phi = 90^o$ (central doublet) and $\phi = 0^o$ (outer doublet). Thus the quadrupole splittings as defined in equation[3.19] ($\phi = 0$) can easily be extracted from this spectrum. The ^{133}Cs unorientated spectrum (figure 3.4c) has a singularity at ϕ=90° and so the splitting between adjacent lines is half that of the quadrupole splittings as defined in equation [3.21].*i.e.* $\Delta\tilde{\nu}(\phi = 90^o) = 1/28|\tilde{q}_{zz}|_s^l S$ The 90° orientation are also clearly seen in the ^{35}Cl unorientated spectrum (figure 3.5c). Although quadrupole splittings can be readily extracted from both ordered and unorientated spectra, it is usually better to work with ordered samples since the lines are much sharper and the signal to noise ratio much greater.

From the spectra of all three nuclei it is thus possible to distinguish between isotropic and ordered phases. Furthermore, in biphasic regions separate signals for the coexisting phases can be observed which enables the precise determination of the upper and lower boundaries to these transitions.

3.5 Determination of Liquid Crystal Phase Boundaries

In determining the phase transition temperatures it is important to approach the transition from a pure phase region. Thus, for example, the upper boundary of the isotropic-to-nematic transition is obtained by cooling from the isotropic phase whereas the lower boundary to the transition is approached from the nematic phase. The importance of the procedure cannot be over emphasised if precise values of the phase transition temperatures are to be obtained. The greater the time period spent in phase coexistance regions, and the larger the density difference between the two phases, the greater the opportunity for phase separation and a consequent concentration gradient within a sample to occur. Spending as little time as practicable in the mixed-phase regions minimizes the phase separation problem.

3.5.1 Isotropic-to-Nematic Phase Transition

Figure 3.6 shows the sequence of ^2H spectra observed as the temperature is lowered from the isotropic micellar solution phase into the nematic phase[7]. At high temperatures the spectrum is a single line with a half width of ≈ 1.2 Hz determined by spin relaxation processes. As the temperature is lowered the line broadens and then splits

Figure 3.6 Sequence of ^2H NMR spectra[7] observed on cooling a CsPFO/^2H_2O (w_a = 0.302) sample from the isotropic phase (a) to (c) into the isotropic/nematic biphasic region (d) and (e).

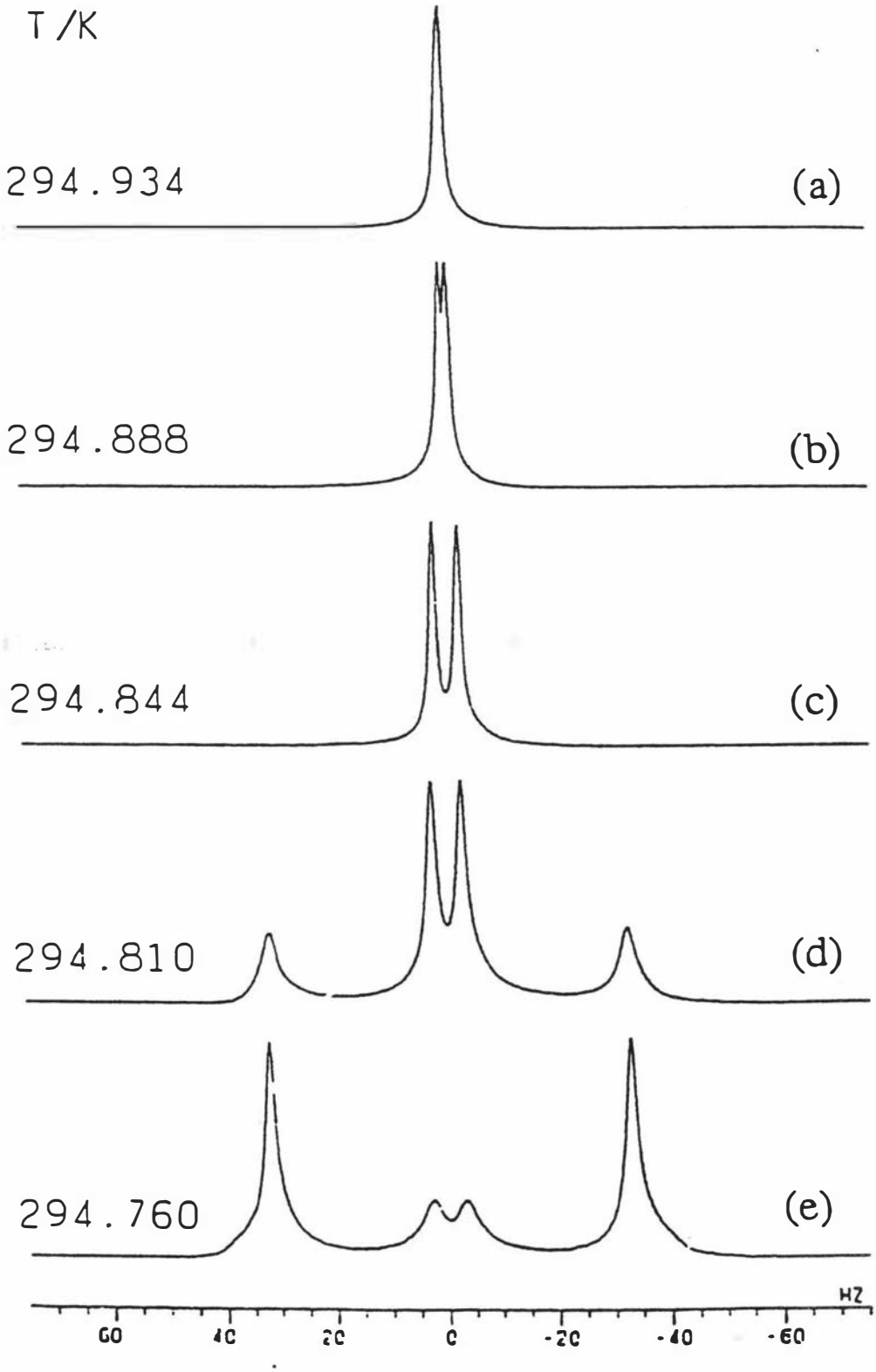

into a doublet whose separation increases rapidly in magnitude until the temperature of the upper boundary to the isotropic-to-nematic transition T_{IN} is reached. This temperature is signified by the appearance of the outer doublet which comes from the nematic phase. T_{IN} can be accurately determined from a plot of the inverse of the quadrupole splittings versus the temperature. The splitting of the isotropic phase signal into a doublet arises from the orientational ordering of the micelles induced by the magnetic field. Using this method the upper boundary to the isotropic-to-nematic transition can be determined with high precision (± 5 mK)[13].

The magnitude of the isotropic splitting depends on the sample concentration and the magnitude of **B**. For practical purposes at **B** = 6.34 T it is not possible to use the field induced order technique for samples with $w_a > 0.40$[13]. For samples with these concentrations it is better to obtain T_{IN} by looking for the first appearance of the nematic ^{133}Cs Zeeman peak which is preceded by the pretransitional broadening of the isotropic peak as is shown in figure 3.7. Alternatively the first appearance of the quadrupole multiplet in both the ^{2}H and ^{133}Cs spectra can be used for this purpose. These tend to be broad, however, and more difficult to detect than the ^{133}Cs Zeeman peak when the proportion of nematic phase is small. Of course, the appearance of the N_D^+ phase peak indicates that the sample is already in the mixed phase region. The maximum error in T_{IN} as a result of this depends on the sensitivity of detection of the nematic phase peak and the temperature range of the mixed-phase region. Typically T_{IN} could be located to a temperature precision of ±0.01 K using this method.

The best method to determine T_{NI}, temperature of the lower boundary to the isotropic-to-nematic transition, makes use of the discontinuity in the temperature dependence of the magnitude of either the ^{2}H or ^{133}Cs quadrupole splittings at this phase boundary (figure 3.8). To determine T_{NI} the sample is rapidly cooled into the nematic phase and left until the sample has time to become well ordered as indicated by the sharpness of the nematic peaks. The temperature dependence of the quadrupole splittings is thendetermined on heating of the sample, making careful measurements close to the discontinuity. The sharp discontinuity in the quadrupole splittings at T_{NI} is a precise indication of this temperature to ≈ 0.01 K. The rapid fall in the quadrupole splittings on approaching T_{NI} is due to the rapid change in S (equation[3.18])close to T_{NI}[6]. While in the mixed-phase region the nematic splitting changes little with temperature as a consequence of the value of S being essentially constant at the nematic-to-isotropic phase transition[5].

Figure 3.7 Sequence of ^{133}Cs NMR spectra[12] for the -1/2 to +1/2 transition as observed on cooling a CsPFO/$^{2}H_2O$ (w_a = 0.500) sample from the isotropic phase into the isotropic/nematic biphasic region. (a) Isotropic micellar solution phase, (b) Isotropic micellar solution phase with broadening of the line as a result of magnetic field induced pretransitional orientational ordering of the micelles. (c) and (d) isotropic/nematic biphasic region. The structure in the isotropic phase signal is due to the orientational ordering of the micelles.

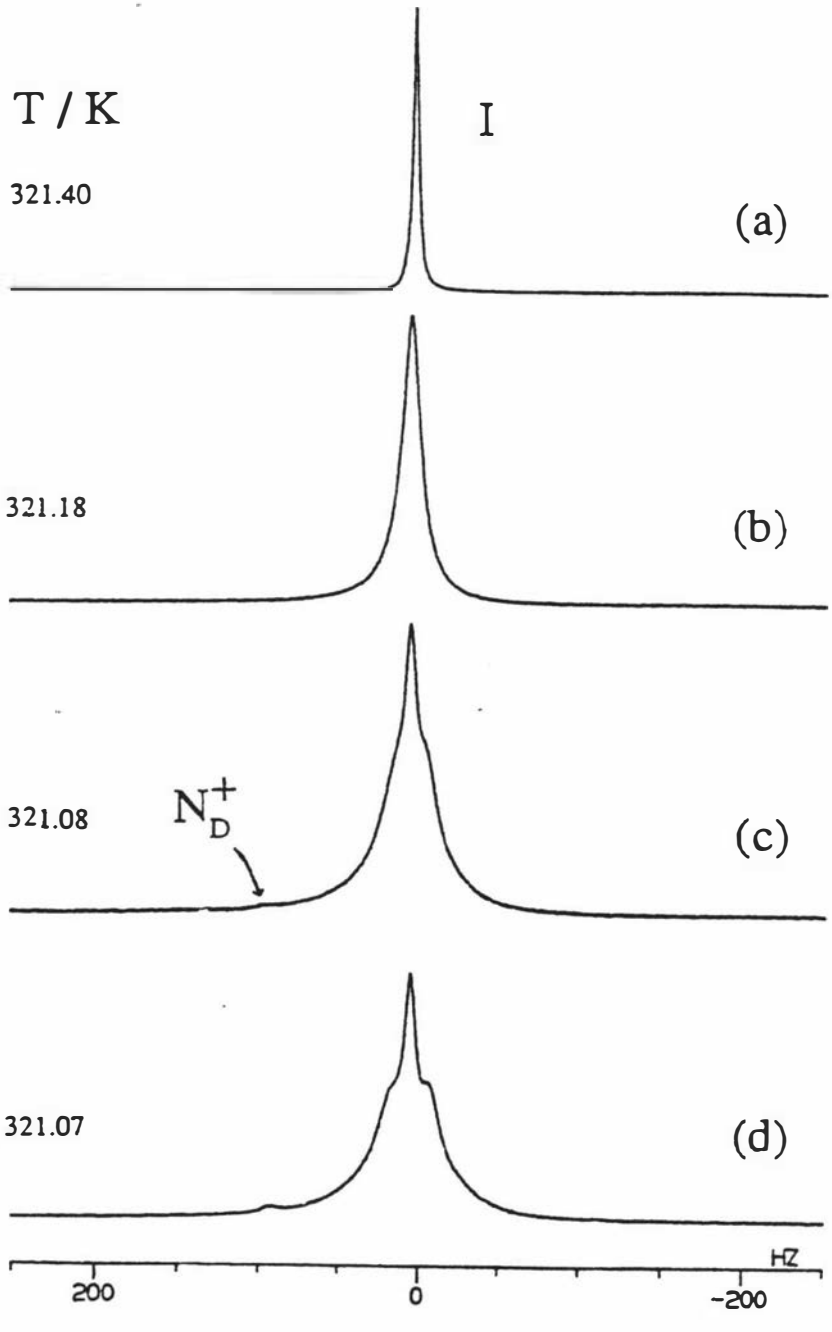

Figure 3.8 The temperature dependence of the partially averaged ^{133}Cs quadrupole splitting for a CsPFO/^2H_2O ($w_a = 0.500$). T_{NI} is clearly identified from the discontinuity in $\Delta\tilde{\nu}(^{133}Cs)$.

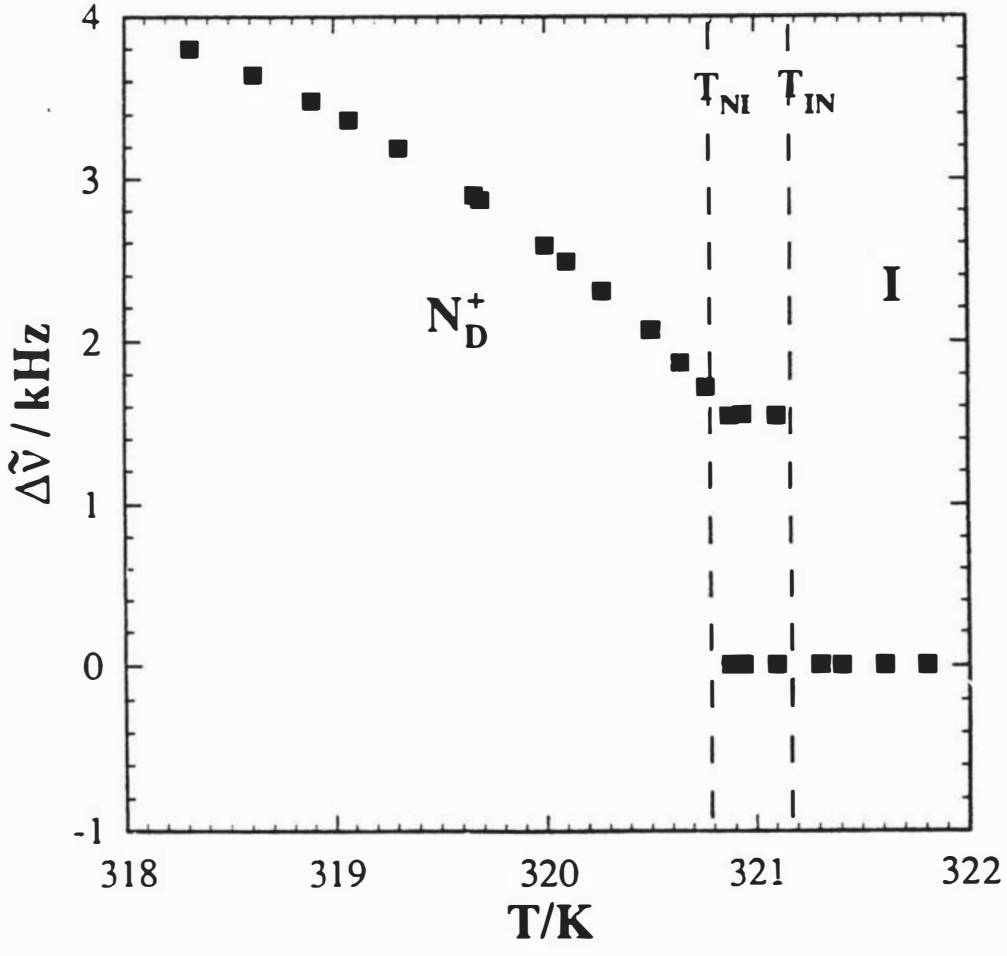

3.5.2 Lamellar-to-Nematic phase transition boundary

The spectra obtained when a sample from the CsPFO/^2H_2O system with an amphiphile mass fraction of w_a = 0.50 is slowly cooled from the nematic phase across the nematic/lamellar biphasic region into the lamellar phase are shown in figure 3.9. Separate lamellar, and nematic signals are resolved, in the phase coexistence region, since the peak separation of nematic and lamellar signals is of the order of 40 Hz (*cf* quadrupole splittings of 5000 Hz). The outer peaks represent the lamellar phase spectrum while the inner peaks represent the nematic phase spectrum. It is interesting to compare the ^{133}Cs spectra with the ^2H spectra at the same temperatures for this sample as shown in figure 3.10. This clearly indicates the greater resolving power of ^{133}Cs in the detection of the L_D and N_D^+ phases, the only indication from the ^2H spectra of ^2H_2O that a biphasic region exists is a slight broadening of the ^2H peaks in the mixed phase region. The appearance of the lamellar peaks on cooling, or nematic peaks on heating to determine T_{NL} or T_{LN}, is an imprecise method for reasons already discussed. A much better determination is achieved by observing the temperature dependence of the quadrupole splittings (figure 3.11a). A discontinuity in quadrupole splittings is observed at T_{NL} the temperature of the upper boundary to the nematic-to-lamellar transition, and T_{LN} the, temperature of the lower boundary to the nematic-to-lamellar transition, which clearly identifies these transition temperatures.

When the intervening biphasic region is so narrow that separate signals from each of the phases are unable to be resolved using NMR the phase transition is determined from the point of inflection of the temperature dependence of the quadrupole splittings. For such a case a plot of the quadrupole splitting versus temperature, figure 3.11b, shows a change in the temperature dependence of the quadrupole splitting at T_{LN}. The maximum slope indicates the T_{LN} transition the downward turn in the quadrupole splitting on the lamellar side of the transition and upward turn on the nematic side (figure 3.11a) are indications of strong pretransitional effects. ^{133}Cs is a better nucleus than ^2H for detecting the narrow mixed phase region. This is because the magnitude of the ^{133}Cs quadrupole splittings and therefore the magnitudes of $\Delta\tilde{\nu}(L) - \Delta\tilde{\nu}(N)$ is greater for this nucleus[14].

Figure 3.9 Sequence of ^{133}Cs NMR spectra[14] observed on cooling a CsPFO/^2H_2O (w_a = 0.500) sample from the nematic phase N_D^+ into the lamellar phase L_D. The two distinct multiplets in (b) indicate the presence of a nematic/lamellar biphasic region.

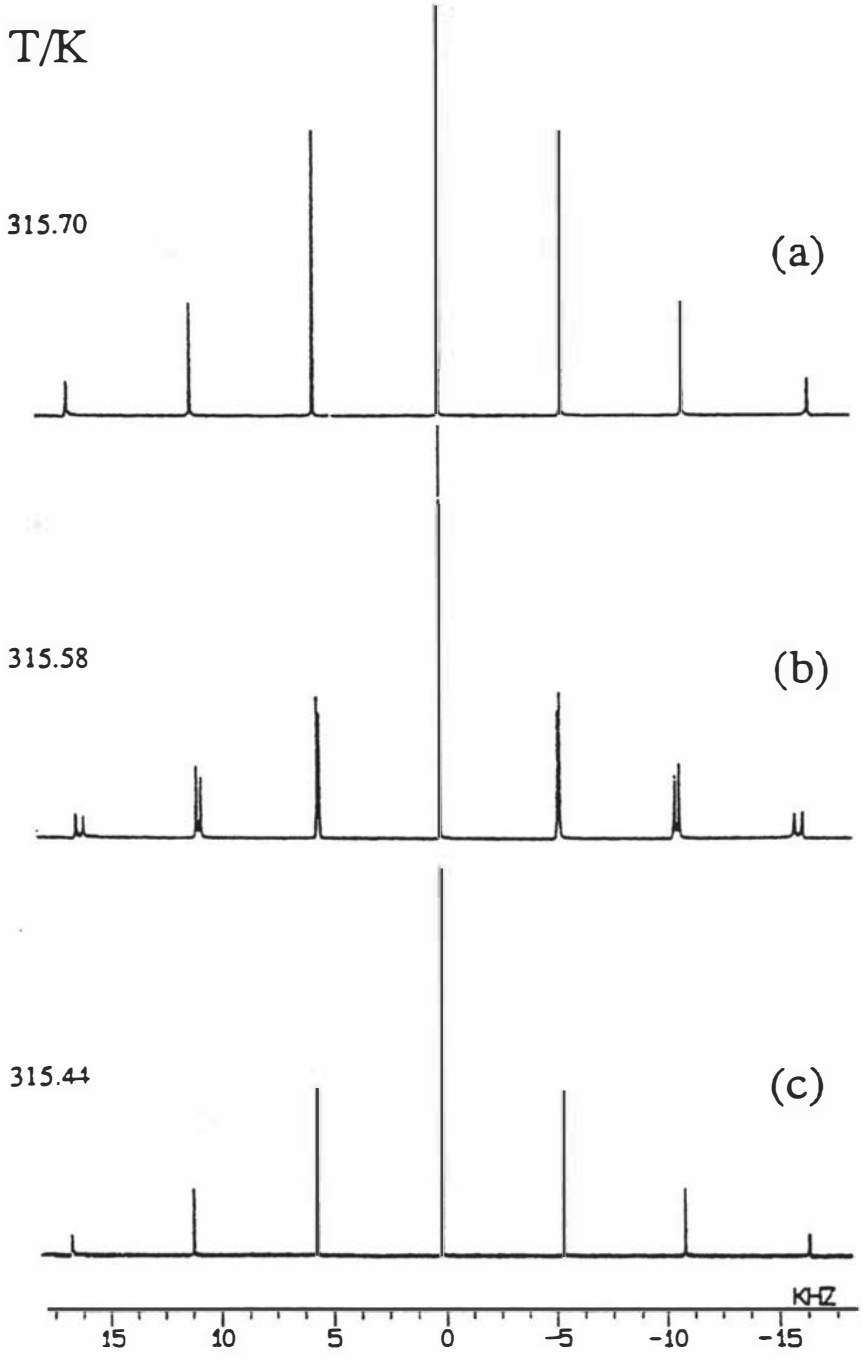

Figure 3.10 Sequence of ^2H NMR spectra [14] observed on cooling a CsPFO/^2H_2O (w_a = 0.500) sample from the nematic phase N_D^+ into the lamellar phase L_D. The ^{133}Cs NMR spectra for the same sample shows two distinct multiplets within the N_D^+/L_D biphasic region (figure 3.9) but the ^2H NMR spectra shows only a slight broadening of the doublet lines as an indication of a N_D^+/L_D biphasic region. This comparison illustrates the greater resolving power of ^{133}Cs NMR compared to ^2H NMR.

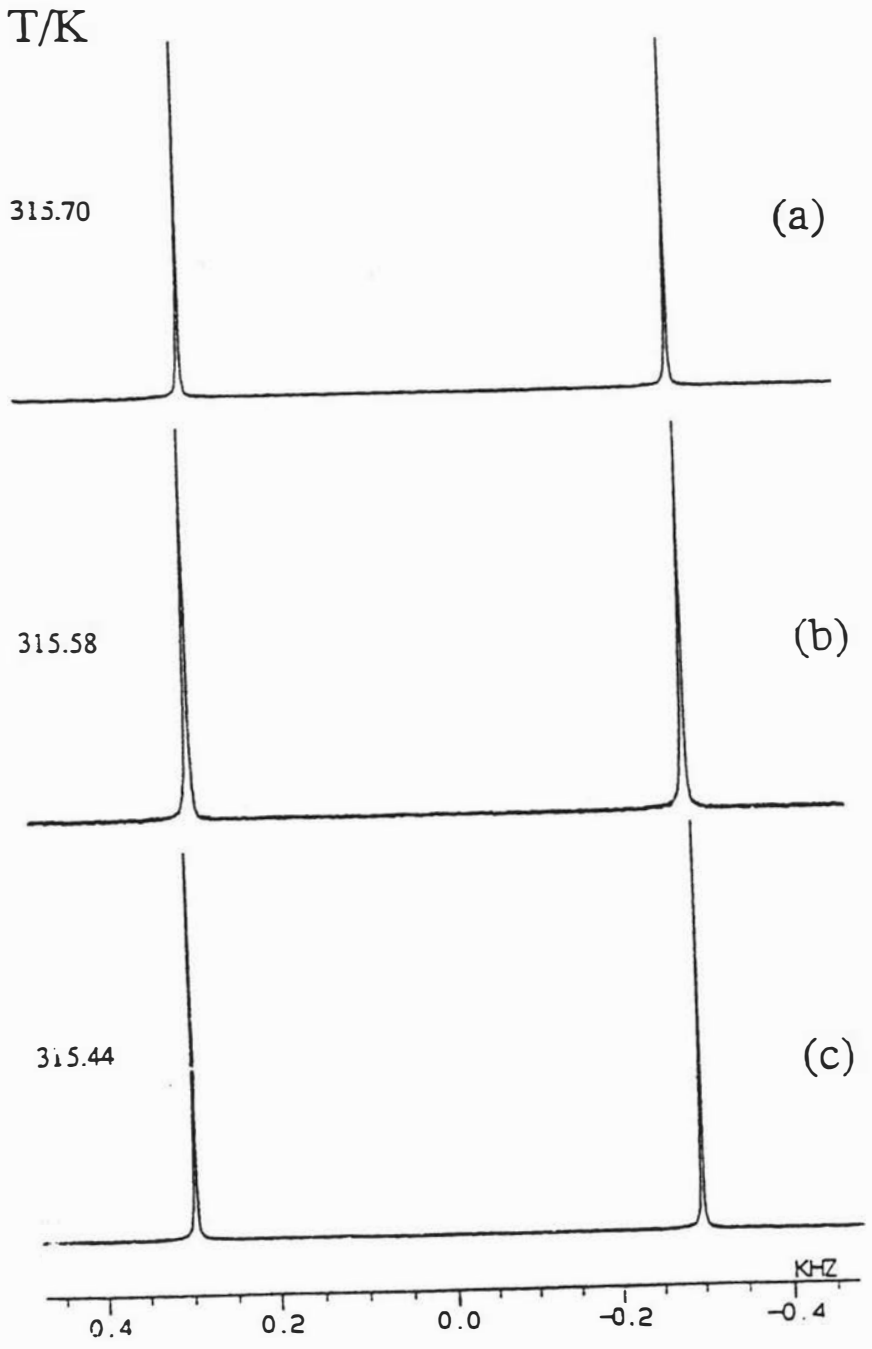

Figure 3.11 The temperature dependence of the partially averaged ^{133}Cs quadrupole splittings $\Delta\tilde{\nu}(^{133}Cs)$ for the samples: (a) CsPFO/^2H_2O (w_a = 0.500) sample ; illustrating the discontinuity in the quadrupole splitting at T_{NL} and T_{LN} , and (b) CsPFO/CsCl/^2H_2O sample with a mass ratio of CsPFO to ^2H_2O of 1:1 and a mass fraction of added CsCl w_c of 0.0126. In (a) T_{LN} and T_{NL} are indicated by discontinuities in the quadrupole splittings. In (b) only T_{LN} is detectable from the discontinuity in the temperature dependence of $\Delta\tilde{\nu}(^{133}Cs)$.

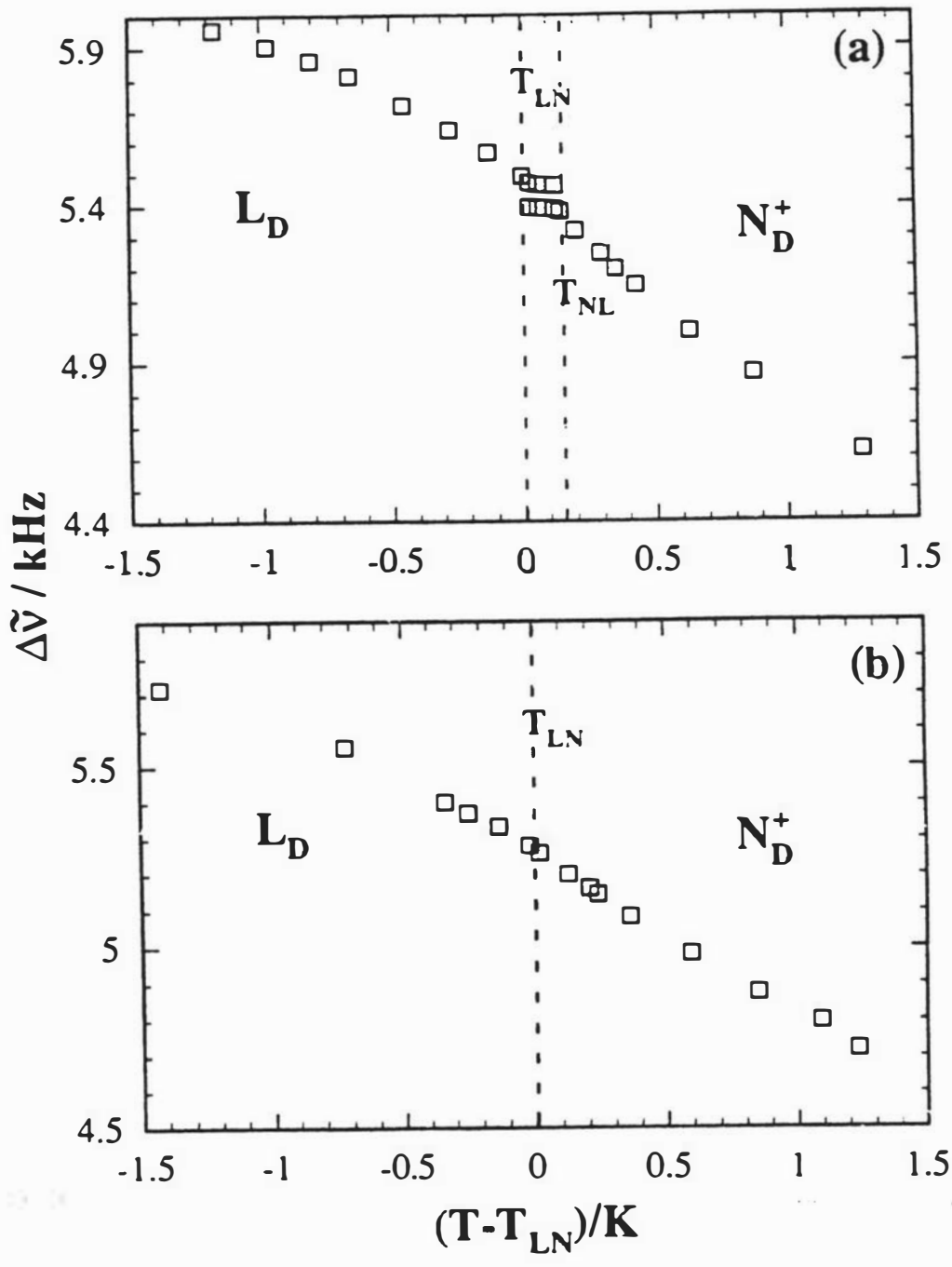

3.5.3 Lamellar-to-Isotropic phase transition boundary

Phase separation is particularly rapid in the isotropic-to-lamellar phase coexistence regions due to the larger density differences between the phases. It is, therefore, particularly important to approach the upper T_{IL} and lower T_{LI} temperature boundaries of the mixed phase region from the pure phase regions. The method of identification of T_{IL} is identical to that used for T_{IN} when the pretransitional quadrupole splitting is too small to monitor. To determine T_{LI} the sample is first cooled rapidly from the homogeneous isotropic phase into the lamellar phase by immersion of the NMR tube in a beaker of water at an appropriate temperature. This is necessary since the temperature width of the I/L_D mixed-phase region is large enough that during the time it takes to cool across this region using the sample temperature control system, macroscopic phase separation can occur[9]. Since this is done outside the magnetic field an unorientated sample is produced but importantly it is homogeneous.

The quadrupole splittings are easily obtained from a polycrystalline sample (the quadrupole splitting is twice the separation of the peaks in a polycrystalline sample[4]) and so a plot of the quadrupole splitting versus temperature is readily constructed. On heating from the lamellar into the mixed phase there is a discontinuity in the quadrupole splitting (figure 3.12), similar to that observed in the detection of T_{NI} . It does not matter that phase separation occurs in the biphasic region as T_{LI} is identified by the discontinuity.

Figure 3.12 is a plot of the temperature dependence of the ^{133}Cs quadrupole splittings but a plot of the temperature dependence of the ^{2}H splittings is equally as good for the purpose of determining T_{LI}. At temperatures close to T_{LI} ($\approx (T_{LI} - 0.5\ K)$) the sample begins to orientate in the magnetic field. This is also the case all along the lamellar-to-nematic transition line. If an orientated sample is required it is simply necessary to wait for a period which is dependent upon the proximity of the sample temperature to T_{LI}[15] .

Figure 3.12 The temperature dependence of the partially averaged ^{133}Cs quadrupole splittings $\Delta\tilde{\nu}(^{133}Cs)$ for a CsPFO/CsCl/^2H_2O sample with a mass ratio of CsPFO to ^2H_2O of 1:1 and a mass fraction of added CsCl w_e of 0.102. The discontinuity in $\Delta\tilde{\nu}(^{133}Cs)$ identifies T_{LI}.

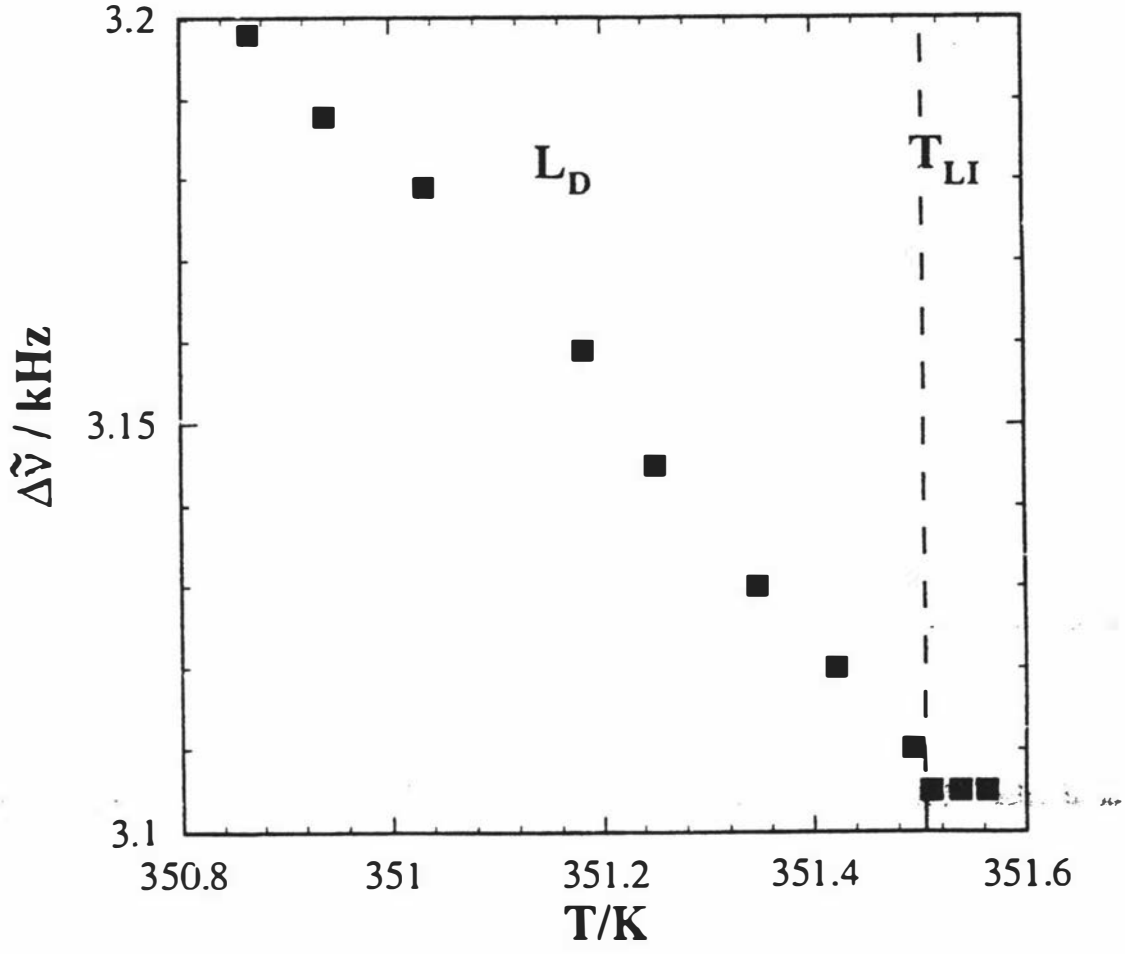

References

1. A. Abragam, *The Principles of Nuclear Magnetism* (Oxford University Press, Oxford, 1961).

2. M. H. Cohen, F. Reif, *Solid State Physics* **5**, 321-395 (1957).

3. N. Boden, S. A. Jones, *N.A.T.O. ASI. Sci. C. Maths. Phys.* **141**, 437 (1985).

4. N.-O. Persson, L. B., *J. Phys. Chem.* **83**, 3015-3019 (1979).

5. N. Boden, S. A. Corne, K. W. Jolley, *J. Phys. Chem.* **91**, 4092-4105 (1987).

6. N. Boden, et al., *J. Physique* **47**, 2135-2144 (1986).

7. M. H. Smith, Ph.D., Massey University (1990).

8. N. Boden, S. A. Jones, *Israel J. Chem.* **23**, 356-362 (1983).

9. N. Boden, K. W. Jolley, M. Smith, *J. Phys. Chem.* **97**, 7678-7690 (1993).

10. H. Wennerström, G. Lindblom, B. Lindman, *Chem. Scr.* **6**, 97 (1974).

11. H. Wennerström, N.-O. Persson, G. Lindblom, B. Lindman, *J. Magn. Reson.* **30**, 133-136 (1978).

12. A. N. Parbhu, Master of Science, Massey University (1990).

13. K. W. Jolley, M. H. Smith, N. Boden, *Chem. Phys Lett.* **162**, 152-156 (1989).

14. N. Boden, K. W. Jolley, M. H. Smith, *Liq. Cryst.* **6**, 481-488 (1989).

15. N. Boden, K. W. Jolley, *Phys. Rev. A* **45**, 8751-8758 (1992).

Chapter 4
Theories of Self-Assembly and Self-Organisation

In order to further the understanding of the self-assembly and self-organisation in micellar systems it is important to compliment the experimental results and the conclusions drawn from them with a comparison of current theoretical models, as neither the experimentalist nor the theoretician should work in isolation. In this chapter three current theoretical models are presented. They comprise of two aggregate self-assembly models from the research groups of McMullen, Ben-Shaul, and Gelbart (MBG)[1-3] and Eriksson and Ljunggren (EL)[4-6], and the self-organisation model of Taylor and Herzfeld (TH)[7], which also allows for self-assembly of the aggregate. This is by no means a comprehensive review of the range of theoretical models for self-assembling lyotropic liquid crystals. Rather, the models have been selected on the basis of their relevance to experiments presented in this thesis.

MBG have developed a phenomenological model to determine the chemical potential of monomers within aggregates and the consequent equilibrium micelle size distribution. The model is presented here in detail as the equations will be used in calculations to qualitatively estimate changes in the aggregate theoretical size distributions with temperature and fluorocarbon chain length. EL have approached the problem of self-assembly by considering the surface thermodynamics and small system thermodynamics of aggregate formation. The EL treatment involves determination of the individual contributions to the excess free energy of a monomer from which aggregate size distributions can be calculated. Only a brief outline of the EL model will be presented as values for the parameters in their model pertinent to the system under study are currently not well defined, and so no specific calculations using this model will be conducted. This model is presented to allow a comparison of their predictions of the effect of salt on the aggregation shape and size distribution, with the findings of the experiments on the ternary CsPFO/CsCl/^2H_2O and APFO/NH_4Cl/^2H_2O systems.

The approach that TH have employed is a phenomenological description of aggregate assembly in conjunction with a scaled particle treatment of fluid configurational entropy and a cell description of periodic smectic density modulations. A brief summary of the development of the model and the predicted phase behaviour of discotic aggregate systems is presented. This predicted phase behaviour will be used to qualitatively compare theoretical results with experimental phase behaviour of these micellar systems.

4.1 Self-Assembly Models

4.1.1 Phenomenological Approach to Self-Assembly

Prior to the approach of MBG[2], self-assembly models assumed that the chemical potential per surfactant molecule was dominated by the "surface" terms $\gamma_I a + c/a$ where γ_I and c represent the interfacial and electrostatic energies associated with the head groups (having area of a) respectively. That is contributions to the chemical potential from energy and entropy terms associated with the packing of hydrophobic chains were ignored. These terms not only depend on the head group area but also on the elastic properties of the chains. MBG[2] argue that the chains are not "passive" as the head group chemical potential cannot be optimized without taking into account the free energy "price paid" by the hydrophobic tails. The following is their phenomenological model where they introduce a "relative stability" parameter y to treat the compressional and splay elasticity contribution to the chemical potential per surfactant molecule. Although this model has been derived for solutions of infinitely dilute non-interacting micelles, inclusion of an inter-micellar interaction term changes the models qualitative predictions only slightly[3,8].

MBG considered the case of spherical, cylindrical and discotic micelles. In the discotic micelle two distinct sites are recognised such that the surfactant can reside in the oblate-cylindrical "body" or the part-toroidal "rim". The different chemical potentials for each environment are expressed by

$$\tilde{\mu}_i^0(a) = h_i(a) + g_i(a), \qquad [4.1]$$

where $h_i(a)$ represents the interfacial tension and electrostatic energy contributions to the "surface" part of $\tilde{\mu}^0$ and $g_i(a)$ corresponds to the "bulk" energy and entropy effects associated with the packing of the hydrophobic tails. Whereas $g_i(a)$ has previously been treated as independent of environment i and headgroup area a, MBG consider its complicated dependence on the area per head group and the nature of the surfactant environment.

MBG assume that the chemical potential $\tilde{\mu}^0$ at each site is optimized, that is it adjusts to the appropriate optimized headgroup area a_0 in each environment of each micelle of interest which allows the following to be written

$$\tilde{\mu}^0_{s,disk} = \tilde{\mu}^0_{cyl,disk} + \frac{s_{rim}}{s}\left[\tilde{\mu}^0_{rim} - \tilde{\mu}^0_{cyl,disk}\right] \qquad [4.2]$$

Here $\tilde{\mu}_i^0 \equiv \min \tilde{\mu}_i^0(a) \equiv \tilde{\mu}_i^0\left(a_0^{(i)}\right)$, where i represents the two environments (1) cylinder of the disc and (2) rim of the disc. s_{rim} denotes the number of surfactants in the rim of an s-disc. The nature of the thermodynamic equilibrium depends on the relative and absolute magnitudes of the chemical potential associated with each of the relevant surfactant environments.

Using straightforward surface/volume geometric relations and assuming that the core of the aggregate is of uniform density filled exclusively by chains, Israelachvili[9] has

shown the area per head group a_i of a surfactant in a given environment i is uniquely related to its thickness, l_i.

$$\frac{a^{(i)}}{v/l_i} = i = \begin{cases} 1, & \text{bilayer(lamellar)} \\ 2, & \text{cylinder(hexagonal)} \\ 3, & \text{sphere} \end{cases} \qquad [4.3]$$

where v is the space filling volume associated with each molecule. As little is known about the actual elasticity effects which determine the contribution of $g(a)$, MBG allowed for it indirectly as follows[2]. For all i $\tilde{\mu}_i^0(a) = \gamma_i a + c/a$ and they define l_i to also be fixed (l). This is essentially the approach of Israelachvili *et al* [9] except that instead of setting $v/l = a_0$ or $2v/l$, they allow the following intermediate cases;

$$a_0 = \frac{v}{l}(1+y) \qquad [4.4]$$

where $0 \le y \le 2$. l is considered the mean of the l_i values associated with the surfactant in question. Similarly, a_0 represents an average of the optimum head group areas. The quantity y accounts for the bulk elasticity effects that have been suppressed. Under these conditions for discotic aggregates to be stable, y must have a value within $0.4 \le y \le 0.43$.

Equation[4.2] can now be rewritten in the more explicit form

$$\tilde{\mu}^0_{s,disk} = \tilde{\mu}^0(a_{disk}) + \frac{s_{rim}}{s}\left[\tilde{\mu}^0(a_{rim}) - \tilde{\mu}^0(a_{disk})\right] \qquad [4.5]$$

Where a_{rim} and s_{rim} can be determined as explicit functions of v, l and s and it can be shown that

$$\tilde{\mu}^0_{s,disk} = \tilde{\mu}^0_{\infty,d} + \alpha_d f_d(s) \qquad [4.6]$$

with

$$\tilde{\mu}^0_{\infty,d} = 2\gamma_l a_0\left[1 + \frac{y^2}{2(1+y)}\right]$$
$$= \tilde{\mu}^0(a_{disk}) = \tilde{\mu}^0_{cyl,disk}$$

$$\alpha_d(s) = \left(\frac{3m}{32}\right)^{1/2} \frac{\pi\gamma a_0}{1+y} \times \left[1 - \frac{y(2+y)}{1 + \frac{m}{s_{rim}}}\right]$$

and

$$f_d(s) = \left(\frac{32m}{3\pi^2}\right)^{1/2} \frac{1}{s} \frac{(1 + s_{rim}/m)^2}{(1 + 2s_{rim}/m)^2}$$

Translational and rotational contributions to the size of micelles have been determined by statistical-thermodynamic treatment of the ideal (molecular) gas partition functions[1]. It has been shown that inclusion of these two terms in the expression for the free energy favour small aggregates, so thus further stablizing the discotic aggregates against the formation of bilayers. As there are no accurate data for the interfacial tension and average optimum head group areas for the system under study, translational and rotational contributions have not been included in this analysis.

It follows from equation [4.6] the equilibrium size distribution of micelles is determined by the s-dependence of $\tilde{\mu}_0$ by the following expression

$$x_s = s x_1^s e^{\beta s(\mu_1^0 - \tilde{\mu}_{1,\infty}^0)} \qquad [4.7]$$

where x_1 and μ_1^0 are respectively the mole fraction and chemical potential of the monomer.

From the above equation it is now possible to predict the size distribution of the micelles in a particular system if values of the interfacial tension, volume and length of the chain, area the head group occupies, and the chemical potential of the monomer in solution are known. Whereas in the fluorocarbon systems being studied in this thesis the volume and length of the chain can be determined, the values of the remaining parameters are not well defined. As MBG have indicated, the specific choice of those values which are not well defined[2], does not effect qualitatively this discussion, therefore the procedure used was to choose reasonable values for the unknown parameters from existing data. The chemical potential of a monomer in a range of micelle sizes was then calculated using equation[4.6] and the micelle size distribution from equation[4.7]. Number average Sn and weight average Sw were calculated from $Sn = \sum_s x_s \Big/ \sum_s \frac{x_s}{s}$ and $Sw = \sum_s s x_s \Big/ \sum_s x_s$ respectively.

Figure 4.1 shows an example of the micelle size distribution for a CsPFO/^2H_2O sample with an amphiphile mole fraction of 0.0094 at 300 K. The values of the parameters used are given in the legend, the choices of these values are more fully explained in chapter five where these calculations are used to qualitatively compare theoretical predictions with experimental observations.

4.1.2 Free Energy Approach to Self-Assembly

The EL treatment of self-assembly involves determination of the individual contributions to the excess free energy ε_s^* of a monomer in an aggregate with an aggregation number of s (* denotes the geometry of the aggregate) . The size distribution of the micelles is readily obtained once ε_s^* is known as a function of s. Contributions to the excess free energy are give by

$$\varepsilon_s^* = \varepsilon_{tan} + \varepsilon_{el}^* + (\varepsilon_s^*)_{conf} + \gamma_{hc/w} a^* + \varepsilon_{pg}^* \qquad [4.8]$$

where ε_{tan} is the contribution from the free energy gained upon removing the hydrophobic chain from a water solution to a hydrophobic environment, ε_{el}^* is the electrostatic free energy which counteracts ε_{tan} as a result of concentrating the ionic headgroups and their counter-ions, $(\varepsilon_s^*)_{conf}$ and $\gamma_{hc/w} a^*$ represent the free energy contributions of the configurational restrictions on the aggregated chains, and hydrocarbon/water contact respectively. Finally ε_{pg}^* is the surfactant headgroup parameter introduced in order to account for several lesser know effects, for example the reduction

Figure 4.1. Micelle size distribution for a CsPFO/^2H_2O sample the mole fraction of amphiphile in an aggregate of size s verses the aggregation number s calculated from equations[4.6] and [4.7]. The total amphiphile mole fraction is $x_a = 0.0094$ and the temperature is set at 300 K. The values of the parameters used in the calculations are: $\mu_1^0 = 15$ k T; $\gamma = 0.025$ J m^{-2}; $y = 0.43$; $l = 1.096$ nm; and $v = 0.360$ nm^3 (see text for definition of parameters). The number average and weight average are calculated to be 115 and 147 respectively.

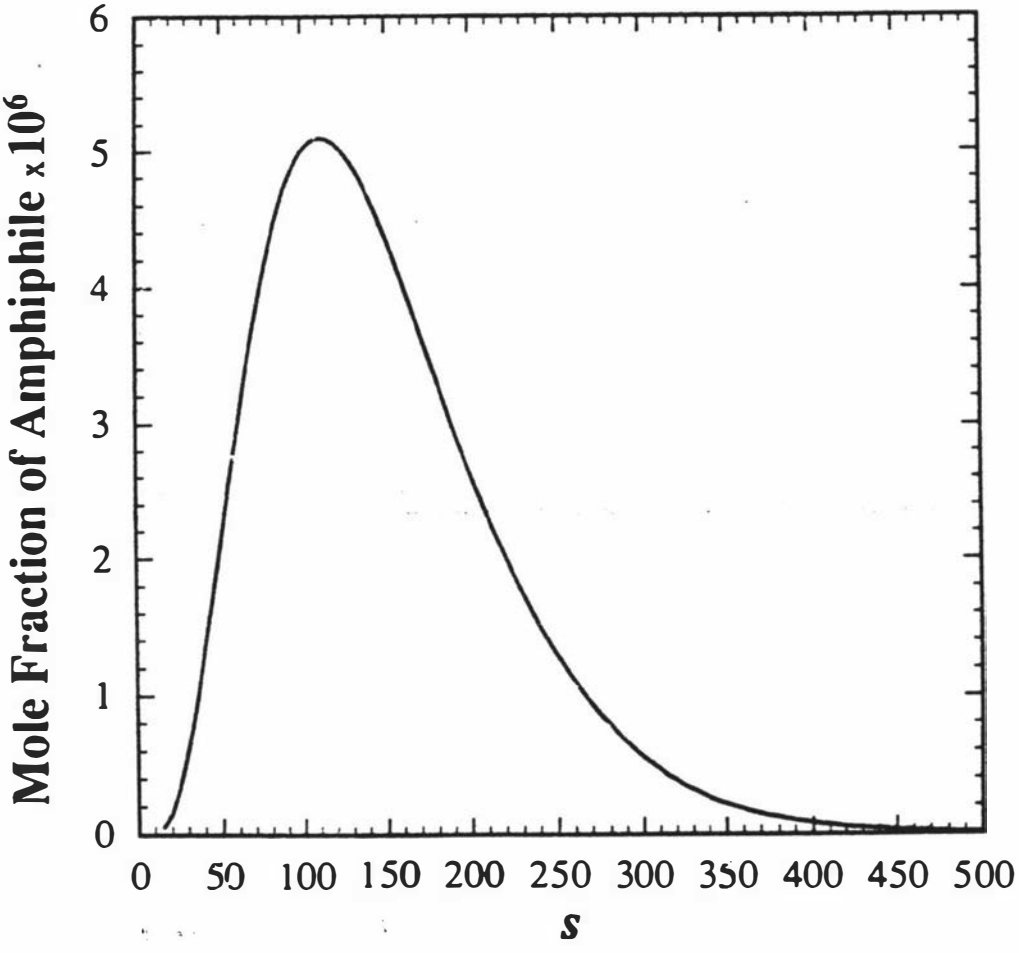

in overall free energy of the hydrocarbon/water contact because of the presence of polar headgroups.

In the case of a disc shaped micelle, which is modelled as being composed of a planer bilayer part joined with a toroidal, semicylindrical rim part, EL have shown that the excess free energy varies as a function of the aggregation number s in the following manner

$$s\varepsilon_s^d / kT = \alpha^t s_{rim} + \beta^b s + \partial(s) \qquad [4.9]$$

where α^t is the contribution to the excess free energy of a monomer in the toroidal, semicylindrical rim. β^b is the free energy difference corresponding to the work needed per monomer to form part of an infinite bilayer out of surfactant ions present in solution, and $\partial(s)$is a term introduced to account for the end to end repulsion resulting from overlap of the junction zone between the bilayer and half toroid.

Once the excess free energy is known as a function of the aggregation number, EL have shown that it is straight forward to compute the volume fraction of disc shape aggregates by means of the expression

$$\phi^d = \exp\left(-s\varepsilon_s^d / kT\right) \qquad [4.10]$$

Using the above expression for the aggregation number dependence of the excess free energy, EL have calculated the distribution of disc shaped aggregates of sodium dodecyl sulfate (SDS) in water, as a function of surfactant and added inorganic salt[4, 6]. They have used experimental data to determine each of the individual contributions in equation[4.8] to the excess free energy.

Figure 4.2 is an example of the micelle size distributions that have been calculated by EL. The micelle distributions are for a monomer concentration of 0.47 mM and α^t = -0.153299. To examine the influence of salt on the micelle size distribution the distribution curves have been calculated at varying values of β^b as indicated on the figure. β^b is inversely proportional to the salt concentration, where β^b = 0.2044 corresponds to an effective salt concentration of 0.5 M, with the two other distributions adapted from this value. The graph indicates that the EL model predicts that there will be an increase in the average aggregate size and the volume fraction of discotic aggregates as the salt concentration is increased. This prediction of an increase in the micelle size distribution as a function of salt concentration will be compared with the experimental results from the effect of adding electrolyte to the mesophase behaviour. EL have also computed aggregate size distributions for spheres, rods and vesicles using the above method. It is predicted that bimodal distributions can exist between different aggregate structures and an evolution in the aggregate structure of spheres→rods→discs→vesicles as a function of increasing salt concentration[4] (see figure 4.3). This is an interesting prediction and will also be used in conjunction with experimental observations in chapter six of the effect of added electrolyte of the self-assembly of lyotropic liquid crystal systems.

Figure 4.2 The predicted discotic micelle size distribution. The mole fraction of amphiphile in an aggregate of size s verses the aggregation number s, calculated from EL model for a SDS concentration of 0.47 mM which gives α_t = -0.153299 and different values of β^b (as indicated on the figure) corresponding to the inverse of the salt concentration.

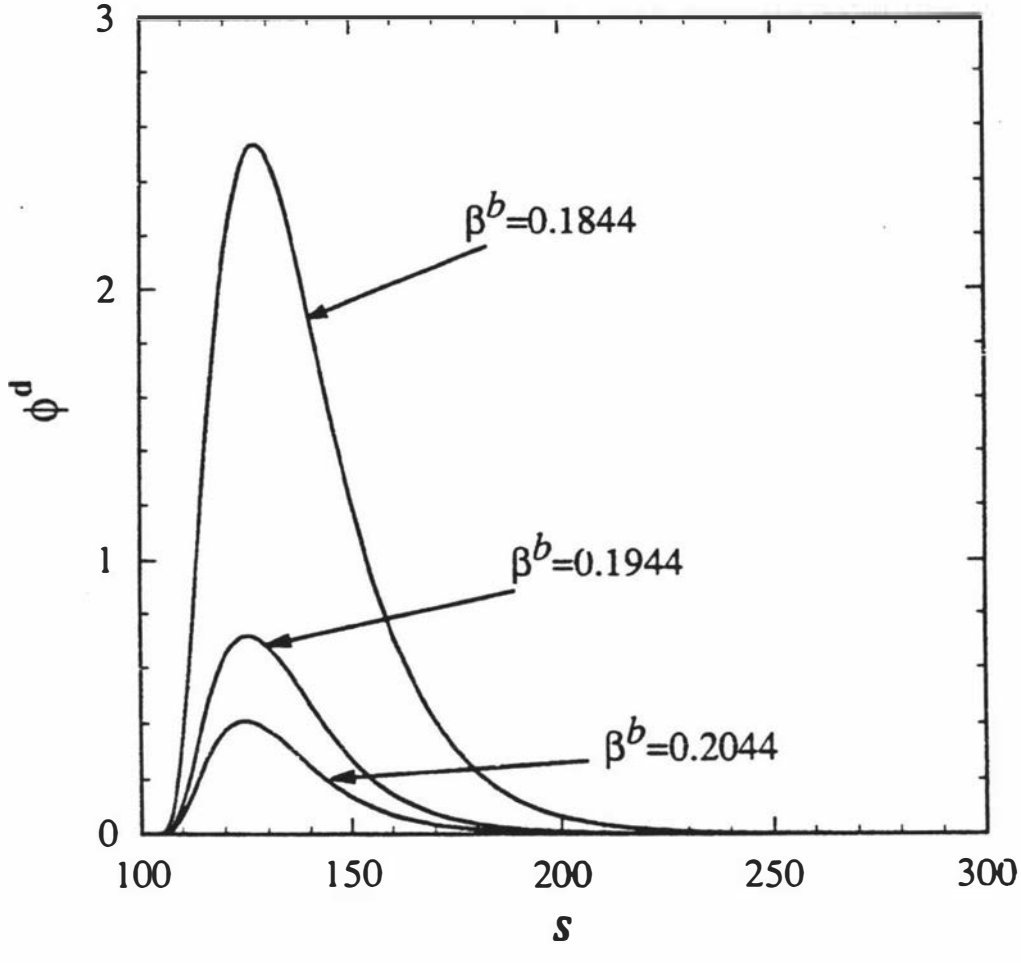

Figure 4.3 Evolution of aggregate structure figure reproduced from reference[4]. The predicted evolution of the structure of the aggregate as a function of the salt and amphiphile concentration.

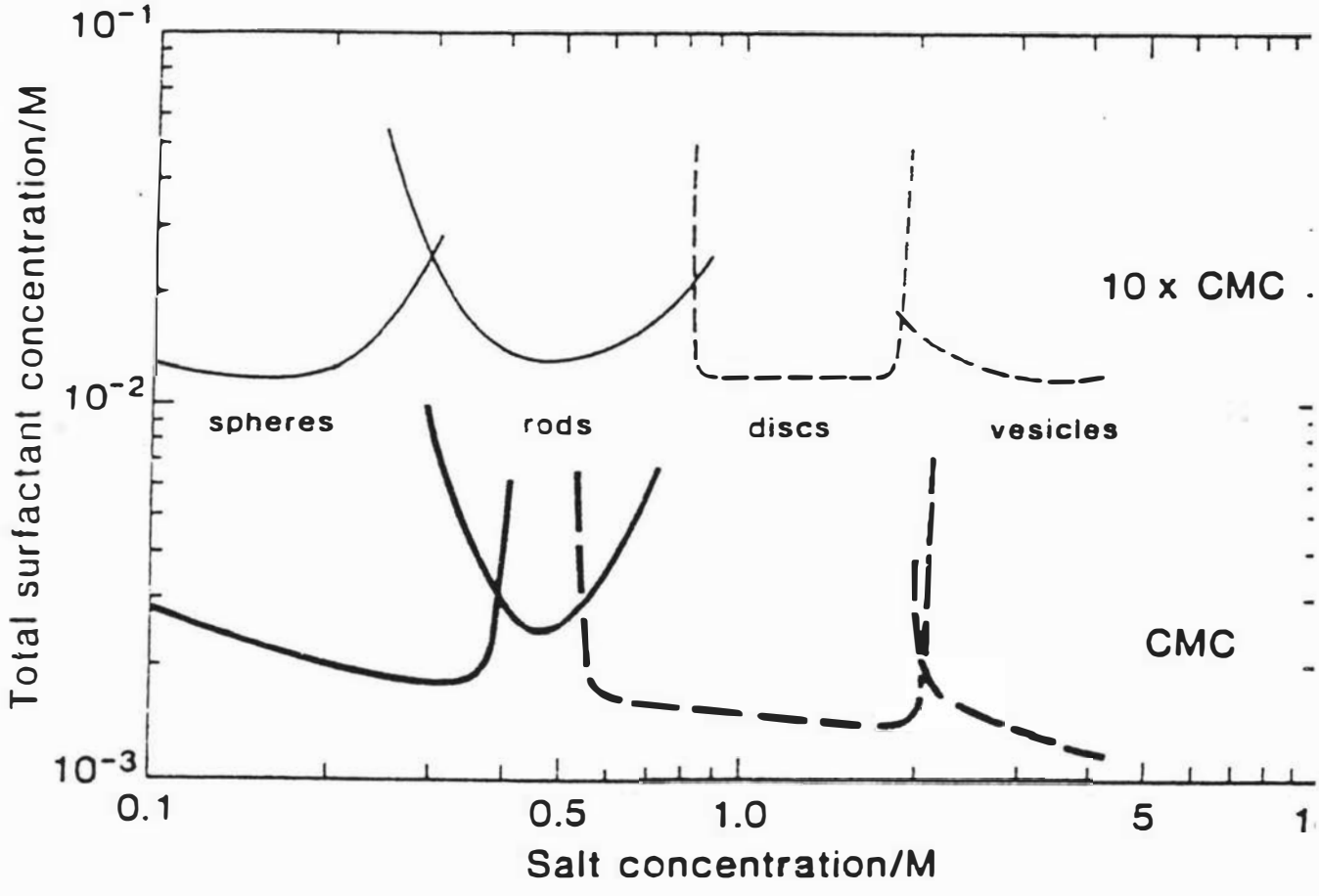

4.2 Self-Organisation Model

4.2.1 Self-Organisation in Reversibly Assembling Lyotropic Systems

Initial theoretical explanations of the orientational ordering in reversibly assembling lyotropic systems were based purely on excluded volume interactions, such as Onsager's hard particle model which demonstrated the existence of an alignment transition in a dilute solution of long thin hard rods[10]. Although these models may appear rather simplistic, especially in consideration of interactions such as van der Waals attraction and electrostatic repulsion, it can be shown from the theory of simple fluids, hard-core interactions play a dominant role in determining fluid structure and long-range attractive potential's can often be treated in a perturbative manner[11]. Another difficultly in modelling order/disorder transitions in self-assembling systems is the variable and polydisperse aggregate size distribution which is generally both concentration and temperature dependent. When considering these problems in the context of order/disorder transitions in lyotropic liquid crystal systems, it appears that the most applicable theory is currently that of Taylor and Herzfeld. They have developed a model based on the scaled particle modification of Onsager theory, for reversibly assembling systems which undergo a series of order/disorder transitions[7]. The following is a brief summary of the model, and presentation of the results. It is introduced to allow a comparison between predicted and experimentally determined phase behaviour.

Taylor and Herzfeld define the model system as a set of polydisperse uniaxial particles (aggregates) in a volume V and temperature T. A given aggregate is characterised by its aggregation number s and its orientation Ω. The fraction of particles which have an aggregation number s and orientation Ω is given by the aggregate number distribution function $N(s,\Omega)/N_p$ where the total number of particles is defined as $N_p = \sum_{s,\Omega} sN(s,\Omega)$. N_p is a variable quantity, while the total particle volume fraction ϕ_p is constant. The Helmholtz free energy of such a reversibly assembling system is given by $A(\phi_p,V,T) = -k_B T \ln Q(\phi_p,V,T)$ where

$$Q(\phi_p,V,T) = \sum_{\{N(s,\Omega)\}_{\phi_p}} \tilde{Q}[N(s,\Omega);V,T] \qquad [4.11]$$

is the canonical partition function, in which the sum extends over all possible size distributions subject to the constraint of a constant ϕ_p.

The intra-aggregate free energy is then described phenomenologically. The average free energy per monomer, of monomer-monomer contacts within a s aggregate is taken as $-[(s-1)/s]\Phi(T)k_B T$ where $\Phi(T)$ is the free energy of association. Thus each s aggregate contributes a Boltzmann factor of $q_s = \exp[-(s-1)\Phi]$ to the corresponding term in the partition function.

The inter-aggregate potential has been modelled as an infinitely hard core (corresponding to the physical dimensions of the particle) surrounded by a short-range soft repulsive step of height J and width ξ. The position and orientation of aggregate i have been defined as x_i and Ω_i respectively, so the interaction energy between two aggregates i and j, which depends on their separation $x_{ij} = x_i - x_j$ and relative orientations $\Omega_{ij} = \Omega_i - \Omega_j$, includes the hard core contribution

$$\beta\mu_0(x_{ij},\Omega_{ij}) = \begin{cases} \infty, & d_{ij} < 0 \\ 0, & d_{ij} > 0 \end{cases} \qquad [4.12]$$

and the contribution of the soft repulsions

$$\beta\mu_1(x_{ij},\Omega_{ij}) = \begin{cases} 0, & d_{ij} < 0 \\ \beta J, & o(\Omega_i - \Omega_j), 0 < d_{ij} < \xi \\ 0, & d_{ij} > \xi \end{cases} \qquad [4.13]$$

where $\beta = 1/k_BT$, d_{ij} is the minimum surface to surface distance between aggregates i and j, and $o(\Omega_i\text{-}\Omega_j)$ is the overlap length of aggregate i with the repulsive step of aggregate j.

To model translational order TH have defined all aggregates in a translationally ordered phase as being parallel to each other, so disordered dimensions of the systems are allowed to be separated from translationally ordered dimensions. Thus the smectic phase is viewed as a two-dimensional fluid confined within a one-dimensional cell corresponding to the thickness of the smectic layer. In the fluid dimensions the interparticle interactions are still described by equations[4.12] and [4.13], while in the translationally ordered dimensions the particle-cell wall interaction takes the form

$$\beta w(x_i) = \begin{cases} \infty & \text{if particle } i \text{ penetrates a cell wall} \\ 0 & \text{otherwise.} \end{cases} \qquad [4.14]$$

This phenomenological description of aggregate assembly, in conjunction with a scaled particle treatment of fluid configurational entropy and a cell description of periodic smectic density modulations is then used to calculate the phase diagram for the disc-like system. In the case of discotic aggregates TH have modelled the system as s symmetric right cylinder monomers of equal height and diameter (l) self-assembled to form a right cylinder disc-like s aggregate of height l. They make the assumption that the disc polydispersity is sufficient to suppress columnar ordering, so the system is expected to form isotropic, nematic and smectic (lamellar) phases.

Their phase diagram of the self-assembling disc-like system is shown, as a function of Φ and ϕ_p, in Figure 4.4. The parameters that were then used in the calculations are a monomer length of l = 9 Å and mass of 500 amu with a repulsive step potential of height $\beta l^2 J = 0.2$ and width $\xi/a = 0.1$. They have assumed that Φ increases linearly with T^{-1} so that the phase diagram can be interpreted as a temperature-concentration phase diagram The phase diagram displays a low temperature nematic phase intervening between a low concentration isotropic phase and a high concentration smectic phase. With increasing temperature the region of nematic stability narrows and finally terminates at an isotropic-nematic-smectic triple point ($\phi_p \approx 0.35$, $\Phi \approx 22.0$) above which there is a direct isotropic

Figure 4.4 TH model phase diagram for a self-assembling disc-like system reproduced from reference[7]. Φ is the magnitude of the free energy of association of each monomer-monomer contact within the aggregate which is assumed to increase linearly with T^{-1}, and ϕ_p is the particle volume fraction.

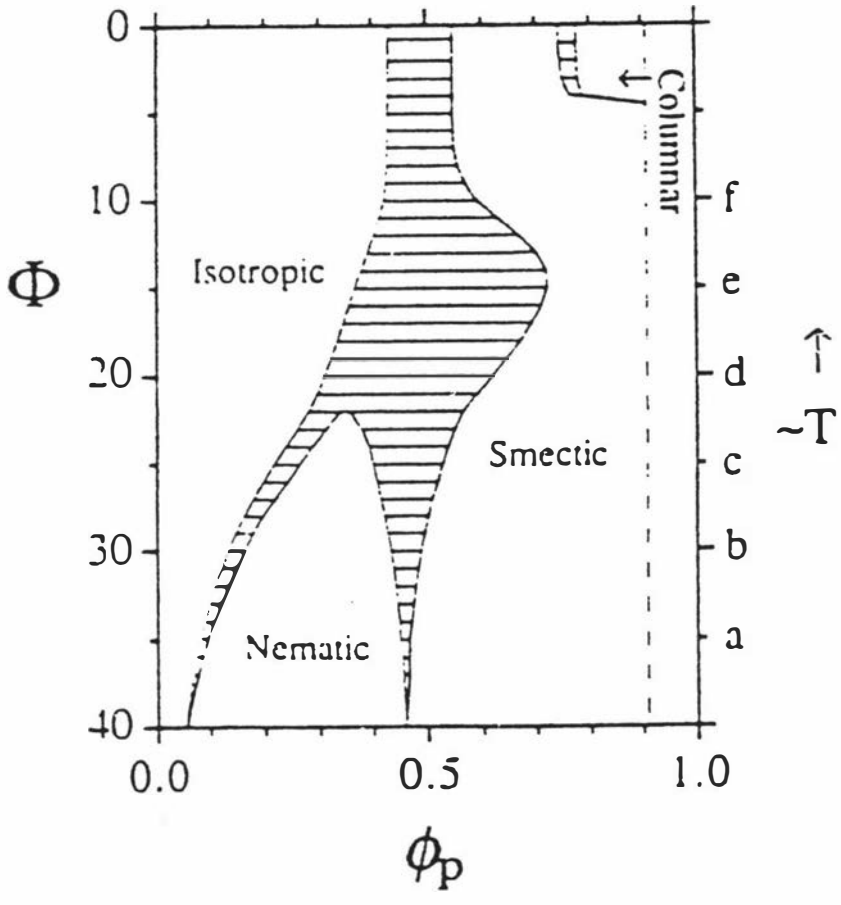

to smectic transition. For most of the temperature range the smectic phase is stable out to close packing. However, at the highest temperatures, when aggregation is very weak, the smectic phase is predicted to be replaced by a columnar phase of symmetric or slightly asymmetric monodisperse discs. The TH model will be compared with the experimentally determined phase behaviour, in later chapters.

References

1. W. E. McMullen, W. M. Gelbart, A. Ben-Shaul, *J. Phys. Chem.* **88**, 6649-6654 (1984).

2. W. E. McMullen, A. Ben-Shaul, W. M. Gelbart, *J. Colloid Interface Sci.* **98**, 523-536 (1984).

3. W. M. Gelbart, A. Ben-Shaul, W. E. McMullen, A. Masters, *J. Phys. Chem.* **88**, 861-866 (1984).

4. J. C. Eriksson, S. Ljunggren, *Langmuir* **6**, 895-904 (1990).

5. J. C. Eriksson, S. Ljunggren, U. Henriksson, *J. Chem. Soc, Faraday Trans II* **81**, 833-868 (1984).

6. S. Ljunggren, J. C Eriksson, *J. Chem. Soc. Faraday Trans. II* **82**, 913-928 (1986).

7. M. P. Taylor, J. Herzfeld, *Phys.Rev. A* **43**, 1892-1905 (1991).

8. A. Ben-Shaul, W. M. Gelbart, *J. Phys. Chem.* **86**, 316-318 (1982).

9. J. N. Israelachvili, S. Marcelja, R. G. Hor.., *Quart. Rev. Biophys.* **13**, 121 (1980).

10. L. Onsager, *Ann. N. Y. Acad. Sci.* **51**, 627-659 (1949).

11. P. J. Hansen, I. R. McDonald, *Theory of Simple Liquids* (Academic, London, 1986).

Chapter 5
Effect of Amphiphile Chain Length on the Self-Assembly and Self-Organisation of Micelles of the Caesium Salts of Perfluorocarboxylic Acids in Aqueous Solutions

5.1 Introduction

Experiments conducted on the APFO/^2H_2O and CsPFO/^2H_2O systems indicate that order/disorder transitions are governed primarily by hard core interactions[1,2]. The implication of this is that, attractive interactions such as dispersive forces, or repulsive electrostatic interactions between micelles are not significant in the mechanism of the order/disorder transitions. To examine the role of these interactions, a systematic investigation was undertaken of the effect of the chain length on the nature and mechanism of the phase transitions in micellar liquid crystals found in aqueous solutions of the salts of perfluorinated carboxylic acids. There are some rudimentary phase diagrams available for the heptadecafluorononanoic salts[3,4] but these are not of sufficient quality for the purpose of the present investigation.

Previous work on the phase behaviour of the CsPFO/^2H_2O system has been extended by accurately measuring the I-to-N_D^+ and N_D^+-to-L_D phase transition temperatures in micellar liquid crystals formed from solutions of the caesium salts of tridecafluoroheptanoic (CsTFH), heptadecafluorononanoic (CsHFN) and nonadecafluorodecanoic (CsNFD) acids in ^2H_2O. NMR was used to monitor the change in the size of the aggregate along the transition lines. Phase transition temperatures were determined precisely and accurately to ± 0.01 K by NMR measurements of quadrupole splittings of ^2H in ^2H_2O as outlined in chapter 3. In addition, the magnitudes of the ^2H quadrupole splittings were used to monitor the variation of micelle size along the I-to-N_D^+ and N_D^+-to-L_D transition.

5.2 The Phase Behaviour

The phase transition temperatures of the CsTFH/^2H_2O (C7), CsHFN/^2H_2O (C9) and CsNFD/^2H_2O (C10) systems are shown superposed on the I-to-N_D^+ and N_D^+-to-L_D transition lines of the CsPFO/^2H_2O (C8) system in figure 5.1. For the CsPFO/^2H_2O system the isotropic, nematic and lamellar phase boundary curves have been recalculated from the high resolution phase diagram of Boden *et al*[5], using the new measured CsPFO density of ρ = 2.32 g cm^{-3} (appendix C). Using this density the nematic phase volume fraction ϕ at Tp(I,N,L) is 0.442(*c.f.* ϕ = 0.426[6]) and the volume fraction at the tricritical point Tcp is 0.26 (*c.f.* ϕ = 0.25[6]). In temperature verses volume

Figure 5.1 Nematic-to-isotropic and lamellar-to-nematic phase transition temperatures for the for the CsTFH/^2H_2O (△), CsHFN/^2H_2O(○), and CsNFD/^2H_2O (□) systems superimposed on a partial phase diagram (solid lines) for the CsPFO/^2H_2O system. All labels refer to the CsPFO/^2H_2O phase diagram. I, isotropic micellar solution phase; N_D^*, nematic phase with discotic micelles; L_D, lamellar phase; Tp(I,N,L), the isotropic micellar solution-nematic-lamellar triple point; Tcp, the lamellar-nematic tricritical point. Tc is the solubility curve and the dotted lines below Tc therefore represent transitions between metastable phases[5, 6].

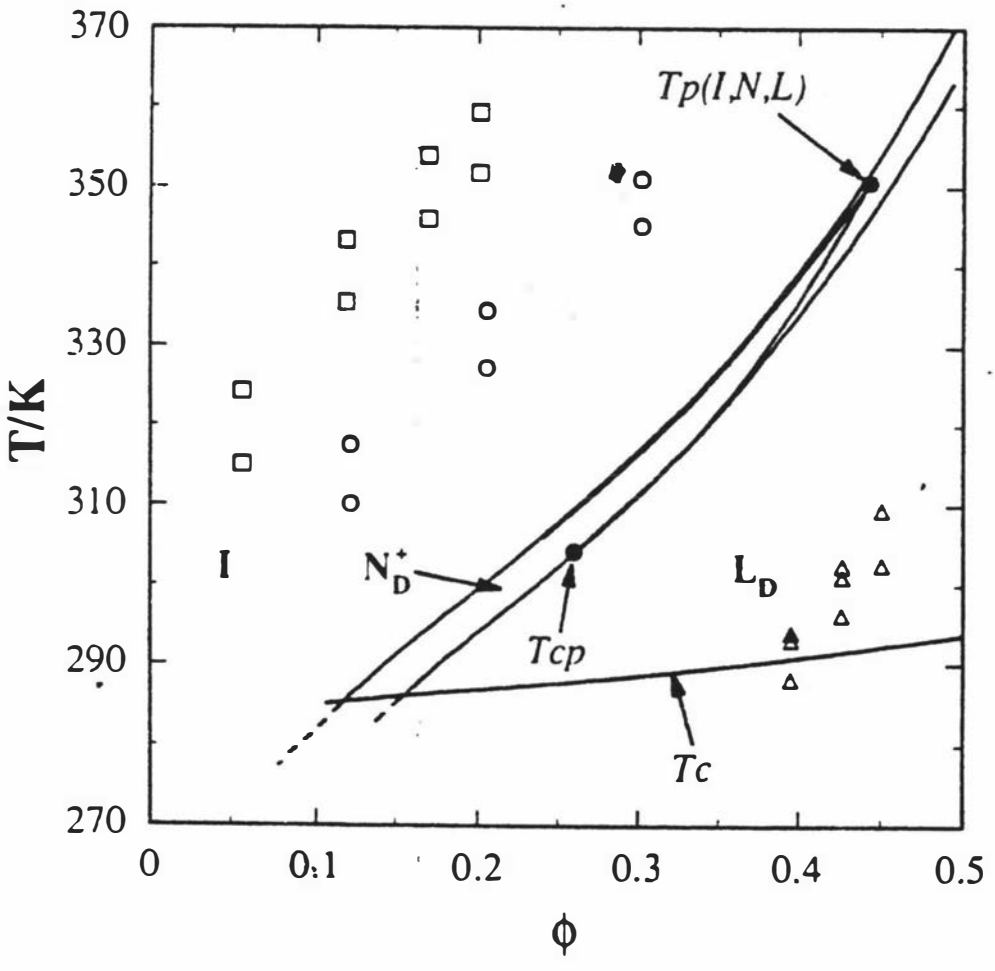

fraction of amphiphile space the phase behaviour of the four surfactants is strikingly similar with the phase transition temperatures being displaced to higher temperatures as the length of the fluorocarbon chain increases. At corresponding volume fractions the temperature range of the nematic range also increases with increasing chain length. The corresponding temperature range of the nematic phase for C7, C8, C9 and C10 are about 5.0 K, 5.5 K, 6.9 K and 7.8 K respectively. But at corresponding volume fractions the width of the isotropic/nematic biphasic region is almost constant irrespective of the chain length. T_{IN}-T_{NI} is plotted as a function of the volume fraction of each of the surfactant systems C7 to C10 in figure 5.2. The figure shows the width of the coexistence region decreases as a function of decreasing amphiphile concentration, from a measured high of ≈ 1.4 K at $\phi = 0.42$ to a low of ≈ 0.10 K at $\phi = 0.10$.

The CsTFH/^2H_2O system is displaced to lower temperatures (by ≈ 45 K) than the CsPFO/^2H_2O system. The triple point Tp(I,N,L) temperature was determined to be 307.3 K (ϕ_I = 0.442, ϕ_N = 0.450, and ϕ_L = 0.468) (see figure 5.3). Tp(I,N,L) was determined by cooling a ϕ = 0.451 sample from the isotropic into firstly the isotropic/lamellar mixed phase region when the lamellar doublet appeared. On further cooling below Tp(I,N,L) the isotropic peak disappeared as a nematic doublet increased in intensity[5]. The onset of the disappearance of the isotropic phase signal indicated the temperature of Tp(I,N,L). The concentration of each phase was determined from the abscissae of the isotropic, nematic and lamellar phase boundary curves at the triple point temperature[5]. There is a remarkable correspondence between the triple point compositions in the CsPFO/^2H_2O and CsTFH/^2H_2O systems. It was not possible to determine Tcp for the sample since this occurred at a temperature well below the solubility curve (figure 5.1).

The CsHFN/^2H_2O system presented (figure 5.1) is displaced to higher temperatures (by ≈ 33 K) than the CsPFO/^2H_2O system with an accessible nematic range that is governed by the upper temperature attainable on our temperature control unit (≈ 370 K). For this system measurements have not been carried out in sufficient detail to accurately locate the tricritical point Tcp along the nematic-to-lamellar transition line. But the temperature width of the N_D^+/L_D phase coexistence regime at ϕ = 0.302 (≈ 0.15 K) is practically the same as that for the corresponding volume fraction of CsPFO/^2H_2O[6]. If it is assumed that the concentration dependence of T_{LN} - T_{NL} is the same as that of the CsPFO/^2H_2O system, which would appear reasonable considering the identical concentration dependence of T_{IN} -T_{NI} for the perfluorinated systems (figure 5.2), then Tcp for the CsHFN/^2H_2O system will occur at the same volume fraction as it does in the CsPFO/^2H_2O system *i.e.* at $\phi = 0.26$[6].

Figure 5.2 Temperature range of the isotropic-to-nematic phase coexistence region as a function of volume fraction of amphiphile ϕ for the CsTFH/^2H_2O (◆), CsPFO/^2H_2O(●), CsHFN/^2H_2O(▲), and CsNFD/^2H_2O(■)systems.

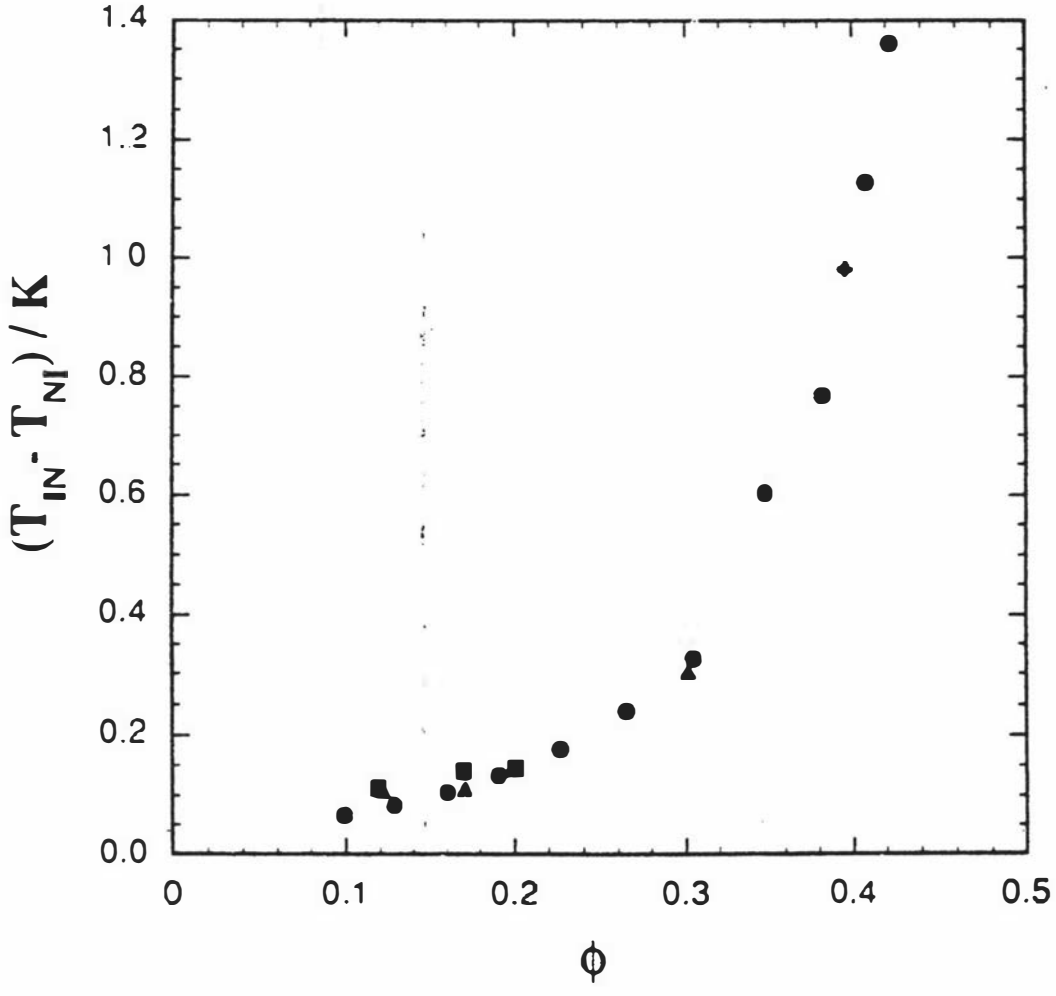

In the CsNFD/^2H_2O system the phase transitions are displaced by about 60 K and the nematic-to-lamellar transition is second order (below Tcp) at the maximum concentration studied (ϕ = 0.20). That is Tcp is located at an inaccessible temperature as far as this study is concerned. At lower volume fractions the isotropic-to-nematic mixed phase region is very narrow (< 80 mK) and exchange of ^2H_2O between isotropic and nematic regimes is usually fast on the time scale of the NMR experiment[5]. This, in combination with field induced ordering of the sample in the isotropic phase, meant that T_{NI} could not be measured to a high precision. Also, at ϕ = 0.05 and lower the samples were very viscous and at a volume fraction of 0.024 shear induced birefringence was observed. This sample exhibited complex phase behaviour which was uncharacteristic of the I-to-N_D^+ and N_D^+-to-L_D series of transitions. The shear induced birefringence is similar behaviour to that observed in the CsPFO/CsCl/^2H_2O system at low volume fractions of surfactant (see triangular phase diagram chapter 6). Phases that exhibit this phenomenon are no longer comprised of discotic aggregates but of large vesicles[7], and the shear induces deformations in the vesicle resulting in birefringence. This phenomenon is interesting and warrants further study, but it is beyond the scope of this investigation.

In the concentration/temperature space where the I-to-N_D^+-to-L_D phase transitions prevail it would appear that, within the temperature and concentration constraints of this study, the major effect of varying the chain length is a vertical shift in the phase boundary curves and it should be possible to represent the phase behaviour for all four systems on a "universal" phase diagram. Such a diagram, which was constructed by assuming that Tcp occurs at the same volume fraction, ϕ = 0.26, for all four systems and treating the Tcp temperature as an adjustable parameter in the CsTFH/^2H_2O, CsHFN/^2H_2O, and CsNFD/^2H_2O systems, is given in figure 5.4. The best fit values for Tcp used in the construction of this figure were 264.5 K, 338.2 K and 365.5 K for C7, C9, and C10 respectively. The universal phase diagram is of practical significance because the extent of any particular aspect of the phase space accessible to experiment is readily discernible.

5.3 Aggregate Size Along Phase Transition Boundaries

A comparison of the aggregate size along the I-to-N_D^+ and N_D^+-to-L_D phase transition lines can be obtained from the ^2H quadrupole splittings. To enable such a comparison to be conducted it must be remembered that at a common volume fraction the mole fraction ratio of amphiphile to ^2H_2O x_a/x_w will depend on the chain length. Considering the contributions to the ^2H quadrupole splitting, equation[3.19], it is important that we account for the variation of x_a/x_w between systems. This can be achieved by simply dividing the quadrupole splitting at any given volume fraction by

Figure 5.3 Partial phase diagram for the CsTFH/^2H_2O system showing the Tp(I,N,L) triple point. The triangles represent experimental points and the lines are best fit second degree polynomials through the data points.

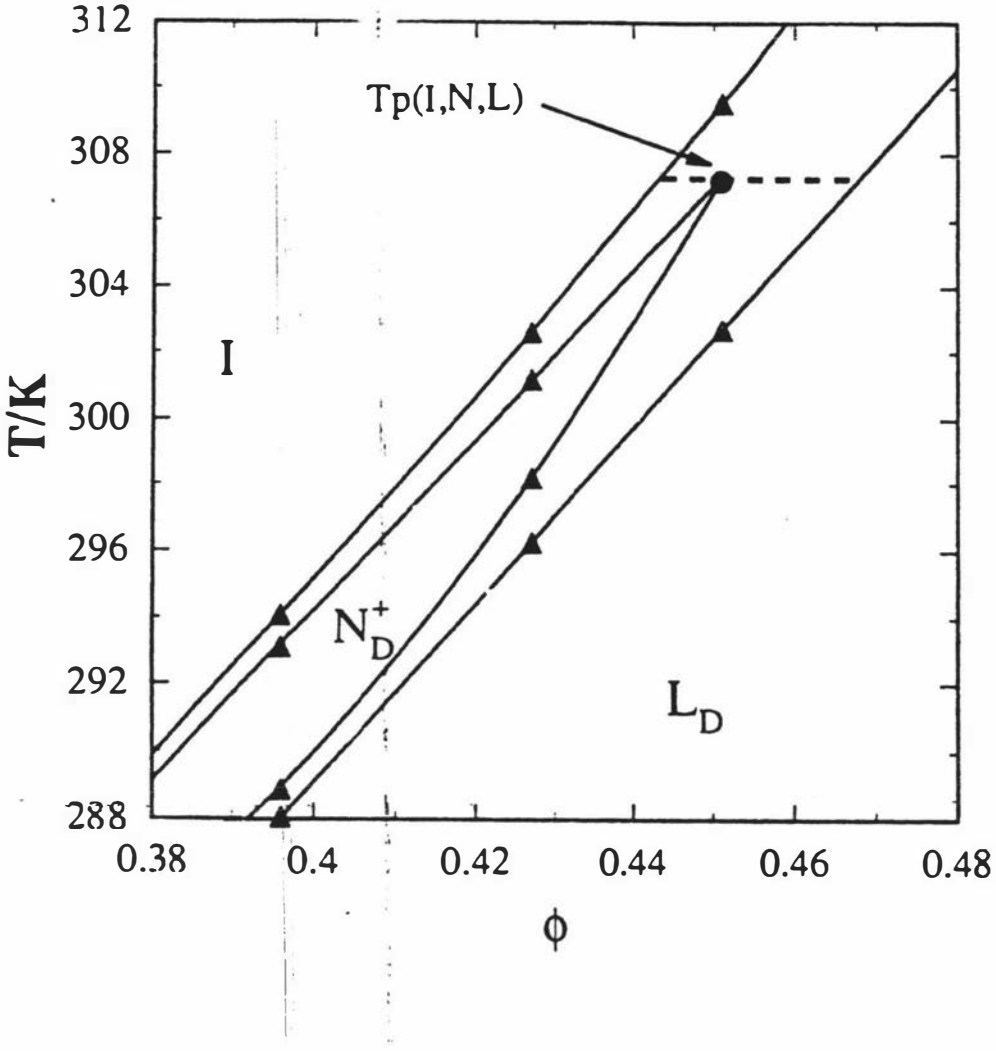

Figure 5.4 Universal phase diagram for the CsTFH/^2H_2O, CsPFO/^2H_2O, CsHFN/^2H_2O, and CsNFD/^2H_2O systems in reduced phase transition temperature T/T(Tcp) volume fraction ϕ space. The values of the tricritical point (Tcp) temperature for the four systems are given in the text. The symbols represent the CsTFH/^2H_2O (△), CsHFN/^2H_2O(○), and CsNFD/^2H_2O (□) systems.

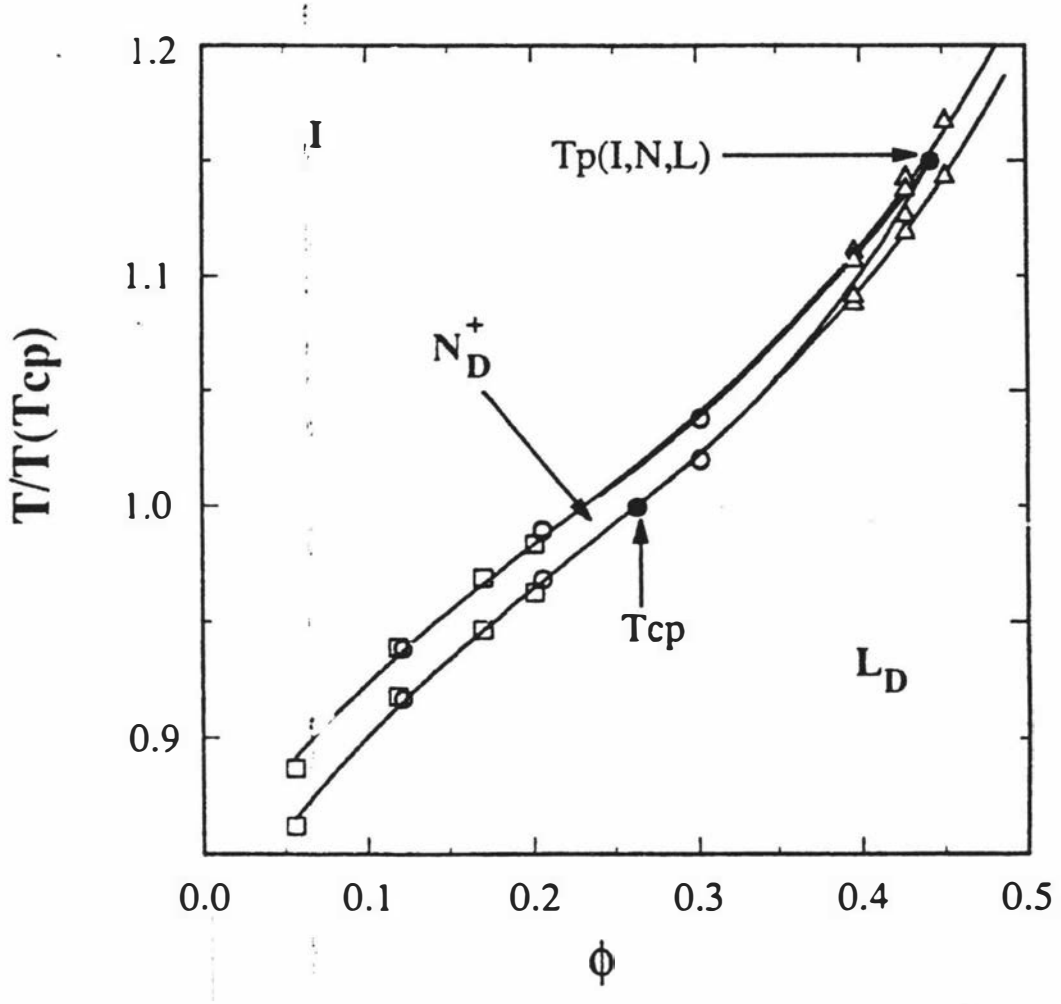

x_a/x_w . It has been shown for the CsPFO/^2H_2O system that the terms χ_D, n_b and S_{OD} remain constant over the temperature and concentration range of the nematic phase[5], and therefore

$$\frac{\Delta\tilde{\nu}(^2H)}{x_a/x_w} = K\langle P_2(\cos\alpha)\rangle_S S$$

where $K(=\frac{3}{2}\chi_D n_b S_{OD})$ contains all the terms which are constant (*c.f.* equation[3.20]). The quantity $\Delta\tilde{\nu}(^2H)/(x_a/x_w)$ is a sensitive function of the micelle a/b ratio through the $\langle P_2(\cos\alpha)\rangle_S$ term[5].

A plot of $\Delta\tilde{\nu}(^2H)/(x_a/x_w)$ as a function of ϕ is given in figure 5.5. The upper curve is for the lamellar-to-nematic phase transition boundary, while the lower curve is for the nematic-to-isotropic one. The coincidence of the $\Delta\tilde{\nu}(^2H)/(x_a/x_w)$ values at corresponding ϕ values for all four systems along the transition curves is striking.

Along T_{LN} the order parameter S is essentially constant[8], so the general decrease in $\Delta\tilde{\nu}(^2H)/(x_a/x_w)$ with increasing ϕ is due to a corresponding decrease in $\langle P_2(\cos\alpha)\rangle_S$[5]. A decrease in $\langle P_2(\cos\alpha)\rangle_S$ corresponds to an increase in the aspect ratio a/b. Considering that a corresponds to the length of the minor axis which is determined by the length of the amphiphile chain the aspect ratio can only increase if b decreases, that is the oblate micelle decreases in diameter. The decrease in micelle size as a function of increasing amphiphile concentration along the T_{LN} transition line is consistent with previous findings[9]. The coincidence of the $\Delta\tilde{\nu}(^2H)/(x_a/x_w)$ vs ϕ along the nematic-to-lamellar curve, irrespective of the length of the amphiphile chain, suggests at least a "corresponding states" kind of behaviour. That is, the nematic to lamellar transition occurs when the micelles attain a given a/b ratio for a particular volume fraction.

Along T_{NI} $\Delta\tilde{\nu}(^2H)$ is determined by changes in both $\langle P_2(\cos\alpha)\rangle_S$ and S. With increasing surfactant concentration S increases and $\langle P_2(\cos\alpha)\rangle_S$ decreases[5]. From ϕ values of 0.45 to 0.20 it is the decrease in S which dominates, but at lower ϕ values the rate of decrease in S is small and the increase in $\langle P_2(\cos\alpha)\rangle_S$ with decreasing ϕ results in the observed increase in $\Delta\tilde{\nu}(^2H)/(x_a/x_w)$. The coincidence of the values of $\Delta\tilde{\nu}(^2H)/(x_a/x_w)$ vs ϕ, irrespective of chain length, along the isotropic to nematic curve, suggests that this transition also occurs when the micelles attain a given a/b ratio at a particular ϕ. The conclusion is reinforced by recalling that the width of the I/N_D^+ phase is independent of chain length. $T_{IN} - T_{NI}$ is related to the strength of the transition and hence to the value of S at T_{NI}. Figure 5.2 suggests that S has the same value at T_{NI} for all the systems.

Figure 5.5 Plot of the quantity $\Delta\tilde{\nu}(^2H)/(x_a/x_w)$ measured along the isotropic-to-nematic transition line (lower trace) and the nematic-to-lamellar transition line (upper trace) versus volume fraction of amphiphile ϕ for the CsTFH/^2H_2O (△), CsPFO/^2H_2O(●), CsHFN/^2H_2O (○), and CsNFD/^2H_2O (□) systems.

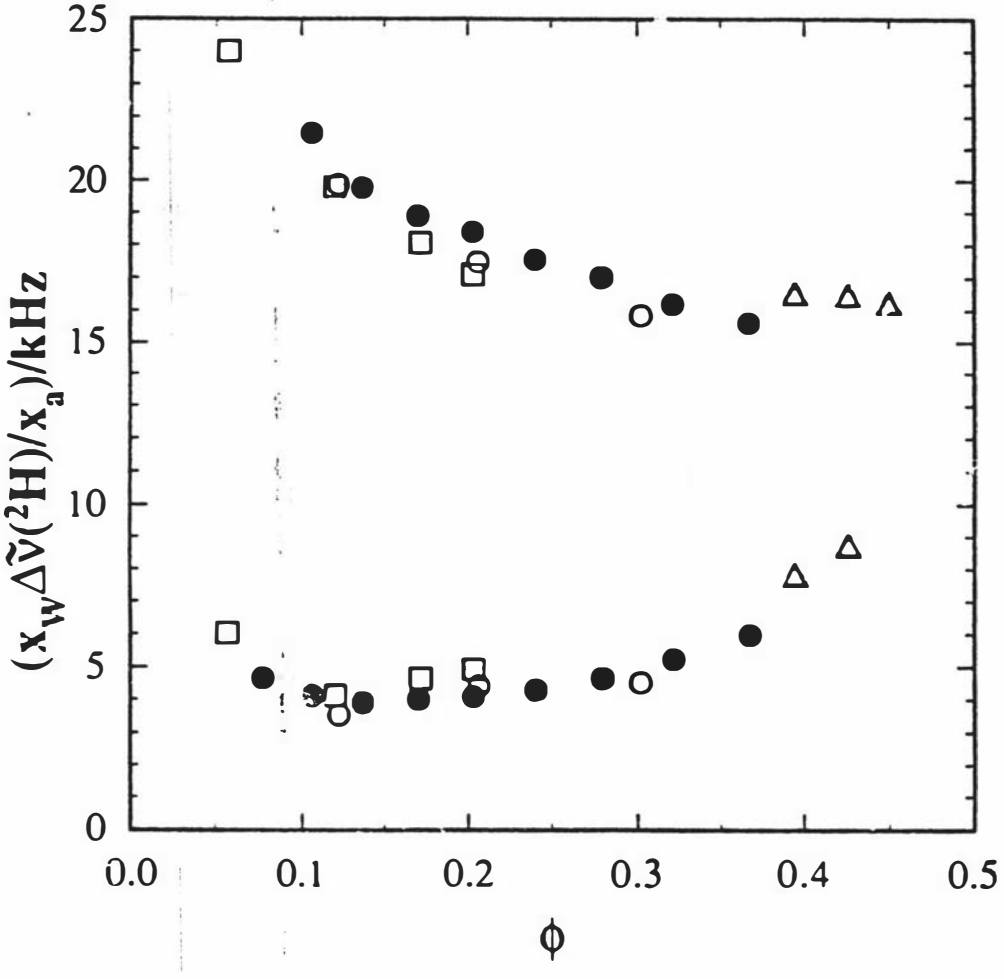

Similar conclusions (to those above) have recently been reached from considering the ^{133}Cs quadrupole splittings along the I-to-N_D^+ and N_D^+-to-L_D transition lines in the two systems CsPFO/H_2O and CsPFO/^2H_2O[9]. In the latter case, however, whilst the micelle axial ratios in the two systems along the N_D^+-to-L_D transition line were identical, there was a small isotope effect along the I-to-N_D^+ transition line.

Along both the I-to-N_D^+ and N_D^+-to-L_D transition lines in figure 5.5 the a/b ratio for the micelle must be the same. This does not, of course, mean that they have the same aggregation number since the chains have different lengths. The only system for which micelle aggregation numbers have been determined is CsPFO/^2H_2O. It is possible to estimate the micelle aggregation numbers for other systems by normalising to these data. Taking a to be the length of the fluorocarbon chain from the terminal fluorine of the CF_3 group to the centre of the α-carbon of the carboxylate carbon (= 0.186+0.130Nc, where Nc is the number of carbons in the fluorocarbon chain[8]) and calculating the volume of the amphiphile from[10] $V_A = \{3.6 + (n-8) \times 0.381\} \times 10^{-28} m^3$, where the volume of CsPFO is $3.6 \times 10^{-28} m^3$ and $0.381 \times 10^{-28} m^3$ is the volume of one CF_2 group[8], we can calculate the micelle aggregation number from $\bar{s} = (4\pi ab^2/3) / V_A$ at any given a/b ratio. At $\phi = 0.2$ for the C8 amphiphile, the axial ratio a/b is 0.278 and $\bar{s} = 200$[11]. The corresponding $\bar{s}$ values for the C7, C9 and C10 systems are 155, 250, and 310 respectively. This is further evidence the transition is mainly driven by excluded volume interactions, since if van der Waals attractive forces were also significant we would expect these to increase as the size of the micelle increased.

The increase in the temperature range of the nematic phase with increasing chain length can also be interpreted in terms of the self-association of the fluorocarbon chains. At $\phi = 0.2$ the nematic temperature range (T_{NI}-T_{LN}) for the C8, C9 and C10 systems are 5.70, 7.18 and 8.56 K respectively. At this concentration the a/b ratio for the CsPFO/^2H_2O system at T_{LN} is 0.24[9]. This represents a growth in $\bar{s}$ for the C8 system from 200 at T_{NI} to 265 at T_{LN}. The corresponding growth for the C9 and C10 systems are from 250 to 340 and from 310 to 420 respectively, *i.e.* the micelle aggregation number needs to increase by progressively greater amounts as the chain size increases in order for the desired a/b ratio to be obtained. It is interesting to note that $\partial\bar{s} / \partial T$ is about 12 for all the systems. Of course, for the explanation of the increases in the temperature range of the nematic phase to be valid, $\partial\bar{s} / \partial T$ must be the same for all four surfactant systems. This may not be the case.

The observation of constant a/b ratios along both the I-to-N_D^+ and L_D-to-N_D^+ transition lines is consistent with a hard particle interaction being the driving force for both transitions. In the following sections this premise will be examined further by comparing the actual a/b ratios at the transitions with those predicted by various hard particle models.

5.4. Comparison of Phase Behaviour with Hard Particle Models

The experimental results have shown that at a fixed volume fraction ϕ the aspect ratio *a/b* of the micelle at the isotropic-to-nematic and nematic-to-lamellar transition is independent of the amphiphile chain length. A plot of both theoretical and experimental values for *a/b* versus ϕ at both the isotropic-to-nematic (a) and nematic-to-lamellar (b) transition is presented in figure 5.6. The experimental results are only represented by the CsPFO/^2H_2O system as this system has experimentally determined axial ratios[5, 9] but as stated above, this plot is representative of all the systems studied. The APFO/^2H_2O system data are also included for a comparison between systems.

The agreement between the TH hard particle model at higher surfactant volume fractions is very good at T_{NI} (figure 5.6(a)). The deviation at lower volume fractions towards smaller than predicted micelles suggest a greater effective diameter increasing with dilution. Correcting for the Debye lengths of 0.420 nm at Tp(I,N,K) and 0.215 at Tp(I,N,L) does not account for the deviations, nor does the inclusion of a hydration ion shell, decreasing in extent with temperature. It has been suggested that a possible explanation is an additional interaction which increases with the micelle anisotropy[5]. The origin of the extra interaction is unclear. It could arise from increasing anisotropic van der Waals forces as the *a/b* ratio decreases but this is pure speculation at this stage.

The poor agreement between the TH model and experimental results along the lamellar-to-nematic transition indicate that the method used to model the onset of translational ordering is inadequate. In the CsPFO/^2H_2O system the volume fraction dependence of the *a/b* ratios at T_{NL} and T_{LN} run parallel to each other with a slight displacement to higher ratios at T_{LN} and in both cases *a/b* increases with increasing volume fraction. The model predicts that along T_{LN} *a/b* decreases with increasing ϕ. In addition at T_{LN} the predicted axial ratios are far too small. Taylor and Herzfeld have acknowledged that their cell description of the lamellar phase is somewhat crude[12]. The parallel behaviour exhibited along T_{NI} and T_{LN} in the CsPFO/^2H_2O system suggests that the driving force for the N_D^+-to-L_D transition is the same as that for the N_D^+-to-I transition.

Since a hard particle description applies equally well to all the systems, the dependence in the observed phase transition temperatures must be a consequence of changes in the aggregate self-assembly. This will now be examined in the context of the MBG model.

Figure 5.6(a) Comparison of the nematic phase volume fractions and aggregate sizes at T_{NI} in the CsPFO/^2H_2O(■) and APFO/^2H_2O(●)with predictions of the Taylor-Herzfeld(TH) model[12]. (b) Comparison of the nematic and lamellar phase volume fractions and aggregate sizes at the T_{LN} with predictions of the TH model.

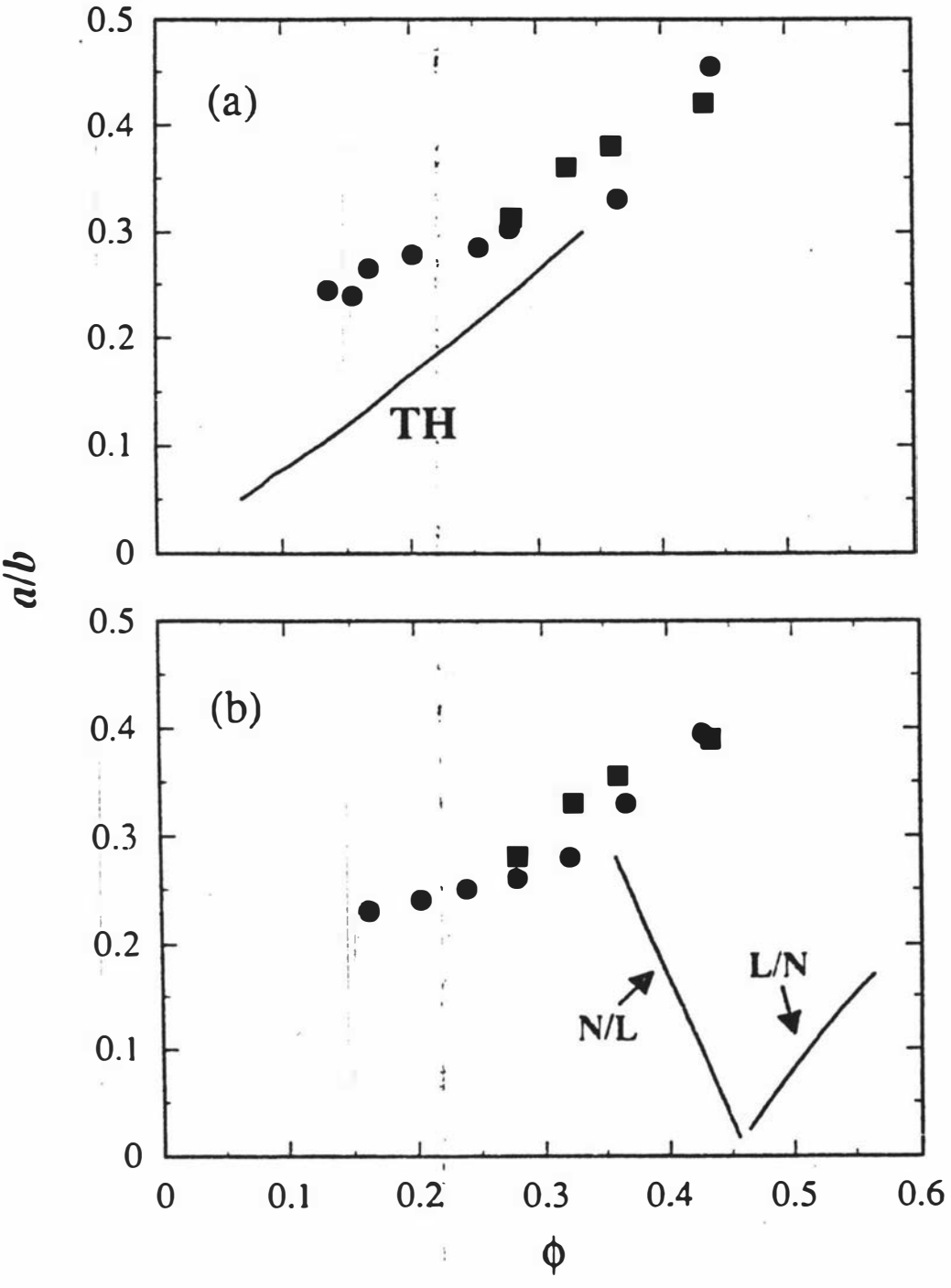

5.4.1. Effect of Changing Chain Length on Micelle Size

The predicted effect of changing the chain length on the aggregation process can be examined using equation[4.6] of the MBG model. A value for y of 0.430 was chosen to be consistent with the region of discotic micelle stability. The dependence of the chemical potential of the isolated monomer on the chain length has been shown to be the order of 1.2 kT per methylene group[13, 14] and in the absence of information on corresponding CF_2 groups this figure will be used here. Calculations were first performed on the C8 system[9] and a value for μ_0^1 of 15 kT was used[15]. Accordingly the value for the C7, C9 and C10 monomers have been assigned respective chemical potentials of 13.8, 16.2 and 17.4 kT. The interfacial tension γ_1 was set at 0.025 J m^{-2} a value which is roughly half that for the perfluorohexane-water interface[9]. The length and volume of the monomer chain can be determined by taking l to be the length of the fluorocarbon chain from the terminal fluorine of the CF_3 group to the centre of the α-carbon to carboxylate carbon ($l = 0.186 + 0.130\,Nc$, where Nc is the number of carbon's in the fluorocarbon chain[10]) and calculating the volume of the amphiphile from $V_A = \{3.6 + (Nc - 9) \times 0.381\} \times 10^{-28}\,m^3$, where the volume of the CsPFO amphiphile[8] is $3.6 \times 10^{-28}\,m^3$ and $0.381 \times 10^{-28}\,m^3$ is the volume of one CF_2 group[10]. The minimum micelle aggregation number is calculated from $s_{min} = (4\pi l^3/3) / V_A$ (see table 5.1). For the purpose of this discussion the actual values chosen are not critical, rather it is the effect that changing the length of the amphiphile chain has on the micelle size distribution.

Table 5.1 Calculated amphiphile dimensions

Number of carbons	Length of chain (nm)	Volume of chain (nm^3)	Minimum micelle aggregation number
7	0.966	.322	12
8	1.096	.360	15
9	1.226	.398	19
10	1.356	.436	24

Comparisons were made at a constant total surfactant mole fraction of 5×10^{-4} and at a fixed temperature of 300 K. The micelle size distributions as a function of chain length are shown in figure 5.7. The figure shows that the model predicts an increase in the micelle size as a function of chain length, the number average aggregation numbers S_n for C7, C8, C9 and C10 have been calculated to be 32, 94, 263 and 964 respectively. To maintain a constant amphiphile mole fraction, x_1 had to be reduced as a function of increasing chain length with the mole fraction of monomer in

Figure 5.7 Micelle size distributions at 300 K and a fixed total amphiphile mole fraction of 5.069 x 10^{-4} as calculated using the MBG model of self-assembly. Details of the calculations and the parameters used are given in the text.

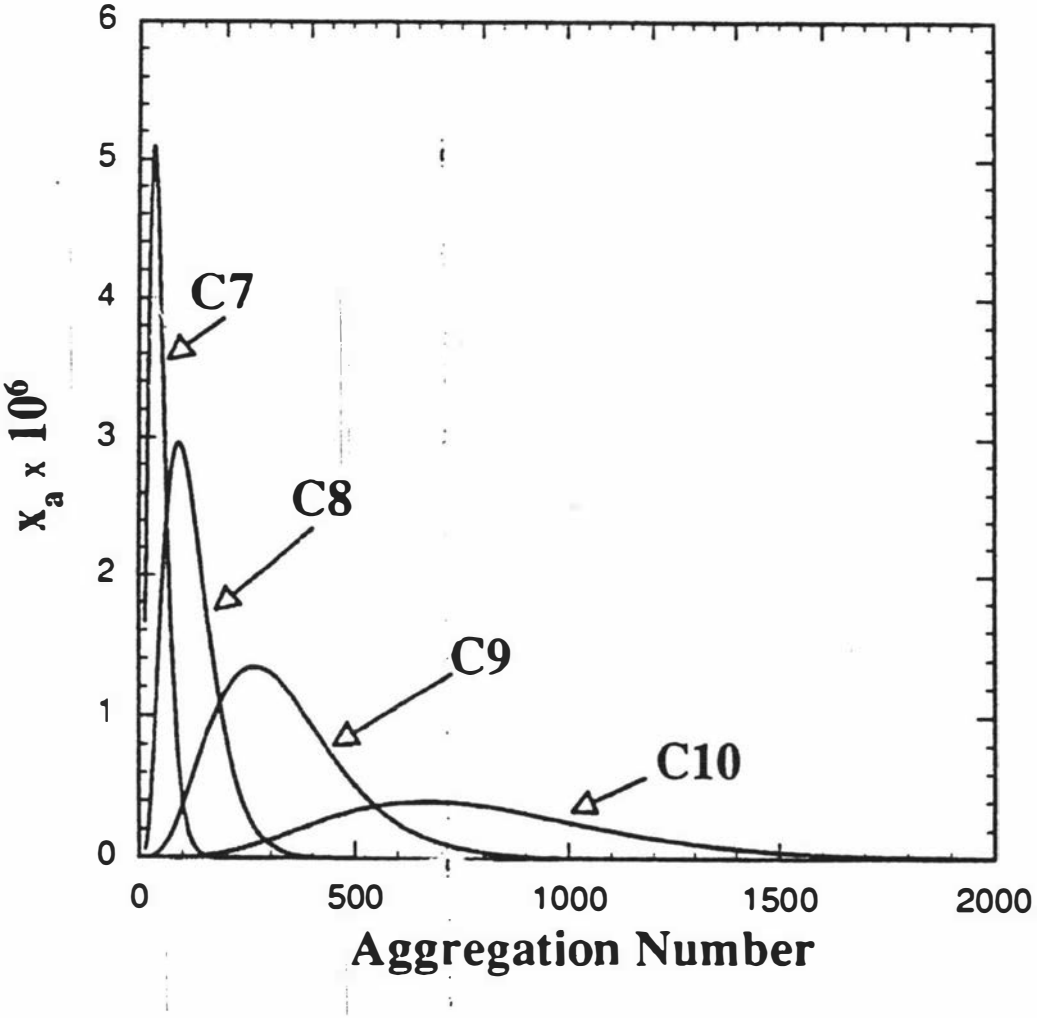

solution for C7, C8, C9 and C10 having mole fractions of $x = 4.167 \times 10^{-4}$, 1.235×10^{-4}, 3.544×10^{-5} and 1.017×10^{-5} respectively, a result which is consistent with the decrease in the cmc value as the amphiphile chain length is increased[3, 16].

The MBG model allows the surfactant molecule in a discotic micelle to reside in one of two sites *i*, the rim or the cap of the disc. The chemical potential of the surfactant in the micelle is the weighted average chemical potential of each of the two sites. Predicted increases in the micelle size distribution as a function of increasing chain length can be understood phenomenologically by considering the surfactant chemical potential in each of the sites. As the chain length increases the rim sites will have a higher chemical potential due to the increase in both the curvature free energy of the chain and the interfacial tension. This may be offset to some extent by a decrease in the electrostatic repulsion. Chains in the cap, however, will experience a greater attraction for each other and this will lead to a decrease in the chemical potential of a cap molecule with increasing chain length. Thus, longer chains favour larger micelles.

An increase in the micellar size distribution with increasing amphiphile chain length is in accord with the experimental observations. It is possible to account for the form of the phase diagram of the analogues in terms of the micelle distribution. As the chain length is increased at any given volume fraction there is an increase in the size of the micellar distribution, therefore the temperature must be increased to decrease the micellar size distribution[8] to attain an appropriate eccentricity for the transition to occur. As the chain length increases the phase transition boundaries are displaced to higher temperatures (figure 5.1).

5.4.2 Effect of Temperature on Micelle Size

Using the MBG model the increase in size of the micelle with increasing fluorocarbon chain length is explained by an increase in the factor $g(a)$ of equation[4.1] due to a concomitant increase in the splay elasticity associated with an increasing radius of curvature of the micelle rim. However, arguments based purely on changes in the rim curvature would predict an increase in micelle size with increasing temperature as the curvature energy of the rim increases, the opposite to what is observed. In addition, the similar temperature dependence of the phase transition temperatures in all four surfactant systems (figure 5.4) is inconsistent with the notion that it is the chain interactions which are responsible for the temperature dependence of micelle size.

The origin of the observed decrease in micelle size with increasing temperature is most likely the effect of temperature on the binding of the ions at the surface of the micelle. The isotope effect on the phase behaviour of the CsPFO/water system on substituting water for heavy water has been attributed to tighter binding of Cs^+ ions to the surface carboxylate groups *via* bridging water molecules in the case of ^2H_2O[9]. The micelle size decreases as the temperature is raised is similarly accounted for in terms of

bonding through a bridging water molecule. On raising the temperature, the hydrogen-bond will weaken, that is, the COO^--Cs^+ distance will increase and the screening of the repulsive force will be reduced. Thus, the average optimum headgroup area a_0 will increase and there will be a corresponding decrease in micelle size.

The TH theoretical phase diagram for the self-assembling discotic system[12] is compared with the phase diagram of the CsPFO/^2H_2O system[5, 8, 17](see figure 5.8). There are similarities between the topology of these two phase diagrams. In both phase diagrams the temperature of the I-to-N_D^+ transition is displaced to higher values with increasing volume fraction as a consequence of a reduction in the aggregate size with increasing temperature. Also in both diagrams the width of the isotropic/nematic mixed phase region increases with increasing volume fraction of micelle but the width of this region is much greater in the theoretical phase diagram. At the triple point the isotropic, nematic, and smectic phases coexist at volume fractions $v_p^I = 0.425$, $v_p^N = 0.431$ and $v_p^S = 0.448$, respectively, which differ from the calculated triple point at $v_p^I = 0.28$, $v_p^N = 0.36$ and $v_p^S = 0.55$. The absence of the nematic-to-lamellar tricritical point from the model phase diagram is due to the crude cell constant description of the smectic phase, which precludes the possibility of a continuous transition from the nematic. The TH phase diagram does however reproduce weakening of the first order nematic-to-lamellar transition with decreasing temperature. The predicted phase diagram also has only a small composition dependence for the nematic-to-lamellar transition, while the CsPFO/^2H_2O system has been shown to have a marked composition dependence to this transition. In addition, the width of the mixed phase region associated with the lamellar-to-nematic transition is predicted to be much greater than is observed for the CsPFO/^2H_2O system. The columnar phase, which is predicted to occur at high temperatures and volume fractions, has not been observed in the CsPFO/^2H_2O system. Overall the model demonstrates many of the features of the real systems phase behaviour especially at the nematic-to-isotropic transition, but there are discrepancies at the nematic-to-lamellar phase transition. The differences between the phase diagrams lies in the difference between a/b vs ϕ curves and the temperature dependence of the soft interactions which are significant at low concentrations. The predominant effect of temperature is to cause a reduction in the size of the micelle which necessitates going to higher concentrations in order to induce the phase transition.

Figure 5.8 Comparison of the theoretical phase diagram for a self-assembling disc-like system (a) with the phase diagram for the CsPFO/^2H_2O system (b). In (a) Φ is the magnitude of the free energy of association of each monomer-monomer contact within the aggregate which is assumed to increase linearly with T^{-1}, and ϕ_p is the particle volume fraction.

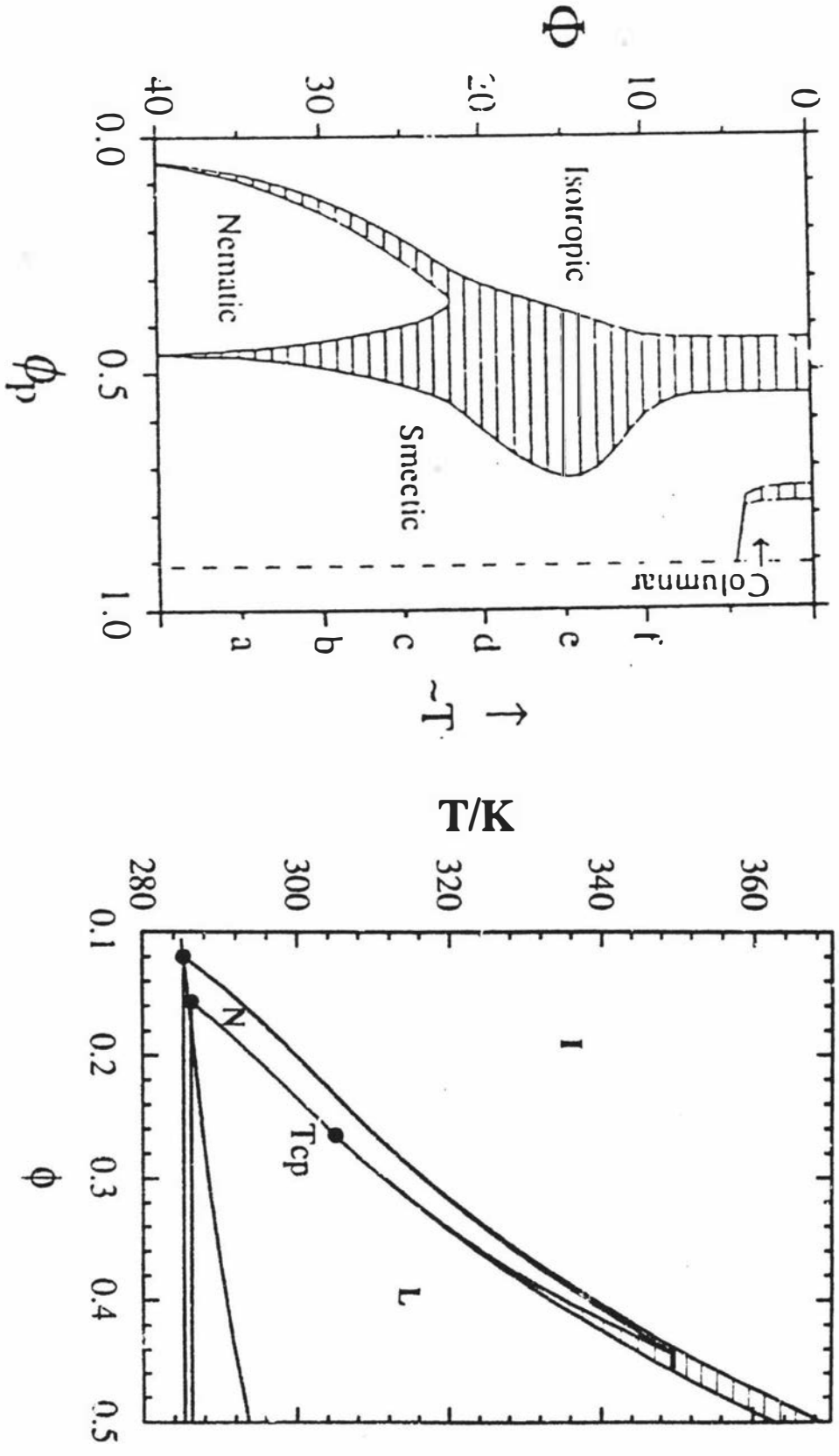

5.5 Concluding comments

The universal phase behaviour, for surfactants of a given counter-ion but with different chain lengths, exhibited by these systems is of practical importance for future studies on the self-association and self-organisation at the extreme concentration regimes. To examine the phase behaviour at high volume fractions, the C7 salt is the obvious choice since the lamellar phase is present over a readily accessible temperature range, similarly, at low volume fraction of surfactant, the C9 or C10 systems are the obvious ones to study.

The isotropic-to-nematic transition line seems to be determined by hard particle interactions at high concentrations whilst longer range soft interactions may become important at lower concentrations. The latter could affect the strong temperature dependence of the phase behaviour, though this is predominantly due to the effects of temperature on the self-assembly of the micelle. The variation of the phase behaviour with fluorocarbon chain length reveals the importance of the curvature free energy of the surfactant film in determining the micelle size. However, this does not account for the decrease in micelle size with increasing temperature. This has been identified as arising from the effects of temperature on the binding of caesium ions to the micelle surface.

References

1. N. Boden, P. J. B. Edwards, K. W. Jolley, in *Structure and Dynamics of Strongly Interacting Colloids and Supramolecular Aggregates in Solution* S.-H. Chen, J. S. Huang, P. Tartaglia, Eds. (Kluwer academic Publishers, Dordrecht, 1992), vol. 369, pp. 433-461.

2. A. N. Parbhu, Master of Science, Massey University (1990).

3. K. Fontell, B. Lindman, *J. Phys. Chem.* **87**, 3289-3297 (1983).

4. K. Reizlein, H. Hoffmann, *Progr. Colloid & Polymer Sci.* **69**, 83-93 (1984).

5. N. Boden, S. A. Corne, K. W. Jolley, *J. Phys. Chem.* **91**, 4092-4105 (1987).

6. N. Boden, K. W. Jolley, M. H. Smith, *Liq. Cryst.* **6**, 481-488 (1989).

7. G. Oriques, Ph. D., University of Leeds (1993).

8. N. Boden, S. A. Corne, M. C. Holmes, P. H. Jackson, D. Parker, K. W. Jolley, *J. Physique* **47**, 2135-2144 (1986).

9. N. Boden, K. W. Jolley, M. Smith, *J. Phys. Chem.* **97**, 7678-7690 (1993).

10. N. Boden, J. Clements, K. W. Jolley, D. Parker, M. H. Smith, *J. Chem. Phys.* **93**, 9096-9105 (1990).

11. M. C. Holmes, D. J. Reynolds, N. Boden, *J. Phys. Chem.* **91**, 5257-5262 (1987).

12. M. P. Taylor, J. Herzfeld, *Physical Review A* **43**, 1892-1905 (1991).

13. M. Jansson, B. Jonsson, *J. Phys. Chem.* **93**, 1451-1457 (1989).

14. R. Nagarajan, E. Ruckenstein, *Langmuir* **7**, 2934-2969 (1991).

15. W. E. McMullen, A. Ben-Shaul, W. M. Gelbart, *J. Colloid Interface Sci.* **98**, 523-536 (1984).

16 S. B. L. Cser, Y. M. Ostanevich, S. Vass, *J. Phys. Chem.* **93**, 7967-7969 (1989).

17 N. Boden, P. H. Jackson, K. McMullen, M. C. Holmes, *Chem. Phys. Lett.* 65, 476-479 (1979).

Chapter 6
Effect of Added Electrolyte on the Self-Assembly and Self-Organization in the APFO/^2H_2O and CsPFO/^2H_2O Systems

Most ionic amphiphile lyotropic liquid crystal systems require the addition of an electrolyte and/or cosurfactant to exhibit a nematic phase. This observation implies that electrolytes can play an influential role in the self-assembly and self-organisation of micellar liquid crystals. Considering that the aggregates of ionic amphiphiles have charged surfaces it is not surprising that electrolyte will have an influence. The question that is posed is what role does the electrolyte play in modifying the nature and mechanism of the phase transitions *i.e.* how does electrolyte effect the intra-and inter-micellar interactions.

The first section of this chapter further develops the use of deuterium quadrupole splittings of ^2H_2O as a probe to determine changes in the size of discotic aggregates of the binary APFO/^2H_2O[1] system, whilst the second section applies ^2H NMR to aggregate structure investigations in the CsPFO/CsCl/^2H_2O and APFO/NH_4Cl/^2H_2O systems. For the CsPFO/CsCl/^2H_2O system, in addition to aggregate structure information from the ^2H quadrupole splittings, information about changes in the counter-ion β_{Cs} and co-ion binding β_{Cl} has been obtained from the ^{133}Cs and ^{35}Cl quadrupole splittings [2, 3](see equations[3.21] and [3.23]).

6.1 The NMR Model to Probe Aggregate Structure

A model of the relationship between the deuterium quadrupole splittings and the mesophase order and aggregate structure has been developed and used in both the APFO/^2H_2O and CsPFO/^2H_2O binary systems[1, 4]. In both these systems it was clearly demonstrated that changes in the ^2H quadrupole splittings could be identified with changes in the orientational order parameter S and $\langle P_2 \cos\alpha \rangle_s$ (equation 3.19) as determined from x-ray and conductivity measurements. For the binary APFO/^2H_2O system the model has only been tested on a APFO/^2H_2O ($w_a = 0.45$) sample from T_{NI} to T_{LN} - 5 K[1], while for the binary CsPFO/^2H_2O system it has been tested along the nematic-to-isotropic transition[4]. The micelles were assumed to be discotic ellipsoids and whilst it is conceivable that in the dilute lamellar phase these discotic micelles are arranged on equidistant planes, at higher concentrations, because of micelle packing constraints and interlayer repulsive forces, more complex lamellar configurations, such as perforated bilayers etc, must ensue until eventually classical bilayers prevail. The assumption of discotic micelles would, therefore, no longer be valid and the model must fail.

In this section the relationship between the ^2H quadrupole splittings and the mesophase structure and order will be tested at other concentrations of the binary APFO/^2H_2O system to determine if the fit of the discotic aggregate model still applies over a range of temperatures and concentrations. Order parameter data from electrical conductivity measurements and axial ratio data from low angle x-ray scattering experiments were provided by co-workers at Leeds University[5], see figures 6.1 and 6.2.

The binary APFO/^2H_2O system is an excellent system to study as its aggregate structure can be directly analysed by low angle x-ray scattering experiments, which is difficult in the CsPFO/^2H_2O system as the caesium ions are strong absorbers of x-rays. A comprehensive phase diagram has been produced for the binary APFO/^2H_2O system (see figure 6.3) and there is a detailed understanding of the phase behaviour[1]. The APFO/^2H_2O system is qualitatively similar and exhibits the same phase behaviour as the CsPFO/^2H_2O system[1].

In order to determine the order parameter and axial ratio from experimental data the geometry of the aggregate has to be defined. Both the order parameters and axial ratios have been calculated assuming that the aggregate consists of oblate ellipsoids. For this geometry $\langle P_2 \cos\alpha \rangle_s$ is related to the axial ratio (a/b) of the micelle by[4]

$$\langle P_2(\cos\alpha)\rangle_s = \frac{1}{2}\left\{3\nu^{-2}\left(\frac{1-p}{1+p}\right)-1\right\} \qquad [6.1]$$

where

$$p = \frac{1-\nu^2}{2\nu}\ln\left(\frac{1+\nu}{1-\nu}\right) \qquad [6.2]$$

and

$$\nu = \sqrt{1-\left(\frac{a}{b}\right)^2} \qquad [6.3]$$

Quantities other than S and $\langle P_2(\cos\alpha)\rangle_s$ that contribute to the ^2H quadrupole splittings (*i.e.* $\chi_D n_b S_{OD}$ see equation[3.19]) were assumed to be constant over the temperature interval of the measurements[4]. It follows from equation[3.19] that in these circumstances, for any given sample[1],

$$\frac{\Delta\tilde{\nu}_T}{\Delta\tilde{\nu}_{T_m}} = \frac{\left(S\langle P_2(\cos\alpha)\rangle_s\right)_T}{\left(S\langle P_2(\cos\alpha)\rangle_s\right)_{T_m}}. \qquad [6.4]$$

Thus, a plot of the quantity on the left hand side verses the quantity on the right hand side of equation[6.4] may be used to test whether the discotic micelle model invoked to determine axial ratios and the order parameter is appropriate.

Figure 6.1 Order parameters S for (a) the APFO/^2H_2O ($w_a = 0.40$) sample and (b) the APFO/^2H_2O ($w_a = 0.50$) sample. For the 0.40 sample crystallisation of the amphiphile occurred in the nematic phase (see phase diagram figure 6.3). Data provided by J. Clements

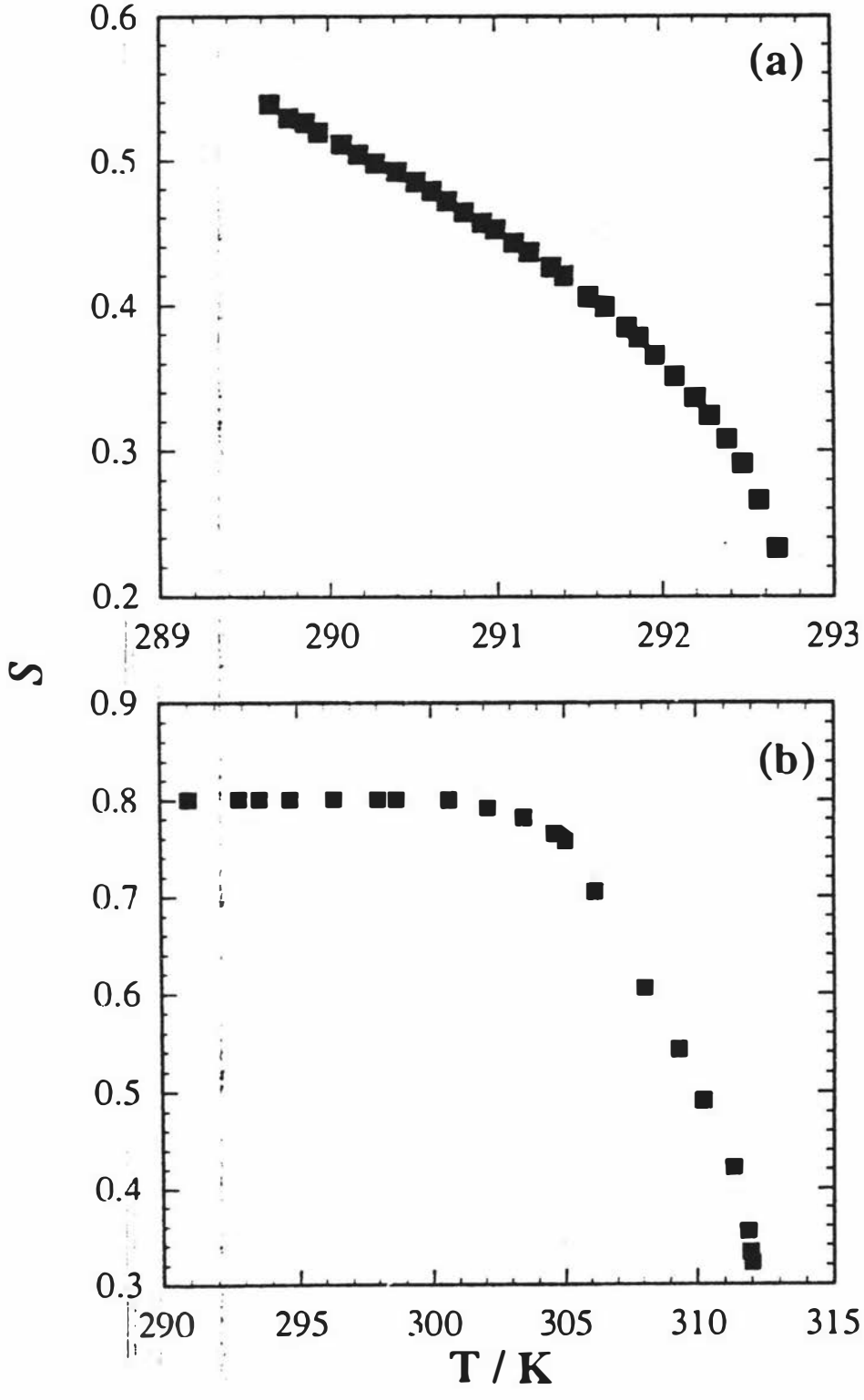

Figure 6.2 Axial ratios *a/b* for (a) the APFO/^2H_2O (w_a = 0.40) sample and (b) the APFO/^2H_2O (w_a = 0.50) sample. Data provided by J. Clements

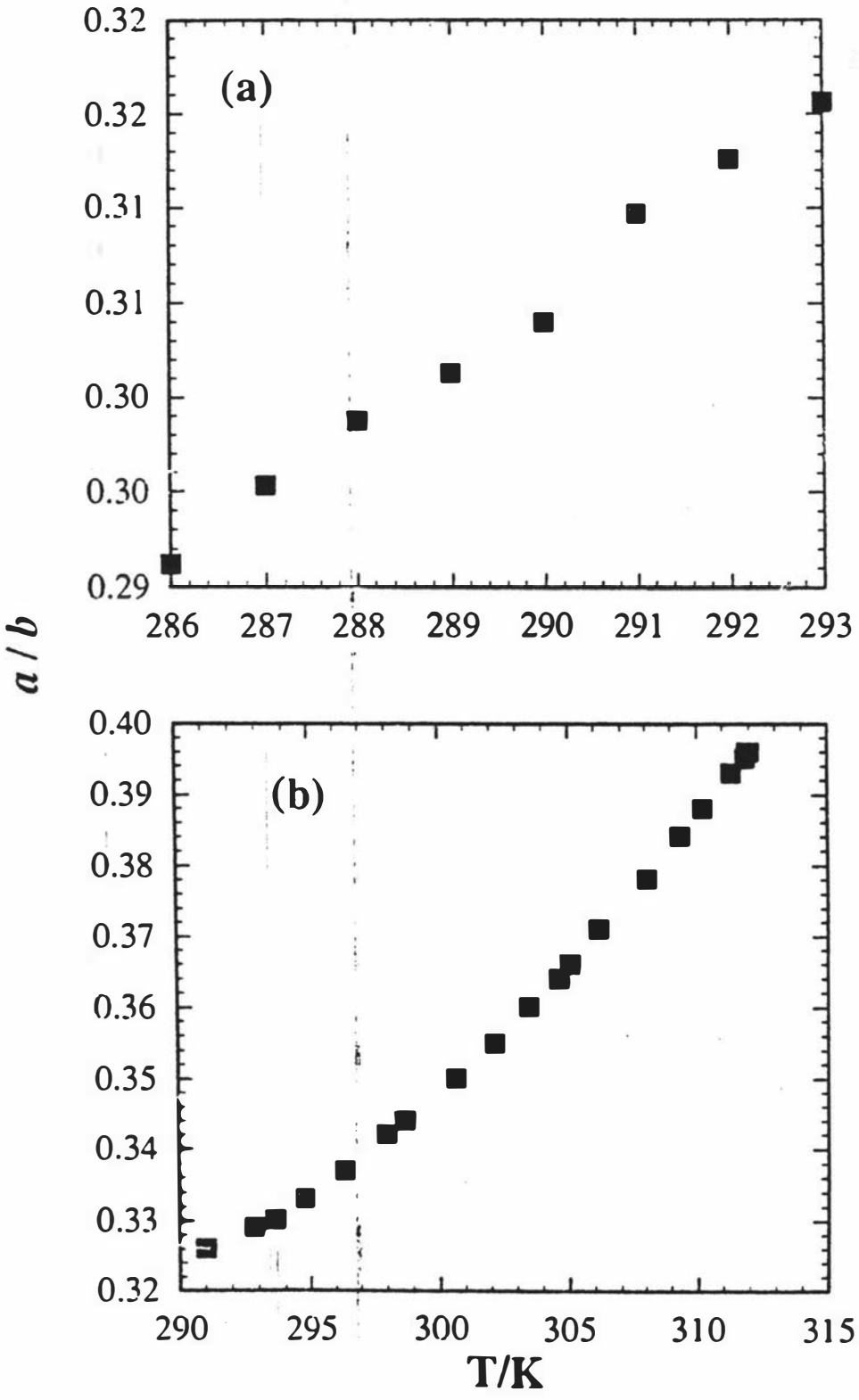

Figure 6.3 Phase diagram for the APFO/^2H_2O system[1]. Nomenclature: I, isotropic micellar solution phase; N_D^+, discotic nematic phase with positive diamagnetic susceptibility; L_D, discotic lamellar phase; K, crystal; Tcp, the lamellar-to-nematic tricritical point; Tp(I,N,K), the isotropic micellar solution-nematic-crystal triple point; Tp(I,N,L), the isotropic micellar solution-nematic-lamellar triple point; Cep, the critical end point.

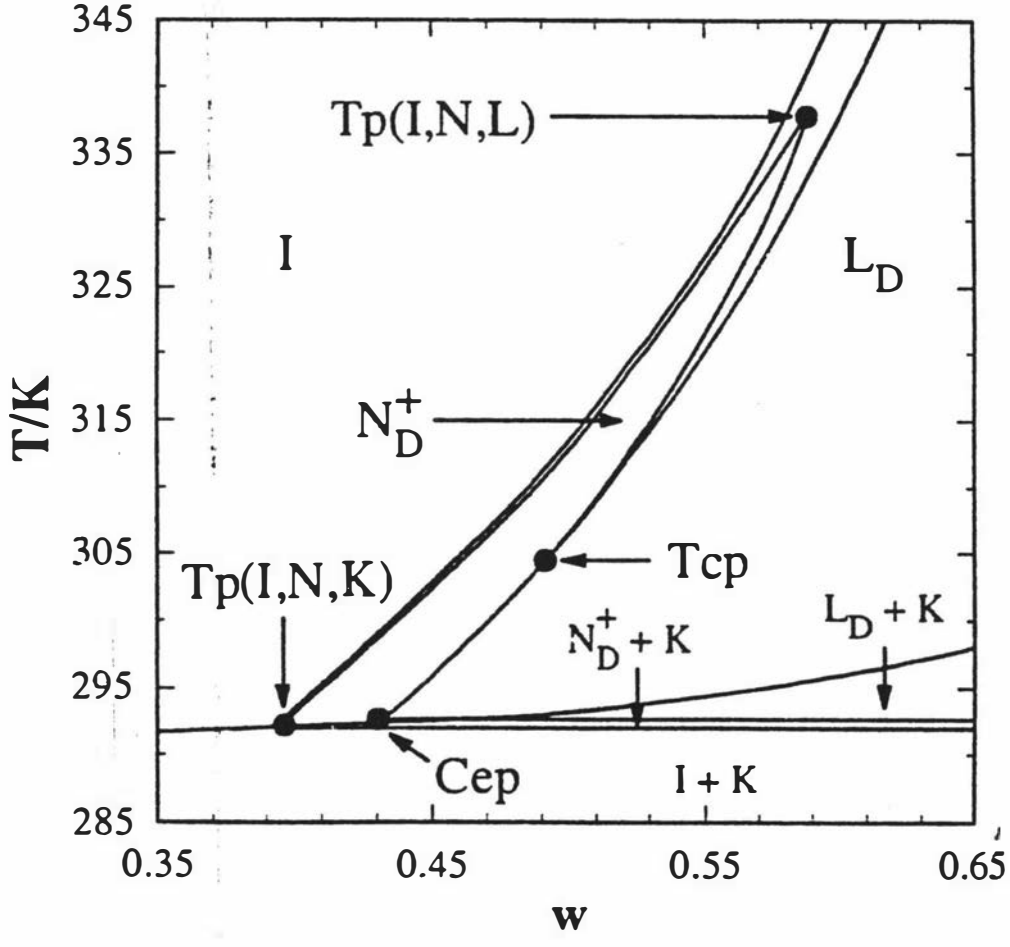

Equation[6.4] was tested from T_{NI} down to T_{NI} - 4 K and T_{NI} - 23 K for the w_a = 0.40 and 0.50 APFO/^2H_2O samples respectively. In both samples there is supercooling below the solubility curve. The actual crystallisation temperatures determine the range of the fit. The results are given in figures 6.4 and 6.5 respectively. Over the temperature range examined for each of the samples the plot of the left hand side verses the right hand side of equation[6.4] is clearly linear with a slope of unity. Thus over the temperature and composition range covered the structures of both the nematic and lamellar phase are consistent with the structural units being oblate ellipsoids. The agreement between both sides of equation[6.4] shows that measurements of the quadrupole splittings can be used to monitor changes in the micelle sizes and mesophase order with temperature and/or composition. The changes in the quadrupole splittings in the nematic phase is largely a consequence of the change in S and $\langle P_2 \cos\alpha \rangle_s$ [1, 4], whilst in the lamellar phase it is predominantly changes in the latter quantity which lead to change in $\Delta\tilde{\nu}(^2H)$.

The ability of NMR to monitor changes in micelle size and to precisely determine phase transition temperatures establishes ^2H NMR as a powerful tool in the investigation of the nature and mechanism of phase transitions in these systems. In the following section we will use the ^2H NMR model to probe the influence of electrolyte on the self-assembly and self-organisation of the APFO/NH_4Cl/^2H_2O and CsPFO/CsCl/^2H_2O systems.

6.2 Ternary Systems

6.2.1 APFO/NH_4Cl/^2H_2O System

A partial phase diagram of the APFO/NH_4Cl/^2H_2O system at a constant mass ratio of APFO to ^2H_2O of 9 : 11 is presented in figure 6.6. For the electrolyte mass fraction w_e = 0 sample the 9 : 11 ratio corresponds to a APFO mass fraction of 0.45. This ratio was chosen so as to give a nematic phase in an accessible temperature "window". The phase diagram in figure 6.6 shows a N_D^+ phase intermediate to an isotropic micellar solution phase I and what is probably a discotic lamellar phase L_D. The N_D^+ phase is stable from w_e = 0 to 0.0175 ± .0005 and from temperatures of 295.3 to 316.6 K. All the phase transition temperatures are seen to increase monotonically with increasing mass fraction of electrolyte w_e, but not to the same extent. The initial effect of adding electrolyte is to increase the temperature range of the nematic region, but as the NH_4Cl concentration increases the nematic range diminishes until it disappears altogether at w_e = 0.0175 ± .0005, T = 316.5 ± 0.05 K. This point is a critical end point Cep, where the line of second order L_D-to-N_D^+ transitions intersects with the lines of first order N_D^+-to-I and L_D-to-I transitions.

Figure 6.4 Plot of equation[6.4] for the APFO/^2H_2O (w_a = 0.40) sample. The straight line has a slope of one and an intercept of zero as predicted. The best fit values of these two quantities are 0.98(2) and -0.01(4), respectively.

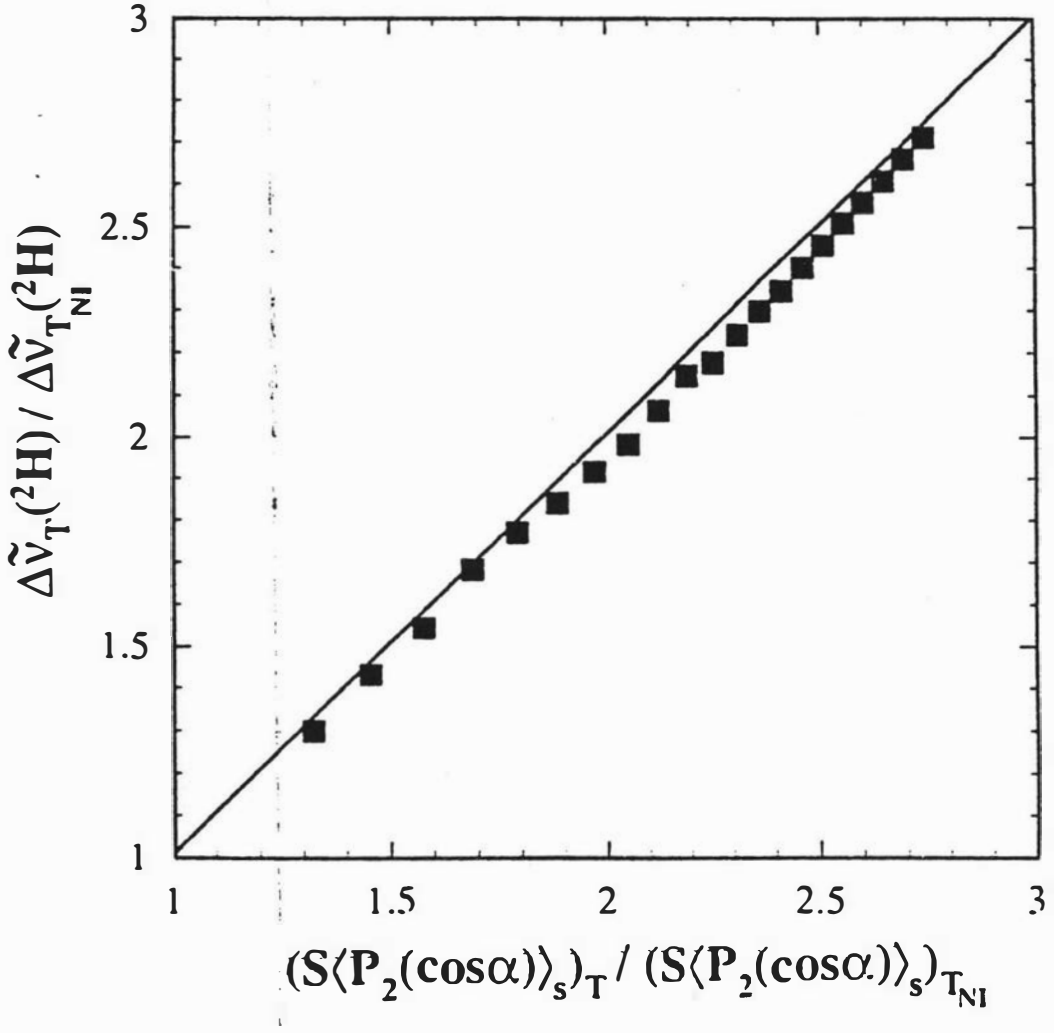

Figure 6.5 Plot of equation[6.4] for the APFO/^2H_2O (w_a = 0.50) sample. The straight line has a slope of one and an intercept of zero as predicted. The best fit values of these two quantities are 1.04(2) and 0.1(1), respectively.

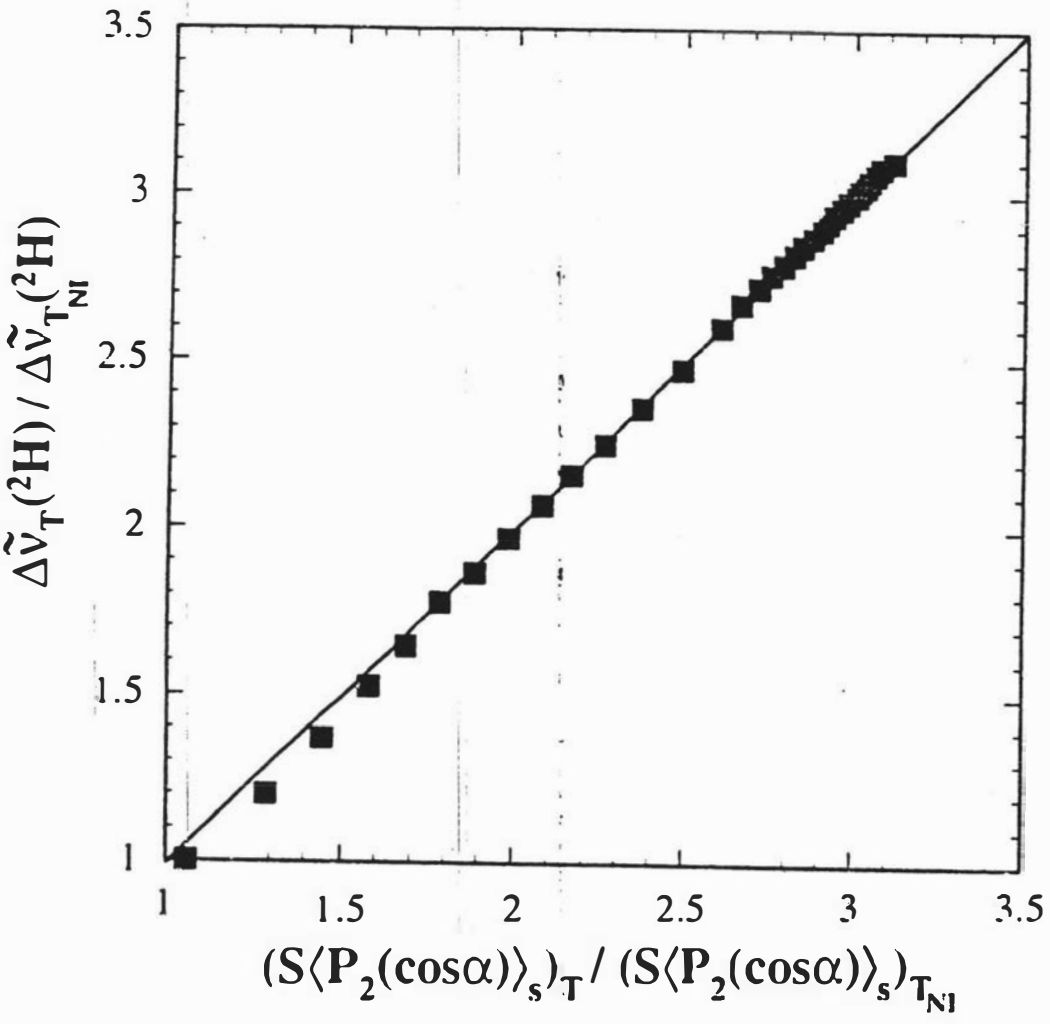

Figure 6.6 Partial phase diagram of the APFO/NH_4Cl/^2H_2O system with a mass ratio of APFO to ^2H_2O of 9 : 11 and an electrolyte mass fraction of w_e (mole ratio of 1 to 26.3).See legend to figure 6.3 for explanation of the labels.

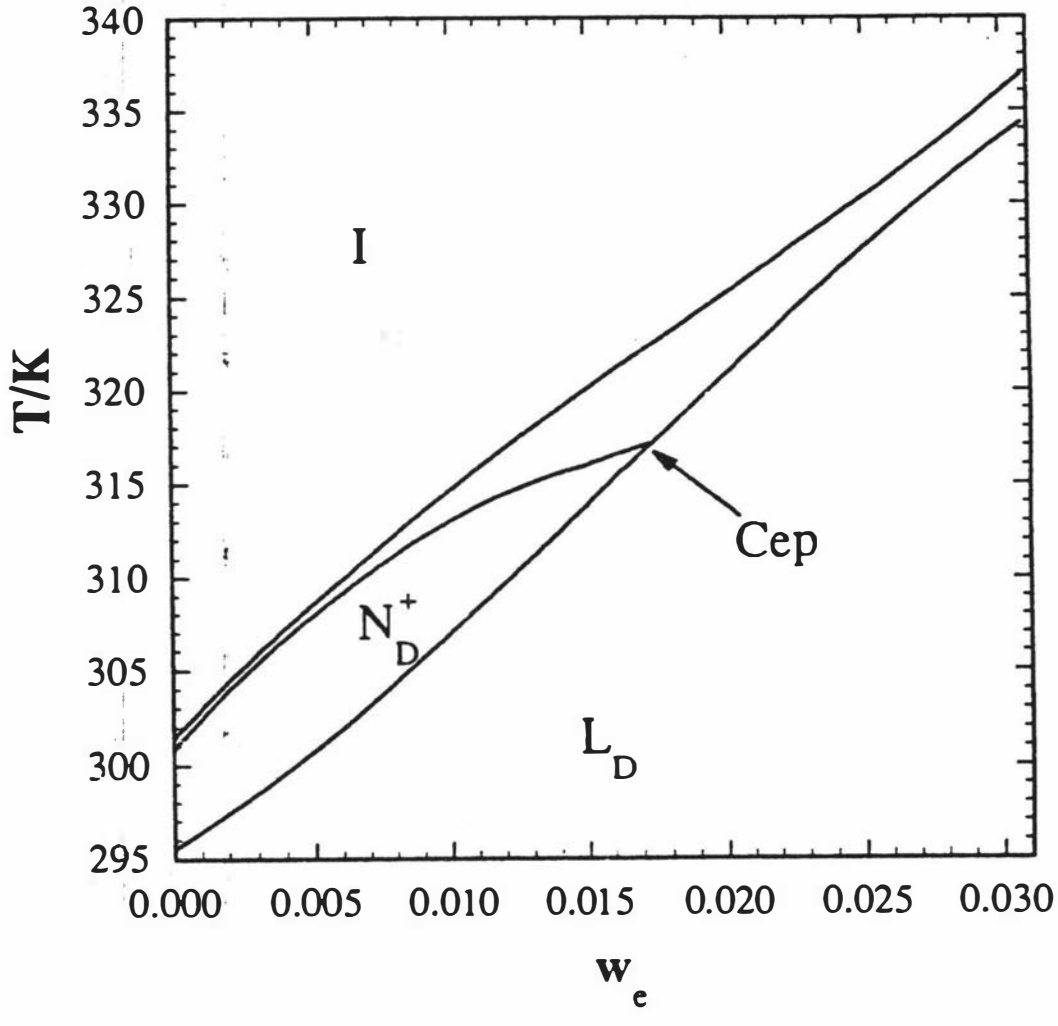

The deuterium quadrupole splittings at T_{LN}, T_{LI}, and T_{NI} are presented in figure 6.7.

The quadrupole splittings along the T_{LN}/T_{LI} boundary are seen to decrease slightly (after an initial increase) as w_e increases. For the samples considered in the present study the ratio x_a/x_w is constant and previous studies have shown that the product $\chi_D n_b S_{OD}$ is also constant over the temperature range of the liquid crystal phases[1, 2, 4]. The variation of $\Delta\tilde{\nu}(^2H)$ is therefore, representative of changes in S and $\langle P_2(\cos\alpha)\rangle_s$[1] with temperature. Equation[3.19] can then be written

$$\Delta\tilde{\nu}(^2H) = c\langle P_2 \cos\alpha\rangle_s S \qquad [6.5]$$

where c represents the terms that are independent of temperature. Along the nematic-to-lamellar transition S is constant[6], so changes in $\Delta\tilde{\nu}(^2H)$ are as a result of changes in $\langle P_2(\cos\alpha)\rangle_s$. Thus $\langle P_2(\cos\alpha)\rangle_s$ must only change slightly along the L_D-to-N_D^+ and L_D-to-I transition lines. The implication of this is that the micellar size and shape changes little along this transition line.

Along T_{NI}, $\Delta\tilde{\nu}(^2H)$ increases with increasing w_e and intersects with the upper curve at Cep. At the nematic-to-isotropic transition $\Delta\tilde{\nu}(^2H)$ is a function of both $\langle P_2 \cos\alpha\rangle_s$ and S. Thus the addition of electrolyte causes an increase in both $\langle P_2 \cos\alpha\rangle_s$ and S until at Cep they are the same. The major effect is from the increase in S. For the $w_e = 0$ sample, for example, $\langle P_2 \cos\alpha\rangle_s$ increases by only 5%[1] across the nematic phase whilst S increases by a factor of about three[7] (compared with an increase in the quadrupole splittings across the nematic phase of 2.9).

A low angle x-ray study of this system was conducted by co-workers at Leeds University[8]. The scattering pattern for a sample in the isotropic phase is a single diffuse ring, while for an aligned nematic sample there is an intense Bragg peak along the meridian arising from the "face to face" separation $d_{//}$ of the micelles parallel to the nematic director. A weaker diffuse scattering along the equator arises from the "side to side" separation $d_\perp$ of the micelles in the plane perpendicular to the director[1]. An example of d-spacings data obtained for a sample with $w_e = .0047$ is shown in figure 6.8.

In order to determine the axial ratio from the d-spacings obtained from the x-ray experiments the micelles that are assumed to be discoidal and hexagonally packed into planes in the ordered phases the volume V_m of the micelle can then be calculated from[1]

$$V_m = \frac{2 d_{//} d_\perp^2 \phi}{\sqrt{3}} \qquad [6.6]$$

where ϕ is the volume fraction of amphiphile. The length of the minor axis a of the discotic micelle is fixed as the length of the fluorocarbon chain, which is 1.1 nm in the APFO/^2H_2O system. Given this, the length of the major axis b can be calculated from[1]

$$b = \sqrt{\frac{3V_m}{4\pi a}}. \qquad [6.7]$$

Figure 6.7 Partially averaged ^2H quadrupole splittings $\Delta\tilde{\nu}(^2H)$ at T_{NI}, T_{LI}, and T_{LN} as a function of the mass fraction of NH_4Cl (w_e) in the APFO/NH_4Cl/^2H_2O system (mass ratio of APFO to ^2H_2O is 9 :11).

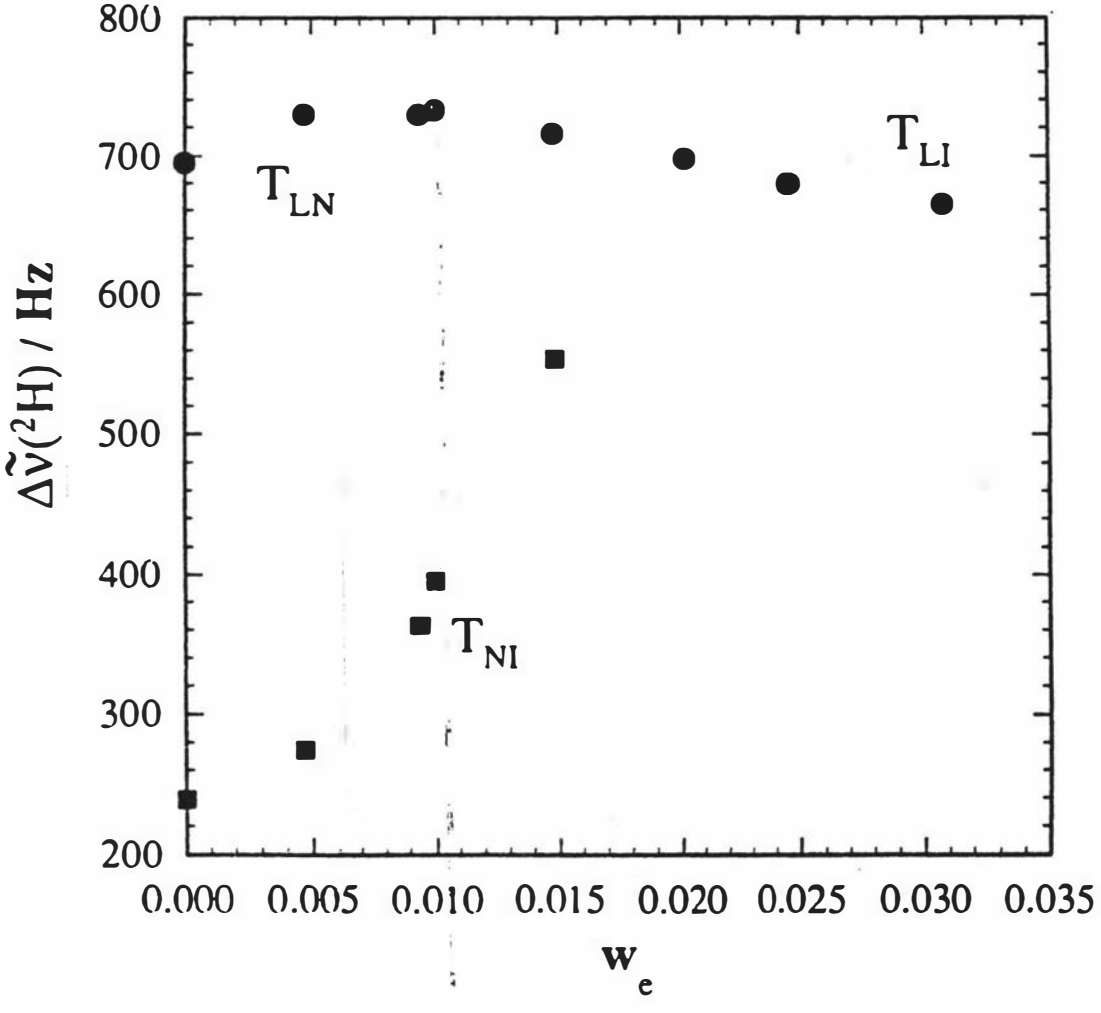

Figure 6.8 *d*-spacings for w_e = 0.0047 from the APFO/NH_4Cl/^2H_2O system with the mass ratio of APFO to ^2H_2O fixed at 9 : 11. The *d*-spacings have been calculated from the maxima of the intensity of the scattering curves. $d_{//}$(■) is the face to face separation of the micelle measured along the meridian, $d_{\perp}$(●) is the side to side separation measured along the equator, and d_0(▲) is the average centre to centre separation measured in the isotropic phase. Data provided by Gerson Oriques[8].

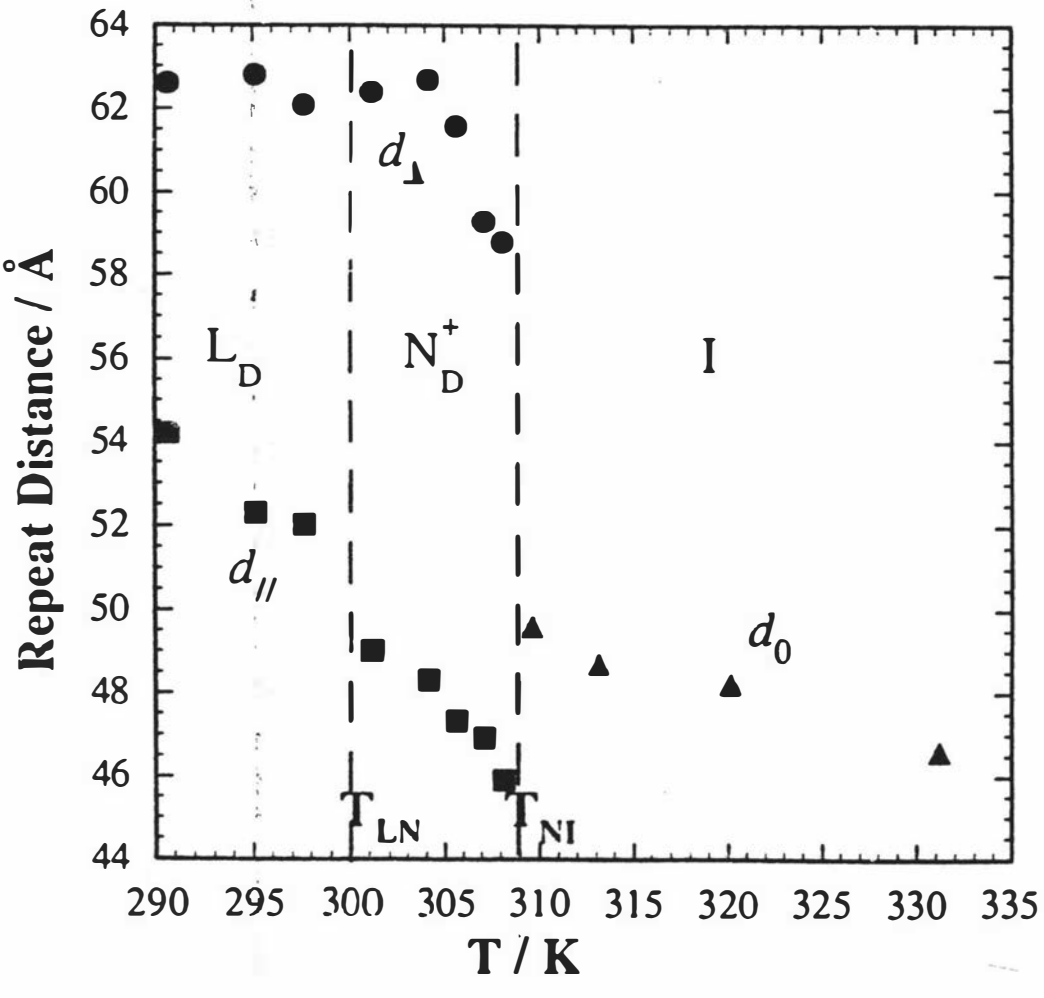

and also the aggregation number s can be simply calculated by

$$s = \frac{m}{V_a} \qquad [6.8]$$

where V_a is the volume of a single amphiphile.

The micelle aggregation numbers calculated at T_{NI} and T_{LI}, from the x-ray data of a range of samples, are shown in figure 6.9 as a function of the added electrolyte mass fraction. The figure shows the $w_e = 0.00$ point has a much lower aggregation number than the other points, which are essentially constant. This initial jump in the aggregation number should correspond to a initial sharp increase in the $\Delta\tilde{\nu}(^2H)$ at T_{NI}, but as the corresponding plot of $\Delta\tilde{\nu}(^2H)$ at T_{NI} shows (figure 6.7) there is initially only a slow increase with increasing w_e and there is no discontinuity between the $w_e = 0$ and $w_e = 0.0047$ point. The average aggregation number for the added electrolyte samples corresponds to an a/b ratio of 0.32 whilst that for the $w_e = 0$ sample corresponds to an a/b of 0.36. The corresponding values for $\langle P_2 \cos\alpha \rangle_s$ are 0.625 and 0.571. Thus if the apparent discrepancy between the binary and ternary micelle sizes is real a discontinuity in $\Delta\tilde{\nu}(^2H)$ of 24 Hz would be expected on addition of electrolyte to the binary sample. There does not appear to be a discontinuity of this magnitude in figure 6.7. There is certainly no discontinuity in the corresponding CsPFO/CsCl/^2H_2O system (figure 6.12). In figure 6.9 the $w_e = 0.00$ data point was measured separately[1] from the remainder of the ternary samples[8] and, in view of the NMR data (figure 6.7), it appears to be anomalous. The a/b ratio for the APFO/^2H_2O sample at $w_a = 0.45$ ($\phi = 0.325$) shown in figure 5.6 also suggests that this measurement may be anomalous. The x-ray experiment really needs to be repeated on a new sample set from $w_e = 0$ onwards. However, in view of the NMR measurements along T_{NI} and the constant values of the aggregation number for the $w_e \neq 0$, samples it is probable that the aggregation number of the $w_e = 0$ sample should be higher and it is reasonable to assume that there is no significant change in the aggregation number along the I-to-N_D^+ and transition line.

Figure 6.10 shows the ^2H quadrupole splittings and axial ratios along the 305 K isotherm in the lamellar phase. $\Delta\tilde{\nu}(^2H)$ is seen to increase monotonically with w_e. The implication of this is that the micelles increase in size with increasing w_e at any given temperature. On the other hand, the x-ray a/b ratios shows an initial increase with w_e which then becomes constant at $w_e = 0.015$. A result which implies a limiting micelle size. In order to understand the difference between the two observations it must be remembered that the axial ratios calculated from x-ray are model dependent, *i.e.* the aggregate is assumed to be an oblate ellipsoid. If the structure can no longer be represented in this way then the calculated a/b values do not have any applicability. The ^2H quadrupole splittings, on the other hand, are a function of $\langle P_2(\cos\alpha) \rangle_s$ which is the contribution to the ^2H quadrupole splittings from the motional averaging arising from diffusive motion of the water molecule over the surface sites. The increase in $\Delta\tilde{\nu}(^2H)$

Figure 6.9 The aggregation number along the isotropic-to-nematic and isotropic-to-lamellar phase transition line of the APFO/NH_4Cl/^2H_2O system with a mass ratio of APFO to ^2H_2O of 9 : 11.

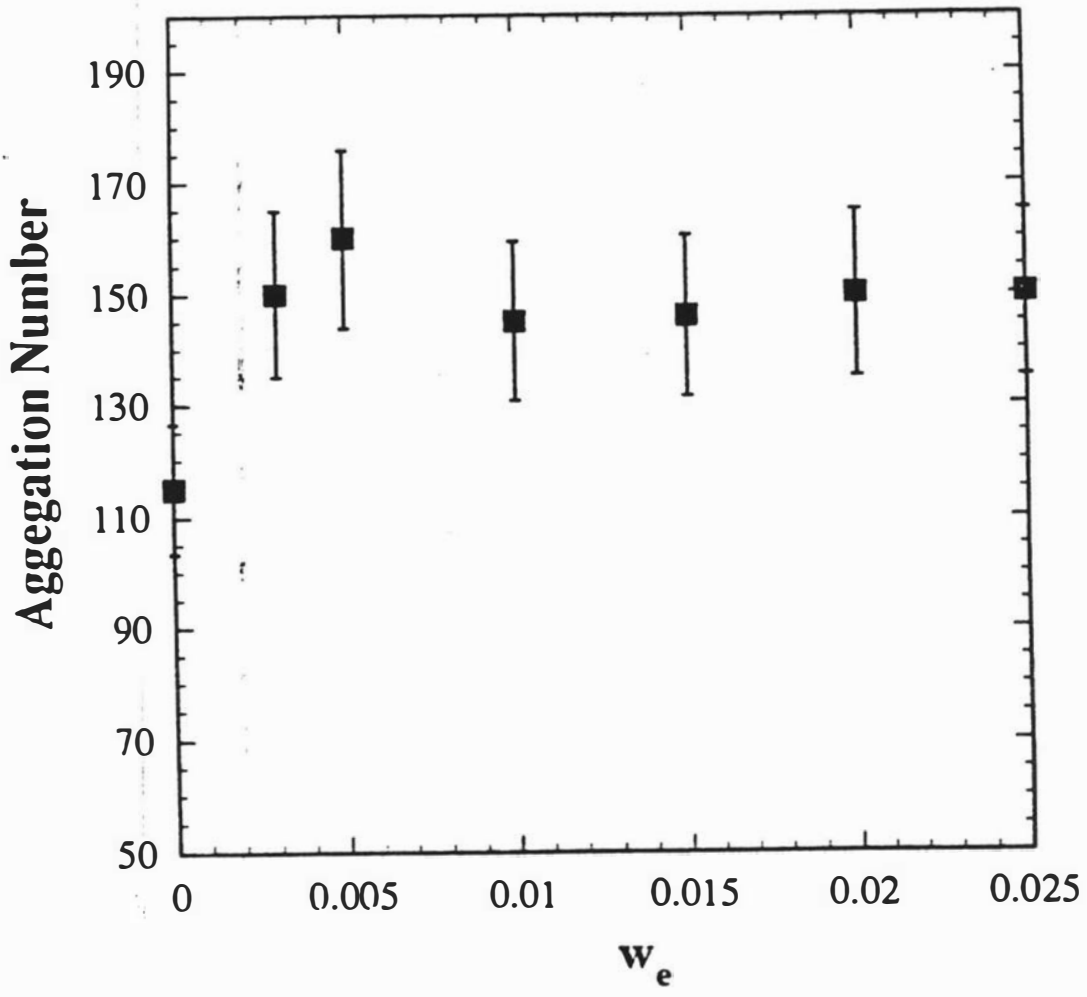

Figure 6.10 Electrolyte concentration dependence of the partially averaged ^2H quadrupole splittings $\Delta\tilde{\nu}(^2H)$ (●)and the axial ratio *a*/*b* (■) of the APFO/NH_4Cl/^2H_2O system with a mass ratio of APFO to ^2H_2O of 9 : 11 along the 305 K isotherm. All points shown are for samples in the lamellar phase. Note the discontinuity in the *a*/*b* plot with increasing w_e and the lack of such a discontinuity in the ^2H quadrupole splittings.

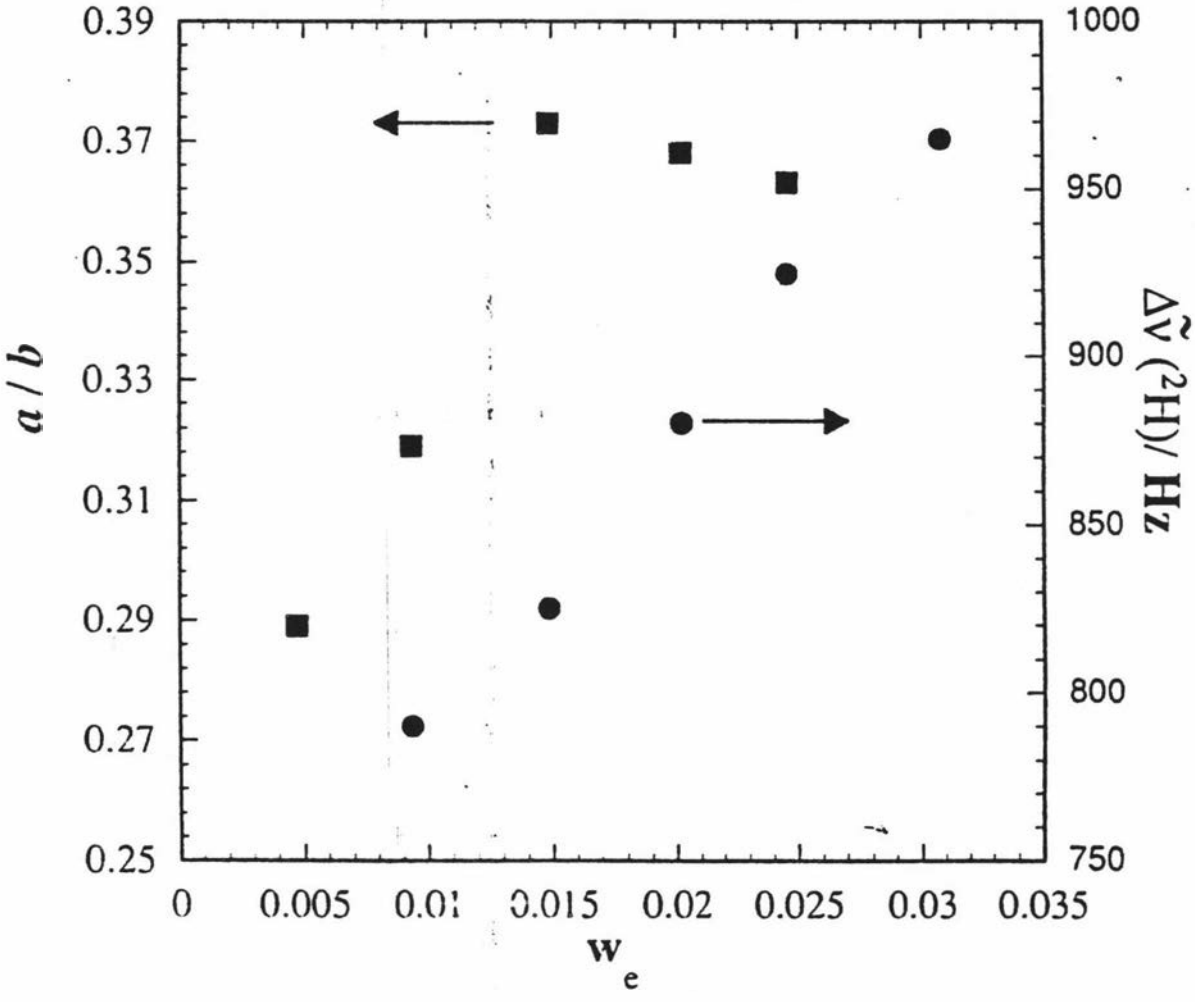

along the isotherm simply indicates that there is a loss in curvature in the system which could indicate that the lamellar phase is tending more to a "classical bilayer" type structure. Thus along the isotherm in the lamellar phase it appears that, at high w_e, the discotic micelle model fails to represent the aggregate structure. The evolution of the structure of the lamellar phase is an interesting and complex problem that will be further addressed in section 6.2.2.4.

6.2.2 CsPFO/CsCl/^2H_2O System

A study of the phase behaviour of the CsPFO/CsCl /^2H_2O system at a fixed mass ratio of CsPFO to ^2H_2O of 1 : 1 has been previously presented[9]. Some of the results of that study will be reproduced here for comparison purposes only. Additional experiments at two new CsPFO : ^2H_2O ratios have also been undertaken.

6.2.2.1 CsPFO/CsCl /^2H_2O System at a fixed mass ratio of CsPFO to ^2H_2O of 1 : 1

The partial phase diagram of the CsPFO/CsCl/^2H_2O system at a fixed mass ratio of CsPFO to ^2H_2O of 1 : 1 is presented in figure 6.11. At this composition the mole ratio of CsPFO to ^2H_2O is 1 to 27.3. The phase diagram shows an nematic (N_D^*) phase intermediate to an isotropic micellar solution (I) and what is possibly a discotic lamellar phase (L_D). The nematic phase is stable from w_e = 0 to 0.078 ± 0.002 and from temperatures of 316.3 to 343.7 K. The overall effect of increasing the salt concentration is to increase the temperature stability of the lamellar phase. At low salt concentrations the nematic phase is also stabilised, and the temperature range of this phase increases. At higher salt concentrations the nematic phase disappears at the critical end point Cep where the line of second order lamellar-to-nematic transitions intersects with the line of first order lamellar-to-isotropic transitions. For the w_e = 0 sample the lamellar-to-nematic transition is first order, but at the lowest added salt sample studied (w_e = 0.0015) it appeared to be second order in that no mixed phase lamellar / nematic coexistence region could be detected. This places Tcp between w_e = 0 and 0.0015. The fact that the addition of electrolyte weakens the L_D-to-N_D^* transition is interesting and will be considered in more detail in section 6.2.2.3. The second point of interest is the critical end point (Cep, w_e = 0.078 ±0.002 T = 344.0 ±0.05 K) where the line of second order L_D-to-N_D^* transitions intersect with the lines of first order N_D^*-to-I and L_D-to-I transitions. At CsCl concentrations greater than w_e = 0.13 the phase behaviour becomes complex and this will be considered in more detail in the section on the triangular phase diagrams.

Figure 6.11 Partial phase diagram of the CsPFO/CsCl/^2H_2O system at a fixed mass ratio of CsPFO to ^2H_2O of 1 : 1 and an electrolyte mass fraction w_e. See legend to figure 6.3 for explanation of the labels.

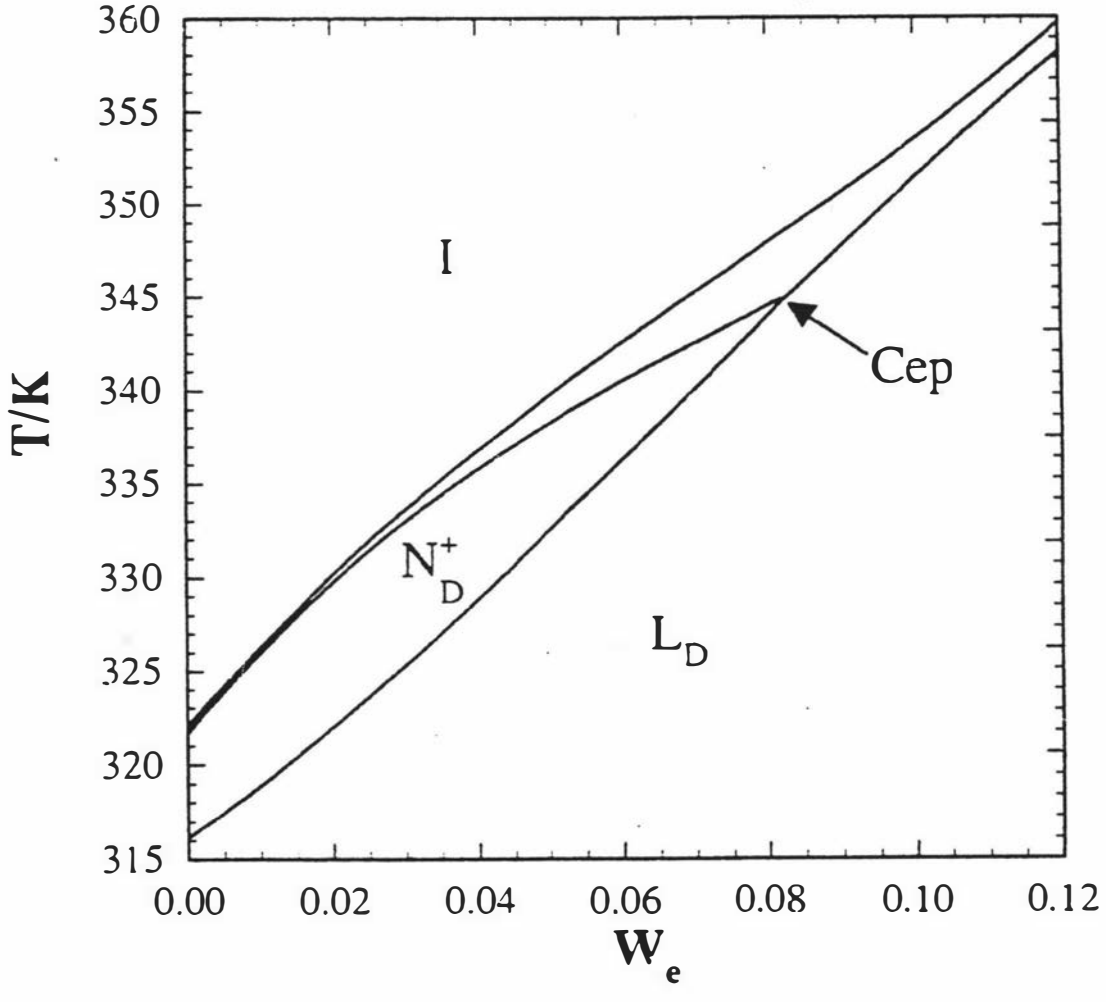

The variation in the ^2H quadrupole splittings at the T_{LN}, T_{NI}, and T_{LI} phase transition temperatures are shown in Figure 6.12 where it is apparent that, as in the APFO/NH_4Cl/^2H_2O system, along the lamellar-to-nematic and lamellar-to-isotropic phase transition lines the ^2H quadrupole splitting are independent of the salt concentration to the first approximation. The value of $\Delta\tilde{\nu}(^2H)$ has a maximum at $w_e \approx 0.035$ which corresponds with the maximum in $T_{IN} - T_{LN}$ and is only about 5% greater than for the $w_e = 0$ sample. The similarity between figure 6.7 for the APFO/NH_4Cl/^2H_2O system and figure 6.12 for the CsPFO/CsCl/^2H_2O system is striking and, in spite of the lack of x-ray data for the latter system, the same conclusions may be drawn as for the APFO/NH_4Cl/^2H_2O system. *i.e.* $\Delta\tilde{\nu}(^2H)$ at T_{NI} increases mainly as a consequence of increases in S, whilst along T_{LN} it is changes in $\langle P_2 \cos\alpha \rangle_s$ which dominate. Similarly the conclusion may be drawn that there is no significant change in aggregate size along the I-to- N_D^+ and I-to-L_D transition lines. This assertion is supported by the result of a recent neutron diffraction study[10] on the CsPFO/CsCl/^2H_2O system (mass ratio of CsPFO : ^2H_2O of 1:1) which showed no change in the $d_{//}$ spacing along this transition.

The dependence of the ^{133}Cs quadrupole splittings at the transition temperatures on the electrolyte concentration is shown in figure 6.13. The steady decrease in the splittings with increasing salt concentration along the N_D^+-to-L_D transition line must be due to an increase in the ratio of free Cs^+ ions in solution in comparison to those bound to the surface, *i.e.* a decrease in β_{Cs}. This does not mean that ions are becoming unbound rather it is the consequence of adding additional free ions. It has been shown that along the lamellar-to-nematic transition line the bound fraction per amphiphile, and hence per micelle, remains constant[9]. Thus both the micelle size and bound ion fraction are invariant along this transition line.

The dependence of the ^{35}Cl quadrupole splittings at the transition temperatures on the electrolyte concentration is shown in figure 6.14, where it is seen that the splittings increase slightly with w_e before eventually reaching a plateau. The implication of co-ion binding will be covered in more detail in the discussion.

The effect of added salt on the ^2H quadrupole splittings in the lamellar phase at a fixed temperature of 313.2 K is shown in figure 6.15, the figure shows a monotonic increase in the quadrupole splittings as the electrolyte concentration increases. In the L_D phase, there is little variation in the orientational order parameter[1, 11] and changes in quadrupole splitting are mainly due to changes in $\langle P_2 \cos\alpha \rangle_s^4$ (*cf* equation[3.19]), *i.e.* change in micelle size or mesophase structure.

Figure 6.12 Partially averaged ^2H quadrupole splittings $\Delta\tilde{\nu}(^2H)$ for the CsPFO/CsCl/^2H_2O system at a fixed mass ratio of CsPFO to ^2H_2O of 1 : 1, and an electrolyte mass fraction w_e, at the T_{NI}, T_{LI}, and T_{LN} phase transition boundaries.

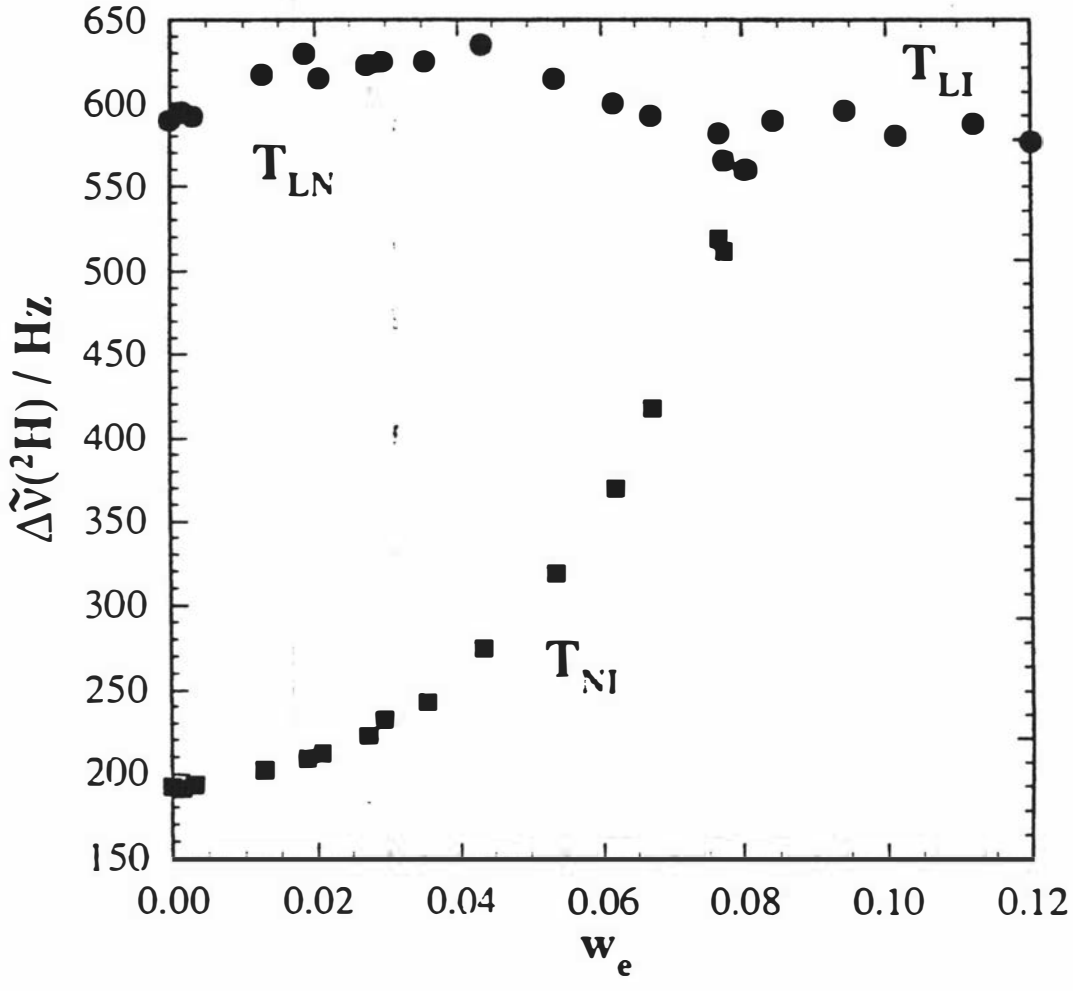

Figure 6.13 Partially averaged ^{133}Cs quadrupole splittings $\Delta\tilde{\nu}(^{133}Cs)$ for the CsPFO/CsCl/^2H_2O system at a fixed mass ratio of CsPFO to ^2H_2O of 1 : 1, and an electrolyte mass fraction w_e, at the T_{NI}, T_{LI}, and T_{LN} phase transition boundaries.

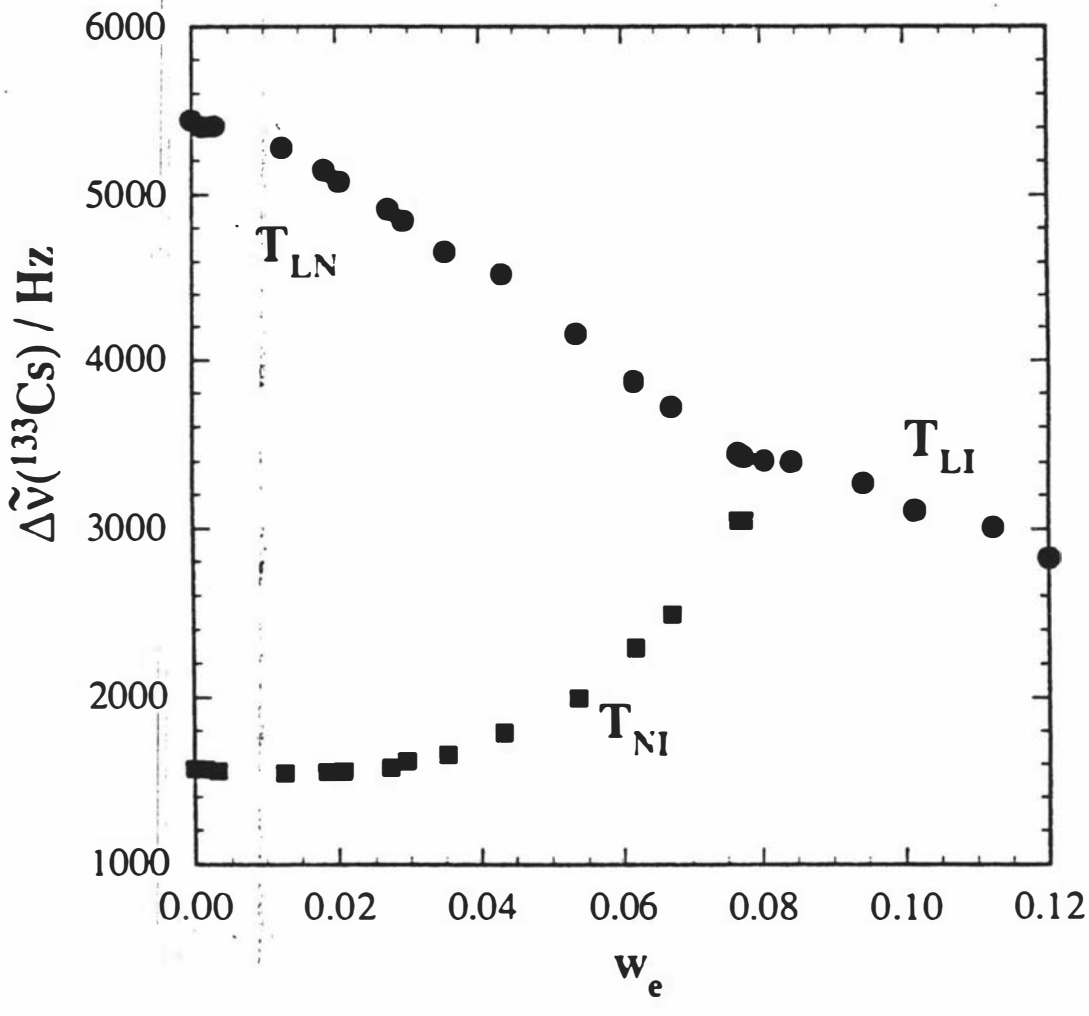

Figure 6.14 Partially averaged ^{35}Cl quadrupole splittings $\Delta\tilde{\nu}(^{35}Cl)$ for the CsPFO/CsCl/^2H_2O system at a fixed mass ratio of CsPFO to ^2H_2O of 1 : 1, and an electrolyte mass fraction w_s, (a) at the T_{NI}, T_{LI}, and T_{LN} phase transition boundaries, and (b) along the 310 K isotherm in the lamellar phase.

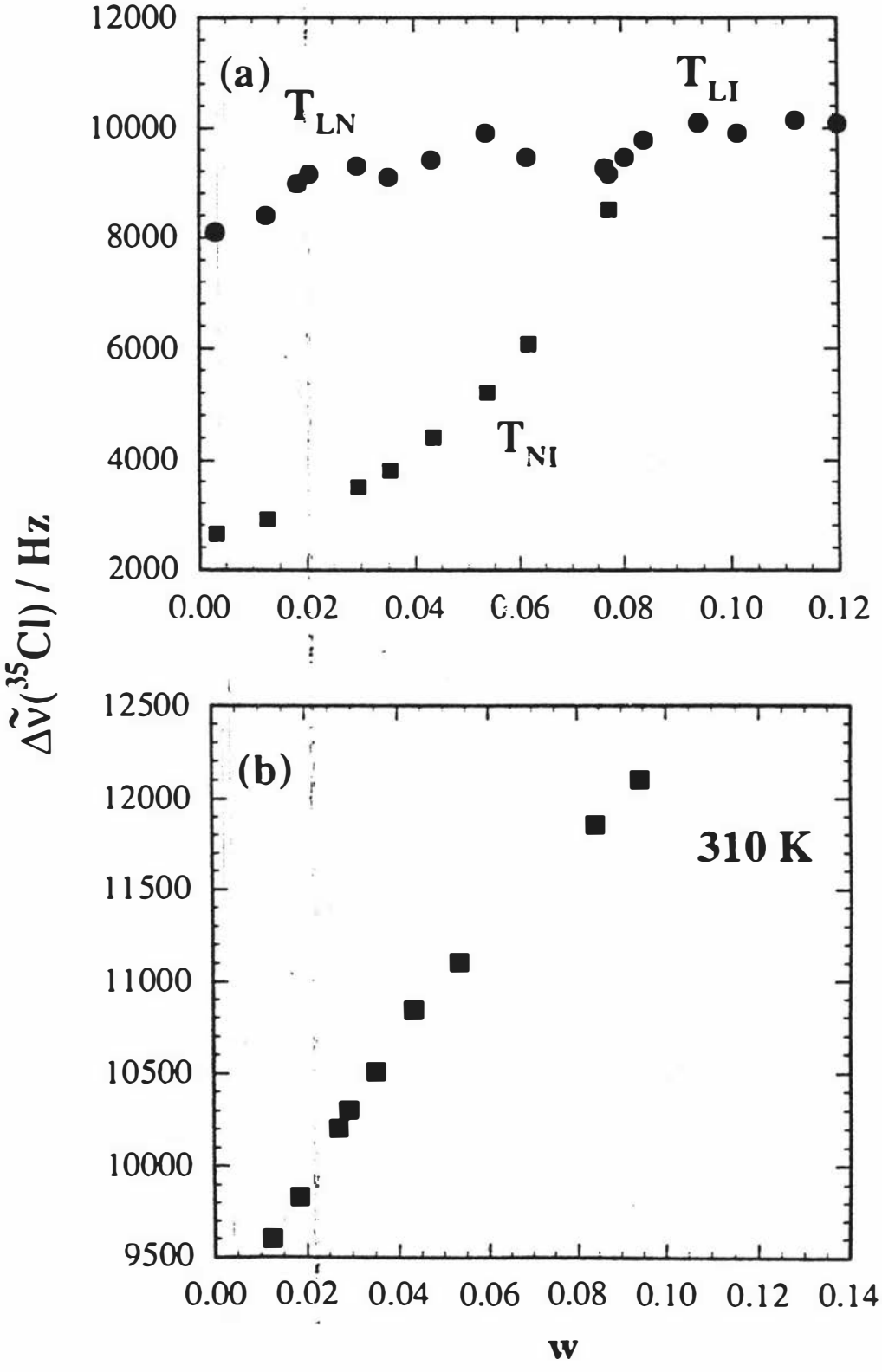

Figure 6.15 Partially averaged ^2H quadrupole splittings $\Delta\tilde{\nu}(^2H)$ (■) at 313.2 K for the CsPFO/CsCl/^2H_2O system at a fixed mass ratio of CsPFO to ^2H_2O of 1 : 1, and an electrolyte mass fraction w_e. All points shown represent samples in the in the lamellar phase.

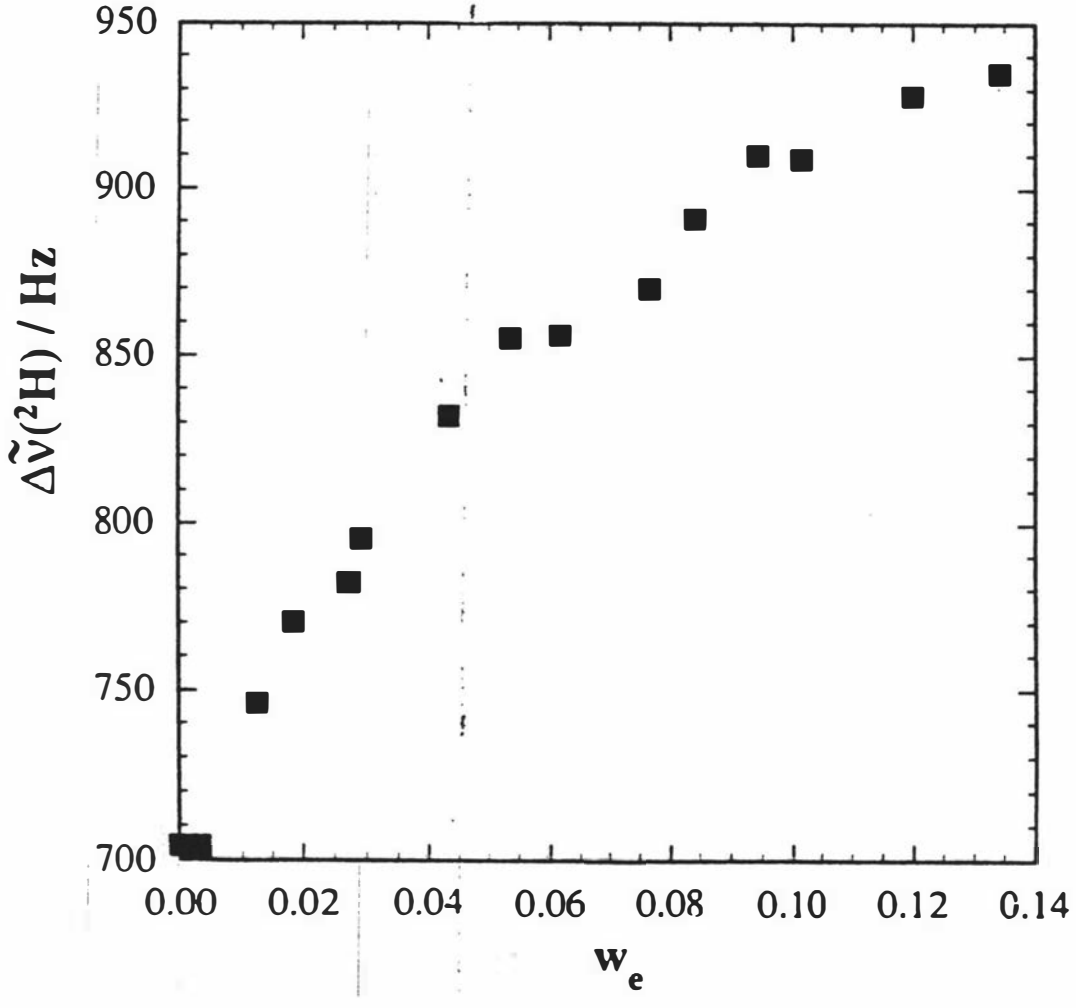

6.2.2.2 CsPFO/CsCl/^2H_2O System at a fixed mass ratio of CsPFO to ^2H_2O of 1 : 4

To examine the effects of added electrolyte in a region of the phase space which is water rich a CsPFO/CsCl/^2H_2O sample with a fixed mass ratio of CsPFO to ^2H_2O of 1 : 4 was investigated.

At low amphiphile volume fractions the binary CsPFO/^2H_2O system has been shown to exhibit pretransitional phenomena associated with the onset of order in the isotropic micellar solution phase immediately prior to the isotropic-to-nematic phase transition[12]. Pretransitional ordering is indicated by a splitting of the isotropic signal into a doublet at temperatures close to T_{IN}. The splitting increases rapidly with increasing temperature and diverges as a hypothetical second-order transition to the nematic phase is approached at a temperature T*. Figure 6.16. shows the field induced quadrupole splitting as a function of temperature for samples with w_c = 0.000 and 0.104. A striking feature of these plots is that the divergence of the quadrupole splitting is quenched at T_{IN}. A detailed description of the origin of the quadrupole splitting and interpretation of the effect of electrolyte on the structure of the aggregate at T_{IN} will be presented in the discussion.

The partial phase diagram of the CsPFO/CsCl/^2H_2O system with a fixed mass ratio of CsPFO to ^2H_2O of 1 : 4 is presented in figure 6.17. There is a decrease in the width of the nematic phase and a stabilization of the lamellar phase with increasing electrolyte concentration. The onset of complex phase behaviour associated with a biphasic region below the I-to-L_D transition occurs at $w_c \approx 0.027$ *cf* a corresponding w_c = 0.13 in the 1:1 mass ratio system (section 6.2.2.1) This complex phase behaviour will be considered in the section on triangular phase diagrams. As the primary objective of this study is to present the disorder/order transitions between pure phase regions, only phase transitions of samples with $w_c \leq 0.027$ will be considered here.

Figure 6.18 shows the ^2H quadrupole splittings at the T_{LN} and T_{NI} phase transition temperatures. There appears to be a slight decrease in $\Delta\tilde{\nu}(^2H)$ along the lamellar-to-nematic transition line as the concentration of w_c increases. However the general form of this figure is in line with figure 6.7 and 6.12 and suggest again that there is no significant change in the aggregate size at T_{NI}.

Figure 6.16 The partially averaged ^2H quadrupole splittings induced by the magnetic field close to T_{IN} for the w_e = 0.00(■) and 0.0104(●) samples of the CsPFO/CsCl/^2H_2O system at a fixed mass ratio of CsPFO to ^2H_2O of 1 : 4. The temperatures have been normalised to T_{IN}.

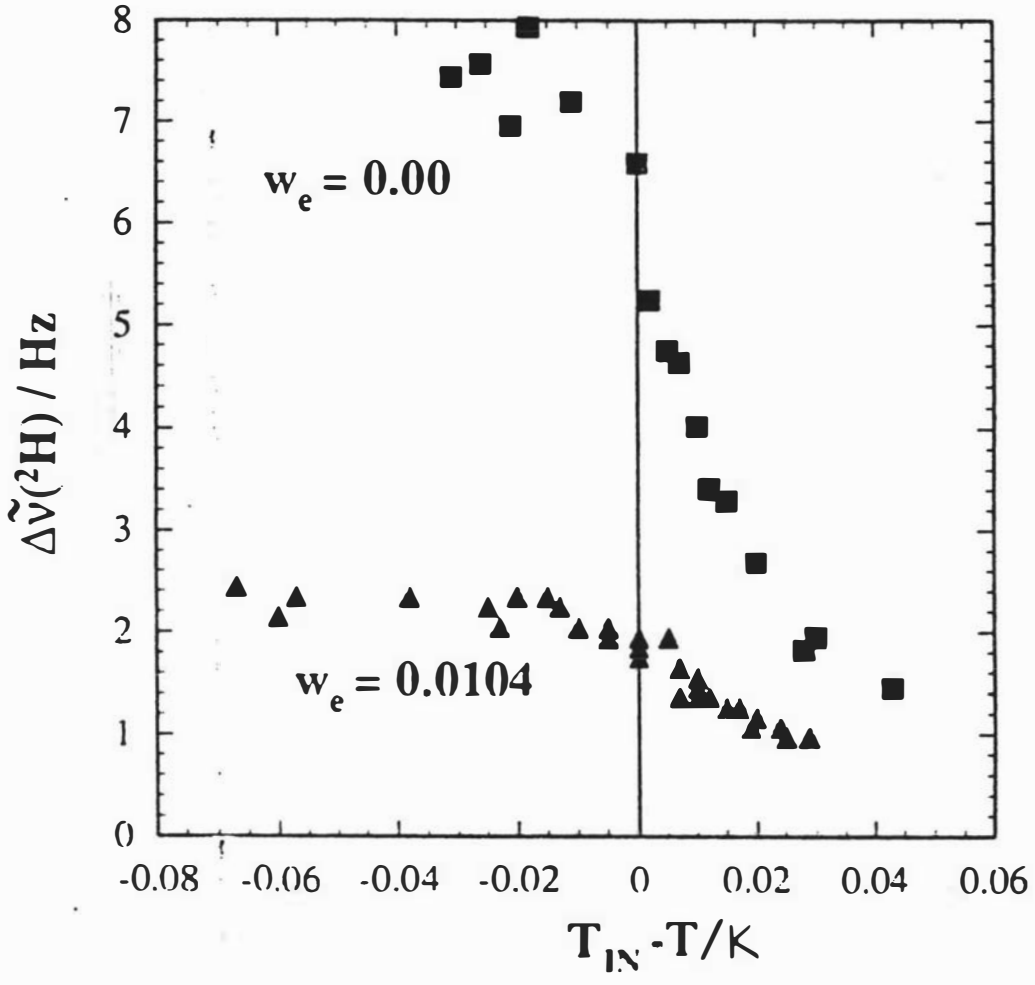

Figure 6.17 Partial phase diagram of the CsPFO/CsCl/^2H_2O system at a fixed mass ratio of CsPFO to ^2H_2O of 1 : 4, and an electrolyte mass fraction w_e. See legend to figure 6.3 for explanation of the labels.

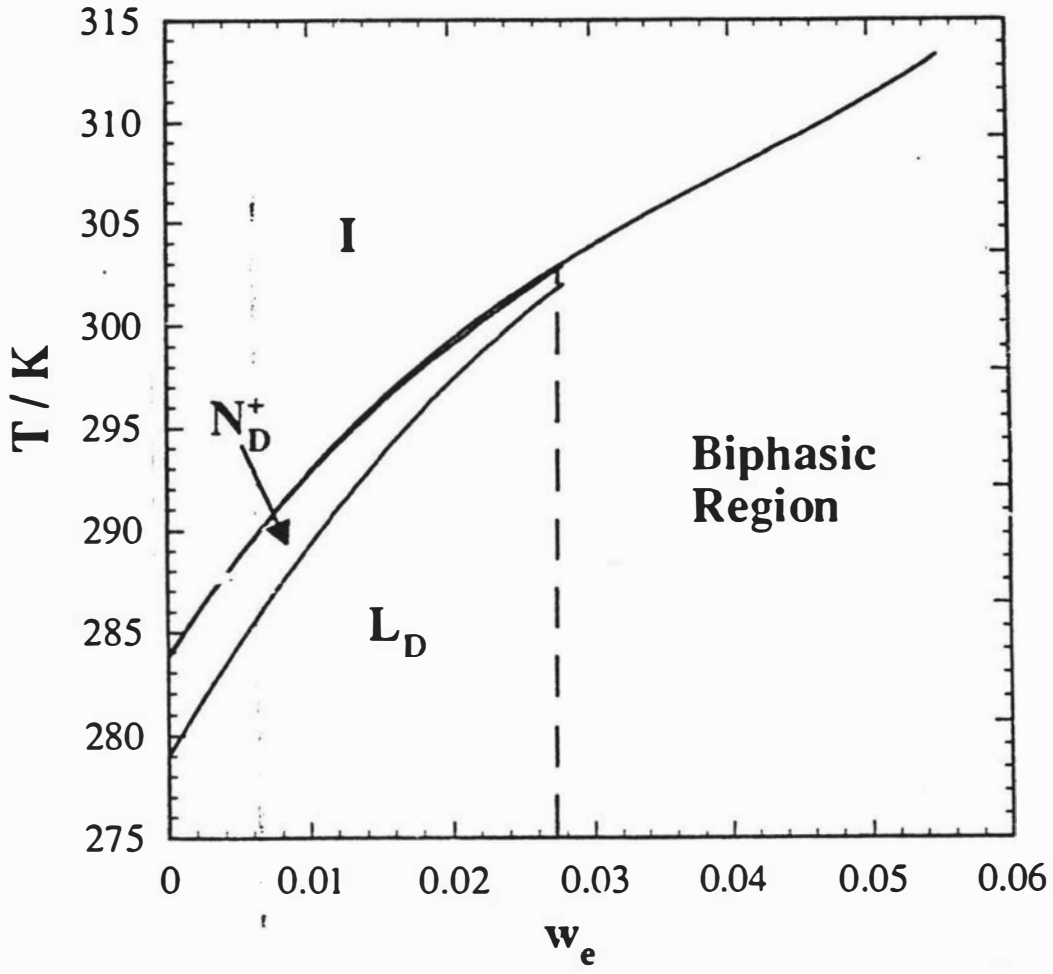

Figure 6.18 Partially averaged ^2H quadrupole splittings $\Delta\tilde{\nu}(^2H)$ for the CsPFO/CsCl/^2H_2O system at a fixed mass ratio of CsPFO to ^2H_2O of 1 : 4, and an electrolyte mass fraction w_e, at the T_{NI} and T_{LN} phase transition boundaries.

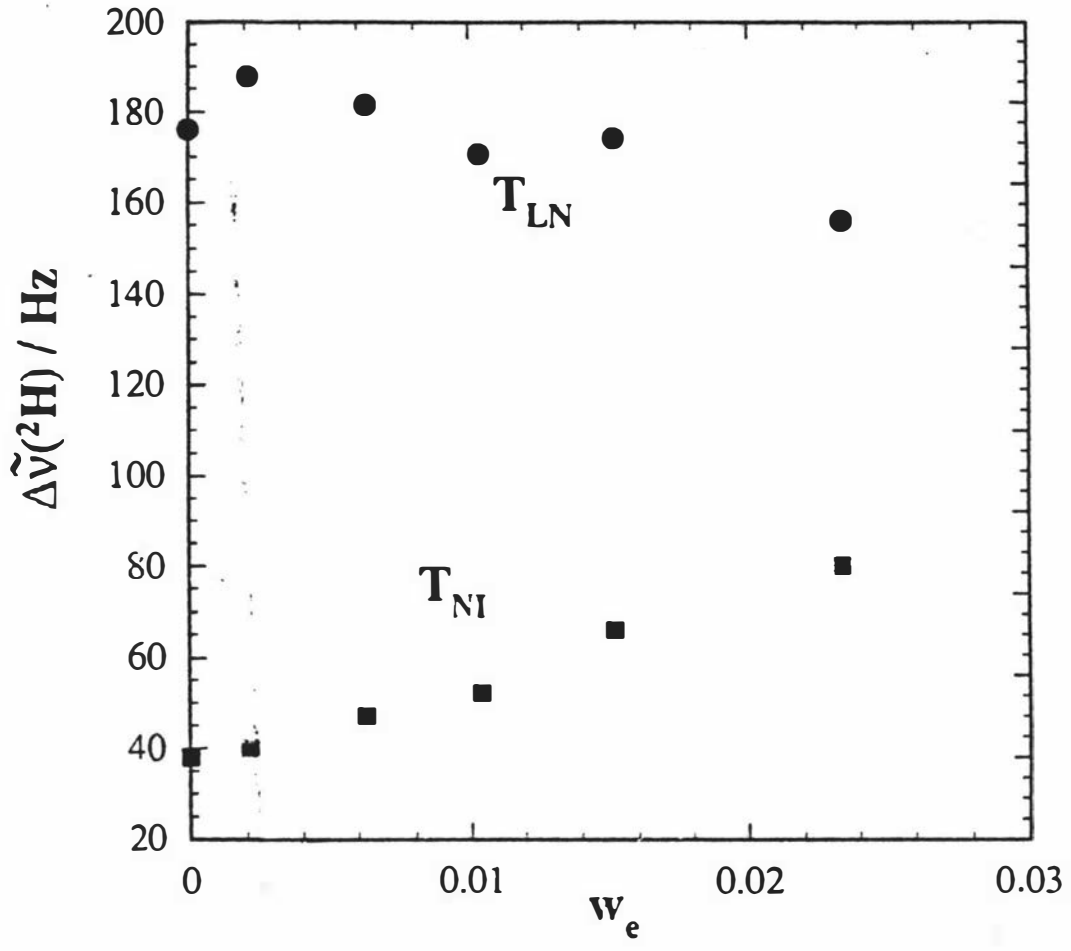

6.2.2.3. Effect of Electrolyte on the First Order Nematic-to-Lamellar Transition

An interesting feature of the phase diagram of the CsPFO/CsCl /^2H_2O system at a fixed mass ratio of CsPFO to ^2H_2O of 1 : 1 (figure 6.11) is the occurrence of a tricritical point Tcp along the lamellar-to-nematic phase transition boundary. A tricritical point occurs on the binary phase diagram of the CsPFO/^2H_2O at a composition of $w_a = 0.43$ and a temperature of 304.80 K[2]. The $w_a = 0.5$ binary sample is well above this concentration and the transition is first order. On the addition of electrolyte, even at the lowest electrolyte concentration, no mixed N_D^+/L_D phase region could be detected and the transition is apparently second order. Thus the presence of electrolyte results in a weakening of the strength of the nematic-to-lamellar transition.

The CsPFO/CsCl /^2H_2O sample at a fixed mass ratio of CsPFO to ^2H_2O of 1 : 1 and a w_e of 0 has a mixed phase L_D/N_D^+ region of only 100 mK and a small amount of CsCl (w_e = 0.001) causes the transition to become second order. The CsPFO/CsCl/^2H_2O system at a fixed mass ratio of CsPFO to ^2H_2O of 53 : 47 and a w_e of 0 has an N_D^+/L_D coexistence region with a width of 400 mK[4], and so this is a suitable sample to use to examine the effect of added electrolyte on this transition. The best method to determine the presence of N_D^+ and L_D signals in a mixed phase region is ^{133}Cs NMR[2]. The phase transition temperatures shown in figure 6.19 were determined in this way.

The partial phase diagram of the CsPFO/CsCl /^2H_2O system at a fixed mass ratio of CsPFO to ^2H_2O of 53 : 47 is presented in figure 6.19. The nematic/lamellar coexistence region is seen to decrease in width with increasing salt concentration, until at $w_e = 0.004$ no N_D^+/L_D coexistence region is present.

The location of Tcp is more accurately determined from a plot of the quadrupole splittings at T_{NL} and T_{LN} (figure 6.20). Along T_{LN} $\Delta\tilde{\nu}(^2H)$ remains relatively constant, while along T_{NL} $\Delta\tilde{\nu}(^2H)$ increases until it coincides with $\Delta\tilde{\nu}(^2H)$ at Tcp. The convergence is simply reflecting a convergence in S as w_e increases, *i.e.* S at T_{NL} increases until it reaches the value of S at T_{LN}. The intersection of the two lines, therefore, is an excellent indication of the location of Tcp.

6.2.2.4 CsPFO/CsCl/^2H_2O Triangular Phase Diagrams

As indicated in the above partial phase diagrams of the ternary CsPFO/CsCl/^2H_2O and APFO/NH_4Cl/^2H_2O systems these three component systems exhibit complex phase behaviour at high salt concentrations. Although this thesis is primarily concerned with the series of order/disorder phase transitions of discotic micelles a more extensive understanding of the ternary system is needed to understand the phase behaviour over a range of system compositions. More importantly the ternary phase diagram enables the

Figure 6.19 Partial phase diagram of the CsPFO/CsCl /^2H_2O system at a fixed mass ratio of CsPFO to ^2H_2O of 53 : 47, and an electrolyte mass fraction w_e. See legend to figure 6.3 for explanation of the labels.

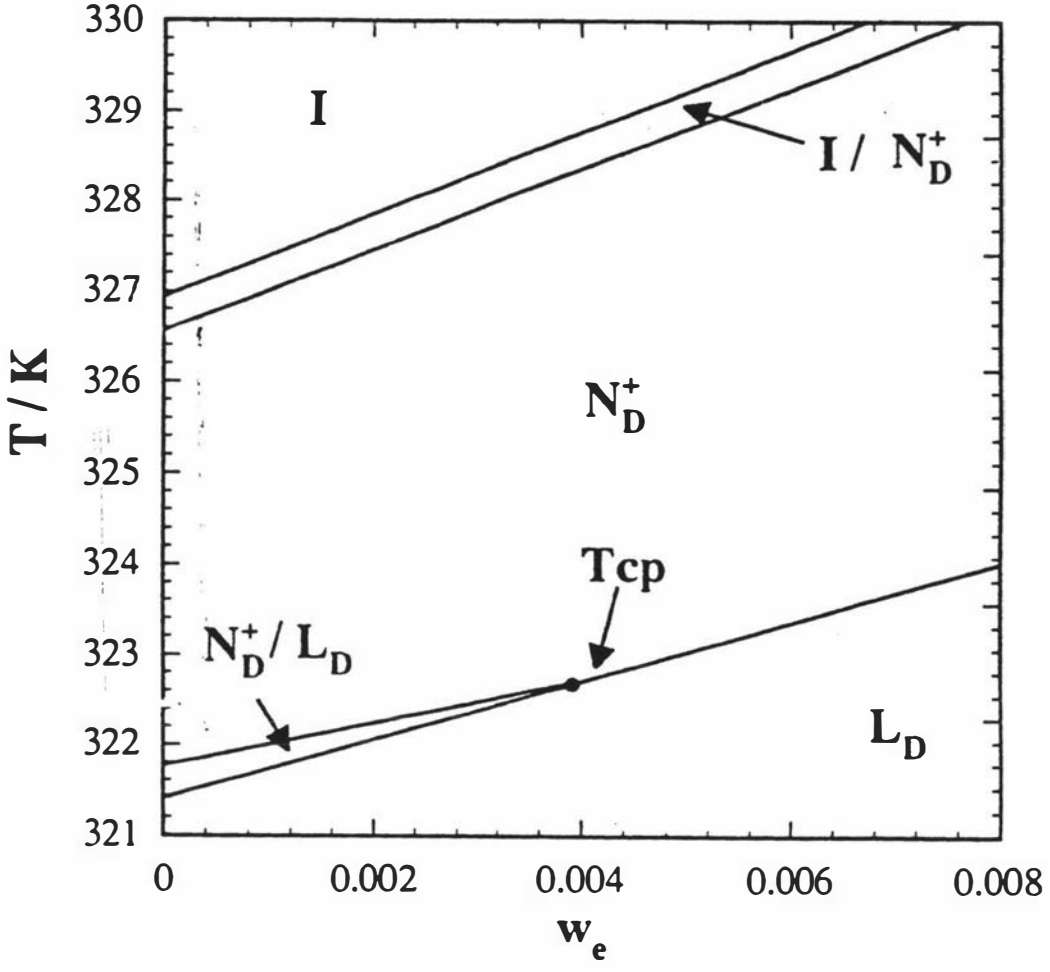

Figure 6.20 Partially averaged ^2H quadrupole splittings $\Delta\tilde{\nu}(^2H)$ for the CsPFO/CsCl/^2H_2O system at a fixed mass ratio of CsPFO to ^2H_2O of 53 : 47, and an electrolyte mass fraction w_e, at the T_{NL} and T_{LN} phase transition boundaries.

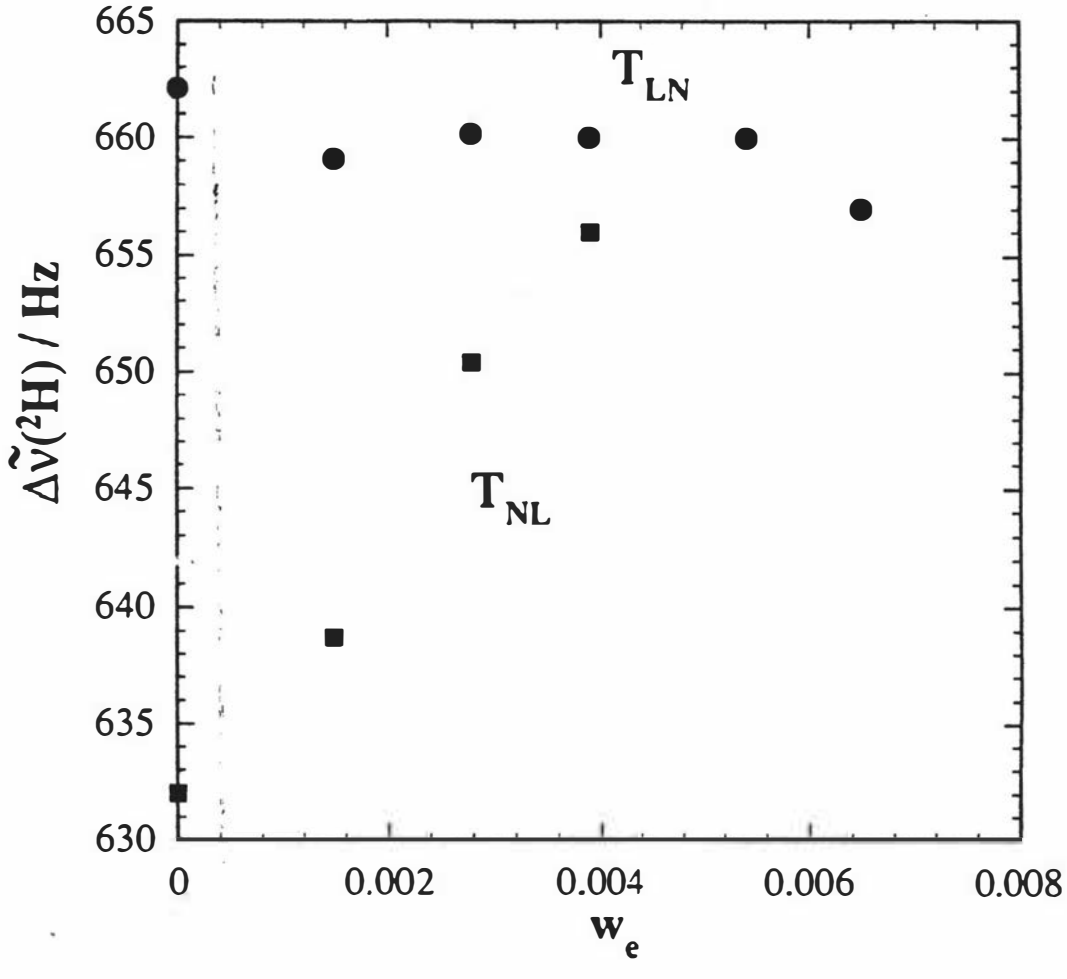

overall effect of electrolyte on the CsPFO/CsCl/^2H_2O system to be determined. Hence ternary phase diagrams of the CsPFO/CsCl/^2H_2O system have been established and are presented here together with a description of the different phase regions.

Partial ternary phase diagrams of the CsPFO/CsCl/^2H_2O system at 303 and 323 K are presented in figure 6.21(a) and (b) respectively. All of the phase transitions were determined by optical birefringence (see chapter 2) and as in all the other systems presented here the pressure was assumed to be constant. The lower axis of these triangular phase diagrams corresponds to the binary CsPFO/^2H_2O system with the amphiphile concentration increases from left to right. Tie lines from the CsPFO/^2H_2O axis to the CsCl apex corresponds to an increase in CsCl concentration at a constant mass ratio of CsPFO to ^2H_2O. The ternary phase diagrams were assembled from data collected from samples of fixed mass fractions of CsPFO to ^2H_2O from w_a = 0.05 to 0.70 in increments of 0.05 to which CsCl was added to constitute samples with electrolyte compositions from w_c = 0 to 0.20 in increments of 0.01. Each sample was observed at temperatures from 283 K to 353 K in 10 K increments. The phase behaviour of this ternary system has a similar form as the APFO/^2H_2O/NH_4Cl system although the phase transition temperatures are displaced[8].

The different regions labelled on the phase diagram are; molecular solution (W); isotropic micellar solution (I); and the liquid crystal region (LC), characterised by optical birefringence. There are three biphasic regions on the phase diagrams. An isotropic solution of monomers and salt in equilibrium with either an isotropic solution of micelles (W+I), a liquid crystalline phase (W+LC), or crystalline amphiphile (W+K).

The upper boundary of the W+I region was identified by the onset of phase separation in the sample to produce two immiscible phases neither of which was birefringent. The upper boundary to the W+LC phase was indicated by the appearance of birefringence in the more dense isotropic phase. The boundary to the W+K region was determined by first cooling the sample until solid crystals appeared and then heating it to determine the temperature at which the crystals redissolved. Supercooling always occurred and the cooling crystallisation temperatures were always lower than the dissolution temperatures. Optical birefringence measurements alone cannot distinguish between the nematic phase and other liquid crystal phases. The nematic region (N_D) has been identified from the NMR experiments and is included for completeness. Obviously there are mixed phase regions between two adjacent phase regions but the resolution of this experiment was too coarse to allow the determination of these mixed phase regions.

A temperature sequence of ternary phase diagrams enables us to observe the temperature dependence of the phase regions. For instance as the temperature increases from 303 to 323K the I phase region becomes more stable while the W+K biphasic region is displaced to higher salt concentrations (figure 6.21). By analysing the stack of triangular phase diagrams over the temperature range (283 to 353 K) it is possible to

Figure 6.21 Triangular phase diagrams of the ternary CsPFO/CsCl /^2H_2O system at fixed temperature of (a) 303 K and (b) 323 K. The different regions labelled on the phase diagram are as follows: the isotropic micellar solution region, I; the nematic phase, N_D; the liquid crystal region, LC; isotropic solution of monomers in equilibrium with an isotropic solution of micelles, W+I; isotropic solution of monomers in equilibrium with a liquid crystalline phase, W+LC; and the isotropic solution of monomers in equilibrium with crystalline amphiphile, W+K.

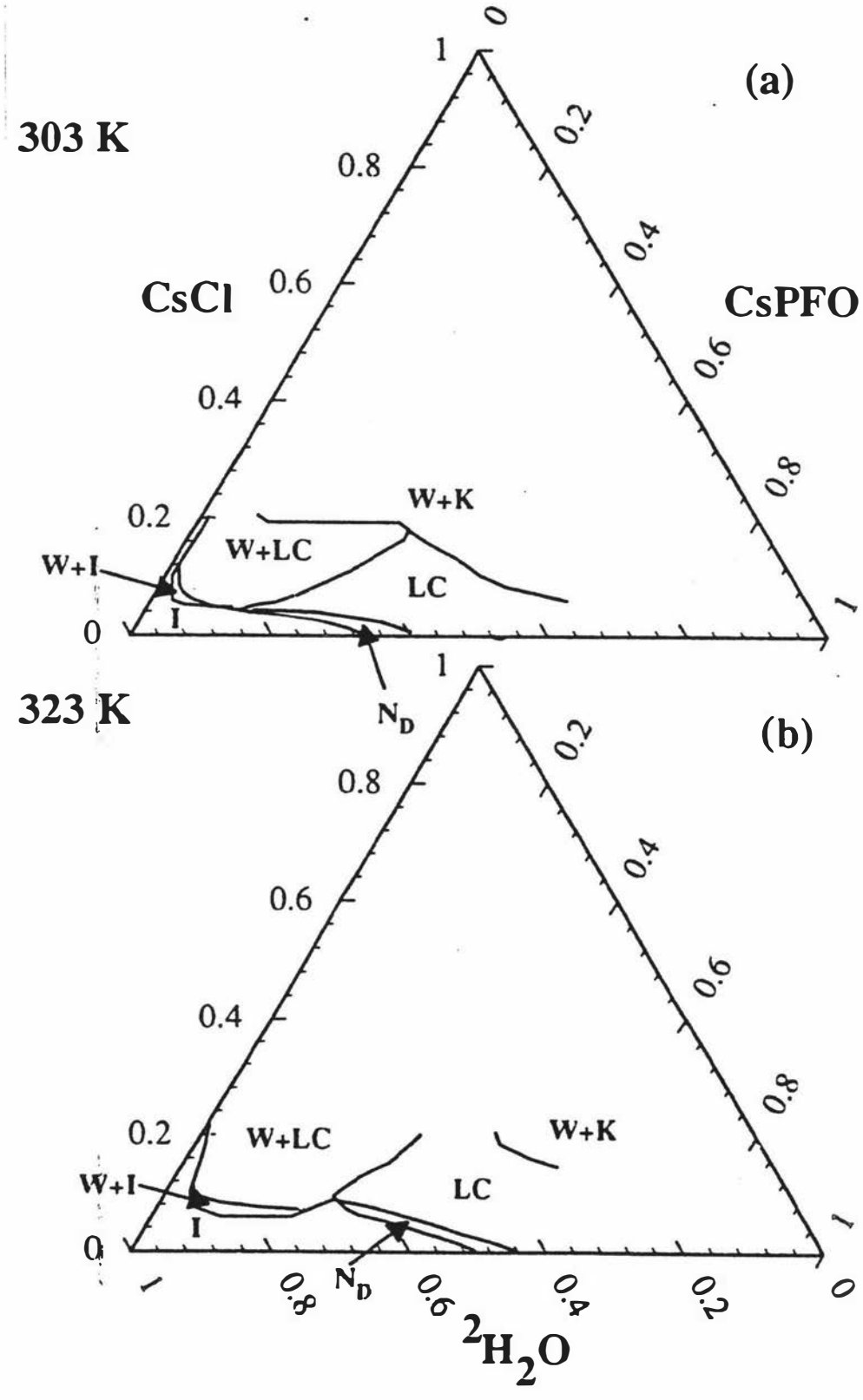

obtain temperature composition slices as in figure 6.22 to 6.24. These figures represent the effects of added electrolyte on the phase behaviour at amphiphile to ^2H_2O ratios of 1:20; 1 : 4; and 1 : 1 respectively. From this sequence of diagrams it is clear that the biphasic regions are pushed to higher temperatures and salt concentrations as the mass ratio of CsPFO to ^2H_2O increases. The partial phase diagrams shown in figures 6.11 and 6.17 for the 1 : 1 and 1 : 4 samples can now be seen in context of the wider phase behaviour shown in figures 6.22, 6.23 and 6.24. At the lowest amphiphile concentrations no nematic phase exists. For the 1 : 4 sample there is a small nematic phase which is stable over a narrow temperature w_e range. At $w_e \geq 0.03$ only mixed phase liquid crystal regions prevail. The nematic range for the 1 : 1 sample is much larger and it needs a salt concentration of $w_e = 0.13$ before the two phase liquid crystal region is seen.

The W+LC region exhibited shear birefringence. On agitation of the sample an apparent single phase region was produced which exhibited a weak birefringence. On leaving the sample for several minutes the birefringence disappeared. On then twisting the sample birefringence was again observed. The behaviour is consistent with a liquid crystal phase structure resembling a classical bilayer. On agitation of the sample the bilayers form vesicles which assume a spherical symmetry when the sample is left undisturbed. A twisting of the tube with the consequent shear force results in a distortion of the vesicles from spherical symmetry and birefringence is observed. The vesicle solution is kinetically stable in that once this phase has been produced it persists indefinitely.

The dilute lamellar phase/vesicle behaviour is reminiscent of dilute phospholipid solutions. By the addition of electrolyte, therefore, it is possible to progressively change the phase behaviour from that of a system of discotic micelles into that associated with extensive bilayer structures. The electrolyte must, therefore, progressively change the lamellar phase structure from discotic micelles into some sort of classical lamellar phase. This evolution is probably progressive since no evidence for a phase transition is observed in the lamellar phase as the electrolyte concentration is increased (see figure 6.15 for example).

Figure 6.22 A cross-sections of the ternary CsPFO/^2H_2O/CsCl system where the mass ratio of CsPFO to ^2H_2O is fixed at 1: 20, and an electrolyte mass fraction w_e, see legend to figure 6.21 for explanation of the labels.

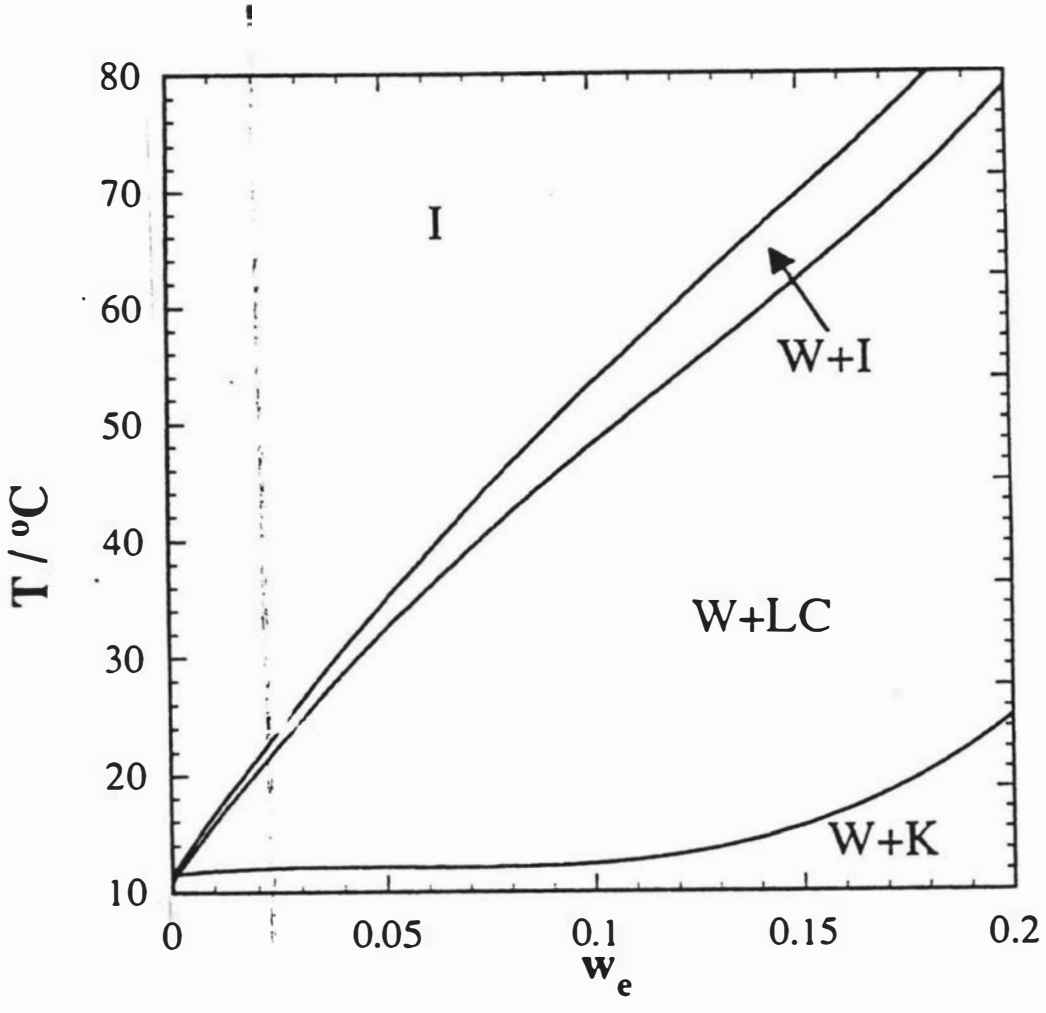

Figure 6.23 A cross-sections of the ternary CsPFO/^2H_2O/CsCl system where the mass ratio of CsPFO to ^2H_2O is fixed at 1: 4, and an electrolyte mass fraction w_e, see legend to figure 6.21 for explanation of the labels.

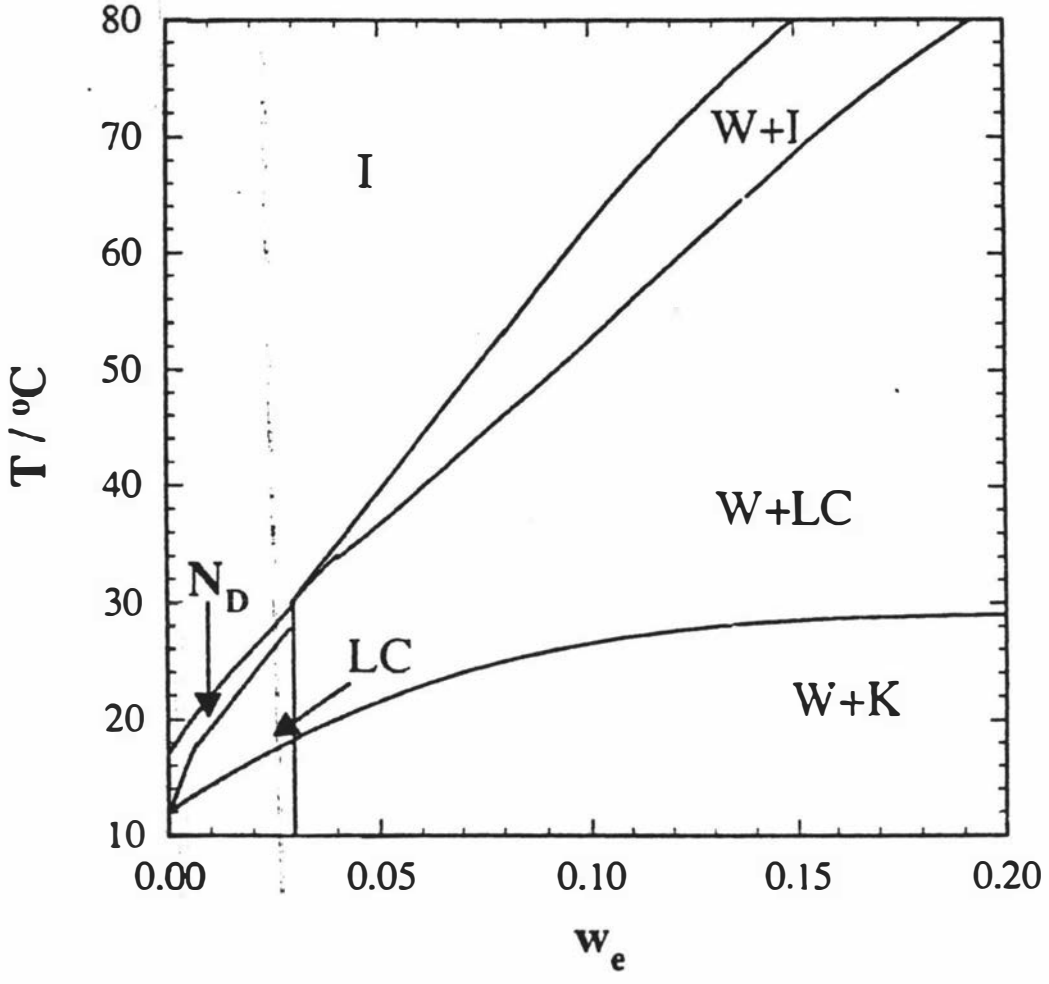

Figure 6.24 A cross-sections of the ternary CsPFO/^2H_2O/CsCl system where the mass ratio of CsPFO to ^2H_2O is fixed at 1: 1 and an electrolyte mass fraction w_e, see legend to figure 6.21 for explanation of the labels.

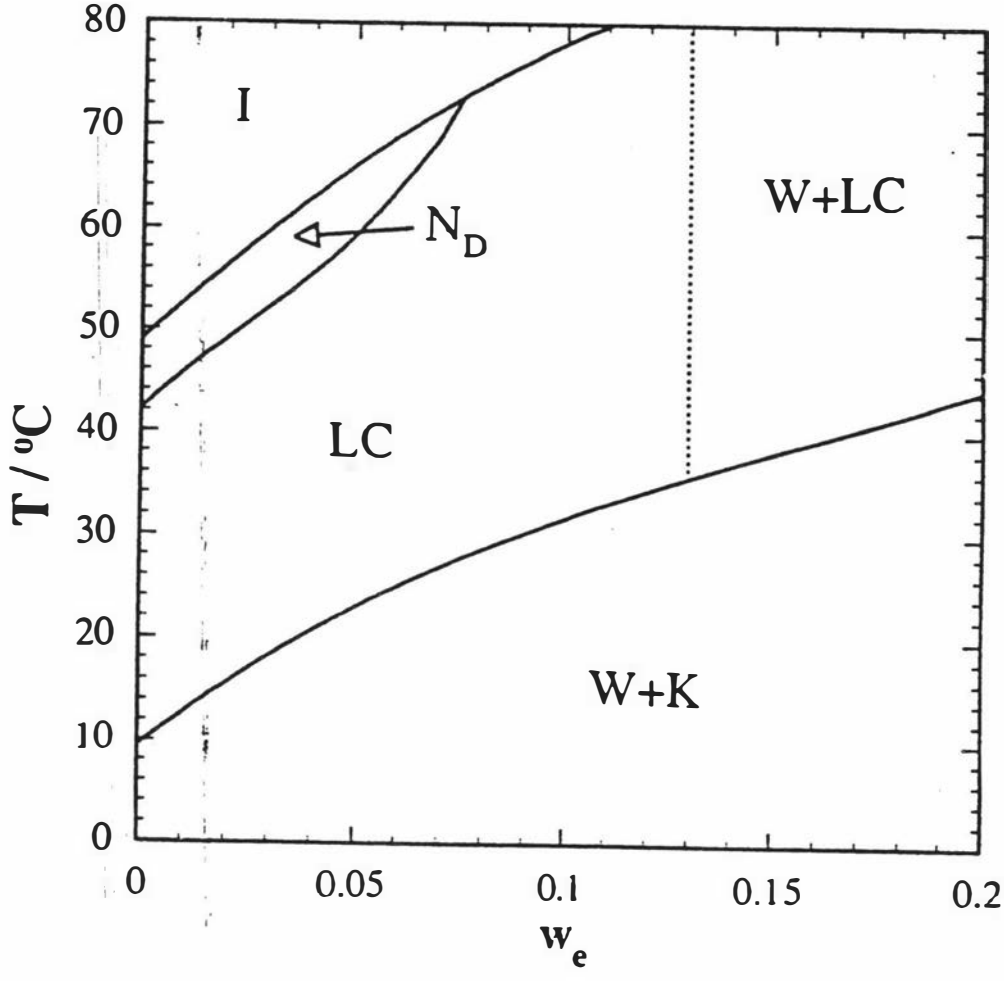

6.3 Discussion

6.3.1 Effect of Electrolyte on Self-Assembling Systems

Influence of Electrolyte on the Phase Behaviour

The partial phase diagrams of the ternary CsPFO/CsCl/^2H_2O and APFO/NH_4Cl/^2H_2O systems are similar in form. As the electrolyte concentration increases there is a monotonic increase in each of the phase transition temperatures. The nematic phase intermediate to the isotropic micellar solution and lamellar phases is initially stabilized at low electrolyte concentrations but ultimately destabilized at higher electrolyte concentrations and eventually disappears at a critical end point Cep. At electrolyte concentrations higher than Cep the isotropic micellar solution phase on cooling undergoes a phase transition directly to a lamellar phase. The magnitude of T_{IN} - T_{NI} reflects the increasing discontinuity in S and $\langle P_2 \cos\alpha \rangle_s$ across the transition as the strength of the transition increases. An example of the w_e dependence of the temperature width of the I/N_D^+ coexistence region is given in figures 6.25(a) and (b) for the CsPFO/CsCl/^2H_2O system with a mass ratio of CsPFO to ^2H_2O of 1 : 1 and the APFO/NH_4Cl/^2H_2O system at a fixed mass ratio of APFO to ^2H_2O of 9 : 11. In the binary CsPFO/^2H_2O system the width of the isotropic/nematic coexistence region increases with increasing mass fraction of amphiphile[4] and the plot is not unlike figures 6.25(a) and (b)

Depending on the initial ratio of amphiphile to ^2H_2O the increasing electrolyte concentration results in single liquid crystal phase regions becoming unstable. The higher the ratio of amphiphile to ^2H_2O the greater the concentration of electrolyte required to destabilize the single liquid crystal phase regions.

The ^2H quadrupole splittings along the phase transition lines for both the CsPFO/CsCl/^2H_2O and APFO/NH_4Cl/^2H_2O systems (figures 6.7, 6.12, 6.18), and the results of x-ray[8] and neutron diffraction experiments[10], show that along the isotropic-to-nematic transition the micelle size is independent of electrolyte concentration.

^2H quadrupole splittings along isotherms in both the CsPFO/CsCl/^2H_2O and APFO/NH_4Cl/^2H_2O systems figures 6.15 and 6.10 show a monotonic increase. This implies either, an increase in the aspect ratio of the disc shaped aggregates as the salt concentration increases, or an effective nett decrease in the curvature of the mesophase aggregates. Thus the picture that emerges is that addition of salt induces a growth of the micelle but there is no change in the micelle size at the transition. As the micelle size has been shown to decrease with increasing temperature[13] the phase transition temperatures are displaced to higher temperatures with increasing salt concentration.

Figure 6.25 The temperature width of the isotropic/nematic coexistence region for the (a) CsPFO/CsCl/^2H_2O system at a fixed mass ratio of CsPFO to ^2H_2O of 1 : 1 as a function of CsCl, and (b) APFO/NH_4Cl/^2H_2O system at a fixed mass ratio of APFO to ^2H_2O of 9 : 11 as a function of NH_4Cl.

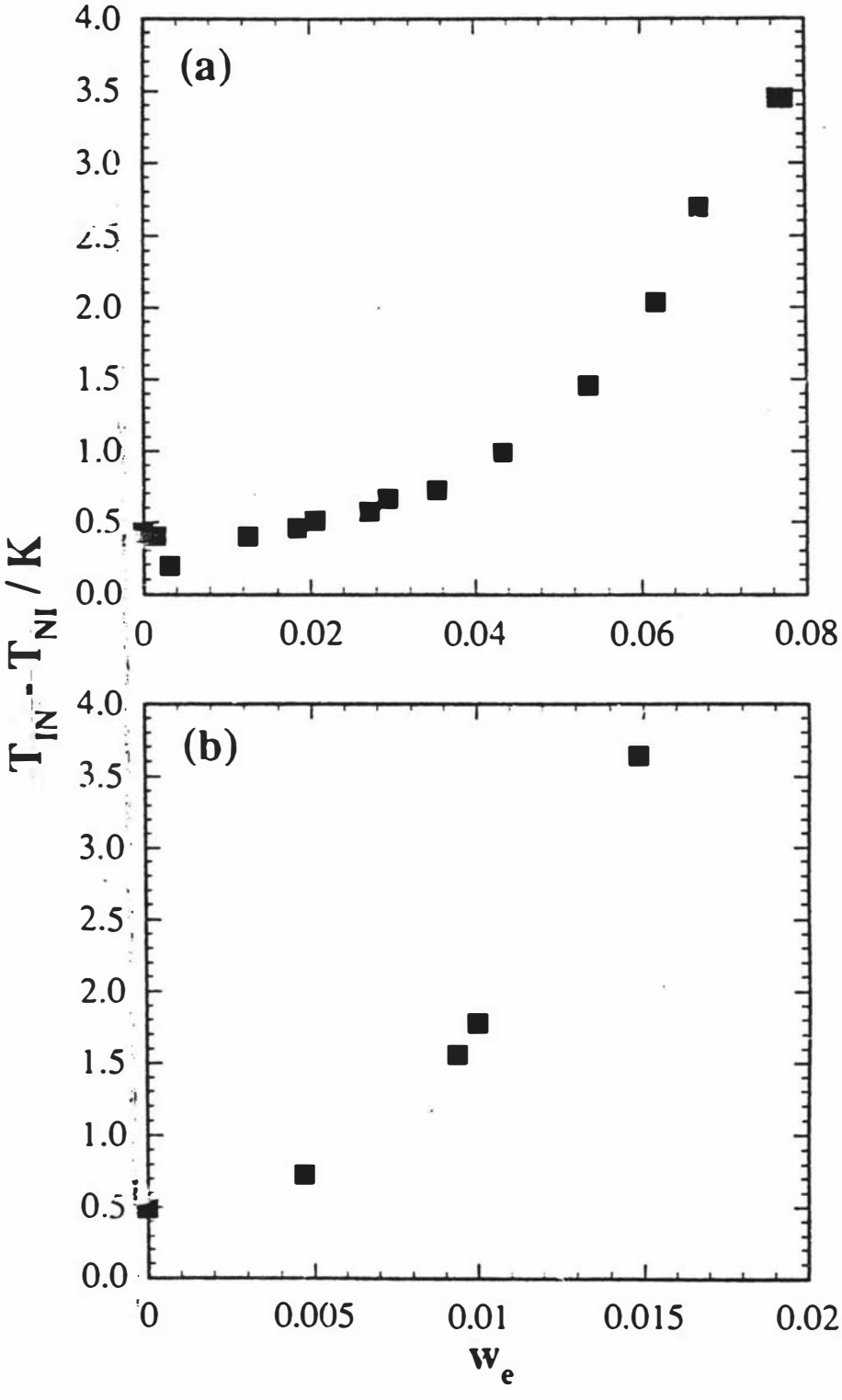

6.3 Discussion

6.3.1 Effect of Electrolyte on Self-Assembling Systems

Influence of Electrolyte on the Phase Behaviour

The partial phase diagrams of the ternary CsPFO/CsCl/^2H_2O and APFO/NH_4Cl/^2H_2O systems are similar in form. As the electrolyte concentration increases there is a monotonic increase in each of the phase transition temperatures. The nematic phase intermediate to the isotropic micellar solution and lamellar phases is initially stabilized at low electrolyte concentrations but ultimately destabilized at higher electrolyte concentrations and eventually disappears at a critical end point Cep. At electrolyte concentrations higher than Cep the isotropic micellar solution phase on cooling undergoes a phase transition directly to a lamellar phase. The magnitude of T_{IN} - T_{NI} reflects the increasing discontinuity in S and $\langle P_2 \cos\alpha \rangle_s$ across the transition as the strength of the transition increases. An example of the w_e dependence of the temperature width of the I/N_D^+ coexistence region is given in figures 6.25(a) and (b) for the CsPFO/CsCl/^2H_2O system with a mass ratio of CsPFO to ^2H_2O of 1 : 1 and the APFO/NH_4Cl/^2H_2O system at a fixed mass ratio of APFO to ^2H_2O of 9 : 11. In the binary CsPFO/^2H_2O system the width of the isotropic/nematic coexistence region increases with increasing mass fraction of amphiphile[4] and the plot is not unlike figures 6.25(a) and (b)

Depending on the initial ratio of amphiphile to ^2H_2O the increasing electrolyte concentration results in single liquid crystal phase regions becoming unstable. The higher the ratio of amphiphile to ^2H_2O the greater the concentration of electrolyte required to destabilize the single liquid crystal phase regions.

The ^2H quadrupole splittings along the phase transition lines for both the CsPFO/CsCl/^2H_2O and APFO/NH_4Cl/^2H_2O systems (figures 6.7, 6.12, 6.18), and the results of x-ray[8] and neutron diffraction experiments[10], show that along the isotropic-to-nematic transition the micelle size is independent of electrolyte concentration.

^2H quadrupole splittings along isotherms in both the CsPFO/CsCl/^2H_2O and APFO/NH_4Cl/^2H_2O systems figures 6.15 and 6.10 show a monotonic increase. This implies either, an increase in the aspect ratio of the disc shaped aggregates as the salt concentration increases, or an effective nett decrease in the curvature of the mesophase aggregates. Thus the picture that emerges is that addition of salt induces a growth of the micelle but there is no change in the micelle size at the transition. As the micelle size has been shown to decrease with increasing temperature[13] the phase transition temperatures are displaced to higher temperatures with increasing salt concentration.

Figure 6.25 The temperature width of the isotropic/nematic coexistence region for the (a) CsPFO/CsCl/^2H_2O system at a fixed mass ratio of CsPFO to ^2H_2O of 1 : 1 as a function of CsCl, and (b) APFO/NH_4Cl/^2H_2O system at a fixed mass ratio of APFO to ^2H_2O of 9 : 11 as a function of NH_4Cl.

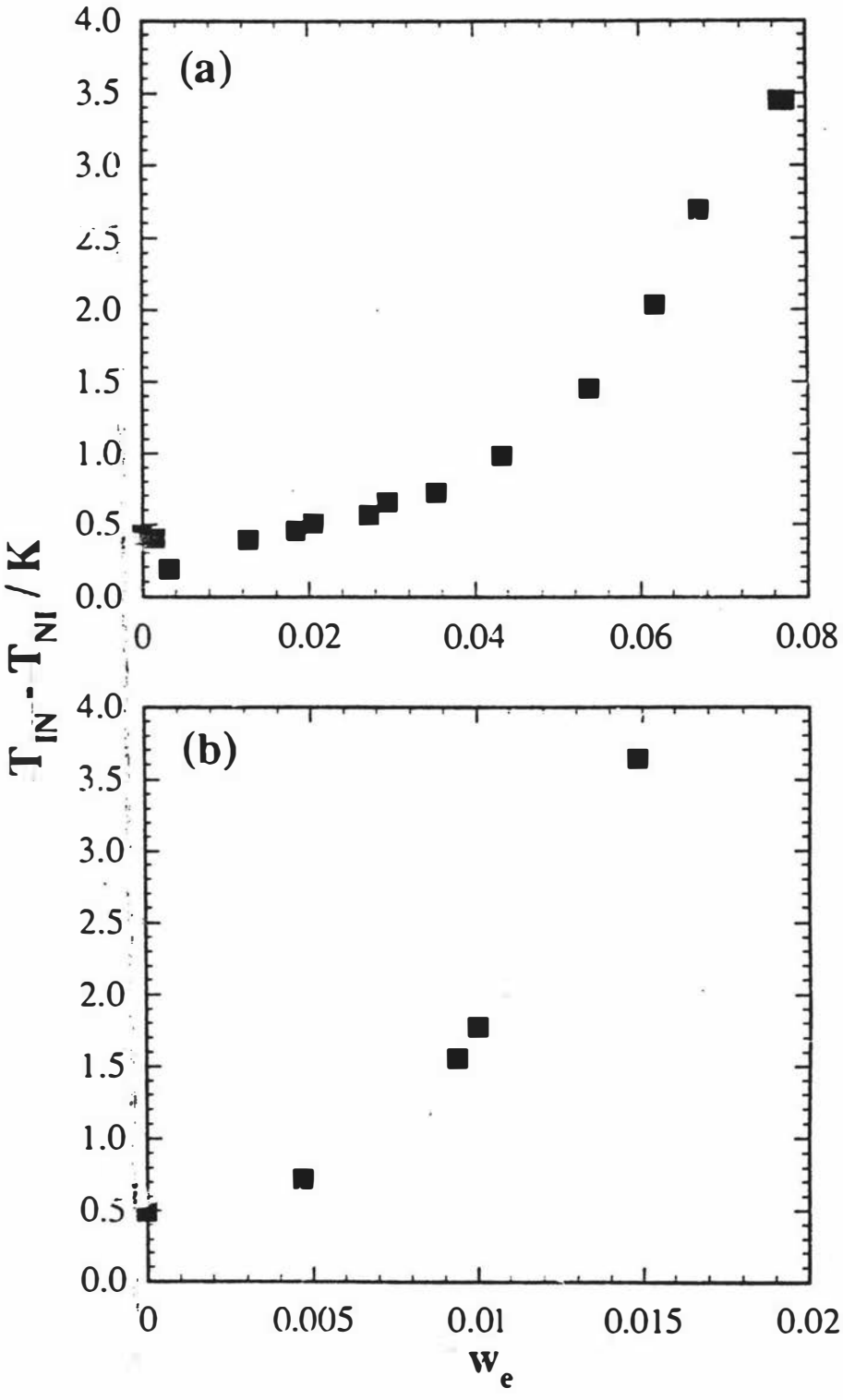

^2H quadrupole splittings have shown that along the L_D-to-N_D^+ and L_D-to-I transition lines at a given volume fraction of amphiphile the aggregate aspect ratio is invariant to electrolyte concentration. Leaver and Holmes have performed a small angle neutron scattering study of the CsPFO/CsCl/^2H_2O system at an amphiphile to ^2H_2O ratio of 1 : 1[10]. Their results confirm the structure of the aggregate at the L_D-to-N_D^+ and L_D-to-I transition is invariant with electrolyte concentration.

Comparison Between The CsPFO/CsCl/^2H_2O and APFO/NH_4Cl/^2H_2O Systems

A comparison of the APFO/^2H_2O and CsPFO/^2H_2O binary systems shows the phase diagrams are very similar when plotted in temperature versus volume fraction coordinates, except that the corresponding transitions are some 23 K higher for the CsPFO/^2H_2O system[14].

In addition it has been shown that at corresponding ϕ values the a/b ratios at the phase transition temperatures are the same[14]. The volume fractions of the amphiphile in the CsPFO/^2H_2O(w_a = 0.5) sample (ϕ = 0.322) is very close to that in the APFO/^2H_2O(w_a = 0.45) one (ϕ = 0.328) and its a/b ratio is 0.32[15]. It is interesting therefore to examine the relative effect of the addition of electrolyte in the two systems. This is shown in figure 6.26 where the quantity $\Delta\tilde{\nu}(^2H)(x_w/x_a)$ (which is proportional to $S\langle P_2\cos\alpha\rangle_s$, see equation[6.5]) is plotted against x_e/x_a where x_e and x_a are the mole fraction of electrolyte and amphiphile respectively. Along the phase transition boundaries the APFO/NH_4Cl/^2H_2O system consistently has a larger value for the quantity $\Delta\tilde{\nu}(^2H)(x_w/x_a)$ than the CsPFO/CsCl/^2H_2O system at a corresponding x_e/x_a. In chapter 7 this will be shown to be attributed to a higher value for n_bS_{OD} (equation[3.19]) in the APFO/NH_4Cl/^2H_2O system. The plot shows that at a given volume fraction of surfactant the APFO/NH_4Cl/^2H_2O system requires less electrolyte per amphiphile than the CsPFO/CsCl/^2H_2O system to destabilize the nematic phase.

In both the CsPFO/CsCl/^2H_2O and APFO/NH_4Cl/^2H_2O systems the isotropic-to-nematic transition occurs when the micelle attains an appropriate a/b ratio at a particular volume fraction, a result that is consistent with a hard particle interaction. In a magnetic birefringence study on the CsPFO/CsCl/^2H_2O system at a CsPFO/^2H_2O ratio of 2 : 3, the micelle aggregation number as measured by a quantity derived from the Cotton Mouton coefficient apparently decreased at T_{NI} as w_e increased[16]. This was interpreted in terms of a decrease in the "effective" size of the micelle as the Debye length decreased with increasing electrolyte concentration. Rosenblatt used the argument that from the standpoint of the entropic free energy[17], the effective micelle diameter increases by a term proportional to and of the size of the Debye length. The present result shows that there is no significant change in the micelle size at the transition, *i.e.* the decreasing Debye length has no effect on the hard particle interaction. The Debye length (κ^{-1}) is calculated from [18]

Figure 6.26 Comparison of the relative ^2H quadrupole splittings $\Delta\tilde{\nu}(^2H)/x_a/x_w$ at the T_{NI}, T_{LI}, and T_{LN} phase transition boundaries between APFO/NH_4Cl /^2H_2O samples with a fixed mass ratio of APFO to ^2H_2O of 9 : 11 and CsPFO/CsCl/^2H_2O samples with a fixed mass ratio of CsPFO to ^2H_2O of 1 : 1.

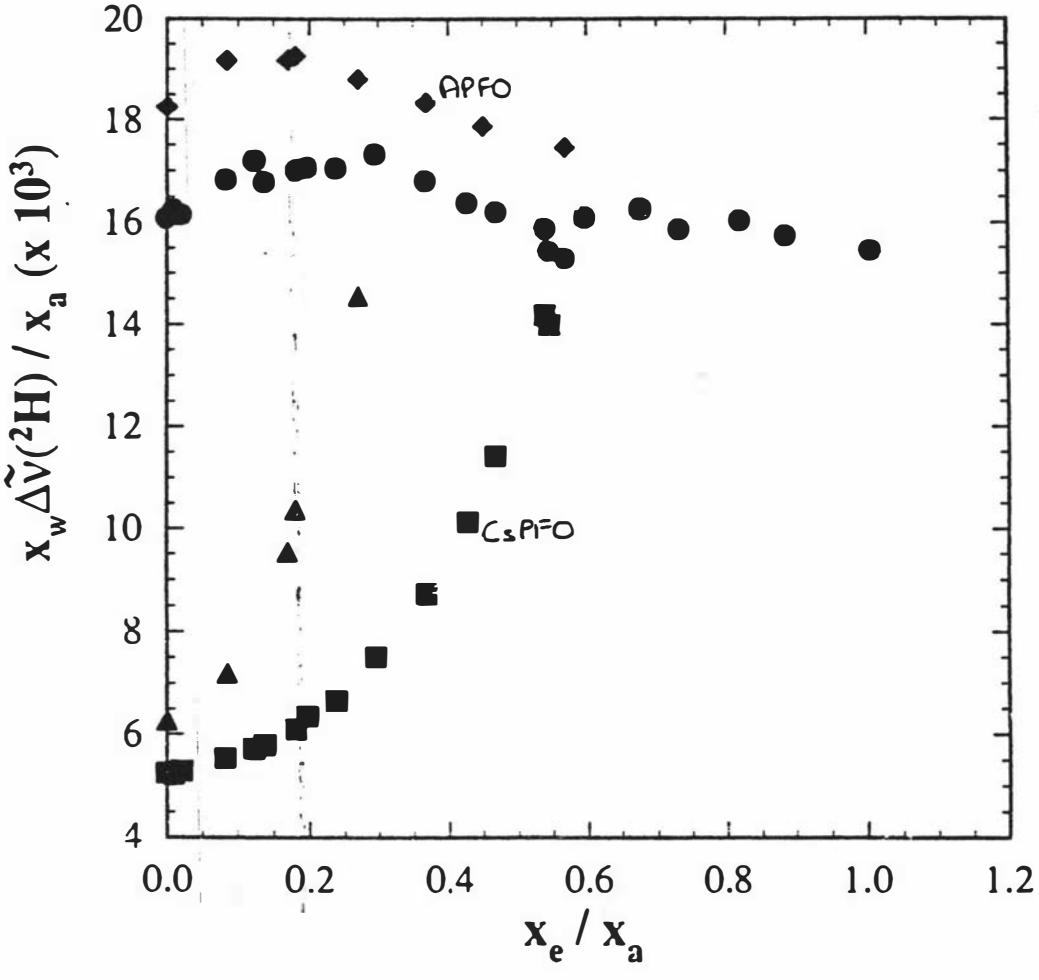

$$\kappa = \left(\frac{\sum_i \rho_{\infty i} e^2 z_i^2}{\varepsilon \varepsilon_o kT} \right)^{1/2}$$

where ρ_{∞} is the number density of the i'th ionic species of charge z_i and ε and ε_o are the relative permittivity and the permittivity of free space respectively.

For the $w_e = 0$ samples κ^{-1} is 0.40 nm and 0.42 nm for the CsPFO and APFO systems respectively. For the CsPFO/CsCl/^2H_2O system at Cep, κ^{-1} has only decreased slightly to a value of 0.34 nm. These distances should be compared with the micelle dimensions of 1.1 nm (*a*) by 3.4 nm (*b*). The size of κ^{-1} is small compared with the particular size and gets smaller as the electrolyte concentration increases. Thus, in contrast to the conclusions of Rosenblatt this study indicates that the inter-micellar interactions do not seem to be affected by addition of electrolyte and for an explanation of the observed effects it is necessary to examine the influence of electrolyte on the intra-micellar interactions, *i.e.* the micellar self-assembly.

Influence of Electrolyte on The Self-Assembly

It has been shown here that the disorder/order phase behaviour of CsPFO/CsCl/^2H_2O and APFO/NH_4Cl/^2H_2O systems can be understood in terms of changes in the aggregate size on the addition of electrolyte. In the previous chapter the effect of temperature on the micellar self-assembly has been considered. This discussion will consider the effect of electrolyte on the micellar self-assembly in the context of the models introduced in chapter 4.

At constant temperature the effect of the electrolyte is to increase the aggregation number of the discotic micelle. The way the micelle grows is to increase the length of the major axis, *i.e.* the micelle becomes more anisometric and the intermicellar anisotropic interaction is increased. But it must be remembered that the axial ratio of micelles cannot continue to decrease continuously in the lamellar phase as a function of increasing w_e, the limit being when it collides with its nearest neighbour at which point discrete micelles are no longer possible. Leaver *et al* [10] have assumed the structure that evolves within the lamellar phase consists of continuous amphiphile layers pierced by irregular water filled holes. With this assumption their scattering experiments have shown that the addition of CsCl anneals out the water filled holes. So even when discrete micelles are not the structural unit in the mesophase, the addition of electrolyte results in a nett reduction in the curvature of the aggregate. At first it would appear that the physics of the phase transitions is overlayed on the chemistry of the self assembly. But this is not strictly valid as increasing w_e eventually results in the nematic phase disappearing at Cep. If it was simply a case of excluded volume driven transitions then a nematic phase would always

be accessible. The aggregate structure probably evolves until the discotic micelles are no longer present at high w_e and thus will account for the disappearance of the N_D^+ phase. However, it is most likely the influence of the electrolyte on the self-assembly that is mainly responsible for this rather than a change in the intermicellar interactions.

The EL model considers the effect of electrolyte for discotic micellar systems and they predict the micelles size distribution increases with increasing electrolyte concentration as shown in figure 4.2. The EL model has also predicts that in addition to increases in aggregate size distributions as a function of increasing electrolyte concentration, there is also an evolution of the aggregate structure. At low amphiphile concentrations there is an evolution of the aggregate structure from spheres→rods→discs→vesicles as shown in figure 4.3. The ternary phase diagrams indicate that there is complex aggregate behaviour at low amphiphile high electrolyte concentrations also $\Delta\tilde{\nu}(^2H)$ results indicate an evolution of the lamellar phase structure from discrete discs to maybe perforated bilayers or even eventually classical bilayer type structures. The evolution of the aggregate structure is an interesting problem that is the subject of on going research but will not be considered here.

In terms of the MBG model the screening of the carboxylic headgroups reduces the contribution of $h_i(a)$ to the chemical potential for the amphiphile in the cylinder of the discotic micelle (equation [4.1]). So there is a decrease in the chemical potential in the cylinder part of the disc with respect to the rim of the disc. This decrease in the difference in chemical potentials therefore accounts for an increase in the size distribution of the discs equation [4.2]. Our observations are qualitatively consistent with the predictions of both of these models.

6.3.2 Influence of Electrolyte on Tcp

It has been shown here that the addition of electrolyte weakens the already weakly first order L_D-to-N_D^+ transition to such an extent that it appears to become second order (figure 6.11). Tricritical points along the L_D-to-N_D^+ transition line have also been observed in the binary CsPFO/water and APFO/water systems[1-3]. In these systems the transition changes from first order to second order with decreasing amphiphile concentration. In the case of the CsPFO/CsCl/^2H_2O system with a fixed amphiphile to ^2H_2O mass ratio of 53 : 47 the inverse of this behaviour occurs in that the transition from first order to second order occurs on increasing the electrolyte concentration. The reason for the occurrence of Tcp, is at this stage not well understood and there is no obvious explanation for the mechanism of this transition. It is clear, however, from figure 6.27 that T_{NL} - T_{LN} appears to become asymptotic to the w_e axis as w_e increases, which is analogous to this quantity becoming asymptotic to the w_a-axis as w_a decreases in the binary[3]. It has been predicted that the nematic-to-lamellar transition of pure thermotropic liquid crystals

Figure 6.27 A plot of the temperature width of the N_D^+/L_D coexistence region verses w_e for the CsPFO/CsCl /^2H_2O system at a fixed mass ratio of CsPFO to ^2H_2O of 53 : 47.

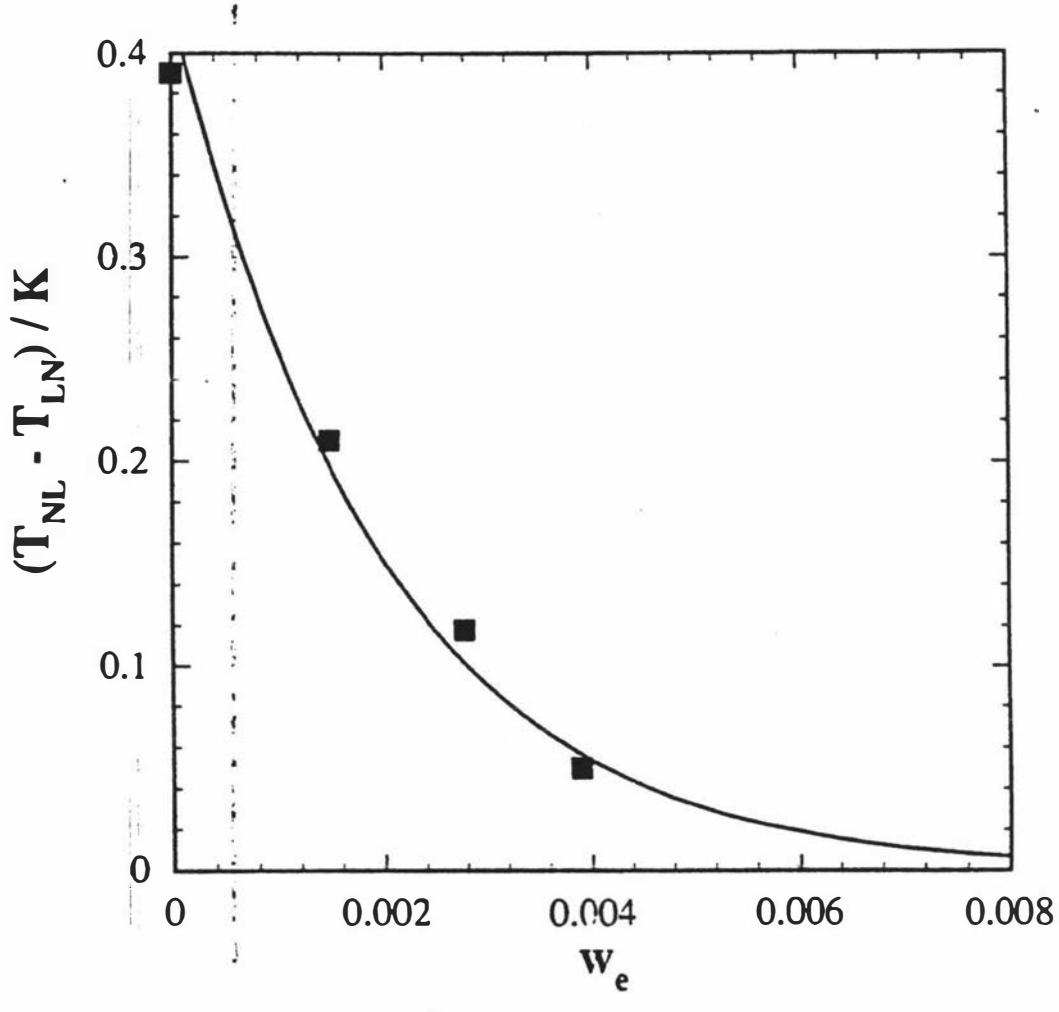

and their mixtures should always be at least weakly first order as a consequence of coupling between director fluctuations and the smectic order parameter[19]. This coupling gives rise to a cubic term in the landau free energy expression for the transition that results in a first order transition. Anisimov *et al* have shown there is a crossover from classical Landau theory behaviour at a solute concentration roughly identified as the Landau tricritical point[20]. Above this concentration the entropy change for the transition is strongly dependent on solute concentration while below the point the concentration dependence is weak, but more importantly, the entropy change is always positive, *i.e.* the transition is first order along the whole of the nematic-to-lamellar transition line. Assuming that T_{NL} - T_{LN} is proportional to the strength of the transition[3], the general appearance of figure 6.27 suggests that this may also be the case for the N_D^+-to-L_D transition in the CsPFO/CsCl/^2H_2O system.

It is interesting to note that Shin *et al* performed specific heat measurements at the nematic-to-lamellar and nematic-to-isotropic phase transitions in the binary CsPFO/H_2O system[21]. They have attributed the existence of Tcp along the L_D-to-N_D^+ transition line to ionic contaminants in the CsPFO. They explain the increase in the temperature width of the nematic-to-lamellar mixed phase region in terms of increasing impurities with increasing total amphiphile concentration. In the present study the addition of an ionic substance to the CsPFO/^2H_2O system has been shown to have the opposite effect, i.e. it causes a weakening of the transition which eventually becomes second order at an apparent Tcp along the lamellar-to-nematic transition line.

6.3.3 The Influence of Co-ions on the Phase Behaviour.

The observation of ^{35}Cl quadrupole splittings in CsPFO/CsCl/^2H_2O samples indicates that some chloride ions must reside in the vicinity of the micellar surface, where the hydration sheath is distorted from spherical symmetry under the influence of the electric field gradient at the micellar surface. According to the Gouy-Chapman model of the diffuse double layer there is a "stirring" effect as a result of thermal motion which allows a dispersal of the rigid wall of counter-ions which define the outer Helmholtz plane. Thus, while the Cs^+ ions cluster close to the micelle surface, a small fraction of Cl^- ions present ions are able to penetrate close enough to undergo distortion of their outer hydration sheaths.

The w_c dependence of the ^{35}Cl quadrupole splittings at the transition temperatures and along the 310 K isotherm in the lamellar phase is shown in figure 6.14. In the latter case, the increase in the values with increasing w_c reflects increases in S, $\langle P_2 \cos\alpha \rangle_s$ and β_{Cl}. The ratio of fraction of bound counter-ions to co-ions can be calculated by comparing the chlorine and caesium quadrupole splittings. It is clear from equations[3.21] and [3.23] that in ordered liquid crystal phases at identical concentrations and temperatures

$$\frac{\beta_{Cs}}{\beta_{Cl}} = \frac{7\chi_{Cl}\Delta\tilde{\nu}_{Cs}}{\chi_{Cs}\Delta\tilde{\nu}_{Cl}} \qquad [6.9]$$

where β_{Cs} is given by $n_{bCs}/(n_a+n_e)$ and β_{Cl} by n_{bCl}/n_e. Here n_a and n_e are the number of moles of amphiphile and electrolyte in the sample respectively. Equation[6.9] can be rearranged to give an expression for the number of bound Cs ions (n_{bCs}) per bound Cl ion (n_{bCl}),

$$\frac{n_{bCs}}{n_{bCl}} = \frac{7\chi_{Cl}\Delta\tilde{\nu}_{Cs}}{\chi_{Cs}\Delta\tilde{\nu}_{Cl}} \times \frac{(n_a + n_e)}{n_e} \qquad [6.10]$$

and assuming an identical electric field gradient, the ratio of the quadrupole coupling constants can be replaced by the ratio of the nuclear electric quadrupole moments. The bound ion ratios calculated using equation[6.10] are in figures 6.28 (a) (at T_{LN}) and (b) (along the 310 K isotherm).

As a test of the assumptions made to obtain this figure the ratio of the bound ion fractions at the micelle surface was calculated from the Boltzmann distribution of ions at a distance x from a plane surface[18]. For x = 0, and using the Debye Huckel model, the ratio of surface concentrations, *i.e.* n_{bCs}/n_{bCl} is

$$\frac{[Cs^+]_0}{[Cl^-]_0} = \frac{[Cs^+]_\infty e^{-e\psi_0/kT}}{[Cl^-]_\infty e^{+e\psi_0/kT}} \qquad [6.11]$$

where ψ_0 is the electrostatic potential at the surface, and the subscripts 0 and ∞ represent the concentration of the ions at the surface and in the bulk respectively. The value of ψ_0 was adjusted to give agreement with the lowest w_e ratio. The actual values are -0.065 V for the ratios along the transition line and -0.064 V for the corresponding ones along the 310 K isotherm which is in good agreement with the calculated electrostatic potential of a 1 : 1 electrolyte at a concentration of 1 M[18]. The agreement between the NMR and theoretical ratios is excellent, and perhaps surprising since the ionic concentrations are high and the Debye Huckel model applies only to dilute solutions. This clearly shows the expected relative increase in the chloride ion bound fraction with increase in electrolyte concentration. An even better fit can be achieved if ψ_0 is allowed to decrease slightly with increasing electrolyte concentration as it is predicted. However, even at the highest w_e value the ratio of Cl to Cs ions is still only 1 : 100 and there would not be expected to be any significant contribution from the co-ion in determining the phase behaviour.

This minor role played by the co-ion in the self-assembly of the fluorocarbon chains is also demonstrated by co-ion substitution experiments where CsF, CsBr and CsI were substituted for the CsCl used in the bulk of this study. The comparison was made at roughly equal salt mol fractions of $\approx 6.0 \times 10^{-3}$ at which concentration addition of CsCl would have resulted in an increase of phase transition temperatures of about 9.9 K over those for the binary system. The actual phase transition temperatures are compared with

Figure 6.28 The ratio of bound Cs^+ ions (n_{bCs}) per bound Cl^- ions (n_{bCl}) (a) along the nematic-to-lamellar transition line and (b) along the 310 K isotherm. The squares(■) have been calculated from the quadrupole splittings (equation [6.10], while the circles (O) are calculated from the Debye Huckel model (equation[6.11]).

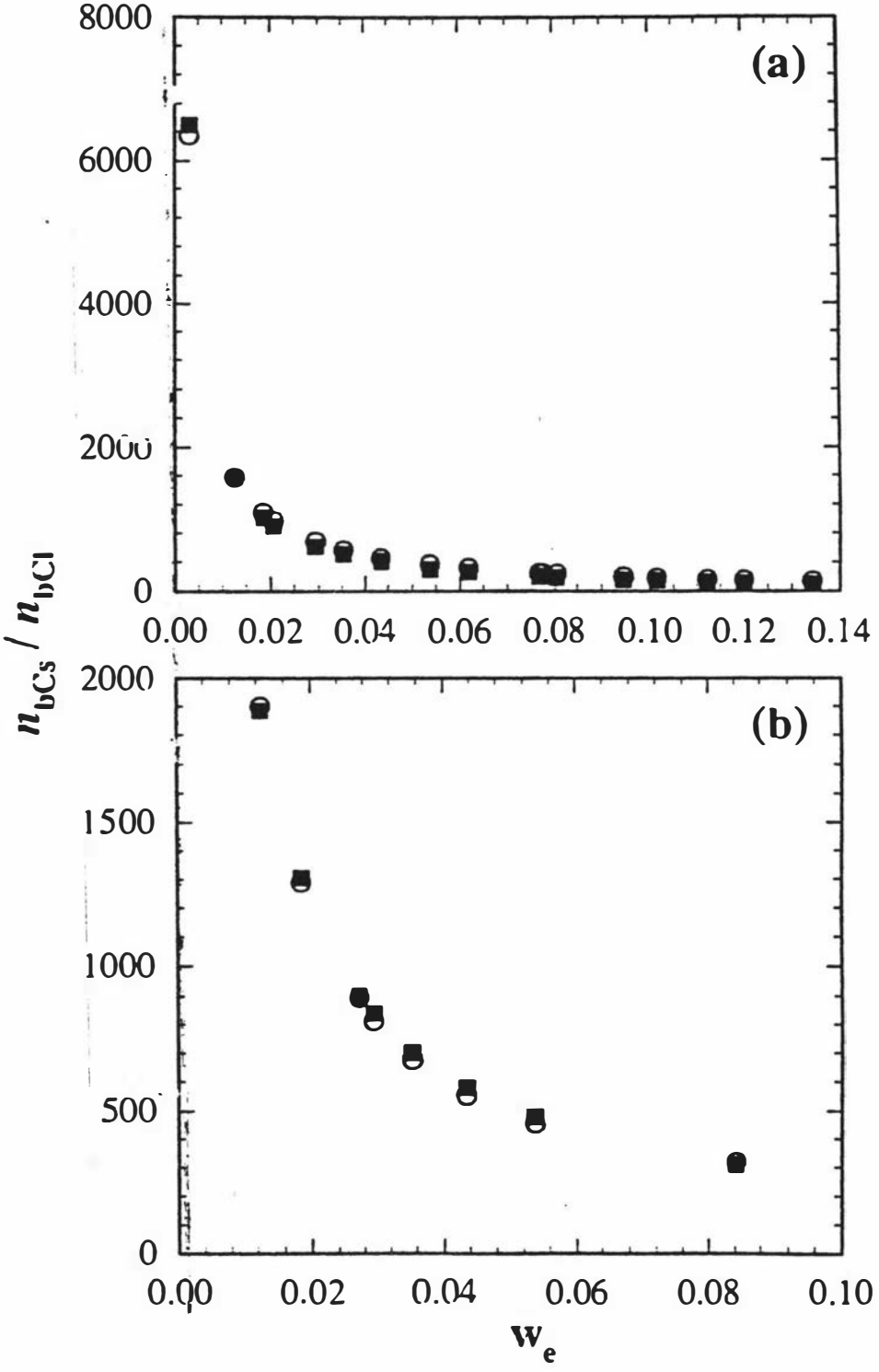

those of the CsCl system in figure 6.29. It is clear that the co-ion plays, at most, only a minor role in aggregate self-assembly.

6.3.4 Field Induced Order

The transition from an isotropic phase to a nematic liquid crystal is first order, but weak in the sense that the molar entropy of the transition is typically only about 0.2 R for thermotropics and even less for lyotropics[22]. A consequence of this is that the isotropic liquid begins to assume characteristics of the nematic phase well before the transition occurs. In liquid crystalline systems the observation of this pretransitional phenomena associated with the onset of order in the isotropic phase immediately prior to the isotropic to nematic phase transition temperature yields valuable information concerning the mechanism of the phase transition. As the isotropic-to-nematic transition is approached the isotropic phase develops more nematic phase characteristics, *i.e.* an increase in the extent of microscopic ordering. In lyotropic liquid crystal systems the nematic-like properties derive from small groups of micelles which have local ordering *i.e.* a degree of orientational correlation between their symmetry axis. These small groups of micelles are anisotropic domains suspended in an isotropic continuum.

In the isotropic phase the CsPFO micelles are discotic and therefore they exhibit an anisotropy in their magnetic susceptibility. Pretransitional behaviour in the isotropic phase of CsPFO/^2H_2O has been studied through the orientational order induced by a magnetic field and detected by optical birefringence[23] and NMR measurements[12]. NMR has an advantage over optical birefringence measurements in that separate NMR signals from the isotropic and nematic phases in the biphasic region can be distinguished, thus permitting measurements to be made across the biphasic region which gives access to information not available from birefringence measurements. Both experiments give values for T_{IN}-T^*, where T^* is the temperature of the theoretical second order transition from the isotropic to nematic phase.

The origin of the ^2H quadrupole splittings in the isotropic phase arises from the orientational ordering of the micelles induced by the magnetic field. This orientational ordering arises from the magnetic torque on the micelle which is enhanced by the build-up in angular correlations of the micelles as the transition is approached. This unquenches the quadrupole interactions of the ^2H spins of the ^2H_2O molecules. The quadrupole splitting of the deuterium signal can be shown to have the following dependence[12]

$$\Delta\tilde{\nu}(^2H) = \frac{|\tilde{q}_{zz}|_s \Delta\chi B^2}{10k(T - T^*)} \qquad [6.12]$$

where $\Delta\chi$ is the anisotropy in the magnetic susceptibility of the micelle and the remaining terms are as defined previously. Taking the inverse of equation[6.12]

Figure 6.29 Comparison of the relative effects of different co-ions on the phase behaviour of the CsPFO/electrolyte/^2H_2O system with a fixed mass ratio of CsPFO to ^2H_2O of 1 : 1. Solid line are the phase transition boundaries of the CsPFO/CsCl /^2H_2O system with a fixed mass ratio of CsPFO to ^2H_2O of 1 : 1. The co-ions substituted for CsCl are CsF(◆), CsBr(O), and CsI(□).

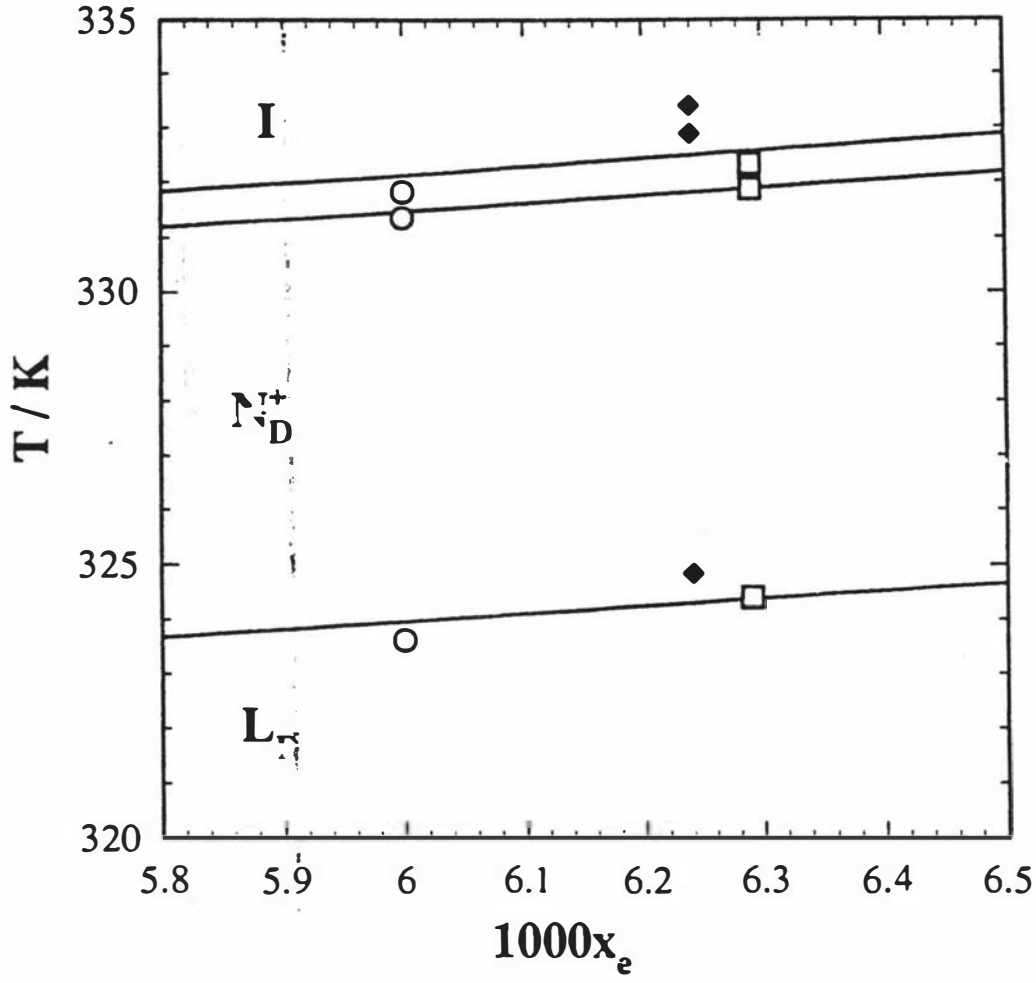

$$\left(\Delta\tilde{\nu}\left(^2H\right)\right)^{-1} = \left(\frac{10k}{\Delta\chi B^2\left|\tilde{q}_{zz}\right|_s}\right)\left(T - T^*\right) \qquad [6.13]$$

indicates that a plot of $(\Delta\tilde{\nu}(^2H))^{-1}$ versus temperature will give a straight line with an intercept of zero at $T = T^*$ *i.e.* the splitting diverges towards T^*. Figure 6.30 shows that this is the case and illustrates the quenching of the divergence in the quadrupole splittings at T_{IN}. Precise values of both T_{IN} and T^* and, in particular, $T_{IN} - T^*$ can be obtained from the plots in figure 6.30.

Over the small temperature range for which the pretransitional quadrupole splittings are measured the micellar aggregation number ($\langle P_2 \cos\alpha\rangle_s$) is practically constant and since the aggregation number influences other factor such as $|\tilde{q}_{zz}|_s$, $\Delta\chi$ and T^*, to a first approximation these also remain constant for any given sample. The magnitude of the quadrupole splitting is a function of the square of the magnetic field strength and $(T - T^*)^{-1}$. In NMR the field strength is dependent on the spectrometer and is therefore a constant for any given experiment. .

A plot of $T_{IN} - T^*$ versus w_e in CsPFO/CsCl/^2H_2O samples (mass ratio CsPFO : ^2H_2O of 1 : 4) is given in figure 6.31.The addition of electrolyte increases the strength of the isotropic-to-nematic transition (increases $T_{IN} - T^*$). Figure 6.31 also shows $1/\Delta\tilde{\nu}(^2H)$ at T_{IN} increases with increasing w_e, i.e. the increase in $1/\Delta\tilde{\nu}(^2H)$ is proportional to $T_{IN} - T^*$(equation[6.13]). The quantity $(T_{IN} - T^*)\Delta\tilde{\nu}(^2H)$ is plotted against w_e in figure 6.32. Within experimental error this quantity and hence $\Delta\chi B^2|\tilde{q}_{zz}|_s$ is constant. B is simply the strength of the spectometer magnetic field, and $\Delta\chi$ and $|\tilde{q}_{zz}|_s$ both depend on the micelle size through the quantity $\langle P_2 \cos\alpha\rangle_s$ ($\Delta\chi = s\Delta\chi_a S_a \langle P_2 \cos\alpha\rangle_s$, where s is the aggregation number, $\Delta\chi_a$ the anisotropy in the magnetic susceptibility of the amphiphile molecule, and S_a the order parameter for the molecule). The only possible term in this expression that could lead to changes in both $|\tilde{q}_{zz}|_s$ (see equation[3.20]) and $\Delta\chi$ is therefore $\langle P_2 \cos\alpha\rangle_s$ and the product of $|\tilde{q}_{zz}|_s$ and $\Delta\chi$ is depends on $\langle P_2 \cos\alpha\rangle_s^2$. The implication of this is that the micelle is the same size along the I-to-N_D^+ phase transition line irrespective of w_e.

Figure 6.30 Plot of the inverse of the field induced quadrupole splittings $1/(\Delta\tilde{\nu}(^2H))$ for the w_e = 0.00 and 0.0104 samples from the CsPFO/CsCl /^2H_2O system with a fixed mass ratio of CsPFO to ^2H_2O of 1 : 4, as a function of T - T_{IN}. The temperature of the theoretical second order transition T* for each sample is the point at which the extrapolated line intercepts the x-axis.

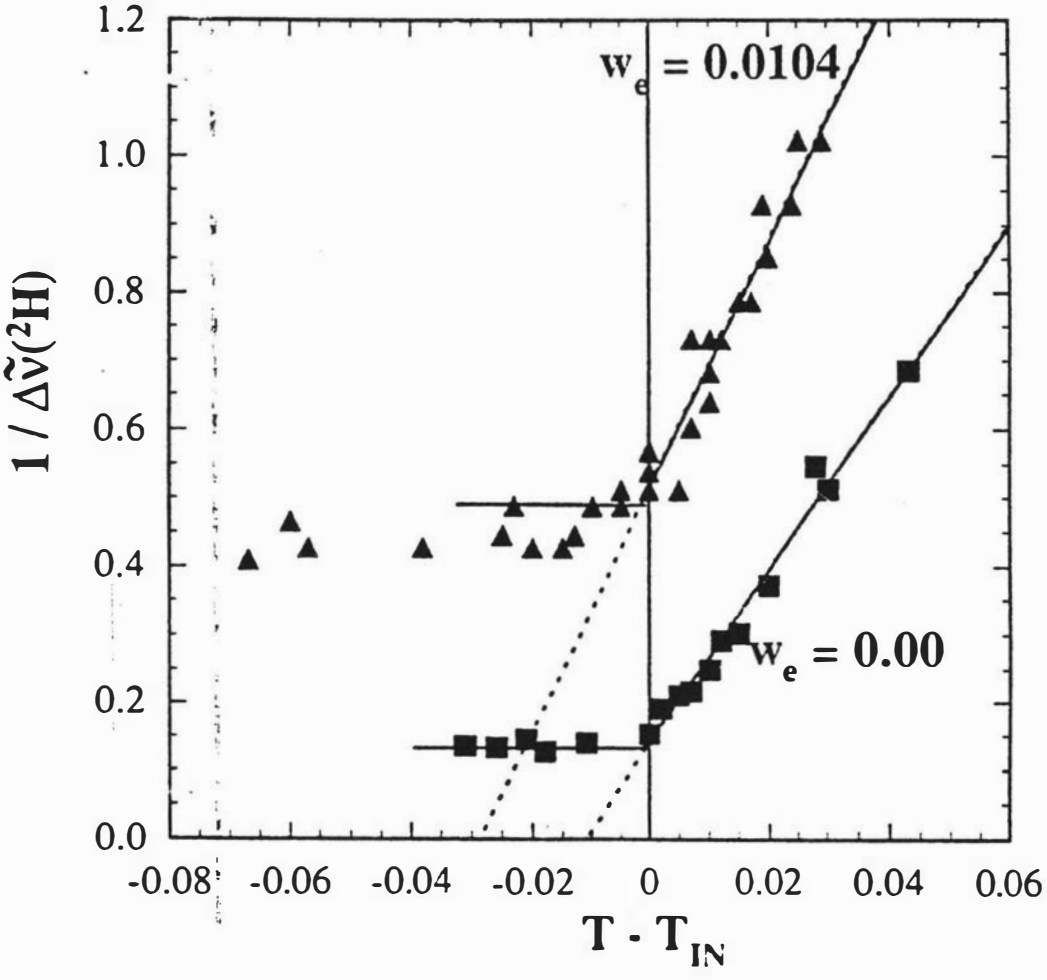

Figure 6.31 The w_e dependence of both $\Delta\tilde{\nu}(^2H)_{T_{IN}}$(■) and T_{IN} - T*(●) for the CsPFO/CsCl /^2H_2O system with a fixed mass ratio of CsPFO to ^2H_2O of 1 : 4.

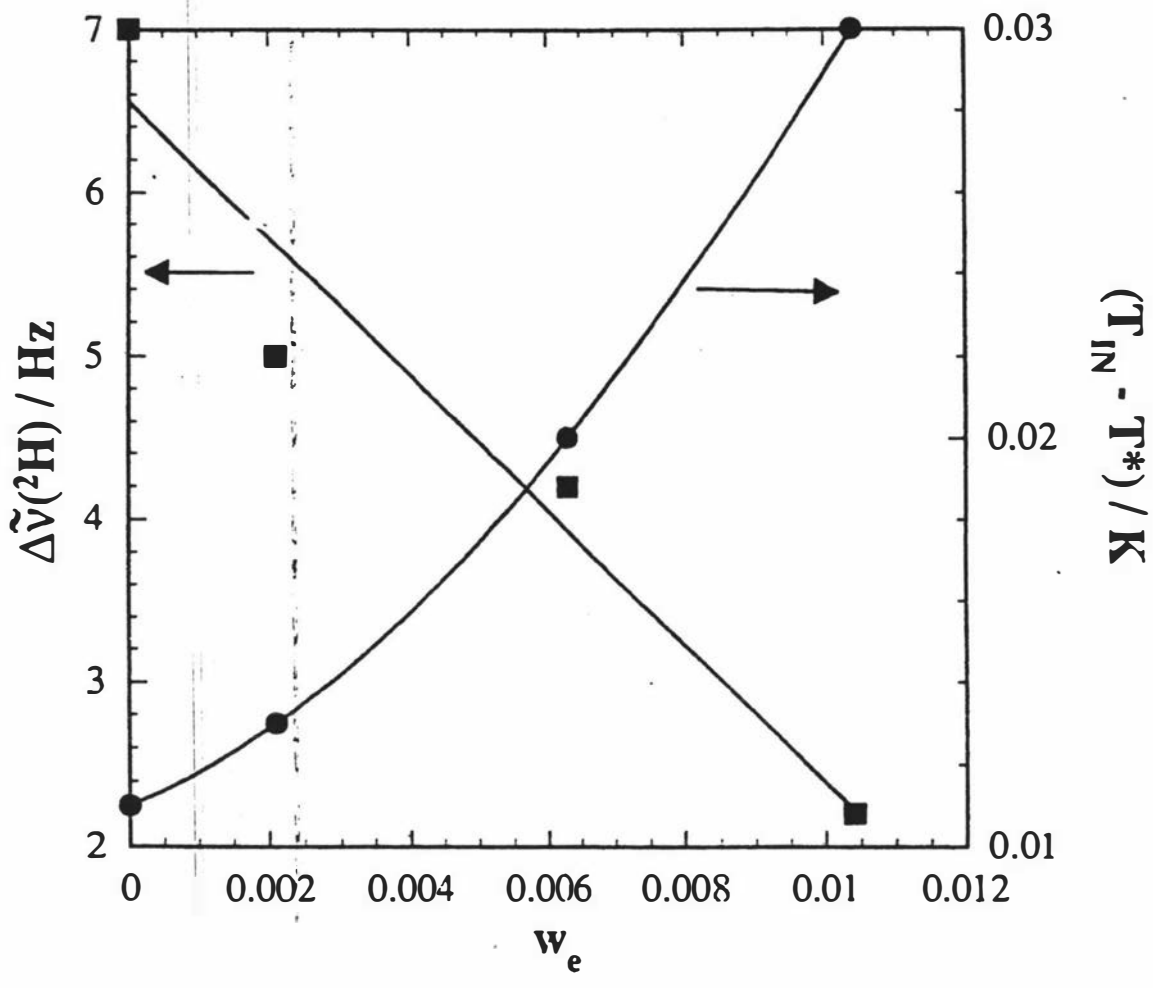

Figure 6.32 $\Delta\tilde{\nu}(^2H)_T$ multiplied by T_{IN} - T* for the CsPFO/CsCl /^2H_2O system with a fixed mass ratio of CsPFO to ^2H_2O of 1 : 4 as a function of w_e. The result shows an invariance to the electrolyte concentration.

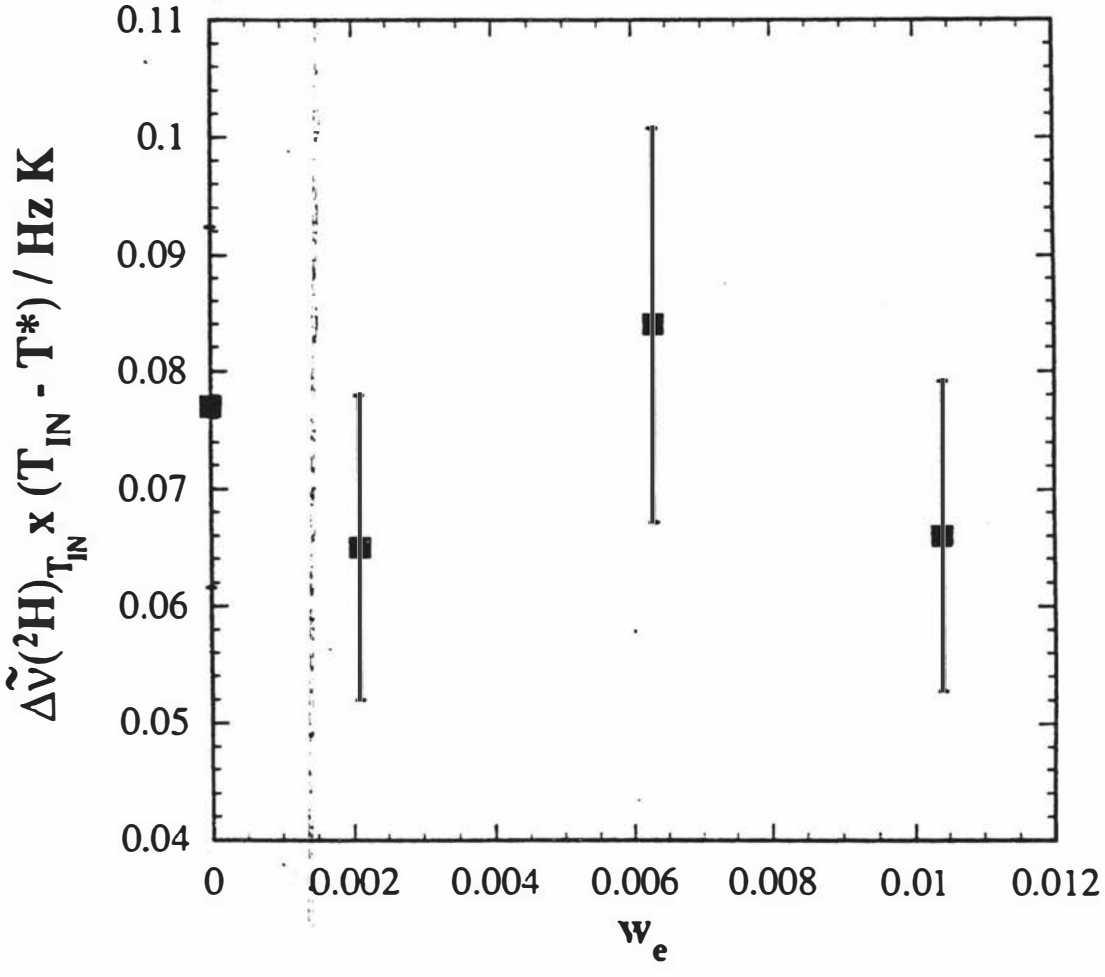

References

1. N. Boden, J. Clements, K. W. Jolley, D. Parker, M. H. Smith, *J. Chem. Phys.* **93**, 9096-9105 (1990).

2. N. Boden, K. W. Jolley, M. H. Smith, *Liq. Cryst.* **6**, 481-488 (1989).

3. N. Boden, K. W. Jolley, M. Smith, *J. Phys. Chem.* **97**, 7678-7690 (1993).

4. N. Boden, S. A. Corne, K. W. Jolley, *J. Phys. Chem.* **91**, 4092-4105 (1987).

5. J. Clements, personal communication, (1991).

6. D. Parker, Ph.D. University of Leeds (1988).

7. N. Boden, K. W. Jolley, *Phys. Rev. A* **45**, 8751-8758 (1992).

8. G. Oriques, Ph. D., University of Leeds (1993).

9. A. N. Parb[illegible], Master of Science, Massey University (1990).

10. M. S. Leaver, M. C. Holmes, *J. Phys. II* **3**, 105-120 (1993).

11. N. Boden, S. A. Corne, M. C. Holmes, P. H. Jackson, D. Parker, K. W. Jolley, *J. Physique* **47**, 2135-2144 (1986).

12. K. W. Jolley, M. H. Smith, N. Boden, *Chem. Phys Lett.* **162**, 152-156 (1989).

13. M. C. Holmes, D. J. Reynolds, N. Boden, *J. Phys. Chem.* **91**, 5257-5262 (1987).

14. N. Boden, P. J. B. Edwards, K. W. Jolley, in *Structure and Dynamics of Strongly Interacting Colloids and Supramolecular Aggregates in Solution* S.-H. Chen, J. S. Huang, P. Tartaglia, Eds. (Kluwer academic Publishers, Dordrecht, 1992), vol. 369, pp. 433-461.

15. N. Boden, J. Clements, K. A. Dawson, K. W. Jolley, D. Parker, *Phys. Rev. Lett.* **66**, 2883-2886 (1991).

16. C. Rosenblatt, N. Zolty, *J. Physique Lett.* **46**, L-1191-L-1191 (1985).

17. L. Onsager, *Ann. N. Y. Acad. Sci.* **51**, 627-659 (1949).

18. J. Israelachvili, *Intermolecular & Surface Forces* (Academic Press Ltd, London, 1992).

19. B. I. Halperin, T. C. Lubensky, S. K. Ma, *Phys. Rev. Lett.* **32**, 292-295 (1974).

20. M. A. Anisimov, P. E. Cladis, E. E. Grorodetskii, D. A. Huse, V. G. Taratuta, W. van Saarloss, V. P. Voronov, *Phys. Rev. A* **41**, 6749 (1990).

21. S. T. Shin, S. Kumar, *Phys. Rev. Lett.* **66**, 1062-1065 (1991).

22. G. S. Attard, P. A. Beckmann, J. W. Emsley, G. R. Luckhurst, D. L. Turner, *Mol. Phys.* **45**, 1125-1129 (1982).

23. C. Rosenblatt, S. Kumar, J. D. Litster, *Phys. Rev. A* **29**, 1010-1012 (1984).

Chapter 7
Effect of Counter-Ion Identity on the Self-Organisation and Self-Assembly

Comparison of the binary APFO/^2H_2O and CsPFO/^2H_2O systems has shown that at corresponding volume fractions of amphiphile the order/disorder phase transitions occurs at the same axial ratio in each system (figure 5.6(a) and (b)). The phase diagrams of the binary APFO/^2H_2O and CsPFO/^2H_2O systems, figures 6.3 and 1.3 respectively, indicate the phase transition temperatures for the APFO/^2H_2O system are lower (by ≈23 K) than the CsPFO/^2H_2O system at a corresponding volume fraction of amphiphile. The implication is that at the transitions the counter-ion appears to have a significant effect on the self-assembly, but little effect on the self-organisation of these micellar liquid crystal systems. In this chapter the influence of the counter-ion on the self-assembly and self-organisation is probed by altering the ratio of NH_4^+ ions to Cs^+ ions at a fixed mole fraction of surfactant.

7.1 Phase Behaviour of the APFO/CsPFO/^2H_2O system

The phase diagram of the APFO/CsPFO/^2H_2O system with the mole fraction of amphiphile x_a fixed at 0.0291 is presented in figure 7.1. At this x_a the sample corresponds to a binary CsPFO/^2H_2O system composition of w_a = 0.45. APFO is substituted for the CsPFO on a molecule for molecule basis. X_{APFO} is the mole fraction of APFO of the total mole fraction of amphiphile. The ratio of the densities of the CsPFO and APFO is 1.26 compared with a molar mass ratio of 1.27 and so the volume fraction of amphiphile is also essentially constant irrespective of the actual composition of the mixed amphiphile. The actual change is $\phi = 0.280$ at $X_{APFO} = 0$ to $\phi = 0.283$ at $X_{APFO} = 1$. The phase diagram (figure 7.1) shows that an increase in the proportion of NH_4^+ ions causes a monotonic decrease in the phase transition temperatures but there is a pronounced curvature in the phase transition boundaries. If there is no preferential counter-ion binding, there should be a linear relationship between the phase transition temperature and X_{APFO}. The curvature indicates that there is a positive deviation from ideal behaviour which indicates preferential binding of Cs^+ ions to the micelle surface.

Figure 7.1. Partial phase diagram of the APFO/CsPFO/^2H_2O system with a constant mole fraction of amphiphile of $x_a = 0.0291$. X_{APFO} is the mole fraction of APFO in the total surfactant, *i.e.* $n_{APFO}/(n_{APFO} + n_{CsPFO})$. Shown are the isotropic micellar solution phase I, the nematic phase N_D^+, and the discotic lamellar phase L_D

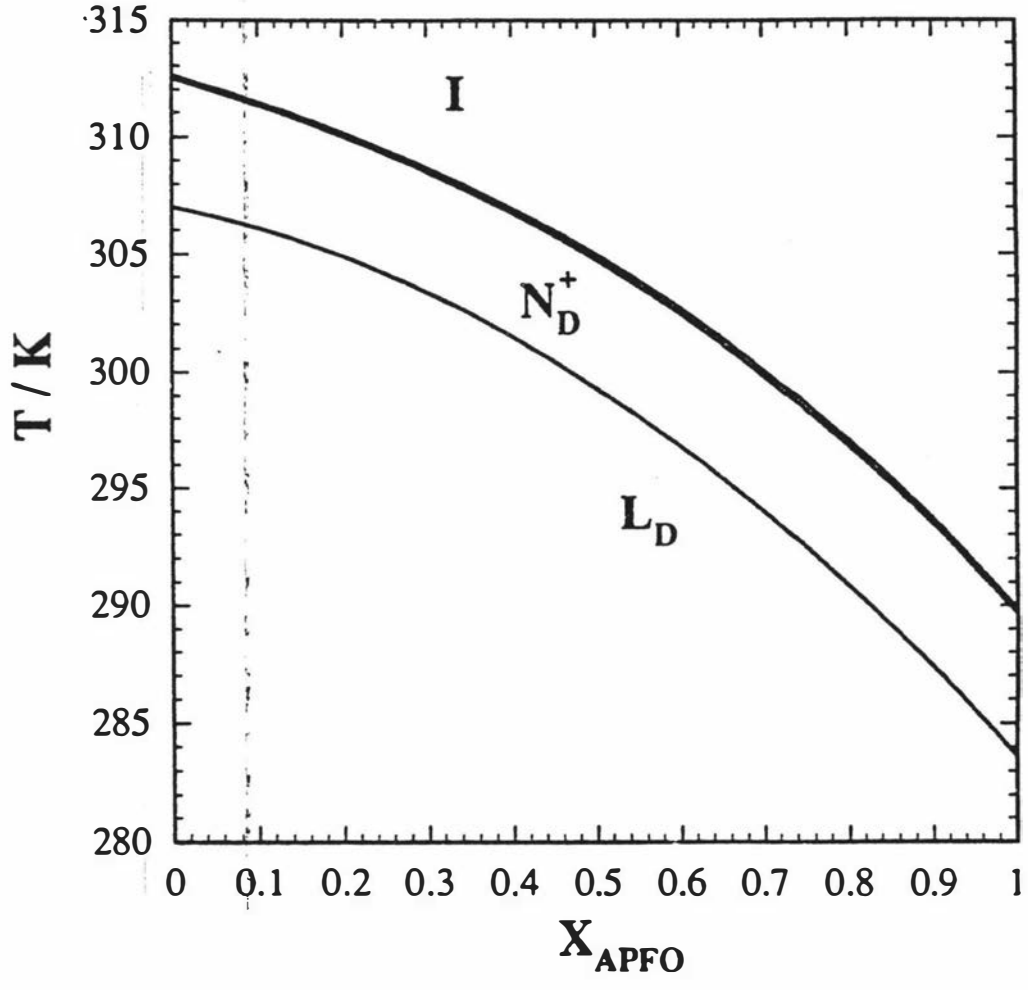

Figure 7.2. Partially averaged ^2H quadrupole splittings $\Delta\tilde{\nu}(^2H)$ for the APFO/CsPFO/^2H_2O system with a constant mole fraction of amphiphile of x_a = 0.0291 at the T_{NI} and T_{LN} phase transition boundaries.

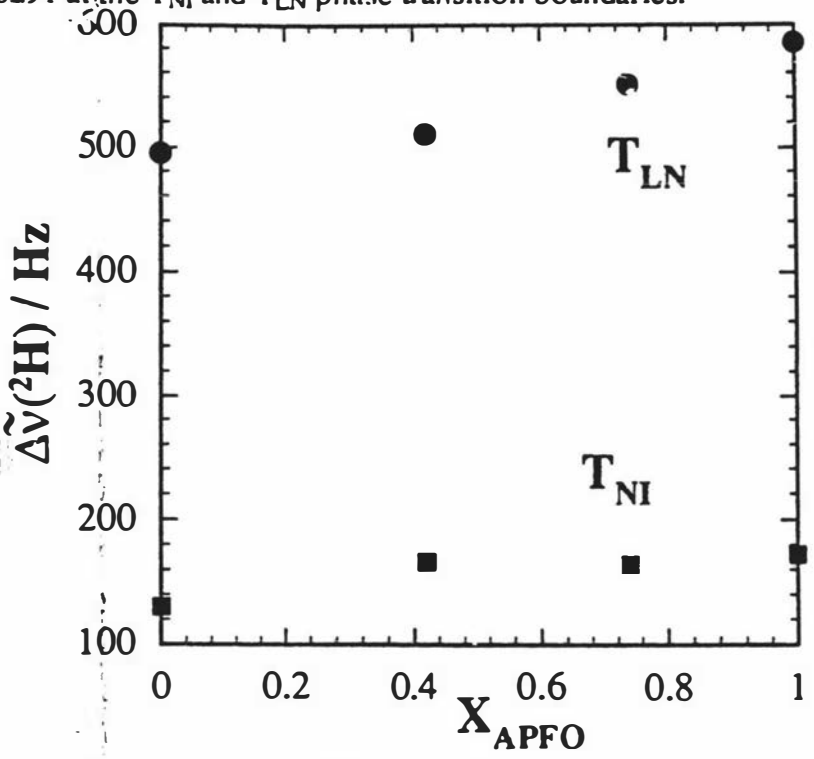

Figure 7.3. Concentration dependence of the partially averaged ^2H quadrupole splittings $\Delta\tilde{\nu}(^2H)$ for the CsPFO/^2H_2O(▲,◆) and APFO/^2H_2O(■,●) binary systems[1] at T_{NI} and T_{LN} divided by x_a/x_w . ϕ is the volume fraction of amphiphile.

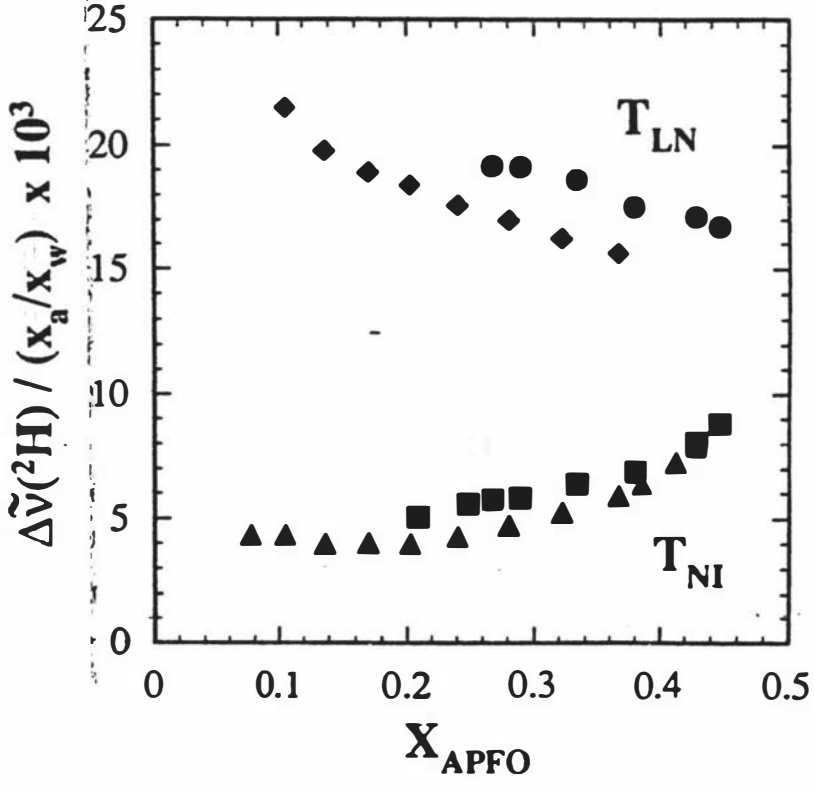

7.2 Micelle Size at the T_{NI} and T_{LN} Transitions

A plot of the $\Delta\tilde{\nu}(^2H)$ along the T_{NI} and T_{LN} phase transition boundaries shows a general increase in the quantity with increasing X_{APFO} (figure 7.2). The origin of this increase can be understood by considering $\Delta\tilde{\nu}(^2H)$ along the phase transition boundaries of the CsPFO/^2H_2O and APFO/^2H_2O binary systems. As x_a/x_w differs between each system at an equivalent volume fraction of amphiphile its contribution to the ^2H quadrupole splittings must be removed to allow a comparison of the relative magnitudes of the ^2H quadrupole splittings between the CsPFO/^2H_2O and APFO/^2H_2O systems. Figure 7.3 shows that at a given volume fraction $\Delta\tilde{\nu}(^2H)/(x_a/x_w)$ for the APFO/^2H_2O system is greater than the corresponding value in the CsPFO/^2H_2O system, although at T_{NI} there appears to be a convergence of the two at high volume fractions (temperatures). The axial ratio along the phase transitions at any given ϕ is the same for both the APFO/^2H_2O and CsPFO/^2H_2O binary systems[2] as is the value of S [3]. The difference in $\Delta\tilde{\nu}(^2H)/(x_a/x_w)$ along the transition must, therefore, lie in the n_bS_{OD} term of the expression for the ^2H quadrupole splittings (compare with equation[3.19]), *i.e.* n_bS_{OD} must be greater in the APFO/^2H_2O system than the CsPFO/^2H_2O system. This would account for the drift to higher quadrupole splittings as shown in figure 7.2 and in this case the higher values for $\Delta\tilde{\nu}(^2H)$ at both T_{NI} and T_{LN}, in the case of the APFO/^2H_2O system, are not a result of larger aggregates in this system.

7.4 Counter-Ion Binding

^{133}Cs quadrupole splittings will reflect changes in the counter-ion binding as the proportion of the Cs^+ to NH_4^+ changes. Figure 7.4 shows $\Delta\tilde{\nu}(^{133}Cs)$ along the T_{LN} and T_{NI} phase transition boundaries as a function of X_{APFO}. Obviously the $X_{APFO} = 1$ sample cannot be included due to the absence of caesium ions. The figure shows an increase in $\Delta\tilde{\nu}(^{133}Cs)$ along the phase transition lines. The only variable contributions to $\Delta\tilde{\nu}(^{133}Cs)$ along the phase transition lines are $\langle P_2 \cos\alpha \rangle_s$ and β_{Cs} (equation[3.21]), and since the micelle size are the same in the two systems at the phase transition temperature then an, increasing $\Delta\tilde{\nu}(^{133}Cs)$ indicates that the bound fraction of caesium ions is increasing with increasing X_{APFO}. Recalling that β_{Cs} is the moles of bound Cs^+ ions n_b divided by the total moles of Cs^+ ions in solution n_t, the increase in β_{Cs} suggests that the decrease in n_b on the addition of APFO is smaller than it would be in the absence of any preferential binding of Cs^+ ions. Normalising to this value and assuming that change in $\Delta\tilde{\nu}(^{133}Cs)$ occur solely as a result of changes in β_{Cs} enables figure 7.5 to be constructed.

Figure 7.4. Partially averaged ^{133}Cs quadrupole splittings $\Delta\tilde{\nu}(^{133}Cs)$ for the APFO/CsPFO/^2H_2O system with a constant mole fraction of amphiphile of x_a = 0.0291 at T_{NI} and T_{LN}.

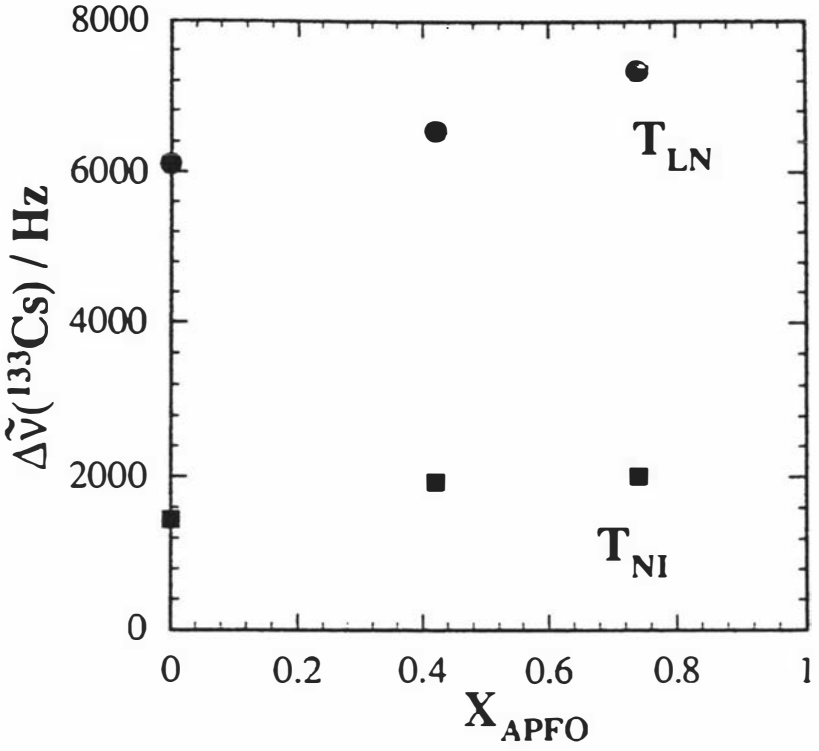

Figure 7.5. Bound fraction of caesium ions β_{Cs} (see text for description of β_{Cs}) at T_{LN} for the APFO/CsPFO/^2H_2O system with a constant mole fraction of amphiphile of x_a = 0.0291.

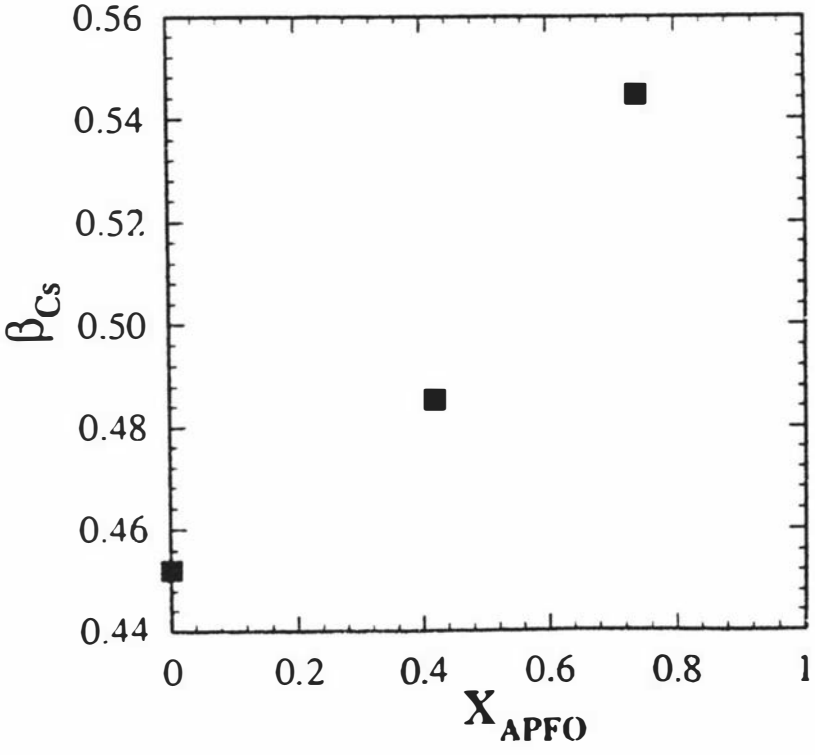

7.5 Conclusion

X-ray measurements have shown that at corresponding ϕ values the *a*/*b* ratios of the micelles are the same in both the CsPFO/^2H_2O and APFO/^2H_2O systems. In spite of the observed increase in the ^2H quadrupole splittings at T_{NI} and T_{LN} on substituting APFO for CsPFO this appears to be the case in the mixed APFO/CsPFO/^2H_2O system also. *i.e.* the increase in $\Delta\tilde{\nu}(^2H)$ is probably due to a corresponding increase in n_bS_{OD} in the APFO/^2H_2O system.

The result is consistent with the findings of Rosenblatt who examined the effect of counter-ion identity on a micellar liquid crystal by substituting rubidium pentadecafluorooctanoate (RbPFO) amphiphile with CsPFO amphiphile at a constant mass fraction of amphiphile in water of $w_a = 0.399$ ($\phi = 0.22$)[4]. The observation of an increase in the bound fraction of Cs^+ ions as X_{APFO} increases indicates that there is a preference for Cs^+ ions to bind to the micellar surface. This is consistent with the observation of a positive departure from ideal mixing in the phase transition temperatures as X_{APFO} increases.

References

1. M. H. Smith, Ph.D., Massey University (1990).

2. N. Boden, P. J. B. Edwards, K. W. Jolley, in *Structure and Dynamics of Strongly Interacting Colloids and Supramolecular Aggregates in Solution* S.-H. Chen, J. S. Huang, P. Tartaglia, Eds. (Kluwer academic Publishers, Dordrecht, 1992), vol. 369, pp. 433-461.

3. N. Boden, J. Clements, K. W. Jolley, D. Parker, M. H. Smith, *J. Chem. Phys.* **93**, 9096-9105 (1990).

4. C. Rosenblatt, *J. Colloid. Interface. Sci.* **131**, 236-241 (1989).

Appendix A
Phase Transition Temperatures

Table A1. Phase transition temperatures for the CsNFD/^2H_2O system. ϕ is the volume fraction of surfactant.

ϕ	T_{IN}	T_{NI}	T_{LN}/T_{LI}
0.056	324.121		315.000
0.119	343.328	343.216	335.450
0.170	354.110	353.970	345.944
0.201	359.495	359.350	351.780

Table A2. Phase transition temperatures for the CsHFN/^2H_2O system. ϕ is the volume fraction of surfactant.

ϕ	T_{IN}	T_{NI}	T_{LN}/T_{LI}
0.122	317.510	317.400	310.100
0.206	334.605	334.5	327.43
0.302	351.150	350.950	344.960

Table A3. Phase transition temperatures for the CsTFH/^2H_2O system. ϕ is the volume fraction of surfactant.

ϕ	T_{IN}	T_{NI}	T_{LN}	T_{NL}
0.396	294.103	293.120	288.051	288.897
0.427	302.620	301.200	298.210	296.260
0.451	309.540		302.700	298.21

Table A4. Phase transition temperatures for the CsPFO/CsCl/^2H_2O system. The CsPFO to ^2H_2O weight ratio is fixed at 1 : 1 and w_e is the weight fraction of CsCl.

w_e	T_{IN}	T_{NI}	T_{LN}/T_{LI}
0.000	322.346	321.920	316.252
0.002	322.700	322.300	316.600
0.003	322.963	322.780	316.880
0.013	327.428	327.035	319.720
0.019	329.850	329.400	321.700
0.021	330.300	329.800	322.100
0.027	332.695	332.130	324.330
0.029	333.575	332.920	325.100
0.035	335.058	334.340	327.120
0.043	337.706	336.720	329.750
0.054	340.836	339.380	333.950
0.062	342.600	340.570	336.850
0.067	344.662	341.970	339.230
0.077	347.400	343.950	343.220
0.078	347.400	343.950	343.220
0.081	348.100		344.240
0.084	348.984		345.460
0.094	351.725		349.100
0.102	353.420		351.510
0.112	357.080		355.020
0.120	359.870		358.680

Table A5. Phase transition temperatures for the CsPFO/CsCl/^2H_2O system. The CsPFO to ^2H_2O weight ratio is fixed at 1 : 4 and w_e is the weight fraction of CsCl.

w_e	T_{IN}	T_{NI}	T_{LN}/T_{LI}
0.000	283.394	283.318	278.950
0.002	286.413	286.332	281.288
0.006	290.209	290.108	285.850
0.010	292.914	292.749	289.587
0.015	296.330	296.120	293.600
0.020	298.760	298.460	296.815
0.023	301.974	301.690	300.740
0.029	302.832	302.600	301.742
0.040	308.114	308.020	307.715
0.052	311.490	311.349	311.295
0.055	313.522		313.420

Table A6. Phase transition temperatures for the CsPFO/CsCl/^2H_2O system. The CsPFO to ^2H_2O weight ratio is fixed at 53 : 47 and w_e is the weight fraction of CsCl.

w_e	T_{IN}	T_{NI}	T_{NL}	T_{LN}/T_{LI}
0.00000	326.906	326.540	321.760	321.370
0.00148	327.574	327.148	322.060	321.850
0.00278	328.347	327.953	322.565	322.447
0.00390	328.631	328.260	322.620	322.570
0.00543	329.533	329.125		323.300
0.00650	329.798	329.350		323.440

Table A7. Phase transition temperatures for the CsPFO/ceasium salt/^2H_2O system. The weight ratio of CsPFO to ^2H_2O is fixed at 1 : 1 and x_e is the mole fraction of the corresponding ceasium salt.

ceasium salt	x_e	T_{IN}	T_{NI}	T_{LN}
CsF	0.00624	333.400	332.870	324.825
CsBr	0.00629	332.330	331.875	324.400
CsI	0.00600	331.830	331.360	323.620

Table A8. Phase transition temperatures for the APFO/NH_4Cl/^2H_2O system. The APFO to ^2H_2O weight ratio is fixed at 2 : 3 and w_e is the weight fraction of NH_4Cl.

w_e	T_{IN}	T_{NI}	T_{LN}/T_{LI}
0.000	293.028	292.770	286.840
0.003	298.487	298.160	291.100
0.005	301.120	300.420	293.830
0.013	308.972	306.870	304.540
0.022	320.301		318.220
0.033	332.930		331.970

Table A9. Phase transition temperatures for the APFO/NH_4Cl/^2H_2O system. The APFO to ^2H_2O weight ratio is fixed at 9 : 11 and w_e is the weight fraction of NH_4Cl.

w_e	T_{IN}	T_{NI}	T_{LN}/T_{LI}
0.00000	301.308	300.820	295.730
0.00470	308.378	307.660	299.890
0.00937	313.657	312.100	305.900
0.01000	315.187	313.420	307.730
0.01485	319.540	315.900	313.640
0.02021	325.280		321.080
0.02457	330.175		326.930
0.03080	336.790		334.420

Table A10. Phase transition temperatures for the APFO/CsPFO/^2H_2O system. The mole fraction of surfactant is fixed at 0.0291 where X_{APFO} is the mole fraction of APFO of the total surfactant.

X_{APFO}	T_{IN}	T_{NI}	T_{LN}
0.00	312.635	312.50	307.02
0.42	306.607	306.40	301.10
0.74	298.960	298.70	292.79
1.00	289.890	289.68	283.63

Appendix B
Quadrupole Splittings at the Phase Transitions

Table B1. ^2H quadrupole splittings along the nematic-to-isotropic and nematic-to-lamellar phase transitions for the CsNFD/^2H_2O system. ϕ is the volume fraction of surfactant.

ϕ	$\Delta\tilde{\nu}(^2H)T_{NI}$ /Hz	$\Delta\tilde{\nu}(^2H)T_{LN}$ /Hz
0.056		92
0.119	36	165
0.170	62	227
0.201	80	263

Table B2. ^2H quadrupole splittings along the nematic-to-isotropic and nematic-to-lamellar phase transitions for the CsHFN/^2H_2O system. ϕ is the volume fraction of surfactant.

ϕ	$\Delta\tilde{\nu}(^2H)T_{NI}$ /Hz	$\Delta\tilde{\nu}(^2H)T_{LN}$ /Hz
0.122	30	192
0.171	52	305
0.302	125	455

Table B3. ^2H quadrupole splittings along the nematic-to-isotropic and nematic-to-lamellar phase transitions for the CsTFH/^2H_2O system. ϕ is the volume fraction of surfactant.

ϕ	$\Delta\tilde{\nu}(^2H)T_{NI}$ /Hz	$\Delta\tilde{\nu}(^2H)T_{LN}$ /Hz	$\Delta\tilde{\nu}(^2H)T_{NI}$/Hz
0.396	442	938	883
0.427	575	1065	873
0.451	700	1240	

Table B4. ^2H Quadrupole splittings along the nematic-to-isotropic and nematic-to-lamellar phase transitions for the CsPFO/CsCl/^2H_2O system. The CsPFO to ^2H_2O weight ratio is fixed at 1 : 1 and w_e is the weight fraction of CsCl.

w_e	$\Delta\tilde{\nu}(^2H)T_{NI}$ /Hz	$\Delta\tilde{\nu}(^2H)T_{LN}$ /Hz
0.000	192	589
0.002	191	595
0.003	193	592
0.013	201	617
0.019	209	630
0.021	212	615
0.027	222	623
0.029	232	625
0.035	243	625
0.043	275	635
0.054	319	615
0.062	370	600
0.067	418	593
0.077	519	582
0.078	512	566
0.081		560
0.084		590
0.084		590
0.094		596
0.102		581
0.112		587
0.120		577

Table B5. ^{133}Cs Quadrupole splittings along the nematic-to-isotropic and nematic-to-lamellar phase transitions for the CsPFO/CsCl/$^{2}H_2O$ system. The CsPFO to $^{2}H_2O$ weight ratio is fixed at 1 : 1 and w_e is the weight fraction of CsCl.

w_e	$\Delta\tilde{\nu}(^{133}Cs)T_{NI}$ / Hz	$\Delta\tilde{\nu}(^{133}Cs)T_{LN}$ / Hz
0.000	1570	5442
0.002	1570	5400
0.003	1558	5405
0.013	1540	5275
0.019	1543	5145
0.021	1550	5075
0.027	1570	4910
0.029	1610	4840
0.035	1650	4660
0.043	1780	4525
0.054	1990	4160
0.062	2285	3875
0.067	2485	3715
0.077	3040	3440
0.078	3040	3420
0.081		3400
0.084		3395
0.094		3270
0.102		3105
0.112		3005
0.120		2826

Table B6. ^{35}Cl Quadrupole splittings along the nematic-to-isotropic and nematic-to-lamellar phase transitions for the CsPFO/CsCl/$^{2}H_2O$ system. The CsPFO to $^{2}H_2O$ weight ratio is fixed at 1 : 1 and w_e is the weight fraction of CsCl.

w_e	$\Delta\tilde{\nu}(^{35}Cl)T_{NI}$	$\Delta\tilde{\nu}(^{35}Cl)T_{LN}$
0.003	2627	8100
0.013	2900	8400
0.019		8980
0.021		9150
0.029	3500	9300
0.035	3800	9100
0.043	4400	9409
0.054	5200	9900
0.062	6075	9460
0.077	9250	9250
0.078	8490	9150
0.081		9450
0.084		9770
0.094		10090
0.102		9900
0.112		10130
0.120		10075

Table B7. ^2H quadrupole splittings along the nematic-to-isotropic and nematic-to-lamellar phase transitions for the CsPFO/CsCl/^2H_2O system. The CsPFO to ^2H_2O weight ratio is fixed at 1 : 4 and w_e is the weight fraction of CsCl.

w_e	$\Delta\tilde{\nu}(^2H)T_{NI}$ /Hz	$\Delta\tilde{\nu}(^2H)T_{LN}.T_{LI}$/Hz
0.000	38	176
0.002	40	188
0.006	47	182
0.010	52	171
0.015	66	174
0.020	71	163
0.023	80	156
0.029	84	157
0.040	95	145
0.052	121	138
0.055		132

Table B8. ^{133}Cs quadrupole splittings along the nematic-to-isotropic and nematic-to-lamellar phase transitions for the CsPFO/CsCl/^2H_2O system. The CsPFO to ^2H_2O weight ratio is fixed at 1 : 4 and w_e is the weight fraction of CsCl.

w_e	$\Delta\tilde{\nu}(^{133}Cs)T_{NI}$ / Hz	$\Delta\tilde{\nu}(^{133}Cs)T_{LN}.T_{LI}$/Hz
0.000	2250	9600
0.002	2750	9600
0.006	2190	8400
0.010	2250	7300
0.015	2290	6553
0.020	2448	5680
0.023	2500	4750
0.029	2566	4725
0.040	2450	3700
0.052	2580	3150
0.055		2830

Table B9. ^{35}Cl quadrupole splittings along the nematic-to-isotropic and nematic-to-lamellar phase transitions for the CsPFO/CsCl/$^{2}H_2O$ system. The CsPFO to $^{2}H_2O$ weight ratio is fixed at 1 : 4 and w_e is the weight fraction of CsCl.

w_e	$\Delta\tilde{\nu}(^{35}Cl)T_{NI}$/Hz	$\Delta\tilde{\nu}(^{35}Cl)T_{LN}$,$T_{LI}$/Hz
0.006	220	790
0.010	300	848
0.020	600	1090
0.023	630	1140
0.029	842	1175
0.052	1016	1270
0.055		1206

Table B10. ^{2}H quadrupole splittings along the nematic-to-isotropic and nematic-to-lamellar phase transitions for the CsPFO/CsCl/$^{2}H_2O$ system. The CsPFO to $^{2}H_2O$ weight ratio is fixed at 53 : 47 and w_e is the weight fraction of CsCl.

w_e	$\Delta\tilde{\nu}(^{2}H)T_{NI}$ /Hz	$\Delta\tilde{\nu}(^{2}H)T_{NL}$/Hz	$\Delta\tilde{\nu}(^{2}H)T_{LN}$ / Hz
0.00000	228	632	662
0.00148	228	638	659
0.00278	231	650	660
0.00390	229	656	660
0.00543	230		660
0.00650	234		657

Table B11 ^{133}Cs quadrupole splittings along the nematic-to-isotropic and nematic-to-lamellar phase transitions for the CsPFO/CsCl/$^{2}H_2O$ system. The CsPFO to $^{2}H_2O$ weight ratio is fixed at 53 : 47 and w_e is the weight fraction of CsCl.

w_e	$\Delta\tilde{\nu}(^{133}Cs)T_{NI}$ / Hz	$\Delta\tilde{\nu}(^{133}Cs)T_{NL}$ / Hz	$\Delta\tilde{\nu}(^{133}Cs)T_{LN}$ / Hz
0.00000	1620	4902	5151
0.00148	1640	4958	5110
0.00278	1610	4990	5068
0.00390	1611	5060	5080
0.00543	1600		4995
0.00650	1590		4920

Table B12 ^{133}Cs quadrupole splittings along the nematic-to-isotropic and nematic-to-lamellar phase transitions for the CsPFO/caesium salt/^2H_2O system. The weight ratio of CsPFO : ^2H_2O is fixed at 1 to 1 and x_c is the mole fraction of the corresponding caesium salt.

ceasium salt	x_c	$\Delta\tilde{\nu}(^2H)T_{NI}$ /Hz	$\Delta\tilde{\nu}(^2H)T_{LN}$/Hz
CsF	0.00624	224	630
CsBr	0.00629	216	620
CsI	0.00600	213	612

Table B13. ^{133}Cs quadrupole splittings along the nematic-to-isotropic and nematic-to-lamellar phase transitions for the CsPFO/caesium salt/^2H_2O system. The weight ratio of CsPFO to ^2H_2O is fixed at 1 : 1 and x_c is the mole fraction of the corresponding caesium salt.

ceasium salt	x_c	$\Delta\tilde{\nu}(^{133}Cs)T_{NI}$ / Hz	$\Delta\tilde{\nu}(^{133}Cs)T_{LN}$ / Hz
CsF	0.00624	1640	5125
CsBr	0.00629	1565	5020
CsI	0.00600	1565	5025

Table B14. ^2H quadrupole splittings along the nematic-to-isotropic and nematic-to-lamellar phase transitions for the APFO/NH_4Cl/^2H_2O system. The APFO to ^2H_2O weight ratio is fixed at 2 : 3 and w_c is the weight fraction of NH_4Cl.

w_c	$\Delta\tilde{\nu}(^2H)T_{NI}$ /Hz	$\Delta\tilde{\nu}(^2H)T_{LN}.T_{LI}$/Hz
0.000	178	588
0.003	210	608
0.005	239	608
0.013	410	590
0.022		562
0.033		543

Table B15. ^2H quadrupole splittings along the nematic-to-isotropic and nematic-to-lamellar phase transitions for theAPFO/^2H_4Cl/^2H_2O system. The APFO to ^2H_2O weight ratio is fixed at 9 : 11 and w_c is the weight fraction of NH_4Cl.

w_c	$\Delta\tilde{\nu}(^2H)T_{NI}$ /Hz	$\Delta\tilde{\nu}(^2H)T_{LN}$,$T_{LI}$/Hz
0.00000	239	695
0.00470	274	730
0.00937	363	730
0.01000	395	733
0.01485	554	716
0.02021		698
0.02457		680
0.03080		665

Table B16. ^2H quadrupole splittings along the nematic-to-isotropic and nematic-to-lamellar phase transitions for theAPFO/CsPFO/^2H_2O system. The mole fraction of surfactant is fixed at 0.0291 where X_{APFO} is the mole fraction of APFO of the total surfactant.

X_{APFO}	$\Delta\tilde{\nu}(^2H)T_{NI}$ /Hz	$\Delta\tilde{\nu}(^2H)T_{LN}$/Hz
0.00	130	495
0.42	166	510
0.74	163	551
1.00	172	585

Table B17. ^{133}Cs Quadrupole splittings along the nematic-to-isotropic and nematic-to-lamellar phase transitions for theAPFO/CsPFO/^2H_2O system. The mole fraction of surfactant is fixed at 0.0291 where X_{APFO} is the mole fraction of APFO of the total surfactant.

X_{APFO}	$\Delta\tilde{\nu}(^{133}Cs)T_{NI}$ / Hz	$\Delta\tilde{\nu}(^{133}Cs)T_{LN}$ / Hz
0.00	1440	6100
0.42	1929	6550
0.74	2002	7350

Appendix C

Density Measurements

Comparison between different systems is usually required to be performed in volume fraction space. In order to do this the density in solution of each of the perfluorinated carboxylic acid salts is required. These densities were determined using an Anton Paar vibrating-tube digital-density meter as outlined in chapter 2.

The apparent molar volumes (V_ϕ) of the caesium salts were calculated from the relationship

$$V_\phi = \frac{1000}{mdd_o}(d_o - d) + \frac{M}{d}$$

where m is the molality of the solution, M is the relative molar mass of the surfactant, d is the density of the solution and d_o is the density of the solvent. The concentration dependence of V_ϕ for aqueous solutions of CsPFO at 25 °C is shown in figure C1. The change in the molar volume on micellization is about 12.2 $cm^3\ mol^{-1}$ which is significantly greater than that found in corresponding hydrocarbon systems[1]. The partial molar volumes of the micelles V_2^- given in Table C1 were obtained by extrapolating the measurements made above the cmc to infinite dilution. The differences in the V_ϕ values between the CsTFH and CsPFO (22 $cm^3\ mol^{-1}$) and the CsPFO and CsHFN salts (25 $cm^3\ mol^{-1}$) are close to the calculated value of 23 $cm^3\ mol^{-1}$ for the volume of a CF_2 group[2].

The CsNFD solutions were too viscous to be easily loaded into the densitometer so its molar volume was determined at 25 °C by measuring the density of a solution with mass fraction w_a of 0.1 using a pycnometer. Assuming ideal mixing and a ^2H_2O density of 1.105 g cm^{-3} at 25 °C[3] gave a CsNFD in solution density of 2.32 g cm^{-3}. This density corresponds to a molar volume of 278 $cm^3\ mol^{-1}$ which is only 18 $cm^3\ mol^{-1}$ larger than the CsHFN value. The most probable explanation for this is that the extrapolation technique has resulted in a CsNFD density which is slightly too big. In view of this we have used a V_ϕ value for CsNFD of 283 $cm^3\ mol^{-1}$ (*ie* 260.3 + 23) in volume fraction calculations.

Table C1 Partial Molal Volume and the Density of Perfluorinated Surfactants used in this Study

Perfluorinated Surfactant	V_2^{∞}	Density of Surfactant (ρ)
CsTFH	210.2	2.36
CsPFO	234.4	2.32
CsHFN	261.4	2.28
CsNFD	278.2	2.32
APFO	234.1	1.84
RbPFO	225.5	2.21

References

1. E. M. Woolley, T. E. Burchfield, *J. Phys. Chem.* **89**, 714 (1985).
2. N. Boden, J. Clements, K. W. Jolley, D. Parker, M. H. Smith, *J. Chem. Phys.* **93**, 9096-9105 (1990).
3. G. S. Kell, *J. Chem. Eng. Data* **12**, 66-69 (1967).

Figure C1 Apparent molar volume V'_ϕ as a function of concentration for caesium pentadecafluorooctanoate in ^2H_2O at 25 °C